UNIVERSITY OF CALIFORNIA, SAN DIEGO

Structural and Functional Analysis of Chemokine Interactions with Glycosaminoglycans and Chemokine Receptors

A dissertation submitted in partial satisfaction of the
requirements for the degree of Doctor of Philosophy

in

Chemistry

by

Catherina L. Salanga

Committee in charge:

Professor Tracy Handel, Chair
Professor Alexander Hoffmann, Co-Chair
Professor Phillip Bourne
Professor Edward Dennis
Professor Douglas Magde

2011

This Dissertation of Catherina L. Salanga is approved, and it is acceptable in quality and form for publication on microfilm and electronically:

_____

_____

_____

_____
Co-Chair

_____
Chair

University of California, San Diego

2011

DEDICATION

Dedicated to my parents and Anthony.
For their unwaivering love and support.

TABLE OF CONTENTS

Signature Page iii

Dedication iv

Table of Contents v

List of Figures xi

List of Tables xiv

List of Abbreviations xv

Acknowledgements xvii

Curriculum Vitae xix

Abstract of the Dissertation xxi

CHAPTER 1 Introduction to the Chemokine Network 1

1.1 The Chemokine Network 1

1.2 Chemokine Oligomerization and GAG Binding 8

1.3 Signaling in the Chemokine Network 13

1.4 Chemokine Receptor Oligomerization and Crosstalk 18

1.5 Chemokines and Chemokine Receptors in Disease 29

1.6 Acknowledgements 34

1.7 References 35

CHAPTER 2 Characterization of MCP-3/CCL7: GAG Interactions Identified by Radiolytic Footprinting with Mass Spectrometry, Mutagenesis and Functional Analysis 49

2.1 Summary 49

2.2 Introduction 51

2.3 Results 57

2.3.1 Hydroxyl radical footprinting analysis by mass spectrometry of MCP-3/CCL7 in complex with heparin octasaccharide 57

2.3.2 Heparin binding assays of MCP-3/CCL7 mutants confirm the contribution of K18K19 and the C-terminal tail K4x lysines to GAG binding 61

2.3.3 Receptor activation measured by calcium flux and chemotaxis across bare filters suggest that K18K19 and K4x epitopes contribute little to receptor binding . 64

2.4 Discussion 66

2.5 Ongoing Work/Immediate Future Directions 73

2.6 Materials and Methods 74

2.6.1 Chemokine expression and purification 74

2.6.2 Radiolysis 75

2.6.3 Proteolytic digestion and mass spectrometry 75

2.6.4 *In vitro* heparin binding assays 76

2.6.5 Generation of stable cell lines 77

2.6.6 Flow cytometry 77

2.6.7 Intracellular calcium flux assays 78

2.6.6 *In vitro* chemotaxis assays 78

2.7 Acknowledgements 79

2.8 References 80

CHAPTER 3 Phosphoproteomic Analysis of Chemokine Signaling Networks 85

3.1 Summary 85

3.2 Introduction 87

3.3 Materials and Methods and Additional Considerations 90

3.3.1: Isolation of chronic lymphocytic leukemia cells 90

3.3.2: CXCL12 stimulation of CLL cells and lysate preparation 90

3.3.3: IMAC phosphopeptide enrichment of CLL samples 91

3.3.4: Reversed-phase liquid chromatography and tandem mass spectrometry.... 96

3.4 Acknowledgements 103

3.4 References 104

CHAPTER 4 Phosphoproteomics Analysis of CXCL12 Signaling in Chronic Lymphocytic Leukemia Cells 108

4.1 Summary 108

4.2 Introduction 110

4.3 Results 114

4.3.1: Normal B cells migrate with higher efficacy and potency to CXCL12 than CLL B cells, despite having lower levels of CXCR4 114

4.3.2: Characterization of phosphopeptides/phosphoproteins in CXCL12-stimulated CLL cells via mass spectrometry 115

4.3.3: Identification of phosphoproteins with prior correlations to CLL and other leukemias 119

4.3.4: Identification of novel downstream targets of CXCL12/CXCR4 signaling in CLL 121

4.3.5: CXCL12 induces the phosphorylation and degradation of PDCD4 122

4.3.6: HSP27 expression and phosphorylation is variable in CLL cells 126

4.4 Discussion 130

4.5 Materials and Methods 138

4.5.1: Cells and reagents 138

4.5.2: Recombinant CXCL12 preparation 138

4.5.3: Migration assays 139

4.5.4: Preparation of CLL lysates for proteomics 139

4.5.5: IMAC phosphopeptide enrichment 140

4.5.6: Mass spectrometry and data processing 141

4.5.7: Western blots and antibody reagents 143

4.5.8: Flow cytometry 144

4.6 Acknowledgements 145

4.7 References 146

CHAPTER 5 Elucidating the Roles of the Chemokine Receptors CXCR4 and CXCR7 in Breast Cancer Growth and Metastasis 151

5.1 Summary 151

5.2 Introduction 153

5.3 Results 155

5.3.1: CXCR4 and CXCR7 localization in MDA-MB-231 cells 155

5.3.2: Tumor growth progression of clonal lines expressing varying levels of CXCR4 and/or CXCR7 157

5.3.3: *In vivo* effects of CXCR7 expression on highly metastatic MDA-MB-231 primary tumor growth and metastasis 162

5.3.4: Effect of CXCR7 expression on CXCL12-mediated signaling in MDA-MB-231 cells 170

5.3.5: Effect of the CXCR4 WHIM mutant on CXCL12 mediated internalization of CXCR4 and CXCR7 174

5.4 Discussion 177

5.5 Ongoing Work/Immediate Future Directions 181

5.6 Materials and Methods 182

5.6.1: Cells and reagents 182

5.6.2: Generation of stable MDA cell lines 183

5.6.3: Flow cytometry 183

5.6.4: Immunofluorescence microscopy 184

5.6.5: *In vivo* mouse studies 185

5.6.6: Calcium flux assays 186
5.6.7: Western blot analysis 186
5.6.8: Internalization assays 187
5.7 Acknowledgements 188
5.8 References 189
CHAPTER 6 Conclusions and Future Directions 193
6.1 Summary 193
6.2 Chapter 2 195
6.3 Chapter 3 and 4 197
6.4 Chapter 5 204
6.5 References 208
APPENDIX I PROTOCOLS 211
A: MCP-3/CCL7 Purification 211
B: MCP-1/CCL2 Purification 216
C: Maintenance and Electroporation of L1.2 Cells 218
D: In Vitro Heparin Binding Assays 220
E: Calcium Flux Analysis 222
F: Bare-Filter Chemotaxis Assays 224
G: Preparing Cap-LC Columns 226
H: Using InsPeCT 229
I: Maintenance of MDA-MB-231 Cells 232
J: Retroviral Transfection and Infection Procedure 234
K: CXCL12 Purification 236
L: ITAC Purification 243
M: RNA Isolation and cDNA Synthesis 248

N: Quantitative Real-time PCR 251
O: Compensation on Flow Cytometer 254
P: Detecting Chemokine Receptor Expression by Flow Cytometry 255
Q: Mammary Fat Pad Injections 258
R: Mouse Tumor Harvests for GFP Imaging, Culturing, and Histology 262
S: Quantification of Lung Fluorescence for GFP-expressing Tumor Cells 267
T: Western Blot Protocol 269
U: Receptor Internalization Assay 275
V: Immunofluorescence Microscopy 278
W: MTT Assay 285
X: Pulldown of HA-tagged Receptor 286

LIST OF FIGURES

Figure 1.1 Cartoon depicting chemokine mediated migration 3

Figure 1.2 Structure of a typical chemokine 4

Figure 1.3 Molecular events in the classical activation of a chemokine receptor 6

Figure 1.4 Various structures of chemokine monomers and higher order oligomers ... 11

Figure 1.5 Surface model of the tetrameric structure of CCL2 with GAG binding sites 13

Figure 1.6 Chemokine receptor signaling in migration and survival/proliferation 16

Figure 1.7 Potential effects of hetero-oligomerization on receptor signaling 21

Figure 1.8 Structure of the CXCR4 dimer 22

Figure 1.9 Potential mechanisms of chemokine receptor crosstalk 28

Figure 2.1 Oligomeric forms of MCP-1/CCL2 with heparin and heparan sulfate 54

Figure 2.2 Sequence alignment of the MCP family 57

Figure 2.3 Dose response curve for the peptide 13-27 60

Figure 2.4 Dose response curve for the peptide 63-76 61

Figure 2.5 Heparin sepharose chromatography results 63

Figure 2.6 MCP-3/CCL7 or mutant mediated intracellular calcium mobilization 65

Figure 2.7 MCP-3/CCL7 or mutant bare-filter chemotaxis assay 66

Figure 2.8 Potential GAG binding epitopes identified by radiolytic footprinting 70

Figure 2.9 Model of MCP-3/CCL7 and MCP-1/CCL2 bound to GAG and/or receptor .. 72

Figure 3.1 IMAC phosphoenrichment strategy 92

Figure 4.1 CXCR7 expression on normal B cells and CLL B cells 111

Figure 4.2 CXCL12-mediated migration of CLL B cells and normal B cells 113

Figure 4.3 Flow chart of CLL phosphoproteomics analysis 116

Figure 4.4 Overlap in phosphoprotein identification between CLL patient cells 118

Figure 4.5 CXCL12 Induces Phosphorylation of PDCD4 at Ser457 124
Figure 4.6 Mass spectra of PDCD4 phosphopeptides 125
Figure 4.7 Mass Spectrum of HSP27 phosphopeptide 127
Figure 4.8 Phosphorylation of HSP27 in subset of CLL patients 129
Figure 4.9 Phosphorylation of PAK2 is present but not induced by CXCL12 132
Figure 4.10 Summary of CXCL12-mediated signaling in CLL 137
Figure 5.1 Cellular distribution of CXCR4 and CXCR7 in MDA-MB-231 cells 156
Figure 5.2 CXCR7 expression in MDA-MB-231 WT and MDA+ CXCR7 cell lines 157
Figure 5.3 CXCR4 expression over time in MDA-MB-231 cultured cells 158
Figure 5.4 Differential CXCR4 and CXCR7 expression levels for MDA clonal line 159
Figure 5.5 Primary tumor growth comparison of mice injected with MDA clonal lines. 160
Figure 5.6 Increase in CXCR4 expression of lung and lymph node metastases 161
Figure 5.7 CXCR4 and CXCR 7 expression of MDA-HM + CXCR7 transfectants 163
Figure 5.8 CXCR4 and CXCR7 expression of MDA-HM injected cell lines 164
Figure 5.9 Comparison of MDA-HM and MDA-HM + CXCR7 tumor sizes 164
Figure 5.10 Primary tumor growth and tumor size comparisons of MDA-HM mice 165
Figure 5.11 Image of lymph node metastases derived from MDA-HM mice 166
Figure 5.12 Lymph node tumor mass comparisons of MDA-HM mice 167
Figure 5.13 GFP fluorescence of lung lobes derived from MDA-HM mice 168
Figure 5.14 Fluorescence quantification of lung metastases from MDA-HM mice 168
Figure 5.15 Representative H & E staining of lungs from MDA-HM mice 169
Figure 5.16 CXCL12 mediated calcium flux of MDA-HM cell lines 171
Figure 5.17 Phosphorylation analysis of PDCD4 following CXCL12 stimulation 172
Figure 5.18 Phosphorylation analysis of Akt, ERK1/2, and PDCD4 173
Figure 5.19 Internalization of CXCR4 and CXCR7 with WHIM mutant 176

Figure 5.20 Quantification of CXCR4 and CXCR7 internalization 177

Figure 6.1 Crosstalk between CLL cells and NLCs 202

Figure 6.2 Silver stained gel of Gelfree fractionation of raw NLC-CLL coculture..... 203

Figure 6.3 Silver stained gel of Gelfree fractionation of depleted NLC-CLL coculture 204

Figure 6.4 Overview of findings from Chapter 5 208

LIST OF TABLES

Table 1.1 Chemokine receptor and chemokine ligand binding partners 5

Table 1.2 Chemokines and their receptors involved in disease..... 31

Table 2.1 Comparative oxidation rate constants for identified peptides 59

Table 2.2 Summary of heparin and sepharose affinity chromatography 63

Table 3.1 Summary of phosphorylations identified in CXCL12-stimulated CLL cells ... 96

Table 3.2 Functional annotation of phosphoproteomics data 102

Table 4.1 Phosphoproteins identified with prior implications in CLL/Leukemia 119

Table 4.2 Select phosphoproteins from phosphoproteomics analysis 121

LIST OF ABBREVIATIONS

ACN……Acetonitrile

Ala……Alanine

AMD3100.....1,1′-[1,4-Phenylenebis(methylene)]bis [1,4,8,11-tetraazacyclotetradecane]

APC.....Allophycocyanin

Arg……Arginine

CID.....Collision induced dissociation

CLL.....Chronic lymphocytic leukemia

Cys……..Cysteine

DMSO.....Dimethyl sulfoxide

DTT……..……Dithiothreitol

ECM.....Extracellular Matrix

EDTA.....Ethylenediaminetetraacetic acid

ESI…….Electrospray Ionization

EtOH…….....……Ethanol

FDR…….....……False discovery rate

FPLC……Fast Performance Liquid Chromatography

GAG……Glycosaminoglycan

GFP……Green Fluorescent Protein

GPCR……..G Protein Coupled Receptor

HAC…….....…Acetic acid

HEK293……..Human Embryonic Kidney cells

His……...Histidine

HIV……..……..Human Immunodeficiency Virus

HPLC……...High Performance Liquid Chromatography

IMAC……..……Immobilized Metal Affinity Chromatography

L1.2 cells…….Mouse pre- B Lymphoma cells

LN_2.....Liquid Nitrogen

Lys……..Lysine

LTQ.....Linear Ion Trap

MALDI……...Matrix Assisted Laser Desorption Ionization

MMP.....Matrix metalloprotease

NaCl……..Sodium chloride

PBMC.....Peripheral blood mononuclear cell

PBS.....Phosphate Buffered Saline

PE.....Phycoerythrin

PFA.....Paraformaldehyde

Ptx.....Pertussis toxin

Ser……..Serine

SCID.....Severe combined immunodeficiency

SPR.....Surface Plasmon Resonance

Thr……Threonine

Ub.....Ubiquitin

Usp2cc.....Ubiquitinase

WT……....Wild-type

ACKNOWLEDGEMENTS

Chapter 1, in part, was published in *Biochemical Journal:* O'Hayre M, Salanga CL, Handel TM, Allen SJ, Chemokines and cancer: migration, intracellular signalling and intercellular communication in the microenvironment. *Biochem J.* 2008; *Cellular and Molecular Life Sciences:* Salanga CL, O'Hayre M, Handel T. Modulation of chemokine receptor activity through dimerization and crosstalk. *Cell Mol Life Sci.* 2009; and, *Expert Opinion in Drug Discovery*: O'Hayre M, Salanga CL, Handel TM, Hamel DJ. Emerging Concepts and Approaches for Chemokine-Receptor Drug Discovery. *Expert Opin.* 2010.

Chapter 2 is currently being prepared for the submission of publication of the material. The following are the contributing authors: Salanga CL, Gupta S, Chance MR, Handel TM. The dissertation author is the primary investigator and author of this paper.

Chapter 3 was published in *Methods in Enzymology*: O'Hayre M, Salanga CL, Dorrestein PC, Handel TM. Phosphoproteomics analysis of chemokine signaling networks. *Methods Enzymol*. **2009.** The dissertation author was a co-investigator and co-first author of this methods chapter.

Chapter 4 was published in *PLoS ONE*: O'Hayre M, Salanga CL, Kipps TJ, Messmer D, Dorrestein PC, Handel T. Elucidating the CXCL12/CXCR4 Signaling Network in Chronic Lymphocytic Leukemia through Phosphoproteomics Analysis. *PLoS ONE*. **2010.** The dissertation author was a co-investigator and co-author of this paper, substantially contributing to the mass spectrometry based portion of this investigation.

The dissertation author and Morgan O'Hayre equally contributed to the material presented in **Chapter 5**. Dr. Jing Yang also substantially contributed to this study by providing expertise, guidance, and technical assistance throughout the investigation.

This work was funded by a Ruth L. Kirschstein NIGMS MARC Predoctoral Fellowship (F31) to CLS and awards from NIAID (RO1-AI37113), DOD (BC060331), NIGMS (RO1-GM081763) and the Lymphoma Foundation to TMH.

I would like to thank the past and present members of the Handel Lab including, Samantha Allen, Arnab Chowdry, Andrew Douglas, Melinda Hanes, Damon Hamel, Ariane Jansma, Li Zhang, Taylor Gilliland, Lauren Holden, John Jones, Alex Le, Lina Mullen, Tetsuya Nawamura, Morgan O'Hayre, Ling Qin, Gloria Sanchez, Kevin Wang, and Chunxia Zhao, for providing such a pleasant work environment to come to everyday. Thank you also for providing me with the technical and/or emotional support during all the ups and downs of my graduate career, I am deeply grateful. I would also like to sincerely acknowledge Tracy Handel for all of her contributions to my personal growth as a scientist. Tracy, you have always been a constant source of support and enthusiasm, amid all the bad luck that I have brought to the table. I truly appreciate you always seeing the silver lining.

I also thank my wonderful family, especially my Mom, Dad, Matt, Ed, Rachel, the girls, and Tita Flor. I am grateful every day to have you all in my life.

Finally, I thank my loving husband, Anthony, and our loving dog, Shelby. Anthony, you are my rock, my best friend and an amazing husband. I immensely appreciate everything you have done to make this journey not quite as tough. I love you. Shelby, thank you for being the sweetest dog in the whole wide world and being a constant source of endorphins for me.

CURRICULUM VITAE

Education

PhD, Biochemistry
University of California, San Diego *San Diego, CA* 2004 – 2011
Handel Laboratory

Dissertation: Structural and Functional Analysis Chemokines with Glycosaminoglycans and Chemokine Receptors

- Characterization of MCP-3/CCL7: GAG Interactions Identified by Radiolytic Footprinting with Mass Spectrometry, Mutagenesis and Functional Analysis
    - Application of hydroxyl radical footprinting to identify potential GAG binding epitopes of the chemokine, MCP-3/CCL7
    - Ala mutagenesis and functional characterization of two novel and topographically varied GAG binding sites using heparin affinity chromatography, calcium flux, and migration assays
- Phosphoproteomic Analysis of CXCL12 signaling in Chronic Lymphocytic Leukemia cells (CLL)
    - Development of a mass spectrometry based phosphoproteomics strategy to study CXCL12 mediated signaling in CLL cells
    - Utilization of immobilized metal affinity chromatography phosphopeptide enrichment with reversed-phase liquid chromatography and tandem mass spectrometry for identifying potentially novel phosphorylation targets of CXCL12 mediated signaling
- Elucidating the Roles of CXCR4 and CXCR7 in Breast Cancer Growth and Metastasis
    - Generation of stable cell lines derived from the human breast cancer cell line (MDA-MB-231) expressing varying levels of CXCR4 and/or CXCR7
    - Use of a *in vivo* mouse tumor model to determine the effects of CXCR4 and/or CXCR7 in breast cancer tumor progression
    - *In vitro* biochemical and functional characterization of MDA lines with CXCR4 and/or CXCR7 by calcium flux, western blot, and internalization assays following ligand (CXCL12) stimulation

BS Chemistry
Northern Arizona University *Flagstaff, AZ* 2002 – 2004
(minor: Studio Art)

Fellowships and Awards

- Ruth L. Kirschstein Predoctoral Fellowship, *NIH* 2006 - 2011
- GAANN Fellowship, *UCSD* 2004 - 2006

Publications

1. **Salanga CL**, Gupta S, Chance M, Handel TM. Characterization of MCP-3/CCL7: GAG Interactions Identified by Radiolytic Footprinting with Mass Spectrometry, Mutagenesis and Functional Analysis. *In Preparation*
2. **Salanga CL,** Handel TM. Chemokine Oligomerization and Interactions with Receptors and Glycosaminoglycans: The Role of Structural Dynamics in Function. *Exp. Cell. Research*. 2011
3. O'Hayre M, **Salanga CL**, Handel TM, Hamel DJ. Emerging Concepts and Approaches for Chemokine-Receptor Drug Discovery. *Expert Opin.* 2010
4. O'Hayre M, **Salanga CL,** Kipps TJ, Messmer D, Dorrestein PC, Handel T. Elucidating the CXCL12/CXCR4 Signaling Network in Chronic Lymphocytic Leukemia through Phosphoprotemics Analysis. *PLoS ONE*. 2010
5. **Salanga CL**, O'Hayre M, Handel T. Modulation of chemokine receptor activity through dimerization and crosstalk. *Cell Mol Life Sci.* 2009
6. O'Hayre M, **Salanga CL**, Dorrestein PC, Handel TM. Phosphoproteomic analysis of chemokine signaling networks. *Methods Enzymol.* 2009
7. O'Hayre M, **Salanga CL**, Handel TM, Allen SJ, Chemokines and cancer: migration, intracellular signalling and intercellular communication in the microenvironment. *Biochem J.* 2008

ABSTRACT OF THE DISSERTATION

Structural and Functional Analysis of Chemokine Interactions with Glycosaminoglycans and Chemokine Receptors

by

Catherina L. Salanga

Doctor of Philosophy in Chemistry

University of California, San Diego, 2011

Tracy Handel, Chair

Alexander Hoffmann, Co-Chair

Chemokines are involved in cell migration and activation during routine immune surveillance, inflammation and even cancer metastasis. The migration of chemokine receptor-bearing cells, including leukocytes and tumor cells, occurs in response to the secretion of chemokines, which accumulate on cell surfaces through interaction with glycosaminoglycans (GAGs) where they effectively serve as traffic signals to guide cell

movement. Engagement of chemokines with their receptors subsequently causes the activation of signaling pathways that result in firm adhesion and extravasation of the cell into tissue, and in the case of leukocytes, activation of defense mechanisms. However, in cancer cells, the signaling pathways can be exploited or redirected, resulting in responses like survival, growth and proliferation. Herein, a structural and functional approach was used to address specific questions about the interactions of chemokines (i) with GAGs and (ii) with chemokine receptors in the context of cancer. Technically, the use of mass spectrometry has been a strong theme throughout these studies. In Chapter 2, a novel application of hydroxyl radical footprinting coupled with mass spectrometry was used to characterize the GAG binding specificity of the chemokine, MCP-3/CCL7. Potential GAG binding epitopes, identified by mass spectrometry, were then validated by mutagenesis and functional assays. In Chapter 3 and 4, a phosphoproteomic mass spectrometry strategy was used to elucidate CXCL12-mediated survival signaling through the receptor, CXCR4, in cells from patients with chronic lymphocytic leukemia (CLL). While signaling cascades involved in chemokine-mediated migration are well established, pathways involved in cell survival and proliferation in cancer, are not. Methods developed for phosphopeptide enrichment, and subsequent analysis via mass spectrometry are described in Chapter 3, and interesting/novel phosphoproteins, potentially involved in CXCL12-mediated CLL survival are described in Chapter 4. In Chapter 5, a functional approach was taken to elucidate the roles of receptors CXCR4 and CXCR7 in breast cancer growth and metastasis. The data show that CXCR7 affects the functional activity of CXCR4 *in vitro*, and decreases the extent of lung metastases *in vivo,* without inhibiting primary tumor growth. Overall, these studies serve to better understand some of the regulatory mechanisms that control chemokine function in normal physiology and in cancer.

CHAPTER 1

Introduction to the Chemokine Network

1.1 The Chemokine Network

Chemokines are small chemoattractant cytokines best known for their role in directing immune cell migration [1]. Upon secretion, chemokines accumulate in localized gradients by binding to cell surface carbohydrate structures and extracellular matrix components, and recruit receptor-bearing leukocytes to sites of inflammation (inflammatory/inducible chemokines) or to secondary lymphoid organs during routine immune surveillance (homeostatic/constitutive chemokines) (Figure 1.1) [2, 3]. Chemokines and their receptors are also involved in many developmental processes including central nervous system development, cardiogenesis, and lymphopoiesis. In addition to their normal physiological roles, aberrant expression and/or regulation of chemokines and their receptors is associated with a number of diseases including inflammatory diseases, atherosclerosis, cancer, and HIV [4].

Four major families of chemokines/chemokine receptors have been classified (CC, CXC, CX3C and XC) according to the pattern of cysteine residues in the ligands, which are small 70-120 amino acid proteins [5, 6]. To date, approximately 44 ligands and 22 receptors have been identified in humans alone [7] and it has been found that many chemokines bind multiple receptors and most receptors bind multiple chemokines

(Table 1.1) suggesting the possibility of functional redundancy. However, emerging evidence indicates specificity in many receptor:ligand interactions not only due to the ability of different ligands to induce different signals from a given receptor [8], termed functional selectivity [9], but also correlating with their spatial and temporal control [5]

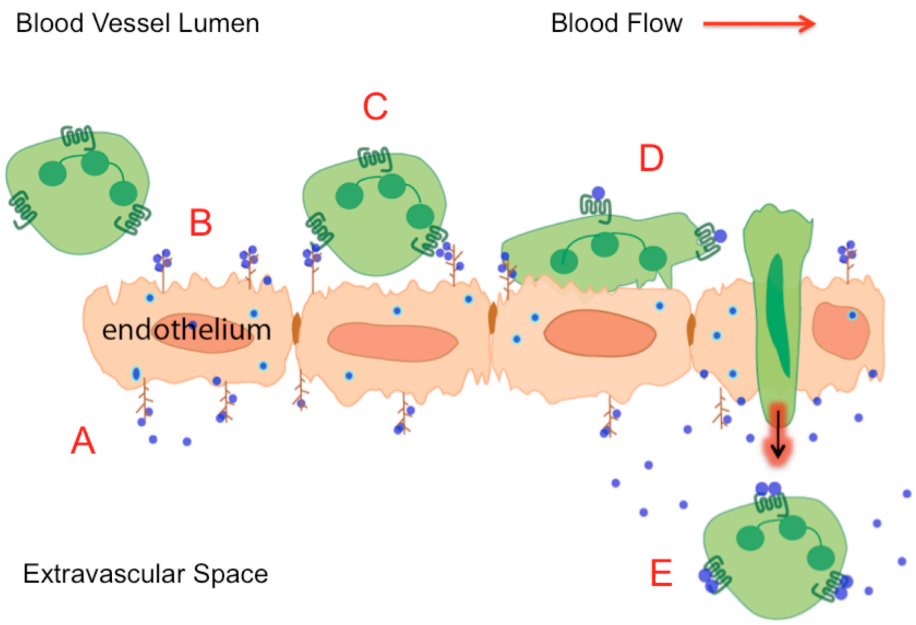

Figure 1.1 Cartoon depicting chemokine mediated migration. (A) Chemokines secreted into the extravascular space bind to GAGs and are transcytosed to the lumenal side of the endothelium where (B) they are presented on the endothelial surface to chemokine receptors on leukocytes in the blood. (C) Chemokines bind to receptors, in some cases causing leukocyte arrest and firm adhesion. (D) The monomeric forms of chemokines cause cell movement. (E) Following extravasation, oligomerized chemokines may provide stop signals and cellular activation. Adapted from [2].

Chemokine ligands

Despite low sequence homology, chemokines have a highly conserved tertiary structure consisting of a disordered N-terminal region, 3 anti-parallel β-sheets and a C-terminal α-helix (Figure 1.2). Chemokines are also known to form dimers and higher order oligomers [10]. Although it has been demonstrated that chemokines bind and signal through their receptors as monomers, at least in the context of migration, the ability of chemokines to dimerize is critical for *in vivo* function; this is thought to be due, at least in part, to the role of oligomeric forms of chemokines in binding to cell surface glycosaminoglycans (GAGs) which in turn facilitates the accumulation of chemokines to localized areas, allowing them to function as directional cues [11]. In support of this

hypothesis, it has been shown that oligomerization deficient and GAG-binding deficient chemokine variants result in impaired migration *in vivo* [11]. Further discussion of the occurrence of chemokine oligomerization and GAG interactions as well as the functional implications associated with these interactions is presented in Section 1.2.

Figure 1.2 Structure of a typical chemokine; shown here is the IL-8 monomer (PDB ID 1IL8) [12]. The N-terminal signaling domain is highlighted; this region of the ligand is postulated to insert into the helical bundle of the receptor, which are heptahelical G protein-coupled receptors (GPCRs).

Table 1.1 Chemokine receptor and chemokine ligand binding partners.

Receptor	Ligands
CCR1	CCL3, CCL5, CCL7, CCL13, CCL15, CCL16, CCL23
CCR2	CCL2, CCL7, CCL8, CCL13, CCL16
CCR3	CCL5, CCL7, CCL8, CCL11, CCL13, CCL15, CCL16, CCL24, CCL26, CCL28
CCR4	CCL17, CCL22
CCR5	CCL3, CCL4, CCL5, CCL8, CCL11, CCL14, CCL16
CCR6	CCL20
CCR7	CCL19, CCL21
CCR8	CCL1
CCR9	CCL25
CCR10	CCL27, CCL28
CXCR1	CXCL6, CXCL7, CXCL8
CXCR2	CXCL1, CXCL2, CXCL3, CXCL5, CXCL6, CXCL7, CXCL8
CXCR3-A	CXCL9, CXCL10, CXCL11
CXCR3-b	CXCL4, CXCL9, CXCL10, CXCL11
CXCR4	CXCL12
CXCR5	CXCL13
CXCR6	CXCL16
CXCR7	CXCL11, CXCL12
XCR1	XCL1, XCL2
CX_3CR1	CX3CL1
CCX-CKR	CCL19, CCL21, CCL25
D6	CCL2, CCL3, CCL4, CCL5, CCL7, CCL8, CCL11, CCL14, CCL17, CCL22
DARC	CCL2, CCL7, CCL8, CCL11, CCL13, CCL14, CCL16, CCL17, CXCL1, CXCL5, CXCL6, CXCL7, CXCL8, CXCL9, CXCL11, CXCL13

Chemokine receptors

Chemokine receptors are seven transmembrane G protein-coupled receptors (GPCRs). Receptor activation occurs when a chemokine agonist binds on the extracellular side of its receptor, and induces a conformational change of the receptor that promotes heterotrimeric G proteins activation on the intracellular face by exposing important motifs such as the DRY box (Figure 1.3). Upon activation of the heterotrimeric G proteins, the $G\alpha$ subunit exchanges GDP for GTP and dissociates from the receptor and from the $\beta\gamma$ subunits, and both G protein complexes go on to activate other downstream signaling events [8] that ultimately lead to a physiological response. Refraction to continued stimuli involves receptor desensitization and internalization by

agonist dependent phosphorylation of the C-terminal tail of the GPCR by GRKs (G protein receptor kinases). Receptor phosphorylation subsequently promotes binding of arrestins, which sterically block further interaction with G-proteins and mediate receptor internalization through clathrin-coated pits [13]. Endocytosis of a GPCR can lead to either lysosomal degradation or recycling back to the cell surface and re-sensitization. In addition to their involvement in internalization, β-arrestins can function as signal transducers by activating pathways such as Akt, PI3K, MAPK and NF-κB, which lead to a variety of cellular responses [14]. On the otherhand, some chemokine receptors, like CXCR7, the focus of Chapter 5, do not canonically couple to G protein; however, CXCR7 has been shown to associate and signal through β-arrestins [15].

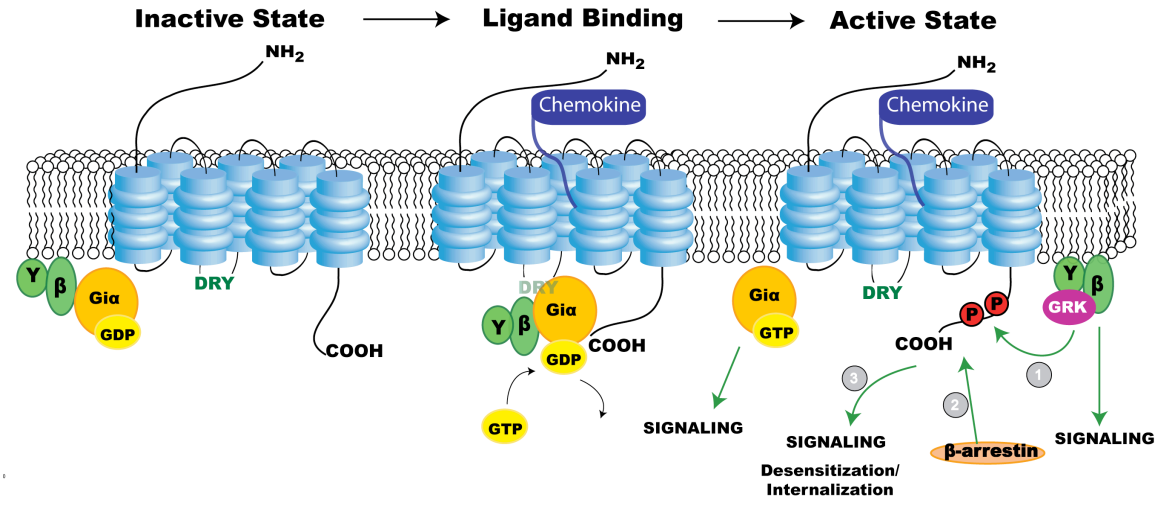

Figure 1.3 Molecular events in the classical activation of a chemokine receptor involving G proteins.

Complex interactions likely provide specificity in chemokine function

Classically, chemokine receptors and other GPCRs have been thought to function as monomers and have been studied as isolated systems to identify particular

pathways activated by a given ligand/receptor. While chemokines function as monomers in some contexts, they homo and hetero-oligomerize and oligomerization is thought to be important for other functions. As described in the next section, chemokines also interact with GAGs, and these interactions may influence localization, interaction with specific receptors, and possibly even signaling output. Further, although the receptors can activate G proteins as monomers [16-18], they are also known to homo- and heterodimerize, an aspect of chemokine receptor biology that is presented in more detail in Section 1.3. Receptors can also engage in direct and indirect crosstalk with other signaling receptors. Evidence for cooperative interactions between receptors and signaling pathways includes additivity, amplification, and synergy in responses [19-21], which are also described in Section 1.3. Another level of complexity/regulation of these signaling networks is the differential expression patterns of chemokines and their receptors that are both tissue specific and dependent on health status, thus allowing chemokine receptors to partner with ligands and activate downstream pathways in a cell- and pathology-dependent manner [5]. These combined complexities create the possibility of unprecedented diversity and multifactorial responses that cast doubt on the long-held belief that the chemokine system is redundant based on the observation that multiple ligands binding to a single receptor, and a single ligand can bind to multiple receptors (Table 1.1). These complex interactions may provide the basis for a high level of specificity dictated by the occurrence of various interactions (e.g. chemokine:chemokine, chemokine:GAG, chemokine:receptor, receptor:receptor) within the chemokine network. Of these, one of the least understood interactions are the chemokine:GAG interactions which are introduced in the next section and investigated in Chapter 2. Chemokine:receptor interactions in the context of CXCL12:CXCR4 signaling in diseased (chronic lymphocytic leukemia) and normal cells (B cells) are the subject of

Chapter 3 and 4. Receptor:receptor interactions either directly or through crosstalk are the subject of a study of CXCR4 and CXCR7 in breast cancer, which is described in Chapter 5.

1.2 Chemokine Oligomerization and GAG Binding Interactions

Despite relatively low sequence homology across the chemokine family, chemokines have remarkably conserved tertiary structures, illustrated by the monomeric structure of MCP-1/CCL2 depicted in Figure 1.2. However, the majority of chemokines have also been found to form oligomers (e.g. dimers, tetramers, and higher order oligomers), and in many instances, these complexes exhibit quite distinct and variable structures (Figure 1.4), which likely contribute to their function [2]. In addition, chemokines interact with glycosaminoglycans (GAGs), which are carbohydrates present on endothelial cells. GAG interactions are important for chemokine sequestration and presentation to receptors on migrating cells. In the absence of such interactions, chemokine gradients formed as directional cues for migrating cells would rapidly diffuse, especially under shear forces from blood flow. The importance of oligomerization and GAG interactions for the activity of certain chemokines has been clearly demonstrated, where GAG-binding deficient mutants and monomeric variants of several chemokines (MCP-1/CCL2, MIP-1β/CCL4 and RANTES/CCL5) were shown to maintain their ability to recruit leukocytes similar to wild-type (WT) *in vitro*, but exhibited a dramatic loss in the ability to recruit cells *in vivo* [22]. These findings and others, supporting the biological importance of chemokine oligomerization and chemokine:GAG interactions, have motivated investigations with a goal of understanding the specificity and molecular determinants involved in these interactions, and ultimately how these interactions

contribute to the biological activity of chemokines. However, at this point, there is still very limited understanding of the diversity of the GAG binding epitopes, the specificity of the interactions, and their functional role. In Chapter 2, studies involving the identification and characterization of GAG-binding motifs for the chemokine MCP-3/CCL7, and how these interactions affect its activity are presented. As a prelude to this chapter, the following sections will provide a more general overview of the structural biology and global implications that chemokine oligomerization and GAG binding can have on the specificity of chemokine interactions within the chemokine network, while more specific details relevant to the characterization of MCP-3/CCL7 and GAG binding interactions are contained in Chapter 2.

Chemokine oligomerization

Although some chemokines, like MCP-3/CCL7 and I-309/CCL11 are monomeric [23, 24], many chemokines form dimers and higher order oligomeric structures, based on NMR and crystallographic studies [12, 25-27]. In particular, two main dimer motifs have been observed among chemokines (Figure 1.4), which include the CC and CXC motifs, represented by dimer structures of MCP-1/CCL2 and IL-8/CXCL8, respectively, and depicted in Figure 1.4. The CC dimer motif has an elongated structure stabilized by a dimer interface involving residues from the largely unstructured N-terminus of each monomer, as illustrated by the MCP-1/CCL2 dimer in Figure 1.4 *B*. By comparison, the CXC dimer is much more compact and involves interactions between the first β-strand of each subunit, as shown for IL-8/CXCL8 in Figure 1.4 *C*. However, there are also chemokines that adopt completely different dimer structures that do not resemble the CC or CXC motifs described, such as Lymphotactin/XCL1, depicted in Figure 1.4 *D*. Finally, chemokines also form tetramers and higher order oligomers that can be quite variable in

structure. For example, the oligomeric structure of MIP-1α/CCL3 was recently solved, revealing a unique double helical polymer arrangement (Figure 1.4 *E* and *F*). While the importance of chemokine oligomerization for the chemotactic activity of certain chemokines has been established [22], the functional relevance of specific oligomeric species, and their contribution to chemokine biology remains to be determined. However, an emerging hypothesis, and the view of our laboratory, is that the structural plasticity of various chemokines may contribute to the specificity of GAG interactions and therefore localization [28, 29], thus providing an additional level of regulation for fine-tuning of the immune response beyond the pairing of ligand with receptor. It is also becoming apparent that different oligomeric forms may also represent "functionally selective ligands". "Functional selectivity" or "ligand bias" is an emerging concept in the GPCR field whereby different ligands of the same receptor have different functional effects; here we suggest the different oligomeric forms of the same ligand may also have different functional effects with respect to receptor signaling. While this is not a major focus of this thesis, GAG interactions may in some cases be responsible for the assembly or stability of different oligomeric forms.

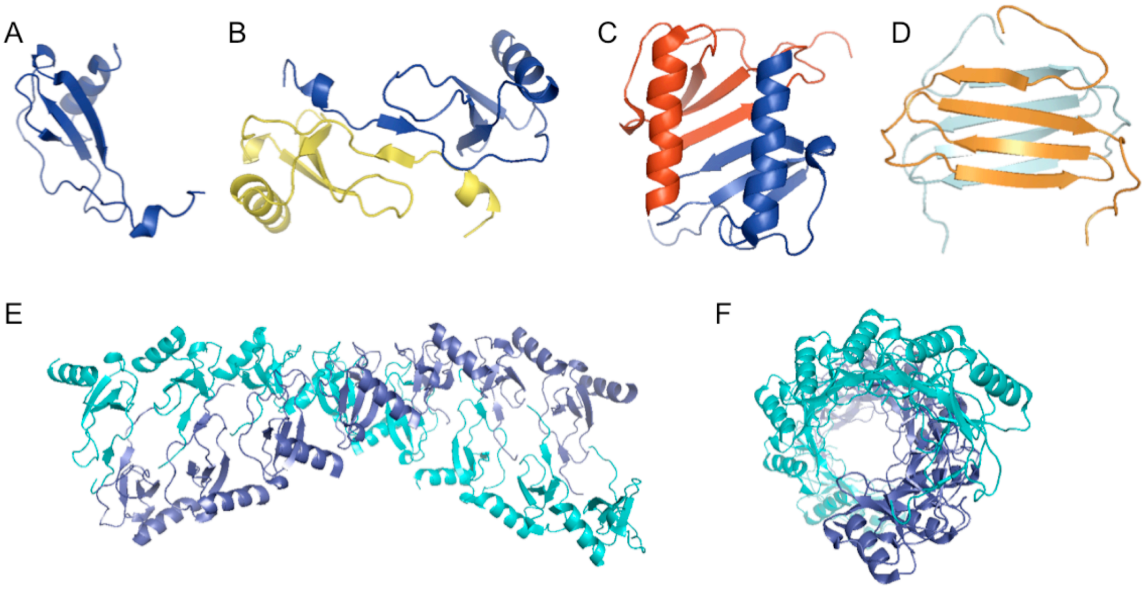

Figure 1.4 Various structures of chemokine monomers and higher order oligomers. (A) Monomeric and (B) dimeric structures of MCP-1/CCL2 (PDB ID IDOM) [30]. (C) Dimer Structure of IL-8/CXCL8 (PDB ID 1IL8) [12]. (D) Non-canonical dimer of lymphotactin/XCL1 (PDB ID 2JP1). This non-canonical structure predominates at high temperature and low ionic strength (40 °C, no salt) and binds to GAGs, whereas the canonical chemokine fold is stabilized by low temperature and high salt concentrations (10 °C, 200 mM NaCl), and binds the lymphotactin receptor [26]. (E and F) Polymeric form of MIP-1α/CCL3 from the side and down the helical axis (PDB ID 2X69) [27].

Chemokine:GAG interactions

GAGs are structurally heterogeneous linear polysaccharides that are typically tethered to the endothelial surface though a membrane bound protein core, forming proteoglycans [31]. There is exceptional diversity among GAGs resulting from the variable sulfation patterns and lengths of the GAG chains. GAGs have an overall negative charge from sulfation, which support interactions with chemokines that are mostly basic proteins. Several classes of GAGs are known including heparan sulfate, Heparin, chondroitin sulfate, dermatan sulfate, keratan sulfate, and hyaluronic acid [32]. Of these, heparan sulfate is the most ubiquitous and widely expressed of the GAG classes, representing 50 to 90% of all proteoglycans on endothelial cells [33]. However,

Heparin, the more easily obtained and less expensive GAG, is highly sulfated and soluble, and is the most commonly used GAG for chemokine interaction studies because of its similarity to heparan sulfate. Although structural differences between the two GAGs could be a potential drawback in these studies, the use of Heparin has led to the correct identification of several functional chemokine:GAG recognition sites [34-37] (see reviews [31, 32, 38] and refs therein) supporting its use *in vitro*. Interestingly, GAG binding epitopes of chemokines can be quite diverse, ranging from linear binding motifs comprised of basic residues to spatially distributed binding sites. While the composition and topological diversity of GAG recognition sites is reserved for discussion in Chapter 2, a brief description of GAG binding to MCP-1/CCL2 is presented here for illustrative purposes.

MCP-1/CCL2 has been well characterized in the context of its oligomeric properties as well as GAG binding interactions [35, 39, 40]. While a CC dimer structure was solved by solution NMR [40], a tetrameric structure of MCP-1/CCL2, solved by X-ray crystallography, is depicted in Figure 1.5 and possesses characteristics of both the CC and CXC dimer motifs. Extensive mutagenesis and functional analysis of MCP-1/CCL2, resulted in the identification of several key residues involved in GAG binding, The GAG binding epitopes, mapped onto the surface model of the MCP-1/CCL2 tetramer, encompass the tetramer in a band-like fashion and reveal a striking basic surface for binding of a highly sulfated linear GAG as shown in Figure 1.5. Indeed, chemokines are known to have higher affinity for longer 10-20mer GAGs compared to smaller GAG fragments [29].

Taken together, it is clear that GAG interactions, and in many cases, oligomerization, are integral to the function and activity of chemokines. Therefore,

elucidation of the molecular mechanisms guiding these interactions will be critical to understanding chemokine function.

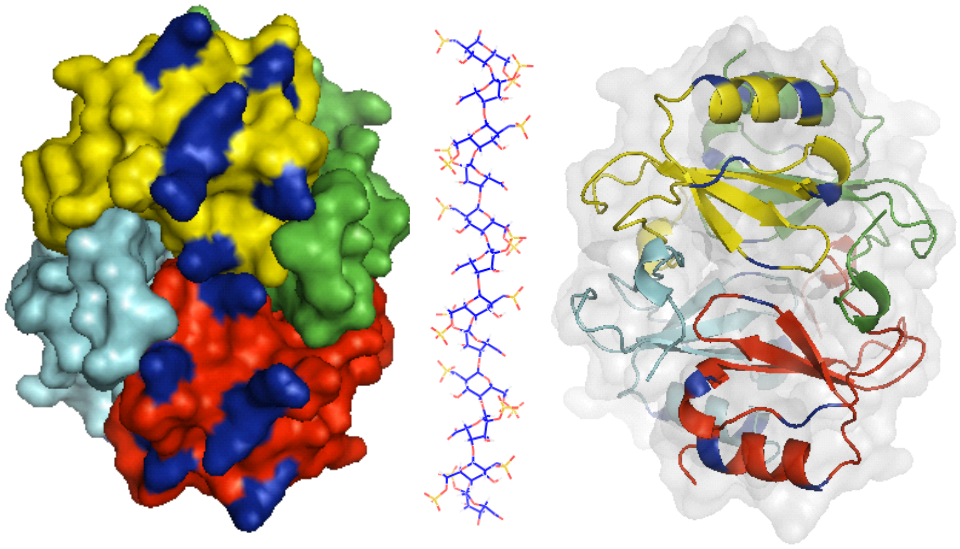

Figure 1.5 Surface model of the tetrameric structure of MCP-1/CCL2 with GAG binding sites highlighted in dark blue. The GAG, Heparin dodecasaccharide, is shown adjacent to the MCP-1/CCL2 tetramer and highlights the complementary structural relationship between the tetrameric complex and an elongated GAG. Adapted from [41].

1.3 Signaling in the Chemokine Network

While chemokines and their receptors are best known for their role in cellular migration, there are many other functions that can also be mediated by chemokine activity including development, survival, proliferation, and angiogenesis. In this context, Chapter 3 and 4 present efforts towards understanding the mechanisms underlying the CXCR4/CXCL12 mediated survival signaling in chronic lymphocytic leukemia (CLL) cells, a disease associated with the accumulation of CLL B cells. Interestingly, despite

high levels of CXCR4 in CLL cells, CLL B cells show little migration in response to CXCL12 compared to normal B cells [42]; instead, CXCL12:CXCR4 seem to be used for survival signaling in these cells. Moreover, using phosphoproteomics, we identified several novel downstream signaling targets of CXCL12, with potential implications in CLL survival. Therefore, in this section, a general overview of pathways involved in chemokine receptor signaling are described and illustrated in Figure 1.6, with a particular emphasis on pathways involved in migration, survival, and proliferation which are relevant to both normal processes as well as cancer.

Signaling in migration

Chemokines and their receptors control cell migration in many contexts: during development, normal patrol and inflammation involving leukocytes, angiogenesis to form new blood vessels from endothelial precursors in cancer, and cancer metastasis. One of the first events in cell migration involves cell polarization in response to a chemoattractant, whereby some receptors and signaling molecules localize toward the source of the chemoattractant, termed the leading edge, while other molecules localize at the trailing edge [43]. This process occurs via chemokine:receptor signaling through the class IB PI3Kγ, which activates Rac and subsequently PAK (p21-activated kinase) as depicted in Figure 1.6. Protrusion of the leading edge to move in the direction of the chemoattractant is mediated by actin polymerization and focal adhesions activated as chemokines bind to their receptors. Gαi-dependent signaling through PI3K and various protein tyrosine kinases induces the activation of Akt, Rac and Cdc42, which lead to downstream F-actin polymerization [44-46] (Figure 1.6). At the trailing edge, activation of ROCK (Rho-associated kinase) downstream of Rho is responsible for actomyosin contraction at the rear so the cell can progress forward [46, 47] (Figure 1.6). Calcium

release and PKC activation downstream of PLC can also play important roles in mediating adhesion events [48]. Activation of FAK, pyk2, and other tyrosine kinases are also important in this process (Figure 1.6). FAK activation is important in establishing focal adhesions and activating other molecules involved in cell movement, such as p130cas, crk and paxillin. Integrin receptors that interact with the ECM to mediate cell adhesion, and secreted proteases such as MMPs, can also be activated downstream of chemokine signaling.

Signaling in survival, growth, and proliferation in cancer

Chemokines, in normal function like development or in the context of cancer (discussed in Section 1.6), can activate a variety of survival and proliferation pathways. This is not surprising given that the two processes bear some resemblance. CXCL12 and its receptor CXCR4, which are very important in development as evidenced by embryonic lethal knockouts [49, 50] play a particularly prominent role in cancer, and have been identified in at least 23 different solid tumors, lymphomas and leukemias [51]. For example, it has been demonstrated that stimulation of numerous cancer cells with CXCL12 (and other homeostatic chemokines) activates the PI3K/Akt pathway [52-57], which is well known to promote survival effects [58]. Although not all chemokines that promote Akt activation enhance the survival of cells, many do, and this pathway seems to be exploited by a variety of cancer cells [59-61].

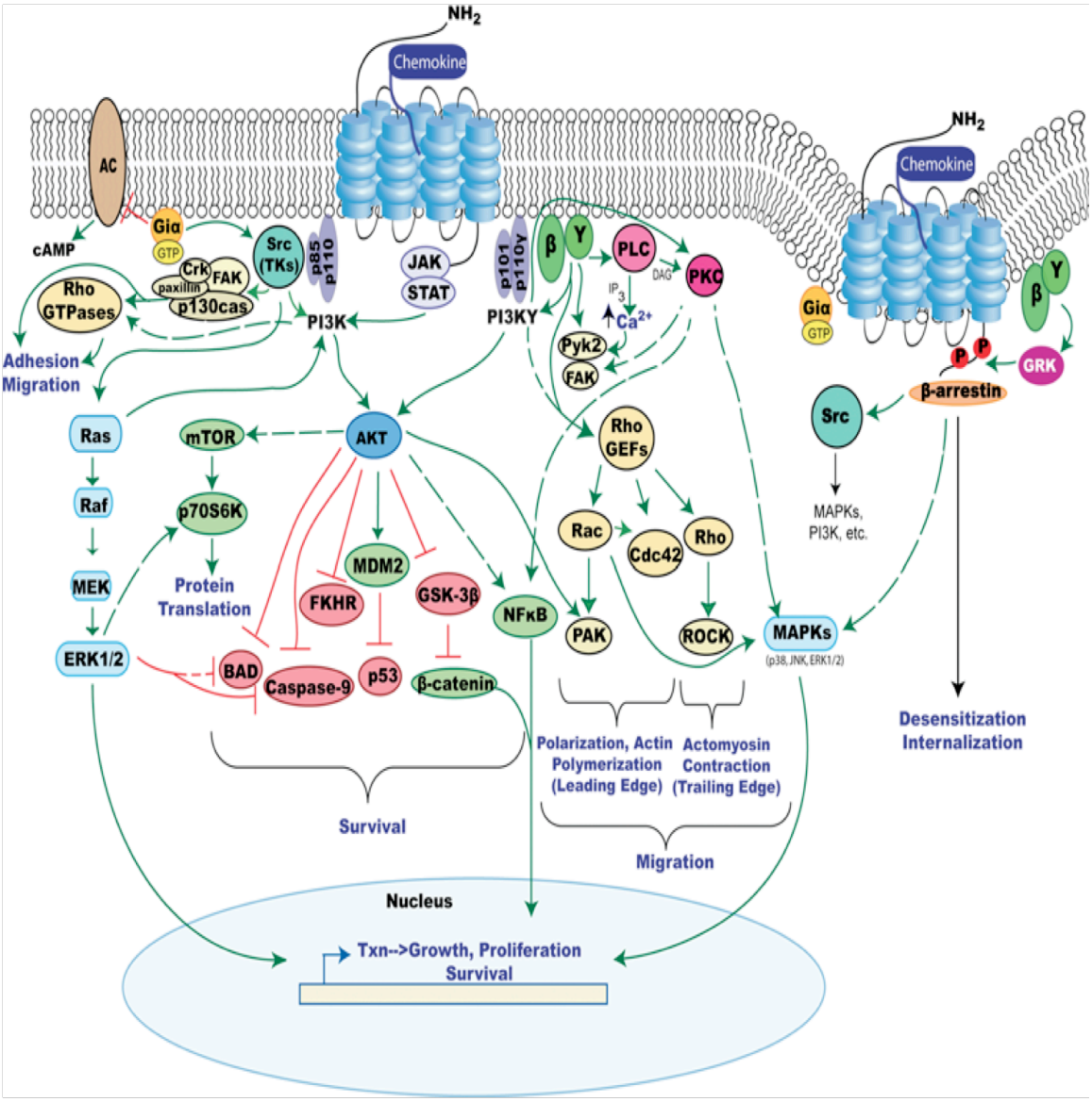

Figure 1.6 Chemokine receptor signaling in migration and survival/proliferation.

Numerous downstream effectors and transcription factors of Akt, ERK1/2, and tyrosine kinase signaling can also promote cell survival and proliferation (Figure 1.6). Chemokine signaling often activates NF-κB, which is commonly downstream of Akt, although it can be activated through other pathways, such as PKC [62]. NF-κB dimerizes and translocates to the nucleus on activation, where it promotes transcription of various

apoptosis inhibitors and cell-cycle-promoting genes [63]. Other downstream targets of Akt include procaspase-9 and the pro-apoptotic Bcl-2 family member, BAD, both of which are inhibited upon phosphorylation (Figure 1.6). The FKHR family of transcription factors, which induce transcription of numerous apoptotic genes, are also inhibited by Akt [48]. Akt-induced activation of Mdm2/Hdm2, leading to p53 degradation and inhibition of GSK-3β, leading to stabilization of β-catenin, also results in downstream inhibition of negative regulators of cell cycle and activation of cell cycle promoting genes (Figure 1.6) [64]. Furthermore, via inhibition of TSC2, Akt leads to mTOR activation, resulting in activation of p70S6K and thus enhanced protein translation of numerous cell growth regulators [58, 65]. ERK1/2 signaling may also contribute to survival through some of these pathways, for example via phosphorylation and inhibition of procaspase-9 and BAD (Figure 1.6) [66]. Furthermore, ERK1/2 can itself localize to the nucleus and activate transcription factors involved in cell-cycle regulation and differentiation, thereby promoting cell proliferation [67]. Other MAPKs, including JNK, have also been implicated in chemokine-induced proliferation [68]. Thus chemokine receptor signaling, resulting in activation of transcription factors involved in anti-apoptotic mechanisms, cell cycle regulation, and growth factor production, are yet other mechanisms whereby cancer cells exploit downstream chemokine signaling pathways. These pro-tumorigenic pathways are likely to be particularly important for the ability of metastatic tumor cells to thrive in foreign environments. Taken together, the pathways presented in this section are especially important in the context of Chapters 3, 4, and 5, which are generally aimed at understanding the role of CXCR4 in mediating survival, growth/proliferation, and metastasis/migration of cancer cells.

1.4 Chemokine Receptor Oligomerization and Crosstalk

Overview of chemokine receptor homo- and heterodimerization

Accumulating evidence indicates that many GPCRs, including chemokine receptors, can form dimers or higher order oligomers. While it has been shown that the β2-adrenergic receptor and rhodopsin can function as monomers with respect to G protein coupling, it has been suggested that dimers represent the basic functional unit of GPCRs [16-18, 69-73]. However, the functional relevance of GPCR oligomerization on GPCR activity is poorly understood, with dimerization of the GABA receptors having the only unambiguous role [69-75]. Receptor homo- and heterodimerization can have far reaching implications with respect to agonist-induced activation and antagonist-induced inhibition, G protein coupling and signaling, and internalization and desensitization of GPCRs. Therefore, it is critical to understand this aspect of GPCRs, especially considering that GPCRs constitute a major target in pharmaceutical industry yet antagonists/agonists could exhibit significantly different consequences in the context of homo- and hetero-dimerization of their target receptors, possibly through mechanisms such as those described in Figure 1.7 [76].

Currently, the strongest evidence for the functional importance of GPCR dimerization involves GPCR biosynthesis and export from the endoplasmic reticulum (ER) to the cell surface. Although there is some debate on how GPCR dimers and higher order oligomers are formed, it is generally thought to occur prior to translocation from the ER to the cell surface [73]. It has been suggested that in some cases, dimer formation stabilizes GPCRs which in turn enables proper exportation from the biosynthetic machinery to the plasma membrane. One classic example of functionally

dependent dimer formation involves the class C gamma-aminobutyric acid $(GABA)_B$ receptor. $GABA_B$-R1 requires dimerization with $GABA_B$-R2 in the ER to help deliver it to the cell surface [74, 75]. Although $GABA_B$-R2 can be properly translocated to the plasma membrane independent of $GABA_B$-R1 binding, it is not functional unless paired with $GABA_B$-R1.

Of the ~ 20 chemokine receptors currently identified, nearly half have been reported to associate with another chemokine receptor, either through homo- or heterodimerization. The chemokine receptor homodimers that have been identified so far include CXCR1, CXCR2, CXCR4, CXCR7, CCR2, CCR5, and DARC [77]. In addition to forming homodimers, several chemokine receptors can physically associate with different chemokine receptors to form heterodimers. In some instances, high sequence homology between receptors is thought to be a good indicator of the propensity for heterodimer formation. However, heterodimers can also form between chemokine receptors with lower sequence identify, and across the CC and CXC subclasses. For instance, although CXCR4 and CCR2 share only 34% sequence identity, they have been shown to form constitutive heterodimers by BRET analysis using HEK293T cells coexpressing both receptors [78, 79]. Below, we present a few examples of chemokine receptor homo- and hetero-oligomerization to highlight the effects that oligomerization can have on modulating chemokine receptor activity, which are also depicted in Figure 1.7.

The identification of the CCR5Δ32 allelic truncation variant present in a small population of HIV-1 resistant individuals [80-82] first shed light on the biological impact that chemokine receptor oligomerization can have on disease phenotype. In homozygous CCR5Δ32 individuals, resistance is conferred by the inability of the mutant receptor to reach the cell surface and facilitate HIV entry as a result of its retention in the

ER. Furthermore, heterozygous CCR5Δ32 individuals are partially protected and progress more slowly to AIDS when infected [83, 84], despite the fact that they produce WT CCR5, an observation which is thought to be due to ER retention of WT CCR5 through dimerization with CCR5Δ32 [85]. In the case of WHIM (Warts, Hypogammaglobulinemia, Infections, and Myelokathexis) syndrome, oligomerization is also thought to result in aberrant function of the WT CXCR4 receptor. WHIM syndrome is a rare genetic immunodeficiency disorder that results in the expression of C-terminal truncation mutants of CXCR4. These receptors show enhanced signaling responses to CXCL12 as a consequence of their reduced ability to undergo ligand-mediated receptor desensitization and internalization [86, 87]. As WHIM syndrome is primarily a heterozygous disease, constitutive heterodimerization of WT and mutant CXCR4 has been proposed as a mechanism by which WHIM CXCR4 can retain WT CXCR4 on the cell surface, leading to similarly enhanced CXCL12-induced responses [87, 88] (Figure 1.7 *C*). Finally, in support of the suggestion that the dimer represents the basic functional unit of GPCRs, the structure of CXCR4 was recently solved and revealed a homodimer in all five crystals solved [89]. Figure 1.8 shows the dimer structure of CXCR4, which is highlighted based on its electrostatic potential to emphasize the complementary nature of the large acidic binding pocket of the receptor, to binding of CXCL12, which like most chemokines, is highly basic in nature.

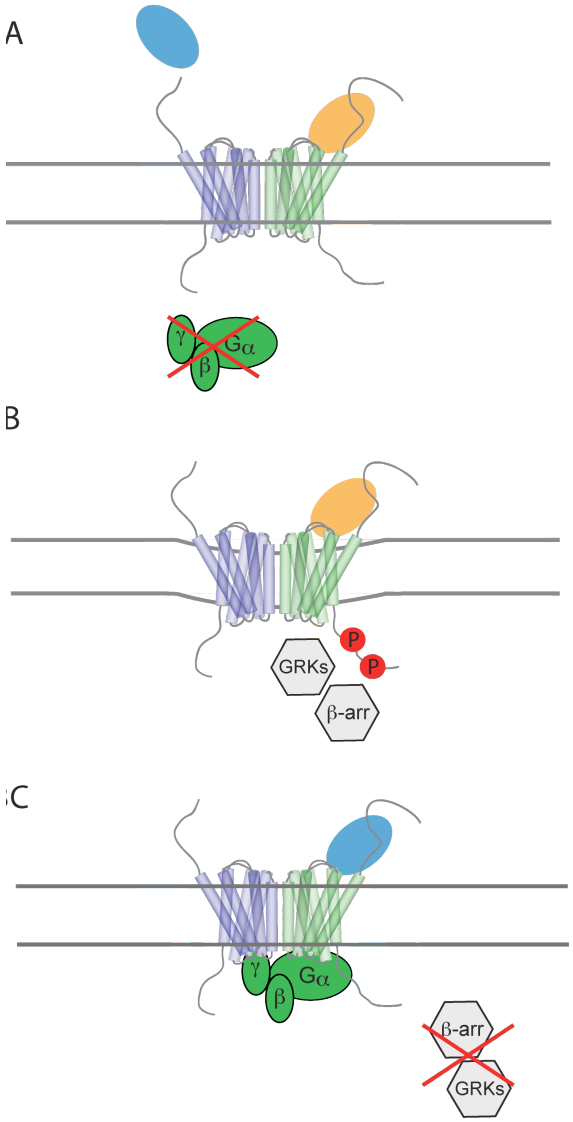

Figure 1.7 Potential effects of hetero-oligomerization on chemokine receptor signaling responses. (A) Binding of a ligand specific for one receptor in a heterodimer could prevent the binding of ligands to the other receptor and/or alter its ability to interact with/signal through intracellular modulators, such as G-proteins. (B) Another potential effect of hetero-oligomerization or receptor cross-desensitization is the downmodulation of one receptor through the ligand selective for another receptor as represented in Panel B. (C) Alternatively, hetero-oligomerization could prevent desensitization and internalization of a ligand activated receptor shown in Panel C, as described for CXCR4 in WHIM syndrome.

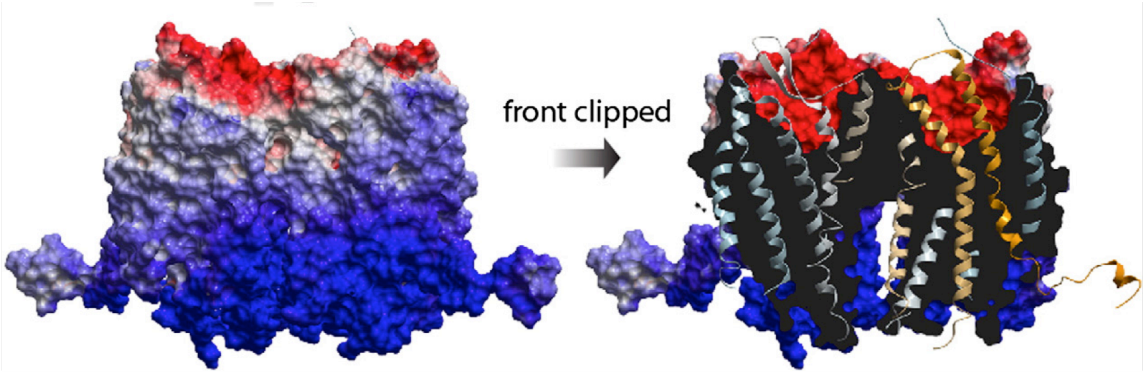

Figure 1.8 Structure of the CXCR4 dimer colored according to the electrostatic potential from red (negative) to blue (positive), in order to highlight the charge complimentarity of these proteins. On the left, the CXCR4 structure is shown from the side of the dimer; the right shows the structure of the CXCR4 dimer, clipped, in order to illustrate the binding pocket. Figure adapted from [2].

A specific example relevant to my thesis work: CXCR4 and CXCR7 heterodimerization

In addition to effects on receptor trafficking as the above examples illustrate, heterodimerization can influence ligand-mediated signaling responses of the involved receptors by affecting ligand binding, G protein coupling or association with other signaling modulators. The topic of CXCR4 and CXCR7 heterodimerization is particularly relevant to the work presented in Chapter 5, which examines the role of coexpression of the chemokine receptors CXCR4 and CXCR7, and their mutual effect on promoting breast cancer tumor growth and metastasis. Since the discovery of the novel chemokine receptor, CXCR7 in 2006 [90], and the finding that CXCL12 is a high affinity ligand for both CXCR4 and CXCR7, several groups have demonstrated that these receptors can form constitutive heterodimers [91-93]. The functional role of the CXCR4:CXCR7 heterodimer is particularly interesting as both receptors are linked to a number of cancers, although little is known regarding how heterodimerization modulates the ligand mediated activity of each receptor in the hetero complex compared to their function alone. In addition to CXCL12, CXCR7 also has a second ligand, CXCL11, though

neither triggers Gαi mediated signaling of CXCR7, which has been attributed to its lack of the classic "DRYLAIV" motif important for G protein coupling [92, 94]. However, Zabel *et al.* and others [95, 96] have shown that despite this lack of Gαi coupling, stimulation by CXCL11 or CXCL12 readily induces association with β-arrestin2, suggesting unique signaling properties of this receptor. Further, they recently probed the role of CXCR7 in tumor cell transendothelial migration (TEM) of CXCR4+/CXCR7+ expressing NC-37 cells using the CXCR7 specific small molecule antagonist, CCX771, as well as its natural protein ligand, CXCL11 [97]. Interestingly, CXCR7 was critical for CXCL12-mediated CXCR4 TEM of these tumor cells, though it did not impact *in vitro* bare filter cell migration. Furthermore, CXCR4-dependent TEM of these cells was potently antagonized by the CXCR7 ligands CCX771 and CXCL11. Notably, CCX771 does not alter the binding affinity of CXCL12 for CXCR4. Nevertheless, it is approximately 20-fold more potent at inhibiting CXCL12-mediated TEM compared to Mozobil, a direct and specific CXCR4 small molecule antagonist. Surprisingly, the antagonist, CCX771, also triggers β-arrestin2 association and with greater potency than CXCL12 [97]. Together these results show several mechanisms by which ligand engagement of CXCR7 is transmitted into the functional regulation of CXCR4, a finding that has important implications for the effectiveness of drugs targeted against the individual receptors. This effect is further supported by findings presented in Chapter 5, suggesting that the coexpression of CXCR7 on CXCR4+ breast cancer cells decreases the extent of CXCR4 mediated breast cancer metastasis in a mouse tumor model. These findings could be explained by receptor heterodimerization and subsequent transinhibition, although the mechanism is still not entirely clear.

There is emerging evidence that chemokine receptors can exist not only as homo- and hetero- dimers, but also as higher order oligomeric complexes [98]. Building

on earlier findings that CCR2, CCR5, and CXCR4 form functional (homodimers) and heterodimers [99-103], Sohy *et al.* recently demonstrated the presence of CCR2, CCR5, and CXCR4 hetero-oligomeric complexes recombinantly expressed in HEK293 cells, through a combination of luciferase complementation and bioluminescence resonance energy transfer (BRET) assays. Importantly, they also found these hetero-complexes endogenously expressed in primary leukocytes through radioligand binding competition assays using receptor-specific chemokines, blocking antibodies, and small molecule antagonists [98]. Furthermore, addition of CCR2, CCR5, or CXCR4 receptor specific antagonists (e.g. TAK-779 and Mozobil) in cells expressing all three receptors resulted in transinhibition of chemokine binding to the other receptors in the oligomeric complex demonstrating their functional interaction in leukocytes. As for CXCR4:CXCR7 oligomers, this example further illustrates that it is important to consider that an antagonist directed at one receptor can potentially inhibit the function of other receptors in the same cell. Depending on the biological context, transinhibition could prove to be beneficial (e.g. by inhibiting the function of other receptors expressed in an inflammatory setting) or alternatively, transinhibition could lead to unfavorable effects with unwanted inhibition of other receptors in the complex that are needed to support normal tissue function. In addition to chemokine receptors oligomerizing among themselves, there are also examples of chemokine receptors oligomerizing with non-chemokine receptors such as the T cell receptor, opioid receptors (delta and kappa) and glycoproteins (e.g. CD26, CD4), or chemokine receptor crosstalk with other signaling molecules [104], which is discussed below.

Chemokine receptor crosstalk and synergy

Given the vast array of extracellular signaling molecules and target receptors, the

potential for interactions between different networks, whether it is to amplify, inhibit, or alter a response, is significant. Nevertheless, there is a high degree of selectivity in crosstalk events, not only in terms of which receptors or signals may interact, but also in terms of cell-type specificity in the occurrence and degree of certain crosstalk events. The protein composition of different cell types is also not the same; they have varying levels of G proteins, cytosolic tyrosine kinases, and other similar signaling molecules may dramatically affect crosstalk interactions and functional response.

Above, the occurrence of homo- and heterodimerization interactions between different chemokine receptors, as well as some of the functional consequences of such interactions, was described. Yet, chemokine receptors not only dimerize with each other, but can also heterodimerize with other types of GPCR and non-GPCR receptors [72, 105]. Receptor heterodimerization and indirect mechanisms of receptor crosstalk confer another level of complexity in the signaling network and diversify the functional effects of chemokines. For example, receptor transinhibition and trans- activation are two commonly encountered crosstalk mechanisms that can occur from physical association and may alter ligand binding, signaling and internalization of the receptors involved. So, although the occurrence of receptor crosstalk has long been established [20, 106], the importance and consequences of crosstalk for chemokine receptor signaling and function is only now becoming more appreciated both in the context of normal cellular function and in disease.

Receptor crosstalk refers to the ability of a particular receptor to influence the signaling and function on another receptor. Different mechanisms of crosstalk are summarized in Figure 1.9 and include the following: (A) Physical association between receptors (oligomerization); (B) activation of cytosolic tyrosine kinases that trans-activate/inhibit signaling of other receptors; (C) induction of ligand levels via

transcriptional regulation, post-transcriptional (e.g. mRNA stability) regulation, or metalloprotease cleavage of tethered ligand; (D) Localization of receptors in specific membrane microdomains (e.g. lipid rafts); (E) Amplification of downstream signaling molecules (e.g. calcium flux).

Chemokine receptor crosstalk can influence the response a cell has to receptor agonists including the amplitude and duration of the signaling, rates of desensitization of receptors, and receptor trafficking [59]. Appreciating the mechanisms and consequences of such crosstalk may help in understanding many nuances in cellular signaling and could prove to be especially important in the context of pharmaceutical development. For example, CXCR4 is largely involved in development, tumor metastasis and also functions as an HIV co-receptor making it a major focus of many chemokine receptor structure-function studies and as a target for therapeutic intervention. In addition to forming homo- and heterodimers with chemokine receptors (e.g. heterodimerization with CXCR7, as discussed above), CXCR4 is also capable of forming dimers with a number of non-chemokine receptors. For example, CXCR4 has been reported to associate with CD26 [107], CD4 [108, 109], the T cell receptor (TCR) [110], the κ-opioid receptor [111] and the δ-opioid receptor (DOR) [112]. In the case of T cells, CXCL12-mediated CXCR4 signaling resulted in prolonged activation of ERK [113, 114]. At the time, the specific mechanism for prolonged ERK activation was unknown; however, it was later shown that CXCL12 triggers heterodimer association between CXCR4 and the TCR on the cell surface of T cells. Kumar *et al.* [110] identified a novel mechanism for CXCL12-induced activation of CXCR4 on T cells, involving ZAP-70, a tyrosine kinase, as well as the immunoreceptor tyrosine-based activation motif (ITAM) domains present on the TCRs. In T cells, ITAM domains of TCRs are phosphorylated when strong agonists bind, causing subsequent recruitment of ZAP-70 that, upon

activation, can trigger downstream signaling cascades. In the case of CXCR4, CXCL12 stimulation is sufficient to cause dimerization, phosphorylation of the ITAM domains and signaling through ZAP-70. Together, these events cause prolonged ERK signaling as well as increased calcium release and enhanced AP-1 transcriptional activity, providing a novel mechanism in CXCR4 signaling.

Recently, CXCR4 was also found to heterodimerize with DOR [112]. In addition to their roles in analgesia and mood, opioid receptors are involved in general immune function. Coexpression of CXCR4 and DOR in MM-1 monocytic cells resulted in inhibition of activation upon simultaneous addition of agonists (CXCL12 and [D-Pen2, D-Pen5] Enkephalin) despite the ligand-binding competency of the coexpressed receptors. Interestingly, the CXCR4/DOR heterodimer was stabilized in its inactive state and was blocked from desensitization. In addition to CXCR4, CCR5 has been shown to interact with the μ-, κ-, and δ-opioid receptors [115-117]. These crosstalk interactions affect ligand-induced receptor signaling by heterologous desensitization of either receptor [115-117]. The ability of chemokine receptors to associate with receptors outside of their own family is a testament to the complicated role that they play in immune trafficking and regulation and is an important consideration to keep in mind when evaluating chemokine mediated signaling of chemokine receptors in various cell types and contexts.

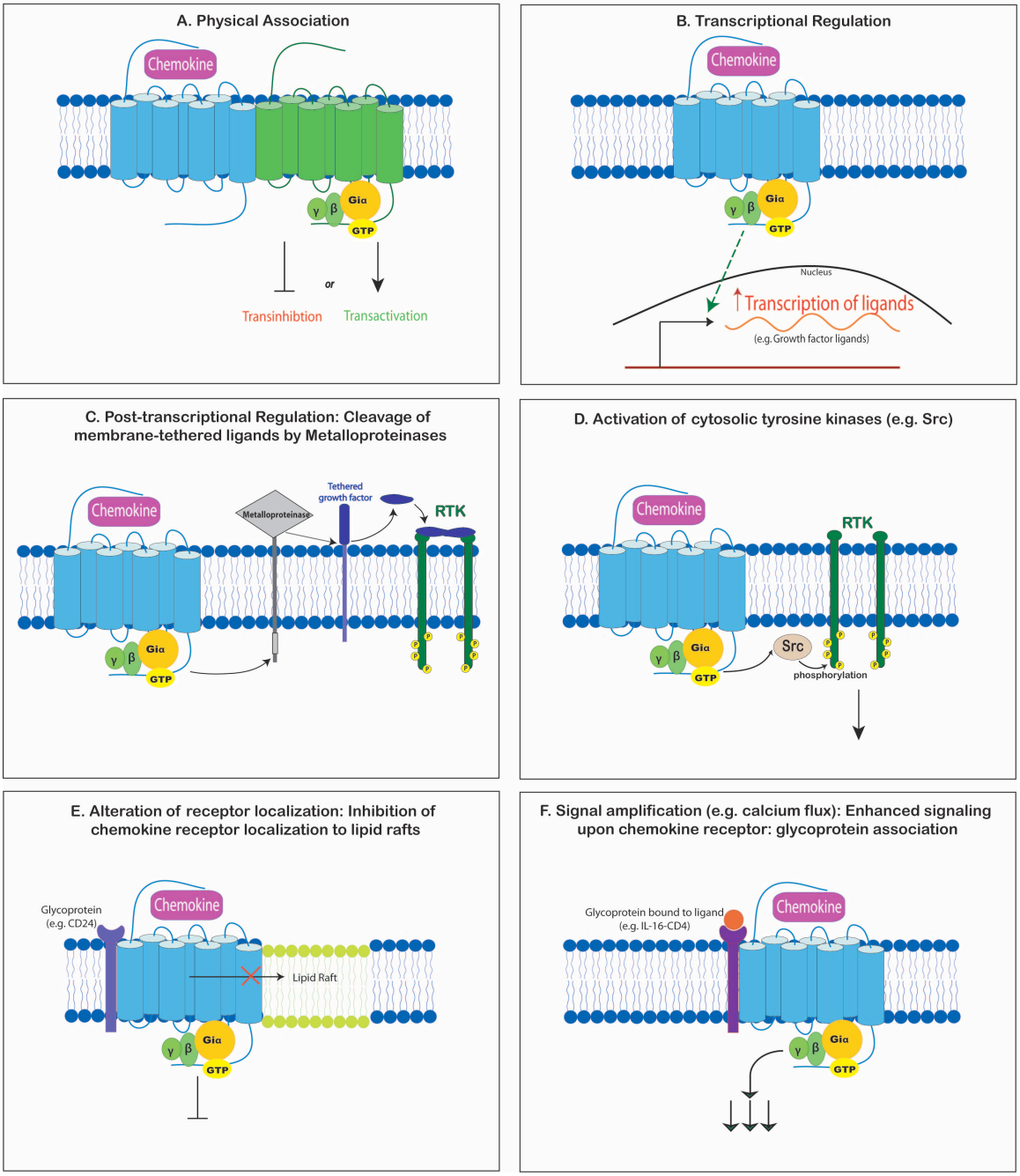

Figure 1.9 Potential mechanisms of chemokine receptor crosstalk. (A) Physical association (e.g. oligomerization); (B) Transcriptional regulation of ligands; (C) Post-transcriptional regulation of ligand levels; (D) Transactivation of receptors via activation of cytosolic tyrosine kinase signaling; (E) Trafficking of receptors to/away from signaling microdomains of the plasma membrane; (F) Downstream signaling amplification (synergy).

1.5 Chemokines and Chemokine Receptors in Disease

Aberrant chemokine/receptor expression or regulation is linked to many diseases, especially those characterized by an excessive cellular infiltrate, such as rheumatoid arthritis and other inflammatory disorders. As alluded to above, there is now overwhelming evidence that chemokines and chemokine receptors are also involved in the progression of cancer, where they function in several capacities [118]. First, specific chemokine/receptor pairs are involved in tumor metastasis. This is not surprising, in view of their role as chemoattractants in cell migration. Secondly, chemokines help to shape the tumor microenvironment, often in favor of tumor growth and metastasis, by recruitment of leucocytes and activation of pro-inflammatory mediators. Emerging evidence suggests that chemokine receptor signaling also contributes to survival and proliferation, which may be particularly important for metastasized cells to adapt to foreign environments. However, there is considerable diversity and complexity in the chemokine network, both at the chemokine/receptor level and in the downstream signaling pathways they couple into, which may be key to a better understanding of how and why particular chemokines contribute to inflammatory disorders, and in some cases, cancer growth and metastasis. In particular, the functional role of the chemokine receptors, CXCR4 and CXCR7, in breast cancer growth and metastasis forms the basis for work presented in Chapter 5 of this dissertation, and provides one example of attempting to delineate the respective roles of specific chemokines and chemokine receptors in disease. Here, a more generalized overview of chemokines and disease will be provided, with an emphasis on cancer, while details of chemokines and their receptors, presented in other chapters, which may have specific disease implications, will be described therein.

Table 1.2 outlines various chemokine/chemokine receptors which are implicated in numerous pathologies including inflammation, autoimmune disease, as well as transplant rejection and cancer, although the exact mechanisms of action are not necessarily well understood for all of the disease listed. One important link between cancer and inflammation is the recruitment of cells, including neutrophils, macrophages, dendritic cells, eosinophils, mast cells, and lymphocytes. Of these, tumor associated macrophages (TAMs) represent an important component of solid tumors and may account for up to half of the tumor mass [53]. TAMS were first observed in tumors in the late 1970s and therefore represent one of the first specific links between the immune system and cancer.

In the last few years, the involvement of chemokines and their receptors in cancer, particularly metastasis, has been firmly established [118-120]. Metastasis is not a random process of cell migration, and, in fact, has many features in common with normal cell migration. However, key differences exist between metastasis and normal migration, and include abnormal chemokine receptor expression, regulation or utilization, often on cells that typically do not migrate. Chemokines provide a physical address for the secondary destination of the tumor cells. The process by which tumors grow and metastasize is complex [121], with many steps required for primary tumor development and establishment of clinically significant secondary tumors as illustrated in Figure 1.10. These steps include: (i) survival and growth of the primary tumor, (ii) detachment of tumor cells from the primary lesion, (iii) invasion into vascular or lymphatic vessels (iv) homing and adherence to the destination organs, and (v) survival, growth, and ‘organogenesis’ of the metastasized cells in their new environment [120, 123].

Table 1.2. Chemokines and their receptors involved in disease. Adapted from [122].

Disease	Chemokine(s)	Chemokine receptor(s)
Acute Inflammation		
Myocardial infarction stroke	CXCL1, CXCL2, CXCL8	CXCR1, CXCR2
Ischemia-reperfusion	CCL2	CCR2
Autoimmune		
Atherosclerosis	CCL2, CCL3, CCL5, CX3CL1, CXCL9, CXCL10, CXCL11	CCR1, CCR2, CCR5, CX3CR1, CXCR3
Multiple sclerosis	CCL2, CCL3, CCL4, CCL5, CXCL9, CXCL10, CCL21	CCR1, CCR2, CCR5, CXCR3, CCR7
Rheumatoid arthritis	CCL2, CCL3, CCL4, CCL5, CXCL9, CXCL10, CXCL12, CXCL1, CXCL5, CXCL8	CCR1, CCR2, CCR5, CXCR3, CXCR4, CXCR1, CXCR2
Psoriasis	CCL4, CCL20, CCL27, CXCL9, CXCL10, CXCL1, CXCL2, CXCL8	CCR5, CCR6, CCR10, CXCR3, CXCR2
Type I diabetes	CXCL9, CXCL10, CCL22	CXCR3, CCR4
Crohn's	CCL25	CCR9
Chronic hepatitis	CCL3, CCL4, CXCL9, CXCL10	CCR5, CXCR3
Lupus	CXCL9, CXCL10, CXCL11, CXCL13	CXCR3, CXCR5
Transplantation		
Allograft	CCL3, CCL4, CCL5	CCR5
	CXCL9, CXCL10	CXCR3
Allergic Inflammation		
Asthma	CCL17, CCL22, CCL1, CCL11, CCL26, CXCL10	CCR4, CCR8, CXCR3
Atopic dermatitis	CCL1, CCL13, CCL17, CCL18, CCL27	CCR4, CCR8, CCR10
Cancer		
Growth	CXCL12	CXCR4, CXCR7
Metastasis:	CCL19, CCL21, CXCL12	CCR7, CXCR4
Lymph node	CXCL9, CXCL10, CXCL11	CXCR3
Gut	CCL25	CCR9
Skin	CCL17, CCL28	CCR4, CCR10
HIV		
R5-tropic	CCL3, CCL4, CCL5	CCR5
X4-tropic	CXCL12	CXCR4

Since alternative environments such as bone marrow and lymph node are not naturally compatible with cells from the breast, for example, cancer cells must both derive and provide signals to favorably shape the tumor microenvironment to become conducive to

survival and growth [55, 124, 125]. The role of chemokines and their receptors in cancer can thus be divided into three broad categories which contribute to one or more of the above processes: (i) providing directional cues for migration/metastasis, (ii) shaping the tumor microenvironment, and (iii) providing survival and/or growth signals.

The well-established properties of chemokines in controlling cell migration have made them clear candidates for involvement in cancer-cell metastasis and inflammatory or autoimmune diseases associated with excessive cellular infiltrate. However, the contribution of chemokines to other aspects of disease, such as growth, proliferation, angiogenesis, and cell survival are also becoming areas of extensive investigation. For example, the focus of Chapters 3 and 4 is aimed at elucidating CXCL12 mediated signaling of CXCR4 in CLL patient cells, with a particular interest in identifying signaling pathways that are potentially involved in the survival or apoptotic resistance of CLL cells. Deciphering signaling pathways activated by chemokines in various cancer cells or other infiltrating cell types will be critical to understanding how chemokines influence disease progression and may reveal potential downstream therapeutic targets and consequences of therapeutic intervention.

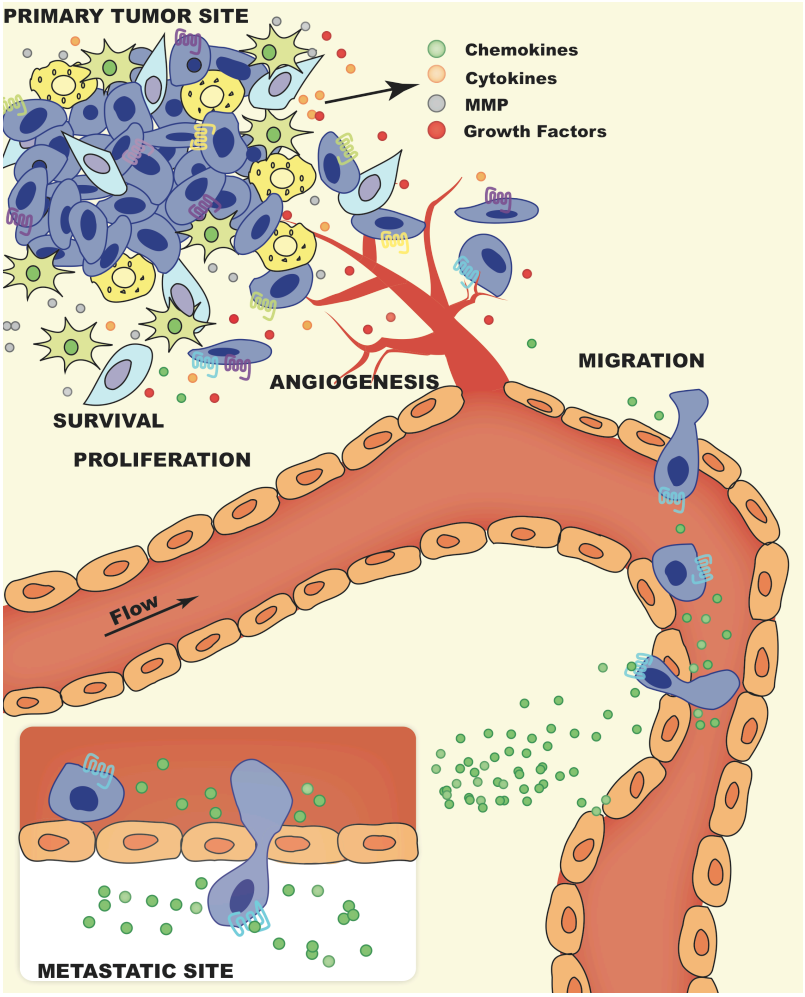

Figure 1.10 Illustration of the various steps in cancer growth and metastasis where chemokines and receptors play a role. In the primary lesion, tumor cells (dark blue) are supported by a network of cells in the microenvironment including fibroblasts (light blue), dendritic cells (green), and TAMs (yellow). Chemokines produced by the tumor cells serve to recruit endothelial cells thereby promoting angiogenesis. They also recruit leukocytes that produce other cytokines, growth factors and MMPs that enhance growth, proliferation, and angiogenesis. Fibroblasts also produce angiogenic and survival/growth promoting chemokines. Metastasis of cells is facilitated by upregulation of particular chemokine receptors like CXCR4 on the tumor cells, which enables them to migrate to secondary tissues where the ligands are expressed. Similar to the primary site, paracrine and autocrine chemokine/cytokine signaling amongst cells within the microenvironment may be especially important for survival and growth of the metastasized cells.

1.6 Acknowledgements

Chapter 1, in part, was published in *Biochemical Journal:* O'Hayre M, Salanga CL, Handel TM, Allen SJ, Chemokines and cancer: migration, intracellular signalling and intercellular communication in the microenvironment. *Biochem J.* 2008; *Cellular and Molecular Life Sciences:* Salanga CL, O'Hayre M, Handel T. Modulation of chemokine receptor activity through dimerization and crosstalk. *Cell Mol Life Sci.* 2009; and, *Expert Opinion in Drug Discovery*: O'Hayre M, Salanga CL, Handel TM, Hamel DJ. Emerging Concepts and Approaches for Chemokine-Receptor Drug Discovery. *Expert Opin.* 2010.

1.7 References

1. Baggiolini, M., B. Dewald, and B. Moser, *Human chemokines: an update.* Annu Rev Immunol, 1997. **15**: p. 675-705.

2. Salanga, C.L. and T.M. Handel, *Chemokine oligomerization and interactions with receptors and glycosaminoglycans: The role of structural dynamics in function.* Experimental Cell Research, 2011. **317**(5): p. 590-601.

3. Moser, B. and K. Willimann, *Chemokines: role in inflammation and immune surveillance.* Ann Rheum Dis, 2004. **63 Suppl 2**: p. ii84-ii89.

4. Gerard, C. and B.J. Rollins, *Chemokines and disease.* Nat Immunol, 2001. **2**(2): p. 108-15.

5. Zlotnik, A. and O. Yoshie, *Chemokines: a new classification system and their role in immunity.* Immunity, 2000. **12**(2): p. 121-7.

6. Bacon, K., M. Baggiolini, H. Broxmeyer, R. Horuk, I. Lindley, A. Mantovani, K. Maysushima, P. Murphy, H. Nomiyama, J. Oppenheim, A. Rot, T. Schall, M. Tsang, R. Thorpe, J. Van Damme, M. Wadhwa, O. Yoshie, A. Zlotnik, K. Zoon, and I.W.S.o.C. Nomenclature, *Chemokine/chemokine receptor nomenclature.* J Interferon Cytokine Res, 2002. **22**(10): p. 1067-8.

7. Nomiyama, H., N. Osada, and O. Yoshie, *The evolution of mammalian chemokine genes.* Cytokine Growth Factor Rev. **21**(4): p. 253-62.

8. O'Hayre, M., C.L. Salanga, T.M. Handel, and S.J. Allen, *Chemokines and cancer: migration, intracellular signalling and intercellular communication in the microenvironment.* Biochem J, 2008. **409**(3): p. 635-49.

9. Galandrin, S., G. Oligny-Longpre, H. Bonin, K. Ogawa, C. Gales, and M. Bouvier, *Conformational rearrangements and signaling cascades involved in ligand-biased mitogen-activated protein kinase signaling through the beta1-adrenergic receptor.* Mol Pharmacol, 2008. **74**(1): p. 162-72.

10. Allen, S.J., S.E. Crown, and T.M. Handel, *Chemokine: receptor structure, interactions, and antagonism.* Annu Rev Immunol, 2007. **25**: p. 787-820.

11. Proudfoot, A.E., T.M. Handel, Z. Johnson, E.K. Lau, P. LiWang, I. Clark-Lewis, F. Borlat, T.N. Wells, and M.H. Kosco-Vilbois, *Glycosaminoglycan binding and oligomerization are essential for the in vivo activity of certain chemokines.* Proc Natl Acad Sci U S A, 2003. **100**(4): p. 1885-90.

12. Clore, G.M., E. Appella, M. Yamada, K. Matsushima, and A.M. Gronenborn, *Three-dimensional structure of interleukin 8 in solution.* Biochemistry, 1990. **29**(7): p. 1689-96.

13. Lefkowitz, R.J. and E.J. Whalen, *beta-arrestins: traffic cops of cell signaling.* Curr Opin Cell Biol, 2004. **16**(2): p. 162-8.

14. Lefkowitz, R.J. and S.K. Shenoy, *Transduction of receptor signals by beta-arrestins.* Science, 2005. **308**(5721): p. 512-7.

15. Rajagopal, S., J. Kim, S. Ahn, S. Craig, C.M. Lam, N.P. Gerard, C. Gerard, and R.J. Lefkowitz, *Beta-arrestin- but not G protein-mediated signaling by the "decoy" receptor CXCR7.* Proceedings of the National Academy of Sciences, 2010. **107**(2): p. 628-32.

16. Bayburt, T.H., A.J. Leitz, G. Xie, D.D. Oprian, and S.G. Sligar, *Transducin activation by nanoscale lipid bilayers containing one and two rhodopsins.* J Biol Chem, 2007. **282**(20): p. 14875-81.

17. Leitz, A.J., T.H. Bayburt, A.N. Barnakov, B.A. Springer, and S.G. Sligar, *Functional reconstitution of Beta2-adrenergic receptors utilizing self-assembling Nanodisc technology.* BioTechniques, 2006. **40**(5): p. 601-2, 604, 606, passim.

18. Banerjee, S., T. Huber, and T.P. Sakmar, *Rapid incorporation of functional rhodopsin into nanoscale apolipoprotein bound bilayer (NABB) particles.* Journal of Molecular Biology, 2008. **377**(4): p. 1067-81.

19. Flaherty, P., M.L. Radhakrishnan, T. Dinh, R.A. Rebres, T.I. Roach, M.I. Jordan, and A.P. Arkin, *A dual receptor crosstalk model of G-protein-coupled signal transduction.* PLoS Comput Biol, 2008. **4**(9): p. e1000185.

20. Hill, S.M., *Receptor crosstalk: communication through cell signaling pathways.* Anat Rec, 1998. **253**(2): p. 42-8.

21. Selbie, L.A. and S.J. Hill, *G protein-coupled-receptor cross-talk: the fine-tuning of multiple receptor-signalling pathways.* Trends Pharmacol Sci, 1998. **19**(3): p. 87-93.

22. Proudfoot, A.E.I., T.M. Handel, Z. Johnson, E.K. Lau, P. LiWang, I. Clark-Lewis, F. Borlat, T.N.C. Wells, and M.H. Kosco-Vilbois, *Glycosaminoglycan binding and oligomerization are essential for the in vivo activity of certain chemokines.* Proc Natl Acad Sci USA, 2003. **100**(4): p. 1885-90.

23. Paolini, J.F., D. Willard, T. Consler, M. Luther, and M.S. Krangel, *The chemokines IL-8, monocyte chemoattractant protein-1, and I-309 are monomers at physiologically relevant concentrations.* J Immunol, 1994. **153**(6): p. 2704-17.

24. Kim, K.S., K. Rajarathnam, I. Clark-Lewis, and B.D. Sykes, *Structural characterization of a monomeric chemokine: monocyte chemoattractant protein-3.* FEBS Lett, 1996. **395**(2-3): p. 277-82.

25. Kuloglu, E.S., D.R. McCaslin, M. Kitabwalla, C.D. Pauza, J.L. Markley, and B.F. Volkman, *Monomeric solution structure of the prototypical 'C' chemokine lymphotactin.* Biochemistry, 2001. **40**(42): p. 12486-96.

26. Kuloğlu, E.S., D.R. McCaslin, J.L. Markley, and B.F. Volkman, *Structural rearrangement of human lymphotactin, a C chemokine, under physiological solution conditions.* J Biol Chem, 2002. **277**(20): p. 17863-70.

27. Ren, M., Q. Guo, L. Guo, M. Lenz, F. Qian, R.R. Koenen, H. Xu, A.B. Schilling, C. Weber, R.D. Ye, A.R. Dinner, and W.-J. Tang, *Polymerization of MIP-1 chemokine (CCL3 and CCL4) and clearance of MIP-1 by insulin-degrading enzyme.* EMBO J, 2010. **29**(23): p. 3952-66.

28. Czaplewski, L.G., J. McKeating, C.J. Craven, L.D. Higgins, V. Appay, A. Brown, T. Dudgeon, L.A. Howard, T. Meyers, J. Owen, S.R. Palan, P. Tan, G. Wilson, N.R. Woods, C.M. Heyworth, B.I. Lord, D. Brotherton, R. Christison, S. Craig, S. Cribbes, R.M. Edwards, S.J. Evans, R. Gilbert, P. Morgan, E. Randle, N. Schofield, P.G. Varley, J. Fisher, J.P. Waltho, and M.G. Hunter, *Identification of amino acid residues critical for aggregation of human CC chemokines macrophage inflammatory protein (MIP)-1alpha, MIP-1beta, and RANTES. Characterization of active disaggregated chemokine variants.* J Biol Chem, 1999. **274**(23): p. 16077-84.

29. Hoogewerf, A.J., G.S. Kuschert, A.E. Proudfoot, F. Borlat, I. Clark-Lewis, C.A. Power, and T.N. Wells, *Glycosaminoglycans mediate cell surface oligomerization of chemokines.* Biochemistry, 1997. **36**(44): p. 13570-8.

30. Lubkowski, J., G. Bujacz, L. Boque, P.J. Domaille, T.M. Handel, and A. Wlodawer, *The structure of MCP-1 in two crystal forms provides a rare example of variable quaternary interactions.* Nat Struct Biol, 1997. **4**(1): p. 64-9.

31. Johnson, Z., A.E. Proudfoot, and T.M. Handel, *Interaction of chemokines and glycosaminoglycans: a new twist in the regulation of chemokine function with opportunities for therapeutic intervention.* Cytokine Growth Factor Rev, 2005. **16**(6): p. 625-36.

32. Handel, T.M., Z. Johnson, S.E. Crown, E.K. Lau, and A.E. Proudfoot, *Regulation of protein function by glycosaminoglycans--as exemplified by chemokines.* Annu Rev Biochem, 2005. **74**: p. 385-410.

33. Ihrcke, N.S., L.E. Wrenshall, B.J. Lindman, and J.L. Platt, *Role of heparan sulfate in immune system-blood vessel interactions.* Immunol Today, 1993. **14**(10): p. 500-5.

34. Ali, S., H. Robertson, J.H. Wain, J.D. Isaacs, G. Malik, and J.A. Kirby, *A non-glycosaminoglycan-binding variant of CC chemokine ligand 7 (monocyte chemoattractant protein-3) antagonizes chemokine-mediated inflammation.* J Immunol, 2005. **175**(2): p. 1257-66.

35. Lau, E.K., C.D. Paavola, Z. Johnson, J.-P. Gaudry, E. Geretti, F. Borlat, A.J. Kungl, A.E. Proudfoot, and T.M. Handel, *Identification of the glycosaminoglycan binding site of the CC chemokine, MCP-1: implications for structure and function in vivo.* J Biol Chem, 2004. **279**(21): p. 22294-305.

36. Grymula, K., M. Tarnowski, M. Wysoczynski, J. Drukala, F.G. Barr, J. Ratajczak, M. Kucia, and M.Z. Ratajczak, *Overlapping and distinct role of CXCR7-SDF-1/ITAC and CXCR4-SDF-1 axes in regulating metastatic behavior of human rhabdomyosarcomas.* Int J Cancer, 2010. **127**(11): p. 2554-68.

37. Proudfoot, A.E., S. Fritchley, F. Borlat, J.P. Shaw, F. Vilbois, C. Zwahlen, A. Trkola, D. Marchant, P.R. Clapham, and T.N. Wells, *The BBXB motif of RANTES is the principal site for heparin binding and controls receptor selectivity.* J Biol Chem, 2001. **276**(14): p. 10620-6.

38. Hamel, D.J., I. Sielaff, A.E. Proudfoot, and T.M. Handel, *Chapter 4. Interactions of chemokines with glycosaminoglycans.* Methods Enzymol, 2009. **461**: p. 71-102.

39. Paavola, C.D., S. Hemmerich, D. Grunberger, I. Polsky, A. Bloom, R. Freedman, M. Mulkins, S. Bhakta, D. McCarley, L. Wiesent, B. Wong, K. Jarnagin, and T.M. Handel, *Monomeric monocyte chemoattractant protein-1 (MCP-1) binds and activates the MCP-1 receptor CCR2B.* J Biol Chem, 1998. **273**(50): p. 33157-65.

40. Handel, T.M. and P.J. Domaille, *Heteronuclear (1H, 13C, 15N) NMR assignments and solution structure of the monocyte chemoattractant protein-1 (MCP-1) dimer.* Biochemistry, 1996. **35**(21): p. 6569-84.

41. Lau, E.K., S. Allen, A.R. Hsu, and T.M. Handel, *Chemokine-receptor interactions: GPCRs, glycosaminoglycans and viral chemokine binding proteins.* Adv Protein Chem, 2004. **68**: p. 351-91.

42. O'Hayre, M., C.L. Salanga, T.J. Kipps, D. Messmer, P.C. Dorrestein, and T.M. Handel, *Elucidating the CXCL12/CXCR4 signaling network in chronic lymphocytic leukemia through phosphoproteomics analysis.* PLoS ONE, 2010. **5**(7): p. e11716.

43. Sanchez-Madrid, F. and M.A. del Pozo, *Leukocyte polarization in cell migration and immune interactions.* Embo J, 1999. **18**(3): p. 501-11.

44. Cancelas, J.A., M. Jansen, and D.A. Williams, *The role of chemokine activation of Rac GTPases in hematopoietic stem cell marrow homing, retention, and peripheral mobilization.* Exp Hematol, 2006. **34**(8): p. 976-85.

45. Tanaka, T., Z. Bai, Y. Srinoulprasert, B.-G. Yang, B. Yang, H. Hayasaka, and M. Miyasaka, *Chemokines in tumor progression and metastasis.* Cancer Sci, 2005. **96**(6): p. 317-22.

46. Li, S., J.L. Guan, and S. Chien, *Biochemistry and biomechanics of cell motility.* Annu Rev Biomed Eng, 2005. **7**: p. 105-50.

47. Tan, W., D. Martin, and J.S. Gutkind, *The Galpha13-Rho signaling axis is required for SDF-1-induced migration through CXCR4.* J Biol Chem, 2006. **281**(51): p. 39542-9.

48. Lee, B.-C., T.-H. Lee, S. Avraham, and H.K. Avraham, *Involvement of the chemokine receptor CXCR4 and its ligand stromal cell-derived factor 1alpha in breast cancer cell migration through human brain microvascular endothelial cells.* Mol Cancer Res, 2004. **2**(6): p. 327-38.

49. Nagasawa, T., S. Hirota, K. Tachibana, N. Takakura, S. Nishikawa, Y. Kitamura, N. Yoshida, H. Kikutani, and T. Kishimoto, *Defects of B-cell lymphopoiesis and bone-marrow myelopoiesis in mice lacking the CXC chemokine PBSF/SDF-1.* Nature, 1996. **382**(6592): p. 635-8.

50. Tachibana, K., S. Hirota, H. Iizasa, H. Yoshida, K. Kawabata, Y. Kataoka, Y. Kitamura, K. Matsushima, N. Yoshida, S. Nishikawa, T. Kishimoto, and T. Nagasawa, *The chemokine receptor CXCR4 is essential for vascularization of the gastrointestinal tract.* Nature, 1998. **393**(6685): p. 591-4.

51. Balkwill, F., *The significance of cancer cell expression of the chemokine receptor CXCR4.* Semin Cancer Biol, 2004. **14**(3): p. 171-9.

52. Curnock, A.P., M.K. Logan, and S.G. Ward, *Chemokine signalling: pivoting around multiple phosphoinositide 3-kinases.* Immunology, 2002. **105**(2): p. 125-36.

53. Nishio, M., T. Endo, N. Tsukada, J. Ohata, S. Kitada, J.C. Reed, N.J. Zvaifler, and T.J. Kipps, *Nurselike cells express BAFF and APRIL, which can promote survival of chronic lymphocytic leukemia cells via a paracrine pathway distinct from that of SDF-1alpha.* Blood, 2005. **106**(3): p. 1012-20.

54. Maxwell, P.J., R. Gallagher, A. Seaton, C. Wilson, P. Scullin, J. Pettigrew, I.J. Stratford, K.J. Williams, P.G. Johnston, and D.J. Waugh, *HIF-1 and NF-kappaB-mediated upregulation of CXCR1 and CXCR2 expression promotes cell survival in hypoxic prostate cancer cells.* Oncogene, 2007.

55. Kulbe, H., N.R. Levinson, F. Balkwill, and J.L. Wilson, *The chemokine network in cancer--much more than directing cell movement.* Int J Dev Biol, 2004. **48**(5-6): p. 489-96.

56. Ganju, R.K., S.A. Brubaker, J. Meyer, P. Dutt, Y. Yang, S. Qin, W. Newman, and J.E. Groopman, *The alpha-chemokine, stromal cell-derived factor-1alpha, binds to the transmembrane G-protein-coupled CXCR-4 receptor and activates multiple signal transduction pathways.* J Biol Chem, 1998. **273**(36): p. 23169-75.

57. Thelen, M., *Dancing to the tune of chemokines.* Nat Immunol, 2001. **2**(2): p. 129-34.

58. Vivanco, I. and C.L. Sawyers, *The phosphatidylinositol 3-Kinase AKT pathway in human cancer.* Nature Reviews Cancer, 2002. **2**(7): p. 489-501.

59. Brand, S., J. Dambacher, F. Beigel, T. Olszak, J. Diebold, J.M. Otte, B. Goke, and S.T. Eichhorst, *CXCR4 and CXCL12 are inversely expressed in colorectal cancer cells and modulate cancer cell migration, invasion and MMP-9 activation.* Exp Cell Res, 2005. **310**(1): p. 117-30.

60. Burger, J.A. and T.J. Kipps, *CXCR4: a key receptor in the crosstalk between tumor cells and their microenvironment.* Blood, 2006. **107**(5): p. 1761-7.

61. Fujita, N. and T. Tsuruo, *Survival-signaling pathway as a promising target for cancer chemotherapy.* Cancer Chemother Pharmacol, 2003. **52 Suppl 1**: p. S24-8.

62. Ye, R.D., *Regulation of nuclear factor kappaB activation by G-protein-coupled receptors.* J Leukoc Biol, 2001. **70**(6): p. 839-48.

63. Karin, M., *Nuclear factor-kappaB in cancer development and progression.* Nature, 2006. **441**(7092): p. 431-6.

64. Diehl, J.A., M. Cheng, M.F. Roussel, and C.J. Sherr, *Glycogen synthase kinase-3beta regulates cyclin D1 proteolysis and subcellular localization.* Genes Dev, 1998. **12**(22): p. 3499-511.

65. Shaw, R.J. and L.C. Cantley, *Ras, PI(3)K and mTOR signalling controls tumour cell growth.* Nature, 2006. **441**(7092): p. 424-30.

66. Allan, L.A., N. Morrice, S. Brady, G. Magee, S. Pathak, and P.R. Clarke, *Inhibition of caspase-9 through phosphorylation at Thr 125 by ERK MAPK.* Nat Cell Biol, 2003. **5**(7): p. 647-54.

67. Kyriakis, J.M., *MAP kinases and the regulation of nuclear receptors.* Sci STKE, 2000. **2000**(48): p. PE1.

68. Sutton, A., V. Friand, S. Brule-Donneger, T. Chaigneau, M. Ziol, O. Sainte-Catherine, A. Poire, L. Saffar, M. Kraemer, J. Vassy, P. Nahon, J.L. Salzmann, L. Gattegno, and N. Charnaux, *Stromal cell-derived factor-1/chemokine (C-X-C motif) ligand 12 stimulates human hepatoma cell growth, migration, and invasion.* Mol Cancer Res, 2007. **5**(1): p. 21-33.

69. Angers, S., A. Salahpour, and M. Bouvier, *Dimerization: an emerging concept for G protein-coupled receptor ontogeny and function.* Annu Rev Pharmacol Toxicol, 2002. **42**: p. 409-35.

70. Bulenger, S., S. Marullo, and M. Bouvier, *Emerging role of homo- and heterodimerization in G-protein-coupled receptor biosynthesis and maturation.* Trends Pharmacol Sci, 2005. **26**(3): p. 131-7.

71. Milligan, G., *G protein-coupled receptor dimerization: function and ligand pharmacology.* Mol Pharmacol, 2004. **66**(1): p. 1-7.

72. Springael, J.Y., E. Urizar, and M. Parmentier, *Dimerization of chemokine receptors and its functional consequences.* Cytokine Growth Factor Rev, 2005. **16**(6): p. 611-23.

73. Terrillon, S. and M. Bouvier, *Roles of G-protein-coupled receptor dimerization.* EMBO Rep, 2004. **5**(1): p. 30-4.

74. Jones, K.A., B. Borowsky, J.A. Tamm, D.A. Craig, M.M. Durkin, M. Dai, W.J. Yao, M. Johnson, C. Gunwaldsen, L.Y. Huang, C. Tang, Q. Shen, J.A. Salon, K. Morse, T. Laz, K.E. Smith, D. Nagarathnam, S.A. Noble, T.A. Branchek, and C. Gerald, *GABA(B) receptors function as a heteromeric assembly of the subunits GABA(B)R1 and GABA(B)R2.* Nature, 1998. **396**(6712): p. 674-9.

75. White, J.H., A. Wise, M.J. Main, A. Green, N.J. Fraser, G.H. Disney, A.A. Barnes, P. Emson, S.M. Foord, and F.H. Marshall, *Heterodimerization is required for the formation of a functional GABA(B) receptor.* Nature, 1998. **396**(6712): p. 679-82.

76. Jacoby, E., R. Bouhelal, M. Gerspacher, and K. Seuwen, *The 7 TM G-protein-coupled receptor target family.* ChemMedChem, 2006. **1**(8): p. 761-82.

77. Salanga, C.L., M. O'hayre, and T. Handel, *Modulation of chemokine receptor activity through dimerization and crosstalk.* Cell. Mol. Life Sci., 2009. **66**(8): p. 1370-1386.

78. Percherancier, Y., Y.A. Berchiche, I. Slight, R. Volkmer-Engert, H. Tamamura, N. Fujii, M. Bouvier, and N. Heveker, *Bioluminescence resonance energy transfer reveals ligand-induced conformational changes in CXCR4 homo- and heterodimers.* J Biol Chem, 2005. **280**(11): p. 9895-903.

79. Sohy, D., M. Parmentier, and J.-Y. Springael, *Allosteric transinhibition by specific antagonists in CCR2/CXCR4 heterodimers.* J Biol Chem, 2007. **282**(41): p. 30062-9.

80. Mellado, M., J.M. Rodriguez-Frade, A.J. Vila-Coro, A.M. de Ana, and A.C. Martinez, *Chemokine control of HIV-1 infection.* Nature, 1999. **400**(6746): p. 723-4.

81. Simmons, G., P.R. Clapham, L. Picard, R.E. Offord, M.M. Rosenkilde, T.W. Schwartz, R. Buser, T.N. Wells, and A.E. Proudfoot, *Potent inhibition of HIV-1 infectivity in macrophages and lymphocytes by a novel CCR5 antagonist.* Science, 1997. **276**(5310): p. 276-9.

82. Agrawal, L., X. Lu, J. Qingwen, Z. VanHorn-Ali, I.V. Nicolescu, D.H. McDermott, P.M. Murphy, and G. Alkhatib, *Role for CCR5Delta32 protein in resistance to R5, R5X4, and X4 human immunodeficiency virus type 1 in primary CD4+ cells.* J Virol, 2004. **78**(5): p. 2277-87.

83. Dean, M., M. Carrington, C. Winkler, G.A. Huttley, M.W. Smith, R. Allikmets, J.J. Goedert, S.P. Buchbinder, E. Vittinghoff, E. Gomperts, S. Donfield, D. Vlahov, R. Kaslow, A. Saah, C. Rinaldo, R. Detels, and S.J. O'Brien, *Genetic restriction of HIV-1 infection and progression to AIDS by a deletion allele of the CKR5 structural gene. Hemophilia Growth and Development Study, Multicenter AIDS Cohort Study, Multicenter Hemophilia Cohort Study, San Francisco City Cohort, ALIVE Study.* Science, 1996. **273**(5283): p. 1856-62.

84. Samson, M., F. Libert, B.J. Doranz, J. Rucker, C. Liesnard, C.M. Farber, S. Saragosti, C. Lapoumeroulie, J. Cognaux, C. Forceille, G. Muyldermans, C. Verhofstede, G. Burtonboy, M. Georges, T. Imai, S. Rana, Y. Yi, R.J. Smyth, R.G. Collman, R.W. Doms, G. Vassart, and M. Parmentier, *Resistance to HIV-1 infection in caucasian individuals bearing mutant alleles of the CCR-5 chemokine receptor gene.* Nature, 1996. **382**(6593): p. 722-5.

85. Benkirane, M., D.Y. Jin, R.F. Chun, R.A. Koup, and K.T. Jeang, *Mechanism of transdominant inhibition of CCR5-mediated HIV-1 infection by ccr5delta32.* J Biol Chem, 1997. **272**(49): p. 30603-6.

86. Hernandez, P.A., R.J. Gorlin, J.N. Lukens, S. Taniuchi, J. Bohinjec, F. Francois, M.E. Klotman, and G.A. Diaz, *Mutations in the chemokine receptor gene CXCR4 are associated with WHIM syndrome, a combined immunodeficiency disease.* Nat Genet, 2003. **34**(1): p. 70-4.

87. Lagane, B., K.Y. Chow, K. Balabanian, A. Levoye, J. Harriague, T. Planchenault, F. Baleux, N. Gunera-Saad, F. Arenzana-Seisdedos, and F. Bachelerie, *CXCR4 dimerization and beta-arrestin-mediated signaling account for the enhanced chemotaxis to CXCL12 in WHIM syndrome.* Blood, 2008. **112**(1): p. 34-44.

88. Balabanian, K., B. Lagane, J.L. Pablos, L. Laurent, T. Planchenault, O. Verola, C. Lebbe, D. Kerob, A. Dupuy, O. Hermine, J.F. Nicolas, V. Latger-Cannard, D. Bensoussan, P. Bordigoni, F. Baleux, F. Le Deist, J.L. Virelizier, F. Arenzana-Seisdedos, and F. Bachelerie, *WHIM syndromes with different genetic anomalies are accounted for by impaired CXCR4 desensitization to CXCL12.* Blood, 2005. **105**(6): p. 2449-57.

89. Wu, B., E.Y.T. Chien, C.D. Mol, G. Fenalti, W. Liu, V. Katritch, R. Abagyan, A. Brooun, P. Wells, F.C. Bi, D.J. Hamel, P. Kuhn, T.M. Handel, V. Cherezov, and R.C. Stevens, *Structures of the CXCR4 chemokine GPCR with small-molecule and cyclic peptide antagonists.* Science, 2010. **330**(6007): p. 1066-71.

90. Balabanian, K., B. Lagane, S. Infantino, K.Y. Chow, J. Harriague, B. Moepps, F. Arenzana-Seisdedos, M. Thelen, and F. Bachelerie, *The chemokine SDF-1/CXCL12 binds to and signals through the orphan receptor RDC1 in T lymphocytes.* J Biol Chem, 2005. **280**(42): p. 35760-6.

91. Levoye, A., K. Balabanian, F. Baleux, F. Bachelerie, and B. Lagane, *CXCR7 heterodimerizes with CXCR4 and regulates CXCL12-mediated G protein signaling.* Blood, 2009. **113**(24): p. 6085-93.

92. Sierro, F., C. Biben, L. Martinez-Munoz, M. Mellado, R.M. Ransohoff, M. Li, B. Woehl, H. Leung, J. Groom, M. Batten, R.P. Harvey, A.C. Martinez, C.R. Mackay, and F. Mackay, *Disrupted cardiac development but normal hematopoiesis in mice deficient in the second CXCL12/SDF-1 receptor, CXCR7.* Proc Natl Acad Sci U S A, 2007. **104**(37): p. 14759-64.

93. Luker, K.E., M. Gupta, and G.D. Luker, *Imaging chemokine receptor dimerization with firefly luciferase complementation.* FASEB J, 2009. **23**(3): p. 823-34.

94. Burns, J.M., B.C. Summers, Y. Wang, A. Melikian, R. Berahovich, Z. Miao, M.E. Penfold, M.J. Sunshine, D.R. Littman, C.J. Kuo, K. Wei, B.E. McMaster, K.

Wright, M.C. Howard, and T.J. Schall, *A novel chemokine receptor for SDF-1 and I-TAC involved in cell survival, cell adhesion, and tumor development.* J Exp Med, 2006. **203**(9): p. 2201-13.

95. Kalatskaya, I., Y.A. Berchiche, S. Gravel, B.J. Limberg, J.S. Rosenbaum, and N. Heveker, *AMD3100 is a CXCR7 ligand with allosteric agonist properties.* Mol Pharmacol, 2009. **75**(5): p. 1240-7.

96. Luker, K.E., J.M. Steele, L.A. Mihalko, P. Ray, and G.D. Luker, *Constitutive and chemokine-dependent internalization and recycling of CXCR7 in breast cancer cells to degrade chemokine ligands.* Oncogene, 2010.

97. Zabel, B.A., Y. Wang, S. Lewen, R.D. Berahovich, M.E. Penfold, P. Zhang, J. Powers, B.C. Summers, Z. Miao, B. Zhao, A. Jalili, A. Janowska-Wieczorek, J.C. Jaen, and T.J. Schall, *Elucidation of CXCR7-mediated signaling events and inhibition of CXCR4-mediated tumor cell transendothelial migration by CXCR7 ligands.* J Immunol, 2009. **183**(5): p. 3204-11.

98. Sohy, D., H. Yano, P. de Nadai, E. Urizar, A. Guillabert, J.A. Javitch, M. Parmentier, and J.Y. Springael, *Hetero-oligomerization of CCR2, CCR5, and CXCR4 and the protean effects of "selective" antagonists.* J Biol Chem, 2009. **284**(45): p. 31270-9.

99. Contento, R.L., B. Molon, C. Boularan, T. Pozzan, S. Manes, S. Marullo, and A. Viola, *CXCR4-CCR5: a couple modulating T cell functions.* Proc Natl Acad Sci U S A, 2008. **105**(29): p. 10101-6.

100. El-Asmar, L., J.Y. Springael, S. Ballet, E.U. Andrieu, G. Vassart, and M. Parmentier, *Evidence for negative binding cooperativity within CCR5-CCR2b heterodimers.* Mol Pharmacol, 2005. **67**(2): p. 460-9.

101. Hernanz-Falcon, P., J.M. Rodriguez-Frade, A. Serrano, D. Juan, A. del Sol, S.F. Soriano, F. Roncal, L. Gomez, A. Valencia, A.C. Martinez, and M. Mellado, *Identification of amino acid residues crucial for chemokine receptor dimerization.* Nat Immunol, 2004. **5**(2): p. 216-23.

102. Issafras, H., S. Angers, S. Bulenger, C. Blanpain, M. Parmentier, C. Labbe-Jullie, M. Bouvier, and S. Marullo, *Constitutive agonist-independent CCR5 oligomerization and antibody-mediated clustering occurring at physiological levels of receptors.* J Biol Chem, 2002. **277**(38): p. 34666-73.

103. Mellado, M., J.M. Rodriguez-Frade, A.J. Vila-Coro, S. Fernandez, A. Martin de Ana, D.R. Jones, J.L. Toran, and A.C. Martinez, *Chemokine receptor homo- or heterodimerization activates distinct signaling pathways.* EMBO J, 2001. **20**(10): p. 2497-507.

104. Salanga, C.L., M. O'Hayre, and T. Handel, *Modulation of chemokine receptor activity through dimerization and crosstalk.* Cell Mol Life Sci, 2009. **66**(8): p. 1370-86.

105. Hereld, D. and T. Jin, *Slamming the DOR on chemokine receptor signaling: heterodimerization silences ligand-occupied CXCR4 and delta-opioid receptors.* Eur J Immunol, 2008. **38**(2): p. 334-7.

106. Milligan, G., S. Wilson, and J.F. Lopez-Gimenez, *The specificity and molecular basis of alpha1-adrenoceptor and CXCR chemokine receptor dimerization.* J Mol Neurosci, 2005. **26**(2-3): p. 161-8.

107. Oravecz, T., M. Pall, G. Roderiquez, M.D. Gorrell, M. Ditto, N.Y. Nguyen, R. Boykins, E. Unsworth, and M.A. Norcross, *Regulation of the receptor specificity and function of the chemokine RANTES (regulated on activation, normal T cell expressed and secreted) by dipeptidyl peptidase IV (CD26)-mediated cleavage.* J Exp Med, 1997. **186**(11): p. 1865-72.

108. Lapham, C.K., J. Ouyang, B. Chandrasekhar, N.Y. Nguyen, D.S. Dimitrov, and H. Golding, *Evidence for cell-surface association between fusin and the CD4-gp120 complex in human cell lines.* Science, 1996. **274**(5287): p. 602-5.

109. Basmaciogullari, S., B. Pacheco, S. Bour, and J. Sodroski, *Specific interaction of CXCR4 with CD4 and CD8alpha: functional analysis of the CD4/CXCR4 interaction in the context of HIV-1 envelope glycoprotein-mediated membrane fusion.* Virology, 2006. **353**(1): p. 52-67.

110. Kumar, A., T.D. Humphreys, K.N. Kremer, P.S. Bramati, L. Bradfield, C.E. Edgar, and K.E. Hedin, *CXCR4 physically associates with the T cell receptor to signal in T cells.* Immunity, 2006. **25**(2): p. 213-24.

111. Finley, M.J., X. Chen, G. Bardi, P. Davey, E.B. Geller, L. Zhang, M.W. Adler, and T.J. Rogers, *Bi-directional heterologous desensitization between the major HIV-1 co-receptor CXCR4 and the kappa-opioid receptor.* J Neuroimmunol, 2008. **197**(2): p. 114-23.

112. Pello, O.M., L. Martinez-Munoz, V. Parrillas, A. Serrano, J.M. Rodriguez-Frade, M.J. Toro, P. Lucas, M. Monterrubio, A.C. Martinez, and M. Mellado, *Ligand stabilization of CXCR4/delta-opioid receptor heterodimers reveals a mechanism for immune response regulation.* Eur J Immunol, 2008. **38**(2): p. 537-49.

113. Tilton, B., L. Ho, E. Oberlin, P. Loetscher, F. Baleux, I. Clark-Lewis, and M. Thelen, *Signal transduction by CXC chemokine receptor 4. Stromal cell-derived factor 1 stimulates prolonged protein kinase B and extracellular signal-regulated kinase 2 activation in T lymphocytes.* J Exp Med, 2000. **192**(3): p. 313-24.

114. Kremer, K.N., T.D. Humphreys, A. Kumar, N.X. Qian, and K.E. Hedin, *Distinct role of ZAP-70 and Src homology 2 domain-containing leukocyte protein of 76 kDa in the prolonged activation of extracellular signal-regulated protein kinase by the stromal cell-derived factor-1 alpha/CXCL12 chemokine.* J Immunol, 2003. **171**(1): p. 360-7.

115. Chen, C., J. Li, G. Bot, I. Szabo, T.J. Rogers, and L.Y. Liu-Chen, *Heterodimerization and cross-desensitization between the mu-opioid receptor and the chemokine CCR5 receptor.* Eur J Pharmacol, 2004. **483**(2-3): p. 175-86.

116. Suzuki, S., L.F. Chuang, P. Yau, R.H. Doi, and R.Y. Chuang, *Interactions of opioid and chemokine receptors: oligomerization of mu, kappa, and delta with CCR5 on immune cells.* Exp Cell Res, 2002. **280**(2): p. 192-200.

117. Szabo, I., M.A. Wetzel, N. Zhang, A.D. Steele, D.E. Kaminsky, C. Chen, L.Y. Liu-Chen, F. Bednar, E.E. Henderson, O.M. Howard, J.J. Oppenheim, and T.J. Rogers, *Selective inactivation of CCR5 and decreased infectivity of R5 HIV-1 strains mediated by opioid-induced heterologous desensitization.* J Leukoc Biol, 2003. **74**(6): p. 1074-82.

118. Balkwill, F., *Cancer and the chemokine network.* Nat Rev Cancer, 2004. **4**(7): p. 540-50.

119. Müller, A., B. Homey, H. Soto, N. Ge, D. Catron, M.E. Buchanan, T. McClanahan, E. Murphy, W. Yuan, S.N. Wagner, J.L. Barrera, A. Mohar, E. Verástegui, and A. Zlotnik, *Involvement of chemokine receptors in breast cancer metastasis.* Nature, 2001. **410**(6824): p. 50-6.

120. Zlotnik, A., *Chemokines and cancer.* Int J Cancer, 2006. **119**(9): p. 2026-9.

121. Gupta, G.P. and J. Massagué, *Cancer metastasis: building a framework.* Cell, 2006. **127**(4): p. 679-95.

122. Viola, A. and A.D. Luster, *Chemokines and their receptors: drug targets in immunity and inflammation.* Annu Rev Pharmacol Toxicol, 2008. **48**: p. 171-97.

123. Murakami, T., A.R. Cardones, and S.T. Hwang, *Chemokine receptors and melanoma metastasis.* J Dermatol Sci, 2004. **36**(2): p. 71-8.

124. Ben-Baruch, A., *Host microenvironment in breast cancer development: Inflammatory cells, cytokines and chemokines in breast cancer progression - reciprocal tumor-microenvironment interactions.* Breast Cancer Res, 2003. **5**(1): p. 31 - 36.

125. Sica, A., T. Schioppa, A. Mantovani, and P. Allavena, *Tumour-associated macrophages are a distinct M2 polarised population promoting tumour progression: potential targets of anti-cancer therapy.* Eur J Cancer, 2006. **42**(6): p. 717-27.

CHAPTER 2

Characterization of MCP-3/CCL7: Glycosaminoglycan Interactions by Radiolytic Footprinting with Mass Spectrometry, Mutagenesis and Functional Analysis

2.1 Summary

Chemokines are mediators of leukocyte trafficking during routine immune surveillance and inflammatory responses where formation of localized chemokine gradients facilitated by interactions with glycosaminoglycans (GAGs) serve to guide cell migration. The importance of chemokine:GAG interactions in the localization and presentation of chemokines to their receptors has been well established; however, it not clear to what extent specificity drives chemokine interactions with GAG and also how chemokine oligomerization contributes to these interactions. As a result, there has been a growing interest in defining GAG-binding sites of specific chemokines to make GAG-binding deficient mutants that allow one to better understand the role and structural mechanisms of these interactions in the biological activity of chemokines. Techniques to identify GAG binding sites typically involve extensive mutagenesis of the basic residues along a chemokine or directed mutation of known GAG-binding motifs (e.g. linear BBxB motifs where B is a basic residue). However, because of oligomerization, GAG-binding epitopes don't have to be linear in sequence, and other motifs may be involved. Thus as

an alternative unbiased approach, we present the novel use of hydroxyl radical footprinting with mass spectrometry for the identification of potential GAG binding sites of MCP-3/CCL7 with Heparin octasaccharide. We then used the hydroxyl radical footprinting results to guide a more directed mutagenesis and functional study for identifying GAG binding determinants of MCP-3/CCL7. Through this approach, we identified and characterized two novel GAG binding sites of MCP-3/CCL7: K18K19 and a K4x C-terminal tail epitope which both spatially separated and do not overlap with receptor binding sites. These sites suggest new ideas about mechanisms by which chemokines interact with GAGs and receptor.

2.2 Introduction

In addition to binding chemokine receptors, interactions with glycosaminoglycans (GAGs) have been increasingly recognized as an important functional component of chemokine activity. As described in the introduction, interactions of chemokines with GAGs provide a mechanism for localizing and concentrating chemokines at specific anatomical sites, and presenting chemokines to their receptors. Additionally, these interactions are thought to be involved in transcytosis of chemokines produced in one compartment such as the extravascular space, across cells where they encounter receptor-bearing cells in another compartment, such as the bloodstream [1]. Chemokine:GAG interactions may even promote intracellular signaling, independent of chemokine receptors, as demonstrated for RANTES/CCL5 binding to the GAG chains of CD44 [2].

Proudfoot and colleagues first demonstrated the requirement of GAG binding for chemokine-induced cell migration [3], and these findings have been further supported with similar studies of other chemokines in recent years [4-6]. In these initial studies, GAG-binding deficient variants of several chemokines (MCP-1/CCL2, MIP-1β/CCL4 and RANTES/CCL5) were found to promote chemokine-induced migration *in vitro,* but exhibited a dramatic loss in the ability to recruit cells *in vivo*, compared to the wild-type (WT) counterparts [3]. Given the established importance of chemokine interactions with GAGs, and the potential contribution of these interactions to the specificity and activity of chemokines, there has been a growing interest in defining the GAG binding epitopes of chemokines. By identifying GAG binding deficient chemokines, such studies are allowing further definition of the role of GAG binding, not only generally in chemokine biology, but for specific chemokines. Secondly, identification of the common features as

well as differences in the GAG binding epitopes and how they present on chemokine surfaces in the context of monomeric and oligomeric structures is gradually providing insight into general mechanisms of recognition as well as the specificity of the interactions. Indeed, the level of specificity in chemokine:GAG interactions remains a big question in the field, but if significant, could provide an enormous additional mechanism for precise control of cell migration and other functions.

As examples of epitopes, MIP-1α/CCL3, MIP-1β/CCL4, and RANTES/CCL5 all contain a BBxB linear GAG binding motif (where B is a basic residue) in the 40s loop region [7-10]. By contrast, IL-8/CXCL8 has been shown to bind GAGs mainly through its C-terminal α-helix [11] and ITAC/CXCL11 through a diffuse epitope involving the 50s loop and Lys^{17} [12]. However, even when similar epitopes are observed, there may be significant differences in the overall GAG binding site in the context of higher order oligomeric species which are often induced upon GAG binding [13] (discussed in Chapter 1.2). For example MIP-1α/CCL3 and MIP-1β/CCL4, which have an overall acidic PI, form the highly helical polymer illustrated in Figure 1.2 E/F [14], whereas RANTES/CCL5, which has a basic PI, forms a more linear polymer (Xu *et al*., under revision for Structure) such that the placement of the GAG binding epitopes would have a different spatial distribution on the surface of the two polymer types. Furthermore, the same chemokine may adopt different oligomeric structures depending on the GAG. For example, the GAG binding site of the tetramer structure of MCP-1/CCL2 is very different than the site presented on the surface of the dimer structure (Figure 2.1), and one can hypothesize that different GAGs might preferentially recognize one structure over the other. Heparin is a uniformly sulfated GAG, and may optimally interact with the continuous basic patch of the tetramer, which has been born out by previous biophysical studies from our lab [15]. On the other hand, heparan sulfate has sulfated domains

separated by unsulfated N-acetylated domains that might better recognize the dimer structure where the two basic patches on the chemokine are separated by a more neutral region; such a model has been suggested for MIP-1α/CCL3 on the basis of experimental data coupled with modeling studies [16]. Thus, the observed differences and potential for variability in chemokine:GAG binding suggests that while GAG interactions are critical for chemokine-mediated cell migration, they may also provide an additional level of specificity since the types of proteins that bind are dictated by the structure of the GAG chains [17]. In other words, while chemokines can bind and activate multiple receptors, it is possible that GAG interactions break this perceived functional redundancy by participating in the control of biological activity in a tissue, cell type, and disease-state dependent manner. That cells change their carbohydrate coats when they become cancerous argues for specificity in protein:GAG interactions. They do so for many reasons, which almost certainly includes the ability to recruit specific cytokines/chemokines that mediate signaling, cell adhesion, proliferation, and migration [18].

Traditional methods for identifying GAG binding sites of chemokines have typically involved mutagenesis of the chemokine (mainly Arg, Lys, and His residues), followed by characterization of the ability of the mutants to bind to GAGs (typically Heparin). Approaches to assess GAG binding include isothermal fluorescence titration, Heparin affinity chromatography, radiolabeled GAG binding assays, and ^{1}H-^{15}N HSQC NMR chemical shift perturbation experiments [19]. These experiments generally require cloning, expression, and purification of many mutants to assess the contribution of specific residues to GAG binding. For example, in the work by Lau *et al.*, an extensive analysis of 35 mutants of MCP-1/CCL2 was conducted [15]; on the otherhand, most other studies have involved significantly fewer mutants, targeting BBXB motifs, which

probably has resulted in missed epitope identifications. As an alternative method for the unbiased identification of GAG binding sites that may help limit the number of mutants that need to be made and subsequently characterized by the traditional methods, herein, we present the novel application of hydroxyl radical footprinting to identify potential GAG binding epitopes of the chemokine, MCP-3/CCL7. Hydroxyl radical footprinting is a mass spectrometry based technique that has been successfully used to characterize protein complexes [20-23], but has not as yet been used to characterize complexes with GAGs.

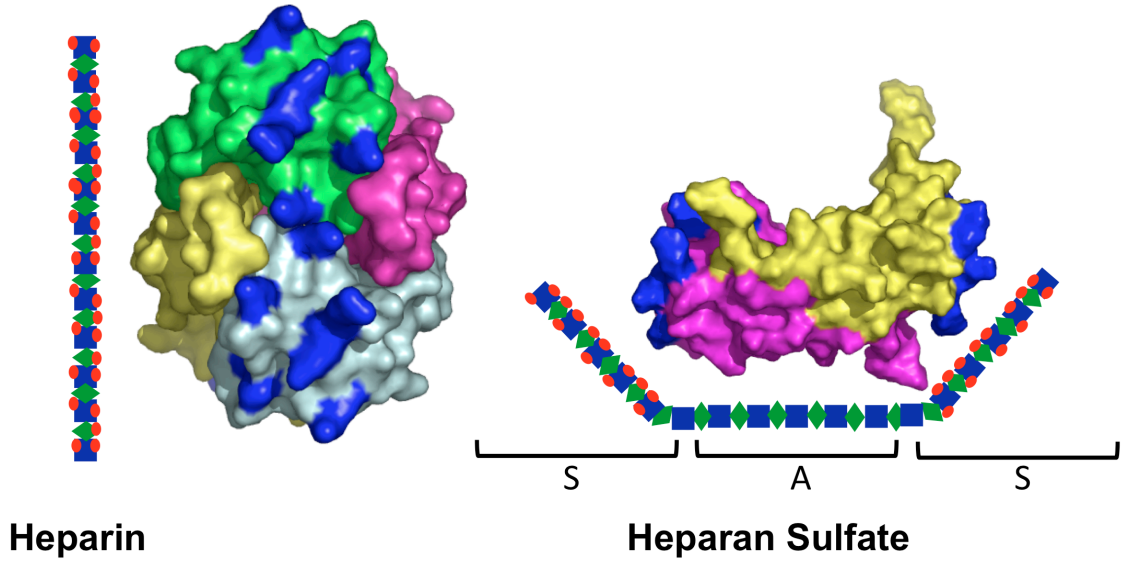

Figure 2.1 Oligomeric forms of MCP-1/CCL2 with Heparin and heparan sulfate. GAG binding epitopes identified previously by our lab [15] are highlighted in blue and illustrate the complimentarity between Heparin and heparan sulfate with different oligomeric structures of MCP-1/CCL2. (*Left*) The tetramer structure of MCP-1/CCL2 (PDB ID IDOL) with a continuous linear band of GAG binding sites identified is depicted adjacent to a highly sulfated (red circles) Heparin chain. (*Right*) Dimer structure of MCP-1/CCL2 (PDB ID IDOM) with basic GAG binding patches (highlighted in blue), spatially separated by a more neutral area of the dimer structure, depicted above a heparan sulfate chain comprised of an unsulfated N-acetylated domain (A) flanked on either side by two sulfated domains (S).

In this method, upon exposure to synchrotron X-ray radiation, protein side chains react with hydroxyl radicals formed from the bulk solvent, resulting in well characterized oxidative modifications of the side chains [21]. Following X-ray exposure, the modifications are then characterized by proteolysis of the protein into peptides followed by mass spectrometry analysis. Since oxidation kinetics for a given side chain type increase with solvent exposure, a comparison of oxidation rates in the presence and absence of GAG should reveal the footprint of the GAG due to protection from solvent. Thus, comparison of free MCP-3/CCL7 to that in complex with GAG should reveal the approximate Heparin binding site.

MCP-3/CCL7 belongs to a subfamily of chemokines, the monocyte chemoattractant proteins, which include MCP-1/CCL2, MCP-2/CCL8, MCP-3/CCL7, and MCP-4/CCL13. All have a high level of sequence similarity ranging from ~60-70% (Figure 2.2) and all bind to the chemokine receptor CCR2. However, MCP-1/CCL2, MCP-3/CCL7, and MCP-4/CCL13 also bind CCR3, MCP-3/CCL7 and MCP-4/CCL13 bind to CCR1, and only MCP-2/CCL8 binds CCR5. Based on the differential expression of receptor binding partners, MCP-3/CCL7 can activate a number of different cell types such as monocytes, eosinophils, basophils, and T cells, making it a very pleiotropic chemokine [24]. In addition, MCP-3/CCL7 is unique among the MCPs because unlike MCP-1/CCL2, MCP-2/CCL8, and MCP-4/CCL13 which form dimers in solution and can oligomerize further in the presence of GAGS [15, 25], MCP-3/CCL7 exists as a monomer at concentrations of up to 20 mg/mL [26] and shows no tendency to form organized oligomers [25]. Our laboratory previously characterized the Heparin binding site on MCP-1/CCL2 and demonstrated the ability of Heparin octasaccharide to induce the tetramer shown in Figure 2.1. As a non-oligomerizing chemokine, we were therefore interested in the differences between MCP-1/CCL2 and MCP-3/CCL7, as their

differences in oligomerization and GAG binding might provide a good example of how two chemokines that share the same receptor are not redundant. Additionally, changes in oxidation rates by radiolytic oxidation would be expected to be purely affected by GAG binding, and not complicated by allosteric changes in the chemokine due to oligomerization, simplifying our first evaluation of the utility of this method.

Using radiolytic footprinting with mass spectrometry, we identified two novel and topographically varied GAG binding sites of MCP-3/CCL7, $Lys^{18}Lys^{19}$ (K18K19) in the 20s loop and $Lys^{65}Lys^{69}Lys^{70}Lys^{75}$ (K4x) along the C-terminal tail. To determine the contribution of these residues to GAG binding and migration activity, alanine mutants were generated and functionally characterized in several biochemical and cell-based assays. The mutants of K18K19 and K4x showed diminished affinity for Heparin in a Heparin binding affinity chromatography assay, compared to WT MCP-3/CCL7. However, they were still able to robustly promote receptor activation as shown by intracellular calcium flux and bare-filter transwell migration assays, suggesting these sites do not overlap with the receptor binding sites.

Together, these data demonstrate the identification of two novel GAG binding interaction sites of MCP-3/CCL7, K18K19 and the K4x C-terminal tail. The separation of the GAG binding and receptor binding sites contrast with MCP-1/CCL2 where they significantly overlap, suggesting different mechanisms for GAG mediated presentation of these two chemokines to their receptors. The results also support the use of radiolytic footprinting as a novel and unbiased approach for the identification of biologically relevant GAG binding sites of chemokines and other cytokines.

Figure 2.2 Sequence alignment of the MCP family with the secondary structure depicted above (cylinder represents α-helix; arrow represents β-strand). Peptides 13-27 and 63-76, which exhibited a decrease in oxidation when GAG was present, are shaded grey in the MCP-3/CCL7 sequence. Within the two peptide regions, basic residues are colored red and residues selected for alanine mutagenesis and follow-up analysis are underlined. Residues previously identified to be important for MCP-1/CCL2 GAG binding are highlighted in red [15].

2.3 Results

2.3.1: Hydroxyl radical footprinting analysis by mass spectrometry of MCP-3/CCL7 in complex with heparin octasaccharide

MCP-3/CCL7, alone or in complex with Heparin octasaccharide, at a 1:5 ratio (chemokine:GAG), was exposed to X-rays from the X-28C beamline for various timepoints ranging from 0 to 20 ms. Irradiated samples were pepsin digested and the peptides were detected by reversed phase liquid chromatography coupled with tandem mass spectrometry (LC-MS/MS). The hydroxyl radical footprinting analysis of MCP-3/CCL7 in complex with GAG, led to the identification of two potential and novel GAG binding epitopes of MCP-3/CCL7, which are presented below.

Oxidatively modified peptides were detected using the software package, ProtMapMS, and the rates of oxidation of peptides over time were compared between MCP-3/CCL7 in complex or alone as has been described previously [27]. Briefly, high flux X-ray exposure of protein for millisecond time points results in modest amounts of oxidative modification of solvent accessible side chains and limits secondary modifications such as backbone cleavage. Proteolytic fragments (modified and

unmodified) are separated by LC-MS/MS and the extent of modification for a select peptide is calculated by integration of peak area, extracted from the total ion current chromatograms, and compared across various exposure times. The fraction of unmodified peptide is quantified as the fraction of unmodified peptide to the total amount of peptide (modified and unmodified). The fraction or percentage of unmodified peptide is then plotted as a function of time (ms) in a pseudo-first order rate reaction to determine the rate of oxidation, using the equation, $y=e^{-kt}$ (where k=rate constant, t=exposure time). Interpretation of the changes in oxidation rates for peptides generated from protein in complex generally correlate with changes in solvent accessibility and protection from modification as a result of binding events or conformational changes. Given that MCP-3/CCL7 is monomeric, the protection from modification when GAG is present is likely due to a binding event, rather than allosteric changes from oligomerization, and is interpreted here as such; the data also shows no evidence of protection due to oligomerization as a CC chemokine, as would be expected for the other MCPs.

Pepsin digest of MCP-3/CCL7 resulted in greater than 90% sequence coverage from replicate experiments. While exposure times were initially collected up to 20 ms, it was found that for the majority of peptides, exposure times greater than 10 ms led to non-linear changes in oxidation probably as a result of over-oxidation and local unfolding of the sample. Therefore, only timepoints of 10 ms or less were used for direct comparison of oxidation rates between MCP-3/CCL7, with and without GAG. From these analyses, 5 peptides were identified in at least two experiments from both MCP-3/CCL7 alone and in complex with GAG, allowing for comparison of the oxidation rates of those peptides (Table 2.1).

Table 2.1 Comparative oxidation rate constants for the MCP-3/CCL7 peptides identified in the presence or absence of the GAG Heparin octasaccharide. The solvent accessibility and oxidized residue(s) for each peptide are also presented in the table. The VADAR computer program was used to calculate solvent accessible surface area ($Å^2$) of MCP-3/CCL7 side chains (PDB ID 1BO0).

Peptide	Sequence	Rate of oxidation (s-1) No GAG	Rate of oxidation (s-1) + GAG
13-27	**YRFINKKIPKQRLES**	36.0 ± 5.1	16.7 ± 2.1
44-59	**KTKLDKEICADPTQKW**	26.8 ± 6.0	19.8 ± 13
51-59	**ICADPTQKW**	3.8 ± 0.8	2.4 ± 0.1
51-62	**ICADPTQKWVQD**	12.8 ± 0.4	12.3 ± 0.6
63-76	**FMKHLDKKTQTPKL**	75 ± 17.8	24.5 ± 14.6

In particular, peptides including residues 13-27 (^{13}YRFINKKIPKQRLES^{27}) and residues 63-76 (^{63}FMKHLDKKTQTPKL^{76}) exhibited a decrease in oxidation rate when GAG was present, suggesting a potential role for residues within these peptides to contribute to GAG binding interactions. Figure 2.3 *A* shows a representative dose response curve for peptide 13-27, in which there is a ~2 fold decrease in oxidation rate when GAG was present. Given that the residues typically involved in GAG binding are Arg, Lys, and His, we first mapped the basic residues within the peptide sequence onto the structure of MCP-3/CCL7, to determine the suitability of the residues to contribute to GAG bindings based on their solvent accessibility. Residues K18 and K19, of peptide 13-27, seemed particularly well suited for GAG binding, considering their solvent exposure as shown in Figure 2.3 *B*. Using the VADAR computer program (PENCE, University of Alberta, Edmonton, Canada) and MCP-3/CCL7 structure (PDB ID 1BO0), the solvent accessible surface area of K18 and K19 was calculated to be 159.8 $Å^2$ and 176.7 $Å^2$, respectively, indicating that these residues are extremely solvent exposed, further supporting their potential to participate in GAG binding. Based on these data, K18 and K19 were further studied to address whether these residues in fact contribute to MCP-3/CCL7:GAG binding interactions, and whether these residues are important for its chemotactic

activity. Additionally, although not probed in the present studies, R14 in the peptide 13-27 is another attractive candidate, with a solvent accessible surface area of 178.1Å^2, and will also be explored for possible contributions to GAG binding.

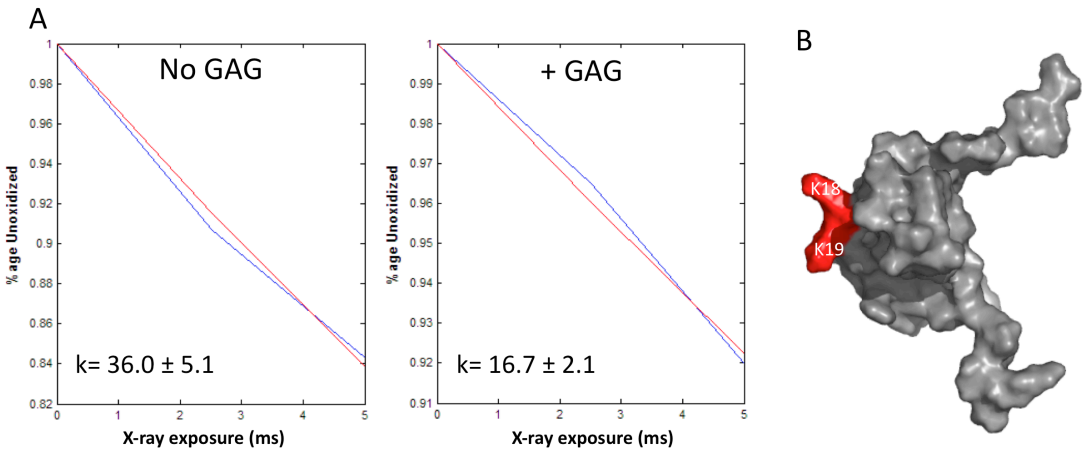

Figure 2.3 (A) Representative dose response curve for the oxidation of the peptide 13-27 in the presence (right) or absence of GAG (left), with average rate constants from triplicate experiments noted (± SD). The blue line shows the percentage of unoxidized peptide for 0, 2.5 and 5 ms exposure times and the red line is a linear fit to the data. (B) Surface model of MCP-3/CCL7 with residues K18 and K19 highlighted in red, using Pymol

Although there was some variability in oxidation rate, the C-terminal peptide (^{63}FMKHLDKKTQTPKL^{76}) consistently showed a decreased rate of oxidation in the presence of GAG compared to MCP-3/CCL7 alone (Figure 2.4 *A*). The variability in the rate constants may be due to the conformational flexibility of the unstructured C-terminal end (amino acids 69-76), which would allow it to adopt multiple conformations. Further suggesting that this peptide could be a genuine binding site for GAGs, it is rich in solvent exposed Lys and His residues including K65, H66, K69, K70, K75, which have solvent accessibilities of 140.4 Å^2, 94.6 Å^2, 124.9 Å^2, 162.8 Å^2, and 147.1 Å^2 (Figure 2.4 B). This epitope represents a particularly interesting potential binding site for GAGs, because it is unlikely to overlap with the receptor binding site which has interesting mechanistic

implications described later [28]. Furthermore, the distance and orientation of this epitope relative to the K18/K19 epitope in peptide 13-27, suggests that they could comprise a contiguous binding site.

In contrast to the above, peptides that were also identified, but did not reveal any significant change in the rate of oxidation include peptide 51-59 and peptide 51-62. Based on the structure of MCP-3/CCL7, these regions are mostly buried, supporting the radiolytic data that they would unlikely contribute to GAG interactions.

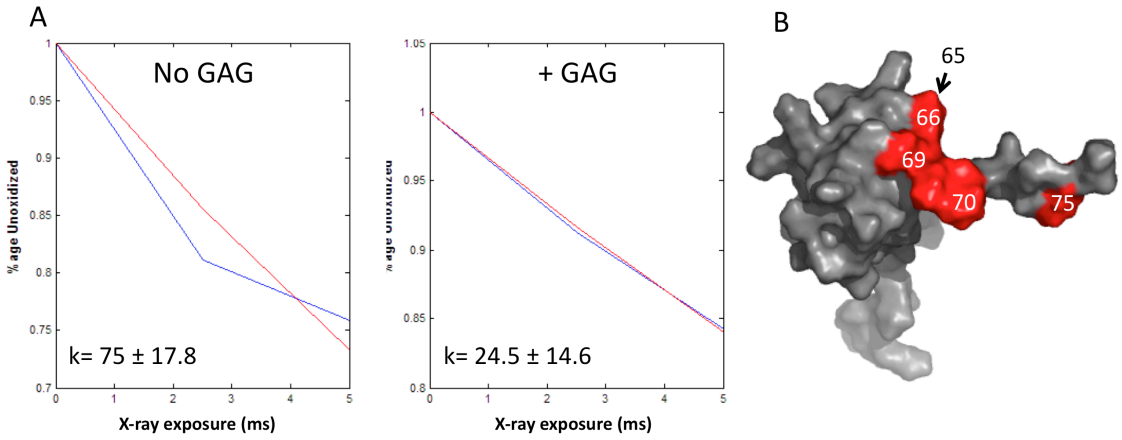

Figure 2.4 (A) Representative dose response curve for the oxidation of the peptide 63-76 in the presence (right) or absence of GAG (left), with the average rate constants from duplicate experiments noted (± SD). The blue line shows the percentage unoxidized of the peptide for 0, 2.5 and 5 ms exposure times and the red line is a linear fit to the data. (B) Surface model of MCP-3 with residues K65, H66, K69, K70, and K75 highlighted in red, generated with Pymol.

2.3.2: Heparin binding assays of MCP-3/CCL7 mutants confirm the contribution of K18K19 and the C-terminal tail K4x lysines to GAG binding

The hydroxyl radical footprinting data suggested a potential role of K18K19 and K4x C-terminal lysines of MCP-3/CCL7 for Heparin binding, based on the reduced oxidation rate of these regions in the presence of saturating amounts of GAG. To validate the contribution of these sites to GAG binding, we generated several alanine mutants and tested them in GAG binding affinity assays. A commonly used method to

determine the relative "affinity" of chemokines or mutants for GAGs is to determine the amount of salt needed for elution from a Heparin sepharose column, where Heparin serves as a model GAG. Alanine mutants were therefore subjected to this assay and the concentration of NaCl required to elute the mutant chemokines from the Heparin resin was compared to the concentration needed to elute WT chemokine (Table 2.2). The difference between mutant and WT ($\Delta[NaCl]_H$) is plotted in Figure 2.5, where larger values suggest greater destabilization of the GAG interaction from the mutation. WT MCP-1/CCL2 and the previously identified GAG binding deficient mutant, MCP-1 /CCL2 R18AK19A [15], were used as controls for comparison of WT and mutant MCP-3/CCL7. Similar to the MCP-1/CCL2 R18AK19A mutant, the MCP-3/CCL7 GAG mutants all displayed a decreased affinity for GAG (Table 2.2). While MCP-3/CCL7 K18AK19A seemed to exhibit the largest effect on Heparin binding, with a $\Delta[NaCl]_H$ of 204 mM, the C-terminal tail residues also affected Heparin binding, with $\Delta[NaCl]_H$ values ranging from ~70-100 mM depending on the number of alanine mutations introduced. For the C-terminal region, each alanine mutation had an additive effect, in that the $\Delta[NaCl]_H$ of 4x K65K69K70K75 > 3x K65K69K70K > 2x K69K70 > single mutations (Figure 2.5 and Table 2.2, data not shown for point mutants). Often, these measurements are done in parallel with determining the amount of salt required to elute mutants from a non-specific S-sepharose column ($\Delta[NaCl]_S$) and compared with the elution from the Heparin sepharose column. This value, $\Delta\Delta[NaCl]$, is often interpreted as a measure of specificity of the protein:Heparin interaction. These numbers are included in Table 2.2 for completeness; however, our opinion is that they can be meaningless values because of differences in variables such as the density of binding sites on the resins. Nevertheless, $\Delta[NaCl]_S$ mirrors the $\Delta[NaCl]_H$ confirming the contribution of K18/K19 and the C-terminal

domain. These epitopes have not been previously associated with the MCP-3/CCL7 GAG interactions, and therefore present new recognition sites.

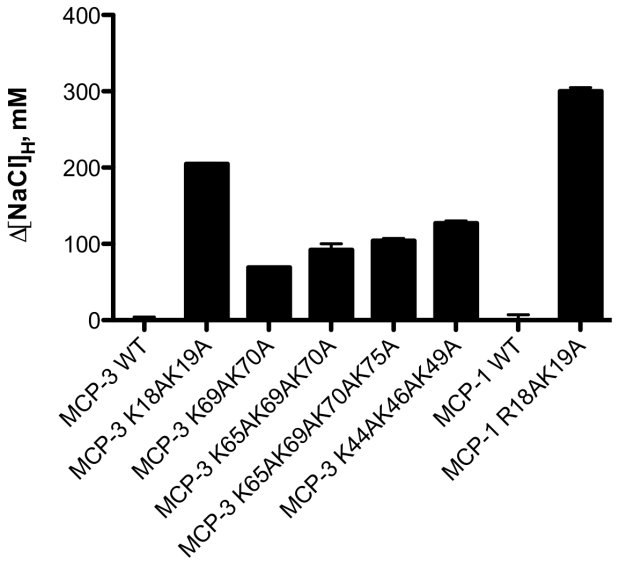

Figure 2.5 Heparin sepharose chromatography results for MCP-3/CCL7, MCP-1/CCL2 and mutants. The difference in the concentration of NaCl (mM) required to elute mutant chemokine from heparin sepharose, compared to WT chemokine, plotted as the average of three experiments (±SD).

Table 2.2 Summary of Heparin and sepharose affinity chromatography data for MCP-3/CCL7, MCP-1/CCL2, and mutants. The concentration of NaCl (mM) required to elute mutant chemokine from either Heparin or sepharose affinity chromatography is compared to WT chemokine.

WT and mutant proteins	$[NaCl]_H$	$\Delta[NaCl]_H$	$[NaCl]_S$	$\Delta[NaCl]_S$	$\Delta\Delta[NaCl]$
MCP-3	733.3		678.7		
MCP-3 K18AK19A	528.7	204.7	464.0	214.7	-10.0
MCP-3 K44AK46AK49A	606.0	127.3	531.0	147.7	-20.3
MCP-3 K46AK69A	620.0	113.3	556.0	122.7	-9.3
MCP-3 K69K70A	664.0	69.3	613.0	65.7	3.7
MCP-3 K65AK69AK70A	641.3	92.0	590.0	88.7	3.3
MCP-3 K65AK69AK70AK75A	629.3	104.0	582.0	96.7	7.3
MCP-1	747.0		592.0		
MCP-1 R18AK19A	446.7	300.3	331.0	261.0	39.3

2.3.3: Receptor activation measured by calcium flux and chemotaxis across bare filters suggest that the K18K19 and K4x epitopes contribute little to receptor binding

To unequivocally establish the biological relevance of a GAG binding motif to the function of a chemokine, *in vivo* cellular recruitment assays comparing the WT and mutant chemokine, are required. However, it is important to first demonstrate what effect the mutations have on the ability to bind and activate the receptor. If receptor activation is unaffected by the mutations, then effects observed on migration *in vivo* can be interpreted as a consequence of impaired GAG binding. If the mutations also significantly affect receptor binding, then the results may be due to a convolution of GAG and receptor binding and the role of GAG binding cannot be cleanly defined.

To test their ability to bind and activate receptor, the alanine mutants K18AK19A and K4xA were evaluated using a calcium flux assay. These assays were done using L1.2 cells, a pre B lymphoma cell line, expressing the receptor CCR1 or CCR2. In both cases, the mutants elicited a robust calcium response similar to WT MCP-3/CCL7 over a range of concentrations (125 nM - 2 μM) in CCR1 expressing cells (Figure 2.6). In addition, MCP-3/CCL7 and mutants mediated very similar time-dependent responses, for all three concentrations of ligand tested, suggesting a high affinity interaction between MCP-3/CCL7 and CCR1, as has been shown previously [29]. Calcium flux of CCR2 expressing cells, mediated by MCP-3/CCL7 and mutants, were also similar (Figure 2.6), suggesting that for both receptors, the two GAG epitopes do not overlap significantly with the receptor.

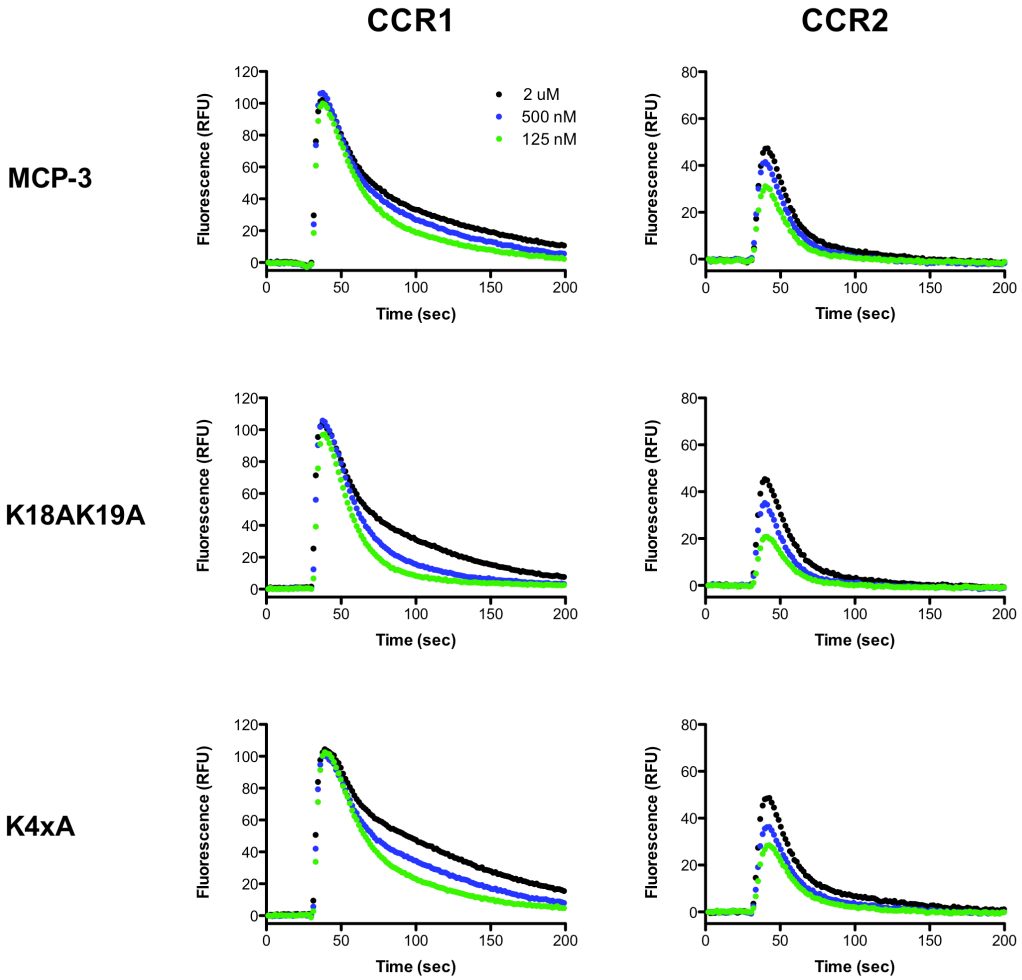

Figure 2.6 MCP-3/CCL7 or mutant mediated intracellular calcium mobilization of CCR1 (*left*) and CCR2 (*right*) expressing L1.2 cells. The calcium flux response upon addition of 2 μM (black), 500 nM (blue), or 125 nM (green) chemokine is plotted over time.

Additionally, the mutants were tested in an *in vitro* bare filter chemotaxis assay. In this Boyden chamber assay, one places chemokine in the bottom well and L1.2 cells in the upper well, separated by a porous filter. Due to the simplicity of the setup, this assay should not require GAGs (unless there is some requirement for interactions on the migrating cells themselves) and thus reflects how well the mutants activate the receptor. As for the calcium flux assay, the mutants were found to elicit a robust migration response of L1.2 cells expressing CCR2 (Figure 2.7). MCP-3/CCL7 induced migration

of CCR2 expressing cells with a maximal migration of ~22% of the total cells at 50 nM chemokine. K18AK19A and K4xA exhibited a slight decrease in potency (~2-fold) and K4xA exhibited a slight loss in efficacy (~17% max migration compared to ~22% max migration of WT). These changes may be due to small effects of the mutations on receptor binding, but are minimal. Thus the mutants are appropriate for testing *in vivo*; in fact, these minor changes are less than the perturbations observed by the R18A/K19A mutant of MCP-1/CCL2, which showed a 20-fold shift in potency.

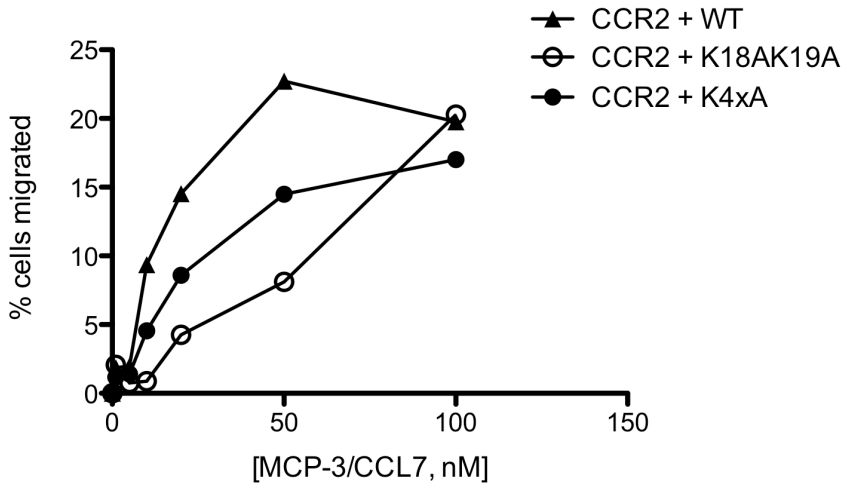

Figure 2.7 MCP-3/CCL7 or mutant mediated migration of CCR2 expressing cells in a bare filter chemotaxis assay showing the % of cells migrated after 2 h in the presence of varying concentrations of chemokine.

2.4 Discussion

While the ability of chemokines to bind and activate their receptors is well recognized as an important component of their functional activity, their interaction with GAGs has only recently been recognized as a critical step in leukocyte recruitment. The

chemokine:GAG interaction is considered especially important for chemokine localization on endothelial surfaces and formation of chemokine gradients to provide directional cues for migrating cells. Presently, a number of GAG-binding deficient chemokine variants have been shown to be ineffective in inducing cell migration *in vivo,* compared to WT chemokine [3-5, 12], supporting the importance of this interaction for biological activity. However, two complementary studies have also demonstrated the importance of GAG binding in transcytosis of IL-8/CCL8 in order to get the chemokine in contact with leukocytes on the correct side of the endothelial barrier [1, 30]. Furthermore, GAG interactions have been reported to be important for RANTES/CCL5 induced apoptosis, and T cell activation [2, 31, 32]. Therefore, chemokine:GAG interactions may have broader significance than currently appreciated. While the molecular details of these interactions remain poorly understood, generation of GAG binding deficient variants has been enormously useful in defining the roles of these interactions for *in vivo* function.

Of the approximately 50 chemokines and 20 receptors that comprise the chemokine network, there is a great deal of overlap with respect to binding partners, where chemokines can bind and activate multiple receptors and vice versa. Although seemingly redundant, we believe that there is a great deal of "functional selectivity" whereby binding of each chemokine to a single receptor activates a different set of signaling pathways, and/or differentially interact with GAGs, thereby defining the cells and tissues where they engage their receptors and signal. Chemokines also possess a highly conserved tertiary structure, but can adopt a variety of oligomeric forms, and emerging data suggest that these oligomeric forms also provide "functional selectivity" where monomers activate some receptor-dependent signaling pathways while oligomers activate others [33]. Of relevance to this study, the various oligomeric structures add

diversity to the potential determinants of GAG binding for a chemokine, depending on the structures formed [19]. However, it has been clearly demonstrated using engineered monomeric chemokine variants, that the monomer is sufficient for binding receptor and inducing cell migration [3, 34, 35]. For example, the chemokine MCP-1/CCL2 readily oligomerizes in solution at low concentrations (nM-μM), however, mutation of proline at position 8 to an Alanine (P8A) abrogates oligomerization, causing MCP-1/CCL2 P8A to be monomeric at millimolar concentrations, although receptor binding to CCR2 is unaffected [34]. In contrast, chemokines such as MCP-3/CCL7 and I-309/CCL11 have been shown to only exist as monomers [26, 36]. In the case of MCP-3/CCL7, it contains a Ser at position 8, unlike MCP-1/CCL2, MCP-2/CCL8, and MCP-4/CCL13, which have a Pro at the corresponding position that supports oligomeric formation. Nevertheless, MCP-3/CCL7 and I-309/CCL11 are still able to promote robust migration *in vitro* and *in vivo* as monomers [3, 5], supporting a biological function for these chemokines. Together, chemokines have a plethora of mechanisms that can contribute to their overall activity (e.g. interactions with chemokines, receptors, and GAGs), although the functional consequences of these complex interactions, and how they contribute to the biological role of individual chemokines, is still not well understood. Therefore, there has been interest in addressing the GAG binding determinants of chemokines, in an attempt to delineate the contribution to specificity of chemokine activity that these interactions support.

In this study, we present an unbiased approach for identifying potential GAG binding sites of the monomeric chemokine, MCP-3/CCL7, through the novel use of hydroxyl radical footprinting with mass spectrometry. The mass spectrometry data provided a global footprint of chemokine bound to Heparin octasaccharide and these findings were modeled onto the known structure of MCP-3/CCL7. MCP-3/CCL7 was

specifically chosen for these studies because it is monomeric; therefore, changes in oxidation when GAG was present could be attributed to GAG binding as opposed to oligomerization. Specific sites were then selected for follow-up investigation by more traditional approaches, including Heparin affinity chromatography and *in vitro* chemokine activity assays, in order to determine the extent of contribution of these regions to the chemotactic activity of MCP-3/CCL7. In particular, two peptides covering residues 13-27 and 63-76 were identified as having decreased rates of oxidation when GAG was present, thereby likely encompassing GAG-binding epitopes. Further investigation localized the binding sites to K18K19 and the Lys rich C-terminal tail motif K4x (Figure 2.8). These sites appeared to be highly suitable for GAG binding, based on their relative orientation in the structure, their basic nature, as well as their largely solvent accessible surface area. Together, these data support the identification of a spatially diverse GAG-binding epitope for MCP-3/CCL7, which deviates from the BBxB linear motif in the 40s loop region identified for some chemokines [7-10].

In order to confirm the relevance of chemokine GAG recognition sites to chemokine activity, *in vivo* recruitment assays are typically performed with the GAG-binding deficient mutants. However, the appropriate interpretation of such findings is reliant on knowing what effects the introduced mutations have on receptor activation. For example, the ITAC/CXCL11 GAG variant mutant (^{5}AAGA^{8}) in the N-terminal region was found to have a dramatic effect on receptor binding, displaying a 225-fold loss in affinity compared to WT [12]. However, the 50s region (^{57}ASAQAA^{62}) and Lys^{17} mutation of ITAC/CXCL11 was found to contribute little to receptor binding. Therefore, the interpretation of the *in vivo* results, showing the decreased ability of ^{57}ASAQAA^{62} and Lys^{17} to recruit cells in a peritoneal recruitment assay, can be attributed to the deficiency in binding GAG, whereas the decrease ^{5}AAGA^{8} cellular recruitment is likely resulting

from a combination of perturbations of receptor binding and activation in addition to GAG binding. Since MCP-3/CCL7 can bind CCR1, CCR2, and CCR3, we tested the effect of mutations on receptor activation using an intracellular calcium flux assay. We found that the mutants induced intracellular calcium flux of CCR1 and CCR2 expressing cells, similar to MCP-3/CCL7 WT, suggesting that K18K19 and the C-terminal tail do not contribute much to receptor activation. Additionally, mutants induced a robust migration response in a bare filter chemotaxis assay that was comparable to that of MCP-3/CCL7 WT (< 3 fold difference in potency and efficacy), further exemplifying that these regions are important for GAG binding, but do not contribute much to receptor activation.

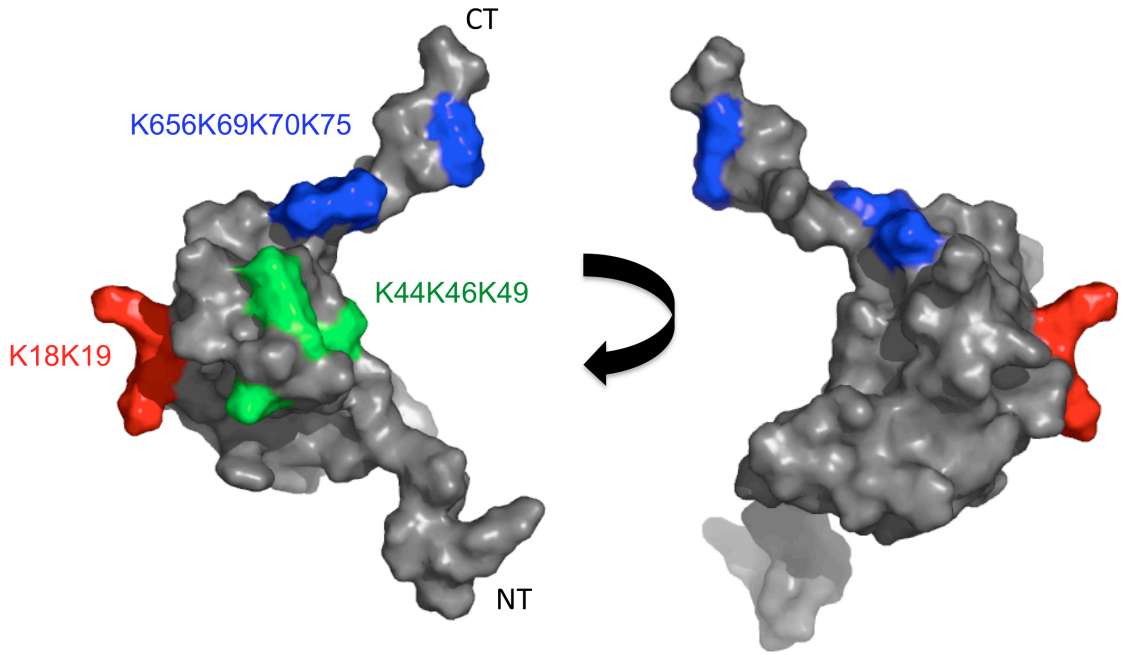

Figure 2.8 Potential GAG binding epitopes identified by radiolytic footprinting mapped (red and blue) onto the surface of MCP-3/CCL7 (PDB ID 1BO0). Peptides containing the residues K18K19 as well as K65K69K70K75 in the C-terminal tail, both exhibited a decreased oxidation rate when irradiated in the presence of GAG. A previously identified GAG binding motif of MCP-3/CCL7 is also shown in green [5], demonstrating the spatial distribution of potential GAG-binding sites. Generated with Pymol.

While the *in vivo* experiments have not yet been carried out, the *in vitro* data strongly suggest that the mutants will have a pronounced decrease in chemotactic activity compared to WT protein *in vivo*, corresponding to their decreased ability to bind GAG.

It is important to note that in addition to the present work, a GAG binding epitope of MCP-3/CCL7 was previously identified in the 40s loop region by Ali *et al*. [5] (Figure 2.8). In that study, the authors focused entirely on the BBxB linear motif present in the 40s loop. Mutational analysis of K44K46K49 in this region showed decreased GAG binding through Heparin sepharose binding assays, although receptor affinity and activation was maintained for CCR1, CCR2 and CCR3. More importantly, injection of the mutants in an *in vivo* air pouch assay showed decreased chemotactic activity, compared to MCP-3/CCL7 WT, supporting the function of this epitope in MCP-3/CCL7 activity. Unfortunately, mass spectrometry analysis of peptides along the 40s loop region of MCP-3/CCL7 were inconclusive, displaying varying levels of oxidation that could not be confidently interpreted with this approach. Nevertheless, the GAG binding sites presented herein were found to mediate an effect on MCP-3/CCL7 activity, at least if not more significantly as the K44K46K49 variant, suggesting that MCP-3/CCL7 has a diverse set of GAG recognition sites. Furthermore, this work highlights the importance of using a global and unbiased approach for determining Heparin binding sites, coupled with traditional chemokine:GAG characterization methods, in order to obtain the most comprehensive analysis possible. It is also important to recognize that the results obtained from the hydroxyl radical footprinting experiments in this study were all carried out using Heparin octasaccharide as the select GAG. However, it is quite possible that some recognition sites may be favored or alternative sites might be utilized in the presence of other GAGs, which could reflect cell type dependence and tissue specificity for regulating chemokine activity.

Overall, we have identified two spatially distinct GAG binding motifs of MCP-3/CCL7: K18K19 and the Lys rich C-terminal tail. We established that mutation of the Lys residues in these motifs resulted in disrupted Heparin binding, although receptor binding remained unaffected. With the GAG binding epitopes of MCP-3/CCL7 being independent from receptor binding, one possible model for MCP-3/CCL7 induced cell migration could involve simultaneous engagement of receptor and GAG through the monomeric forms of this chemokine (illustrated in Figure 2.9, *right*).

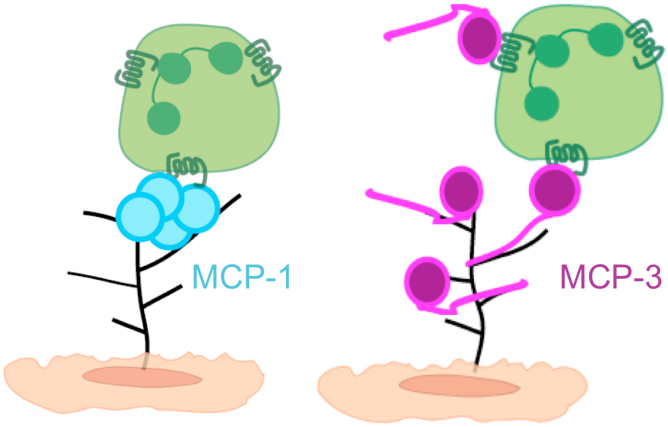

Figure 2.9 Model of monomeric MCP-3/CCL7 (*right*) and tetrameric MCP-1/CCL2 (*left*) simultaneously binding to GAG and chemokine receptor. Since MCP-1/CCL2 receptor binding sites overlap with GAG binding sites, tetrameric MCP-1/CCL2 could allow presentation by GAG on some subunits while concurrently binding to receptor with other subunits. By contrast, since MCP-3/CCL7 has separate GAG and receptor binding epitopes, it could simultaneously engage receptor and GAGs, which is consistent with the fact that it does not oligomerize.

This model contrasts with other chemokines such as MCP-1/CCL2 where there is considerable overlap of the receptor and GAG binding sites, necessitating oligomerization for simultaneous interaction of the receptor through some subunits of the oligomer and interactions with GAGs through other subunits (Figure 2.9, *left*). Finally, it

is possible that the chemokine GAG binding deficient variants can be used to antagonize WT chemokine function *in vivo*, as has been shown for variants of MCP-3/CCL7, SDF-1α/CXCL12 and CCL5/RANTES [5, 37-39].

2.5 Ongoing Work/Immediate Future Directions

While substantial characterization of the MCP-3/CCL7 GAG mutants has already been presented above, three remaining experiments are necessary to complete this work, including radiolabeled ligand competition binding assays to determine affinities of the mutants for receptors CCR1, CCR2 and CCR3, and *in vivo* cellular recruitment assays to unequivocally demonstrate that the GAG mutations affect recruitment *in vivo*. The ligand competition assays are straightforward and routine in our lab. Furthermore, based on the ability of the MCP-3/CCL7 mutants to flux calcium and promote migration *in vitro* similar to WT MCP-3/CCL7, it is unlikely that the binding affinities of MCP-3/CCL7 mutants are significantly affected; nevertheless we need the data for completeness of the paper. Secondly, as a prelude to the *in vivo* studies, we will perform *in vitro* transendothelial migration (TEM) assays with the MCP-3/CCL7 GAG binding deficient mutants since TEM assays are often used to examine specific steps in the migration and can be predictive of function *in vivo*. For example, migration across endothelial cell layers provides an indirect test of chemokine transcytosis and or establishment of a gradient across the endothelial cells, which is thought to require GAGs [1, 30]. Due to likely requirement of GAG binding in TEM assays, we expect the MCP-3/CCL7 mutants to exhibit decreased migration in comparison to WT. Finally, the most important remaining experiments are the *in vivo* cellular recruitment assays of the mutants. Since these experiments require extensive optimization and expertise, we

have formed a collaboration with Dr. Mauro Teixeira (Minas Gerais, Brazil) who is an expert in performing these studies. These data will then form the basis of a first author paper for the dissertation author.

2.6 Materials and Methods

2.6.1: Chemokine expression and purification

MCP-1/CCL2 and MCP-3/CCL7 were subcloned into the pHUE construct (kindly provided by Rohan T. Baker) and expressed as a His-ubiquitin fusion protein as described previously [40]. MCP-3/CCL7 was solubly expressed in BL21(DE3)pLysS *Escherichia coli* cells grown at 30 °C (see Appendix I, protocol A). Cells were induced with isopropyl-D-1-thiogalactopyranoside (IPTG) at an OD ~0.4 and harvested after 3 h. Protein was purified with Ni-Sepharose affinity chromatography using an AKTA FPLC (GE Healthcare, Piscataway, NJ). The Ub-MCP-3/CCL7 fusion was passed over a reversed-phase high-pressure liquid chromatography (HPLC) C18 semi-prep column and then lyophilized and stored at -80 °C. To obtain MCP-3/CCL7, the fusion protein was cleaved with 1:100 (chemokine:ubiquitinase, molar ratio) ubiquitinase for 3 h at room temperature, passed over Ni-nitrilotriacetic acid affinity chromatography (Ni-NTA) to remove unwanted cleavage products followed by a final HPLC purification step. Protein was lyophilized and stored at -80 °C. Protein identity and purity was confirmed by electrospray-ionization mass spectrometry. MCP-1/CCL2 was insolubly expressed as inclusion bodies in BL21(DE3)pLysS *Escherichia coli* cells grown at 37 °C, induced with IPTG at an OD ~0.6-0.8 and grown for 3 h before being harvested (see Appendix I, protocol B). Inclusion body pellets were purified by Ni-NTA chromatography, refolded

with Hampton Fold-it Buffer #11 (FoldIt Screen, Hampton Research, Aliso Viejo, CA), concentrated with a 10 kD MWCO filter followed by dialysis into ubiquitinase cleavage buffer (20 mM Tris, pH 8, 200 mM NaCl). The MCP-1/CCL2 fusion was then cleaved with ubiquitinase and purified in the same manner as MCP-3/CCL7. Alanine mutants were generated by QuikChange site-directed mutagenesis (Stratagene) and mutants were purified in the same manner as the wild-type protein.

2.6.2: Radiolysis

MCP-3/CCL7 was prepared with 10 mM Na-cacodylate buffer (pH 7.2) to a final concentration of 10 μM. Using a flow setup, samples were exposed to the X-28C beamline of the National Synchrotron Light Source (Brookhaven National Laboratory, Upton, NY) for 0, 2.5, 5, and 10 ms in the presence or absence of Heparin octasaccharide (Neoparin, San Leandro, CA) at a 1:5 molar ratio (chemokine:Heparin) with beam currents ranging from 210 to 253 mA. All experiments were carried out at ambient temperature. Following exposure, free hydroxyl radicals were quenched with 10 mM Methionine-NH_2 and the samples were stored at -80 °C.

2.6.3: Proteolytic digestion and mass spectrometry

Irradiated samples were diluted 5-fold in 25 mM Ammonium Bicarbonate buffer, pH 8.2, reduced with DTT to a final concentration of 10.5 mM for 20 min at 60 °C, and alkylated with iodoacetamide to a final concentration of 100 mM for 30 min at room temperature in the dark. Samples were then acidified with 1 M HCl to pH ~2 and digested with freshly prepared porcine pepsin (Worthington, Lakewood, NJ) in 0.1% trifluoroacetic acid (TFA) to a 1:5 ratio (w/w) for pepsin to chemokine for 24 h at RT and then frozen at -20 °C to terminate the pepsin reaction. To remove excess salts, digested

samples were passed over 50 mg Sep-pak C18 cartridges (Waters Corp, Milford, MA), washed with 1% acetic acid (HAC), eluted with 80% acetonitrile (ACN)/0.1% HAC and lyophilized. For mass spectrometric analysis, ~ 1 pmol of digest was loaded onto a Dionex high pressure reversed phase liquid chromatography system (Sunnyvale, CA). Peptides were separated with a 15 cm x 75 µm (3 µm, 100 Å) Acclaim PepMap100 C18 column (Dionex) using a linear gradient of 5-50% B over 60 min (*Buffer A*: 20% ACN/0.1% formic acid (FA); *Buffer B*: 80% ACN/0.1% FA). Mass spectrometry data was acquired in the positive mode on a LTQ-FT mass spectrometer (Thermo Fisher Scientific, CA) equipped with a nanospray ion source using a spray voltage of 2 kV. Mass spectra were collected in a data dependent manner where the eight most abundant peptide ions were selected and subsequently fragmented by collision-induced dissociation to produce MS/MS ion fragmentation. Data was processed using the ProtMapMS software package [27], and in some cases, manually validated using XCalibur (ThermoFinnigan) by integration of peak area extracted from chromatograms of the total ion current, and compared across exposure times.

2.6.4: In vitro heparin binding assays

150 µg of WT or mutant protein was loaded onto either a 1 mL HiTrap Heparin HP column (GE Healthcare) or a 1 mL HiTrap SP HP column (GE Healthcare) connected to an AKTA FPLC system (See Appendix I, protocol D). Samples were eluted over a linear gradient of 0-2 M NaCl in 10 mM Na-Phosphate, pH 7.2 at a flow rate of 0.5 mL/min. The amount of NaCl required to elute protein was determined by the % B required to elute each sample; protein elution was monitored by absorbance at 280 nm. The assay was run at least twice for each protein. To determine the effects of

alanine mutations on Heparin binding, the difference in the concentration of NaCl required to elute WT versus mutant protein was calculated according to Eq. 1.

$$\Delta[NaCl]_H = [NaCl]_{H,WT} - [NaCl]_{H,mutant} \qquad \text{(Eq. 1)}$$

The difference in the concentration of NaCl required to elute WT versus mutant protein from S-Sepharose resin was also calculated (Eq. 2).

$$\Delta[NaCl]_S = [NaCl]_{S,WT} - [NaCl]_{S,mutant} \qquad \text{(Eq. 2)}$$

The specificity index was then calculated by Eq. 3, although as described in the text, we do not put much weight in these numbers.

$$\Delta\Delta[NaCl] = \Delta[NaCl]_H - \Delta[NaCl]_S \qquad \text{(Eq.3)}$$

2.6.5: Generation of stable cell lines

Murine pre-B lymphoma L1.2 cells were kindly provided by B. Zabel and maintained in RPMI-1640-Glutamax (Invitrogen) supplemented with 10% fetal bovine serum (FBS), 1% Non-essential amino acids, 1% Na-pyruvate, 0.1% beta-mercaptoethanol at 37 °C/5%CO_2 at a density of 0.5 – 4 x 10^6 cells/mL. L1.2 cells stably expressing CCR1 and CCR2 were generated by electroporation of 10 µg of pcDNA3.1-CCR1 or pcDNA3.1-CCR2 plasmid into 1 x 10^7 cells (see Appendix I, protocol C). Two days after electroporation, cells were selected with 0.7 mg/mL of G418 and clonal populations of high expressers were identified following limiting dilution. Surface expression of CCR1 and CCR2 were detected by mAb staining and flow cytometry analysis (see below). All cell culture materials were obtained from Invitrogen (Carlsbad, CA).

2.6.6: Flow cytometry

Chemokine receptor expression of L1.2 stable lines were assessed by flow cytometry using mAb against CCR1, CCR2, and CCR3 conjugated to PE (R & D,

Minneapolis, MN) or PE-IgG_{2A} or PE-IgG_{2B} isotype controls (R & D) according to manufacturer specifications (See Appendix 1, Protocol P). Briefly, cells were resuspended in 0.5% bovine serum albumin (BSA) in PBS buffer, stained with antibody for 20 min on ice, and washed three times with 0.5% BSA-PBS buffer. Flow data was collected on a BD FACSCaliber Cytometer and analyzed with FlowJo software (Tree Star, Inc., Ashland, OR).

2.6.7: Intracellular calcium flux assays

MCP-3/CCL7 mediated calcium flux of L1.2-CCR1 and L1.2-CCR2 cell lines were measured using the FLIPR Calcium 4 assay kit (Molecular Devices, Sunnyvale, CA) (see Appendix I, protocol E). Cells resuspended in assay buffer (1 x Hanks balanced salt solution, 20 mM HEPES, pH 7.4, 0.1% BSA) were seeded onto a 96 well plate with 150,000 cells/well and incubated with 100 µL of calcium 4 dye for at least 1 h at 37°C/5% CO_2. WT MCP-3/CCL7 or mutant was prepared at varying concentrations, and intracellular calcium flux was measured upon addition of chemokine to dye-loaded cells using a FlexStation (Molecular Devices). Experiments were performed in triplicate.

2.6.8: In vitro chemotaxis assays

Chemotaxis assays were performed using 24-well transwell plates with 5 um pore size filter inserts (Corning, Corning, NY) (see Appendix I, protocol F). WT MCP-3/CCL7 and mutant protein stocks were freshly prepared from lyophilized powder in 10 mM HEPES, pH 7.2 and diluted into the bottom well at varying concentrations (e.g. 0.1-500 nM) using RPMI-1640 + 10% FBS in a total volume of 600 µL. L1.2 cells were resuspended at a concentration of 2.5 x 10^6 cells/mL in RPMI-1640 + 10% FBS and 100 uL of cells were distributed into the upper part of each well. Wells with no chemokine

were used to account for background migration and wells with cells only (no filter) were used to quantify maximal migration. Cells were allowed to migrate for 2 h at 37°C/5%CO_2 after which time cells that migrated to the bottom chamber were counted on a BD FACSCaliber cytometer by counting the number of events in 30 s. Migration was normalized to background migration (no chemokine added) and plotted as the percent of cell migrated to the total number of cells possible (no filter) (± SD). Transendothelial chemotaxis assays were performed in a similar manner to bare filter chemotaxis assays with the exception that filters were first coated with fibronectin (25 μg/mL), then seeded with human umbilical vein endothelial cells (HUVEC) cells (100,000 cells/filter), and allowed to grow for 2 days prior to migration assays with L1.2 cells.

2.7 Acknowledgements

Chapter 2 is currently being prepared for the submission of publication of the material. The following are the contributing authors: Salanga CL, Gupta S, Chance MR, Handel TM. The dissertation author is the primary investigator and author of this paper.

2.8 References

1. Wang, L., M. Fuster, P. Sriramarao, and J.D. Esko, *Endothelial heparan sulfate deficiency impairs L-selectin- and chemokine-mediated neutrophil trafficking during inflammatory responses.* Nat Immunol, 2005. **6**(9): p. 902-10.

2. Roscic-Mrkic, B., M. Fischer, C. Leemann, A. Manrique, C.J. Gordon, J.P. Moore, A.E. Proudfoot, and A. Trkola, *RANTES (CCL5) uses the proteoglycan CD44 as an auxiliary receptor to mediate cellular activation signals and HIV-1 enhancement.* Blood, 2003. **102**(4): p. 1169-77.

3. Proudfoot, A.E., T.M. Handel, Z. Johnson, E.K. Lau, P. LiWang, I. Clark-Lewis, F. Borlat, T.N. Wells, and M.H. Kosco-Vilbois, *Glycosaminoglycan binding and oligomerization are essential for the in vivo activity of certain chemokines.* Proc Natl Acad Sci U S A, 2003. **100**(4): p. 1885-90.

4. Peterson, F.C., E.S. Elgin, T.J. Nelson, F. Zhang, T.J. Hoeger, R.J. Linhardt, and B.F. Volkman, *Identification and characterization of a glycosaminoglycan recognition element of the C chemokine lymphotactin.* J Biol Chem, 2004. **279**(13): p. 12598-604.

5. Ali, S., H. Robertson, J.H. Wain, J.D. Isaacs, G. Malik, and J.A. Kirby, *A non-glycosaminoglycan-binding variant of CC chemokine ligand 7 (monocyte chemoattractant protein-3) antagonizes chemokine-mediated inflammation.* J Immunol, 2005. **175**(2): p. 1257-66.

6. O'Boyle, G., P. Mellor, J.A. Kirby, and S. Ali, *Anti-inflammatory therapy by intravenous delivery of non-heparan sulfate-binding CXCL12.* The FASEB Journal, 2009. **23**(11): p. 3906-16.

7. Graham, G.J., P.C. Wilkinson, R.J. Nibbs, S. Lowe, S.O. Kolset, A. Parker, M.G. Freshney, M.L. Tsang, and I.B. Pragnell, *Uncoupling of stem cell inhibition from monocyte chemoattraction in MIP-1alpha by mutagenesis of the proteoglycan binding site.* EMBO J, 1996. **15**(23): p. 6506-15.

8. Koopmann, W. and M.S. Krangel, *Identification of a glycosaminoglycan-binding site in chemokine macrophage inflammatory protein-1alpha.* J Biol Chem, 1997. **272**(15): p. 10103-9.

9. Koopmann, W., C. Ediriwickrema, and M.S. Krangel, *Structure and function of the glycosaminoglycan binding site of chemokine macrophage-inflammatory protein-1 beta.* J Immunol, 1999. **163**(4): p. 2120-7.

10. Proudfoot, A.E., S. Fritchley, F. Borlat, J.P. Shaw, F. Vilbois, C. Zwahlen, A. Trkola, D. Marchant, P.R. Clapham, and T.N. Wells, *The BBXB motif of RANTES is the principal site for heparin binding and controls receptor selectivity.* J Biol Chem, 2001. **276**(14): p. 10620-6.

11. Kuschert, G.S., A.J. Hoogewerf, A.E. Proudfoot, C.W. Chung, R.M. Cooke, R.E. Hubbard, T.N. Wells, and P.N. Sanderson, *Identification of a glycosaminoglycan binding surface on human interleukin-8.* Biochemistry, 1998. **37**(32): p. 11193-201.

12. Severin, I.C., J.-P. Gaudry, Z. Johnson, A. Kungl, A. Jansma, B. Gesslbauer, B. Mulloy, C. Power, A.E.I. Proudfoot, and T. Handel, *Characterization of the chemokine CXCL11-heparin interaction suggests two different affinities for glycosaminoglycans.* J Biol Chem, 2010. **285**(23): p. 17713-24.

13. Salanga, C.L. and T.M. Handel, *Chemokine oligomerization and interactions with receptors and glycosaminoglycans: The role of structural dynamics in function.* Experimental Cell Research, 2011. **317**(5): p. 590-601.

14. Ren, M., Q. Guo, L. Guo, M. Lenz, F. Qian, R.R. Koenen, H. Xu, A.B. Schilling, C. Weber, R.D. Ye, A.R. Dinner, and W.-J. Tang, *Polymerization of MIP-1 chemokine (CCL3 and CCL4) and clearance of MIP-1 by insulin-degrading enzyme.* EMBO J, 2010. **29**(23): p. 3952-66.

15. Lau, E.K., C.D. Paavola, Z. Johnson, J.-P. Gaudry, E. Geretti, F. Borlat, A.J. Kungl, A.E. Proudfoot, and T.M. Handel, *Identification of the glycosaminoglycan binding site of the CC chemokine, MCP-1: implications for structure and function in vivo.* J Biol Chem, 2004. **279**(21): p. 22294-305.

16. Stringer, S.E., M.S. Nelson, and P. Gupta, *Identification of an MIP-1alpha -binding heparan sulfate oligosaccharide that supports long-term in vitro maintenance of human LTC-ICs.* Blood, 2003. **101**(6): p. 2243-5.

17. Whitelock, J. and J. Melrose, *Heparan sulfate proteoglycans in healthy and diseased systems.* Wiley Interdiscip Rev Syst Biol Med.

18. Sasisekharan, R., Z. Shriver, G. Venkataraman, and U. Narayanasami, *Roles of heparan-sulphate glycosaminoglycans in cancer.* Nat Rev Cancer, 2002. **2**(7): p. 521-8.

19. Hamel, D.J., I. Sielaff, A.E. Proudfoot, and T.M. Handel, *Chapter 4. Interactions of chemokines with glycosaminoglycans.* Methods Enzymol, 2009. **461**: p. 71-102.

20. Charvátová, O., B.L. Foley, M.W. Bern, J.S. Sharp, R. Orlando, and R.J. Woods, *Quantifying protein interface footprinting by hydroxyl radical oxidation and molecular dynamics simulation: application to galectin-1.* J Am Soc Mass Spectrom, 2008. **19**(11): p. 1692-705.

21. Takamoto, K. and M.R. Chance, *Radiolytic protein footprinting with mass spectrometry to probe the structure of macromolecular complexes.* Annu Rev Biophys Biomol Struct, 2006. **35**: p. 251-76.

22. Kiselar, J.G., R. Mahaffy, T.D. Pollard, S.C. Almo, and M.R. Chance, *Visualizing Arp2/3 complex activation mediated by binding of ATP and WASp using structural mass spectrometry.* Proc Natl Acad Sci USA, 2007. **104**(5): p. 1552-7.

23. Angel, T.E., S. Gupta, B. Jastrzebska, K. Palczewski, and M.R. Chance, *Structural waters define a functional channel mediating activation of the GPCR, rhodopsin.* Proceedings of the National Academy of Sciences, 2009. **106**(34): p. 14367-72.

24. Menten, P., A. Wuyts, and J. Van Damme, *Monocyte chemotactic protein-3.* Eur Cytokine Netw, 2001. **12**(4): p. 554-60.

25. Crown, S.E., Y. Yu, M.D. Sweeney, J.A. Leary, and T.M. Handel, *Heterodimerization of CCR2 chemokines and regulation by glycosaminoglycan binding.* J Biol Chem, 2006. **281**(35): p. 25438-46.

26. Kim, K.S., K. Rajarathnam, I. Clark-Lewis, and B.D. Sykes, *Structural characterization of a monomeric chemokine: monocyte chemoattractant protein-3.* FEBS Lett, 1996. **395**(2-3): p. 277-82.

27. Kaur, P., J.G. Kiselar, and M.R. Chance, *Integrated algorithms for high-throughput examination of covalently labeled biomolecules by structural mass spectrometry.* Anal. Chem., 2009. **81**(19): p. 8141-9.

28. Allen, S.J., S.E. Crown, and T.M. Handel, *Chemokine: receptor structure, interactions, and antagonism.* Annu Rev Immunol, 2007. **25**: p. 787-820.

29. Liang, M., M. Rosser, H.P. Ng, K. May, J.G. Bauman, I. Islam, A. Ghannam, P.J. Kretschmer, H. Pu, L. Dunning, R.M. Snider, M.M. Morrissey, J. Hesselgesser, H.D. Perez, and R. Horuk, *Species selectivity of a small molecule antagonist for the CCR1 chemokine receptor.* Eur J Pharmacol, 2000. **389**(1): p. 41-9.

30. Middleton, J., S. Neil, J. Wintle, I. Clark-Lewis, H. Moore, C. Lam, M. Auer, E. Hub, and A. Rot, *Transcytosis and surface presentation of IL-8 by venular endothelial cells.* Cell, 1997. **91**(3): p. 385-95.

31. Czaplewski, L.G., J. McKeating, C.J. Craven, L.D. Higgins, V. Appay, A. Brown, T. Dudgeon, L.A. Howard, T. Meyers, J. Owen, S.R. Palan, P. Tan, G. Wilson, N.R. Woods, C.M. Heyworth, B.I. Lord, D. Brotherton, R. Christison, S. Craig, S. Cribbes, R.M. Edwards, S.J. Evans, R. Gilbert, P. Morgan, E. Randle, N. Schofield, P.G. Varley, J. Fisher, J.P. Waltho, and M.G. Hunter, *Identification of amino acid residues critical for aggregation of human CC chemokines macrophage inflammatory protein (MIP)-1alpha, MIP-1beta, and RANTES. Characterization of active disaggregated chemokine variants.* J Biol Chem, 1999. **274**(23): p. 16077-84.

32. Murooka, T.T., M.M. Wong, R. Rahbar, B. Majchrzak-Kita, A.E. Proudfoot, and E.N. Fish, *CCL5-CCR5-mediated apoptosis in T cells: Requirement for glycosaminoglycan binding and CCL5 aggregation.* J Biol Chem, 2006. **281**(35): p. 25184-94.

33. Jansma, A., T.M. Handel, and D.J. Hamel, *Chapter 2. Homo- and hetero-oligomerization of chemokines.* Methods Enzymol, 2009. **461**: p. 31-50.

34. Paavola, C.D., S. Hemmerich, D. Grunberger, I. Polsky, A. Bloom, R. Freedman, M. Mulkins, S. Bhakta, D. McCarley, L. Wiesent, B. Wong, K. Jarnagin, and T.M. Handel, *Monomeric monocyte chemoattractant protein-1 (MCP-1) binds and activates the MCP-1 receptor CCR2B.* J Biol Chem, 1998. **273**(50): p. 33157-65.

35. Laurence, J.S., C. Blanpain, J.W. Burgner, M. Parmentier, and P.J. LiWang, *CC chemokine MIP-1 beta can function as a monomer and depends on Phe13 for receptor binding.* Biochemistry, 2000. **39**(12): p. 3401-9.

36. Paolini, J.F., D. Willard, T. Consler, M. Luther, and M.S. Krangel, *The chemokines IL-8, monocyte chemoattractant protein-1, and I-309 are monomers at physiologically relevant concentrations.* J Immunol, 1994. **153**(6): p. 2704-17.

37. Ali, S., G. O'Boyle, P. Hepplewhite, J.R. Tyler, H. Robertson, and J.A. Kirby, *Therapy with nonglycosaminoglycan-binding mutant CCL7: a novel strategy to limit allograft inflammation.* Am J Transplant, 2010. **10**(1): p. 47-58.

38. Ali, S., G. O'Boyle, P. Mellor, and J.A. Kirby, *An apparent paradox: chemokine receptor agonists can be used for anti-inflammatory therapy.* Mol Immunol, 2007. **44**(7): p. 1477-82.

39. Johnson, Z., M.H. Kosco-Vilbois, S. Herren, R. Cirillo, V. Muzio, P. Zaratin, M. Carbonatto, M. Mack, A. Smailbegovic, M. Rose, R. Lever, C. Page, T.N.C. Wells, and A.E.I. Proudfoot, *Interference with heparin binding and oligomerization creates a novel anti-inflammatory strategy targeting the chemokine system.* J Immunol, 2004. **173**(9): p. 5776-85.

40. Catanzariti, A.-M., T.A. Soboleva, D.A. Jans, P.G. Board, and R.T. Baker, *An efficient system for high-level expression and easy purification of authentic recombinant proteins.* Protein Sci, 2004. **13**(5): p. 1331-9.

CHAPTER 3

Phosphoproteomic Analysis of Chemokine Signaling Networks

3.1 Summary

Chemokines induce a number of intracellular signaling pathways by activating second messengers (e.g. calcium) and phosphorylation cascades in order to mediate a myriad of functions including cell migration, survival and proliferation. Although there is some degree of overlap in chemokine receptor–mediated pathway activation, different chemokines will often elicit distinct signaling events. Factors such as cell type, receptor expression levels, G protein availability, and disease state will also influence the signaling response from chemokine-induced receptor activation. Improvements in mass spectrometry, enrichment strategies, and database search programs for identifying phosphopeptides have made phosphoproteomics an accessible biological tool for studying chemokine-induced phosphorylation cascades. Although signaling pathways involved in chemokine-mediated migration have been fairly well characterized, less is known regarding other signaling cascades elicited by chemokines (e.g. to induce proliferation) or the potential for distinct pathway activation in a disease state such as cancer. CXCL12(SDF-1)/CXCR4 signaling has been shown to play an important role in the survival of chronic lymphocytic leukemia (CLL) cells, and thus provides a good system for exploring chemokine signaling, particularly in the interest of survival pathway

activation. In this chapter, we describe the use of immobilized metal affinity chromatography (IMAC) phosphopeptide enrichment followed by reversed-phase liquid chromatography and tandem mass spectrometry (LC-MS/MS) analysis for exploring CXCL12-mediated signaling in human CLL patient cells.

3.2 Introduction

As chemokines bind their respective chemokine receptors, they induce conformational changes in the receptors leading to activation of intracellular signaling molecules including G proteins and β-arrestins [1]. These intracellular signaling molecules activate a variety of downstream signaling pathways primarily through the initiation of phosphorylation cascades.

In eukaryotic organisms, phosphorylation, a key reversible post-translational modification, is critical for the rapid transduction of messages from extracellular stimuli to elicit a cellular response. Thus, it is not surprising that an estimated 2 to 3% of the human genome is directly involved in phosphorylation (kinases, which catalyze the addition of phosphate groups, and phosphatases, which catalyze their removal) [2, 3], and an estimated 30 to 50% of proteins are proposed to exhibit phosphorylation at some point in time [4]. Phosphorylation is known to alter the activity, stability, localization, and interaction properties of molecules, and has been linked to a number of cellular processes including cell growth, metabolism, differentiation, movement, and apoptosis [5, 6]. However, the study of protein phosphorylation has been limited due to a number of challenges, including low abundance of many phosphoproteins, the low stoichiometry of phosphorylation, the heterogeneity of phosphorylation sites on a given protein, and the transient/reversible nature of phosphorylation [7].

Classically, immunoblot (Western blot) analysis using phosphorylation-specific antibodies to a target of interest has been the gold standard for probing phosphorylation cascades activated in response to extracellular stimuli. Immunohistochemistry, immunofluorescence, and flow cytometry are additional methods for probing these signaling events; however, all of these techniques target specific proteins and require

highly specific phosphoantibodies. The high costs and limited availability of phosphoantibodies restrict the use of these techniques, which are generally used when there is prior knowledge or association with a particular signaling pathway. These methods are not amenable to global examination of phosphorylation events or for the identification of new phosphorylation sites. Classic methods to identify new phosphorylation sites including Edman sequencing and ^{32}P mapping are generally tedious and not commonly performed [7]. These limitations in understanding global (as opposed to *a priori* knowledge and targeted) protein phosphorylation events and in identifying novel phosphorylation sites have been a strong driving force for the development and implementation of phosphoproteomics techniques.

Utilizing phosphoproteomics to investigate intracellular signaling provides an unbiased approach for globally investigating cellular response to stimuli. The ability to simultaneously examine many phosphoproteins within a single sample and discover novel phosphorylations has also made phosphoproteomics a very attractive alternative from traditional approaches. However, implementation of mass spectrometry (MS)–based phosphoproteomics has its own set of challenges including negative ion suppression effects, limited dynamic range of detection, and difficulties in confidently identifying phosphopeptides [6, 8]. Nevertheless, the development and improvement of phosphoprotein and phosphopeptide enrichment strategies to counteract dynamic range problems and database search algorithms incorporating post-translational modifications have made this technique more accessible and feasible for signaling studies [6, 8].

Given the improvements in phosphoproteomics strategies, this technique can be employed to generate a wealth of information on cellular response to stimuli such as chemokines. Although there is some functional redundancy in the chemokine system given the approximate 50 chemokine ligands and 20 chemokine receptors [9], many

chemokine/receptor pairs will activate distinct pathways and responses [10]. Furthermore, differences in cell type and factors such as G protein availability and expression of specific isoforms and/or levels of particular signaling molecules can have dramatic effects on the signaling pathways utilized and functional response to chemokine stimulation [11]. It is also largely unknown how different disease states such as chronic inflammation or cancer may alter the response to chemokines, potentially through misregulation of known pathways, activation of alternative pathways, or targeting of different downstream effectors.

Here we present the use of MS-based phosphoproteomics method to investigate the signaling pathways induced by CXCL12 in chronic lymphocytic leukemia (CLL) cells. CLL is the most common form of adult leukemia in the Western world and is characterized by the accumulation of a monoclonal population of $CD5^+$ B cells in the blood, bone marrow, and secondary lymphoid tissues [12]. CLL cells are known to overexpress the chemokine receptor, CXCR4 [13], and its ligand, CXCL12, is thought to be an important microenvironmental factor contributing to the survival of these cells [12]Access to primary CLL cells (not immortalized or passaged cell lines) and the relevance of the CXCL12/CXCR4 axis to cancer pathogenesis [14] make this an ideal system for studying phosphorylation signaling cascades induced by CXCL12. It is important to note that while the method described here is specific to CXCL12 stimulation of CLL cells, it can also be used as a starting point for alternative studies involving chemokine/receptor signaling networks as well as non–chemokine signaling networks. Within these methods, there are many possibilities for optimization, as well as additional manipulations that can be exploited to obtain the most comprehensive results possible.

3.3 Materials and Methods and Additional Considerations

3.3.1: Isolation of chronic lymphocytic leukemia cells

Primary CLL cells were obtained in collaboration with Dr. Thomas Kipps at the University of California, San Diego, Moores Cancer Center. Briefly, leukopheresis blood was collected from consenting CLL patients, in agreement with institutional guidelines. Peripheral blood mononuclear cells (PBMCs) were isolated by Ficoll-Paque (Amersham Biosciences, Piscataway, NJ) density gradient centrifugation. Any contaminating red blood cells were lysed at room temperature (RT) for 5 min with red blood cell lysis buffer (Roche Diagnostics, Indianapolis, IN). The PBMCs from the CLL patient used for this particular phosphoproteomics data were determined to contain more than 90% $CD19^{+}/CD5^{+}/CD3^{-}$ B cells as assessed by flow cytometry.

3.3.2: CXCL12 stimulation of CLL cells and lysate preparation

CXCL12 preparation

CXCL12 was insolubly expressed in inclusion bodies as a His tag fusion in *Escherichia coli*. The protein was purified over a Ni-NTA column and refolded with Hampton Fold-It Buffer #8 (Hampton Research, Aliso Viejo, CA). Following dialysis and protein concentration, the His tag was cleaved at RT overnight using enterokinase (NEB, Ipswich, MA) at a 1:100,000 molar ratio. CXCL12 was purified by HPLC, and MS was performed to verify protein identity and purity. Transwell migration assays (Corning, Corning, NY) using Jurkat cells (ATCC, Manassas, VA) were performed to validate the functionality of purified CXCL12.

Stimulation of CLL cells

To prepare cell lysates for phosphoproteomic analysis, 3×10^9 CLL PBMCs were washed with sterile PBS, and resuspended at 1×10^7 cells/ml in serum-free, RPMI-1640 media (Gibco, Rockville, MD). Sixty milliliters of CLL cell suspension were distributed into each of five 15 cm plates (Corning Inc, Corning, NY) and cultured for 2 h at 37°C/5% CO_2 prior to stimulation with CXCL12. A CXCL12 stimulation time course was conducted such that one plate remained unstimulated and the other four were stimulated for 3 min, 10 min, 30 min, or 60 min, with 30 n*M* CXCL12, and all plates were harvested at the same time on ice. Cells were lysed on ice for 30 min with 3 ml ice cold cytoplasmic lysis buffer containing 10 m*M* HEPES, pH 7.9, 1.5 m*M* $MgCl_2$, 10 m*M* KCl, 0.5 m*M* dithiothreitol (DTT) (Sigma, St. Louis, MO), Complete protease inhibitor cocktail (Roche Diagnostics, Indianapolis, IN), and Halt phosphatase inhibitor cocktail (Pierce, Rockford, IL). Plates were scraped with cell scrapers (Sarstedt, Newton, NC) and the cell lysates were collected, sonicated on ice for 15 s pulse (3 s on, 2 s off), and then centrifuged at 20,000 rcf for 20 min at 4°C. The supernatants were distributed into protein LoBind Eppendorf tubes (Eppendorf, Westbury, NY) and lysates and pellets were stored at –80°C. Finally, the total protein concentration of the CLL lysates was determined using a BCA protein assay (Pierce, Rockford, IL). Two milligrams of CLL lysate from each time point were used for phosphoproteomic analysis.

3.3.3: IMAC phosphopeptide enrichment of CLL samples

The IMAC methods presented herein are based on the protocol described by [15]; however, adjustments to the protocol have been made for our system using CLL cells. Given that several phosphoproteomic platforms are available [16], factors such as sample amount/availability, instrument access, time, and cost must be considered in

determining the best approach for a particular study. The strategy (Fig. 3.1) employed for the current study was selected based on available resources as well as the primary goal to rapidly identify many potentially interesting downstream targets of CXCL12 stimulation in CLL cells. Several other techniques could be used in conjunction with, or alternatively to, the methods described below, and will be mentioned throughout.

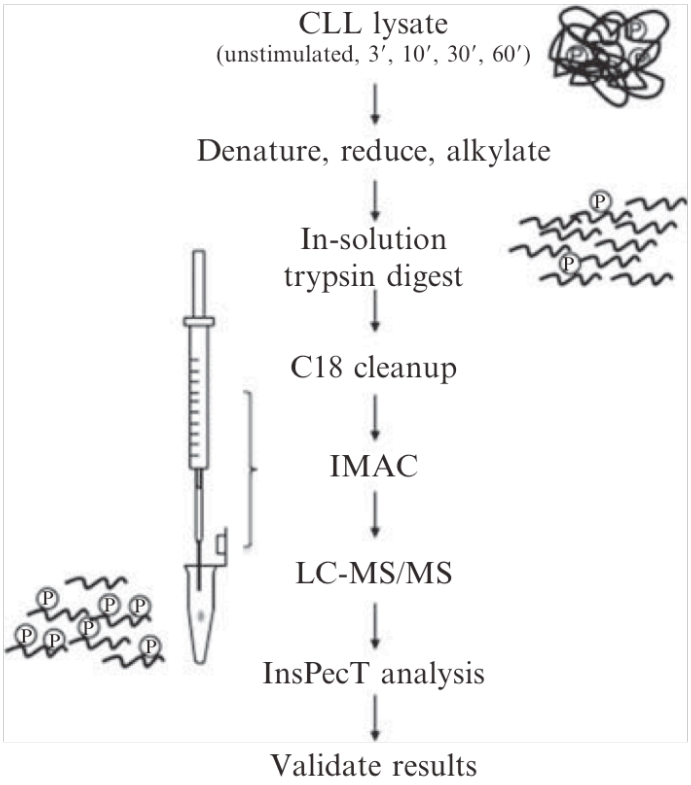

Figure 3.1 IMAC phosphoenrichment strategy. Brief outline of the MS-based methods using IMAC for phosphoenrichment of CXCL12-stimulated CLL cells. Following enrichment and LC-MS/MS analysis, phosphopeptides were identified by InsPecT and then manually validated.

Denaturation, reduction, and alkylation

To prepare lysates for tryptic digest and IMAC enrichment, CLL lysates were denatured with 1% sodium dodecyl sulfate (SDS) (Fisher Scientific, Pittsburgh, PA).

Disulfides were then reduced by the addition of freshly prepared DTT (final concentration = 10.5 m*M*) and heated to 60 to 65°C. After 20 min, lysates were cooled to RT for 30 min. Because reduction is reversible, samples were alkylated with fresh iodoacetamide (Sigma, St. Louis, MO) to a final concentration of 100 m*M* and left to incubate at 25°C for 30 min in the dark. Following SDS, DTT, and iodoacetamide treatment, protein was precipitated by addition of 3 to 4× the starting volume of 50% ethanol/50% acetone/0.1% acetic acid (HAC) in order to remove the detergent. To aid precipitation, samples were thoroughly mixed and stored at –80°C for 10 min. The precipitation reactions were then centrifuged at 1500 rcf for 10 min. The supernatants were removed and the pellets were washed again with an equivalent volume of 50% ethanol/50% acetone/0.1% HAC plus 20% volume of H_2O. The washed pellets were centrifuged at 1500 rcf for 10 min, the supernatant was completely removed and the protein pellets were left to dry overnight.

Trypsin digest

Protein pellets were resuspended in 200 µl of 6 M urea/0.1 M Tris, pH 8.0, and vortexed (volume dependent on amount of starting material). Prior to trypsin digest, the urea concentration was diluted five-fold by addition of 50 m*M* Tris, pH 8.0. Protein was digested using sequencing- grade modified trypsin (Promega, Madison, WI) by resuspending trypsin in 50 mM Tris, pH 8.0, and 1 mM $CaCl_2$ (final concentration) and adding to sample at a ratio of 1:50 (trypsin: protein). Digests were vortexed, parafilmed, and stored at 37°C while shaking. Following an overnight incubation, trypsin was inactivated by acidification of the digests with trifluoroacetic acid to 0.3 to 0.5% (v/v) and stored at 4°C (for long-term storage, freeze and store at –80°C).

C18 cleanup

Peptide mixtures were desalted with 50 mg Sep-pak C18 cartridges (Waters Corp, Milford, MA). Prior to use, C18 cartridges (one per time point) were hydrated with methanol, and then rinsed with 80% acetonitrile (ACN) /1% HAC and equilibrated with 1% HAC. Peptides were loaded onto the columns, washed twice with 1% HAC, and eluted with 400 µl of 80% ACN/0.1% HAC. Fractions were collected in LoBind Eppendorf tubes, dried on a speed-vac at 50°C for 1 h, and stored at 4°C. Pellets were resuspended in 100 µl of 1% HAC and centrifuged at 1500 rcf for 2 min. Supernatants were saved and used for subsequent IMAC enrichment steps.

IMAC bead preparation and enrichment

IMAC beads were prepared by removing the resin from 2 Ni-NTA spin columns (Qiagen, Valencia, CA) and replacing the Ni for Fe. Nickel resin was stripped by rotating with 50 mM EDTA, 1 M NaCl in 50 ml for 1 h, and then centrifuged in a swinging bucket rotor at 1500 rcf for 2 min. The supernatant was removed and the pellet was washed with 50 ml of Milli-Q H_2O followed by 50 ml of 0.6% HAC. The resin was then charged with 50 ml of 100 m*M* $FeCl_3$ (Fluka reagent, Sigma, St. Louis, MO) in 0.3% HAC for 1 h while rotating (Note: prior to $FeCl_3$ stock use, allow any impurities to settle from the solution for at least 1 month). Finally, supernatant was removed to make a 50:50 IMAC bead slurry (600 µl). Individual IMAC columns were generated with the freshly prepared IMAC beads using gel-loading tips (Fisher Scientific, Pittsburgh, PA) affixed with a 1 cc syringe to control flow rate. Each column was plugged with a small amount of glass wool and pinched at the tip before adding 60 µl of IMAC bead slurry. Before each sample was loaded onto its own gel loading tip, the IMAC beads were conditioned with 25% ACN/0.1% HAC. Nonspecific peptides were removed by washing twice with 30 µl of 25% ACN/0.1% HAC/0.1 *M* NaCl, and then twice with 0.1% HAC, and finally twice with 30 µl

of Milli-Q H_2O. Phosphopeptides were eluted with a total volume of 50 µl over three elutions with 1% phosphoric acid. All fractions were collected in protein LoBind Eppendorf tubes, speed-vac dried, and stored at –20°C until MS analysis.

Additional phosphoenrichment strategies and considerations

In addition to Fe^{3+}, Ga^{3+} is another commonly used metal for IMAC [8]; ZrO_2 [17] and TiO_2 [18, 19] have also been widely used for phosphopeptide enrichment, typically in a tip or column format. To obtain optimal enrichment, each approach must be tested and optimized individually to determine its suitability for a given application. Each of these phosphoenrichment strategies has slightly different phosphopeptide selectivity based on their variable chemistry, which leads to identification of some nonoverlapping phosphopeptides [20]. Therefore, utilization of multiple phosphoenrichment strategies will yield complementary data [8]. Phosphoprotein enrichment, particularly for phosphotyrosine proteins, performed by immunoprecipitation with phosphotyrosine antibodies, in conjunction with phosphopeptide enrichment, has also been quite successful [8]. An important consideration and potential shortcoming to IMAC phosphoenrichment is the ability of IMAC resin to bind to highly acidic peptides (i.e. rich in Asp and/or Glu), which can “contaminate” a data set. However, methyl esterification is one option for reducing this phenomenon [21]. In our work, despite not doing methyl esterification, we were still able to obtain an average phosphoenrichment of 30% for all data sets (Table 3.1). Preferential enrichment and strong binding of multiply phosphorylated peptides has also been considered a drawback to IMAC enrichment [8]. However, we mostly recovered peptides containing a single phosphate, consistent with observations that acidic elution conditions mostly yield monophosphorylated peptides [22], and may also be related to retention of multiply phosphorylated peptides or the

challenge of proteomics software to provide a confident identification of multiphosphorylated peptides. Therefore, additional strategies, such as SIMAC (sequential elution from IMAC) can be employed to isolate multiple phosphorylated peptides from monophosphorylated peptides in a complex sample [22]. Additionally, LC-MS/MS analysis of IMAC flow-through and wash fractions recovered few phosphopeptide identifications (1 phosphopeptide per 1000 peptides). The few phosphopeptides identified from the wash fractions were highly abundant in IMAC elution fractions, suggesting efficient enrichment.

Table 3.1 Summary of phosphorylations identified in CXCL12 stimulated CLL cells.

30 nM CXCL12 timepoint:	Unstimulated	3'	10'	30'	60'
Total peptides	550	734	770	754	737
Phosphopeptides	161	249	236	209	158
False positives[a]	8	9	11	13	11
False positive rate (%)	1.5%	1.2%	1.4%	1.7%	1.5%
Phosphoenrichment (%)	29.3%	33.9%	30.6%	27.7%	21.4%
Phosphoproteins[b]	93	131	133	104	103

Notes:
The total number of phosphorylation events and correlating false discovery rate and percent of phosphoenrichment are summarized for each time point data set of CXCL12-stimulated CLL cells.
[a] Estimated by use of a decoy database approach.
[b] Number of phosphoproteins identified within a time point data set.

3.3.4: Reversed-phase liquid chromatography and tandem mass spectrometry

Phosphoenriched CLL peptides were analyzed by reversed-phase, capillary liquid chromatography and tandem mass spectrometry (LC-MS/MS) on a Thermo Finnigan LTQ ion trap mass spectrometer. The capillary LC columns (~17 cm) were packed in-house using deactivated fused silica (100 μm) (Agilent, Santa Clara, CA) with C18 resin (5 μm, 300 Å) (Michrom Bioresources, Auburn, CA). Capillary columns were prepared by drawing a 360 μm O.D., 100 μm I.D. deactivated, fused silica tubing with a

Model P-2000 laser puller (Sutter Instruments, Novato, CA) (heat: 330, 325, 320; vel: 45; del: 125) and were packed at ~600 psi to a length of ~10 cm with C18 reversed-phase resin suspended in methanol. While purchasing capillary columns has distinct advantages, such as improved column-to-column reproducibility, they are about 150 times more expensive than the columns prepared in our laboratory. To prepare samples for running on LC-MS/MS, dried eluate was resuspended in 50 µl of Milli-Q H_2O. The resuspension volume should be adjusted according to the amount of starting material and column capacity, as well as the sensitivity of the mass spectrometer used. Approximately 15 µl of the resuspension was added to a 96-well plate (Axygen, Union City, CA) of which 10 µl was loaded onto the capillary column for LC-MS/MS analysis. To minimize sample evaporation, the 96-well plate was covered with a sealing film (Axygen, Union City, CA). Angiotensin II (Sigma-Aldrich, St. Louis, MO) was used as a control for column performance and run after every two CLL sample runs. The standard method used for all samples was as follows: 95% A/5% B (buffer A = 0.1% HAC in HPLC-grade Milli-Q H_2O, buffer B = 0.1% HAC in HPLC-grade ACN) for 20 min, 60% A/40% B for 30 min, 20% A/80% B for 6 min, followed by a final washing step of 95% A/5% B for 30 min at 250 µl/min. The flow of solvent was split before it reached the column resulting in a flow rate of 200 to 500 nl/min through the capillary column. Samples were run in data-dependent mode, where the spectrometer performed one full MS scan followed by six MS/MS scans of the top six most intense ions in the parent spectrum with a *m/z* ranging from 400 to 2000. A dynamic exclusion list was applied with a repeat count of 1, a repeat duration of 30 s, an exclusion size of 100, exclusion duration of 180 s, and an exclusion mass width of 1.50. The spray voltage was 1.8 kV. Because the instrument cannot fragment all the peptides in the parent spectrum, the sample can be run several times to saturate the proteomic space for a given method. At

this time, the gold standard in proteomics is three runs for each sample, but one will miss some of the possible phosphopeptides that can be identified. Five runs on a given method and identical sample will nearly saturate all the possible candidate peptides and 10 would be better for a higher degree of confidence.

On average, the scan rate in this experiment ranged from four to eight scans per second. The higher the scan rate, the more peptides one will be able to identify for a given LC run, which is an important consideration when designing an experiment and/or purchasing a mass spectrometer for proteomics. While we have provided the parameters for a starting method for the phosphoproteomic analysis, changing the HPLC gradient, changing the data-dependent analysis of different top intensity ions (e.g. 7th to the 13th most intense ions in the parent spectrum) and dynamic exclusion parameters influences the type and amount of data collected. Once the data is collected, prior to InsPecT analysis, RAW data files were converted to mzXML data files using the program ReAdW (http://tools.proteomecenter.org/ReAdW.php).

Additional phosphopeptide separation techniques

Additional separation of phosphopeptides, which can be carried out prior to LC-MS/MS, include strong cation exchange (SCX) chromatography [23, 24]. Both techniques produce an orthogonal method of separation to reversed-phase LC and have been shown to significantly increase the number of phosphopeptides identified. However, given the limited amount of starting material from the primary CLL cells (these are not a renewable source) and increased risk of sample loss associated with additional steps, these techniques were not utilized in the present study. Nevertheless, SCX and HILIC present an attractive means for enhanced phosphopeptide separation and detection.

Phosphopeptide identification with InsPecT

Data analysis was carried out with the open-access database search tool, InsPecT (http://proteomics.ucsd.edu/index.html), which allows for rapid identification of post-translationally modified peptides such as phosphopeptides [25]. InsPecT is particularly useful for identification of post-translational modifications on peptides in a complex mixture. Its employment of tag-based filters reduces the overall number of peptides considered from the database early on, significantly reducing the processing time compared to most other search algorithms available [25]. Additionally, modifications to the InsPecT program have been made recently to specifically improve the recognition of phosphopeptides. A highly enriched and validated phosphopeptide data set was used to develop better recognition and scoring parameters for phosphopeptide spectra [15]. This is important because during collision-induced dissociation (CID) MS/MS, phosphoric acid is typically lost. The resulting spectral patterns of phosphopeptides are characterized by a strong neutral loss peak and weaker y- and b-ion fragments. Because of the decreased intensity of the various fragments, it becomes a difficult and time consuming task for search databases to correctly identify phosphopeptides. However, since the training set for improving the phosphopeptide identification and scoring was collected on an ion trap using CID to generate MS/MS data, the program is especially good at recognizing these phosphopeptide signatures. Gentler dissociation methods, like electron capture dissociation (ECD) and electron transfer dissociation (ETD) are alternative methods to CID, and generally retain the phosphate group on a phosphopeptide facilitating a more precise phosphate localization on a peptide [8].

MS/MS spectra were processed using the UniProt human database, the UniProt shuffled human decoy database as well as common contaminants databases (e.g. keratin). Peptide sequencing searches were also defined for variable modification of up

to two phosphorylation sites (Ser, Thr, or Tyr) on a peptide, and tryptic cleavage search restraints. Using the target decoy database as a measure of the overall quality of MS/MS data, spectra from each time point were sorted by *p*-values. Peptides with a false discovery rate (FDR) of less than 1 to 2% were manually validated for positive identification. Although there are some drawbacks associated with the use of decoy databases [26, 27], they are generally an acceptable approach for approximating the confidence of reliable spectra assignments particularly for tryptic digests [28].

Positive hits from each stimulation time point were combined into a comprehensive list and sorted by protein. Collectively, the five time points resulted in the identification of 1036 unique phosphopeptides and a total of 251 unique proteins (Table 3.1). Taking into consideration the limited amount of starting material used in this study, the overall number of phosphorylation events detected in our analysis is comparable to other phosphoproteomic studies involving complex biological samples [29]. Phosphorylated protein targets of interest were further probed by alternative mechanisms. In some instances, phospho-specific antibodies were available for the phosphorylated protein of interest and could be probed by Western blot for validation. However, in most cases, no phosphoantibodies existed, and comparisons between time points had to be determined by other means. The CLL peptide samples were rerun three times, and exclusion list restraints were varied in order to obtain more data for spectral counting comparison. Spectral counting is a straightforward, cost-saving, semi-quantitative approach to determining the differential levels of relatively abundant proteins in a dataset [30-33]. However, less abundant peptides are not ideal for this method because there is too much stochastic variation. Alternatively, a $^{16}O/^{18}O$ trypsin digest can be used. This semi-quantitative method involves postdigestion labeling of peptides by exchanging ^{16}O for ^{18}O in a trypsin-catalyzed reaction [34]. The exchange of ^{16}O for ^{18}O

is a specific process in which the C-termini of tryptic peptides are generally labeled with two ^{18}O atoms, resulting in a 4-Da shift between coeluting labeled and unlabeled peptides. Other chemical modification methods available for quantitative proteomics include isotope-coded affinity tags (ICAT), isobaric tags for quantification (iTRAQ), and phosphoramidate chemistry (PAC), and have been reviewed elsewhere [6, 35]. Lastly, the development of stable isotope labeling with amino acids in cell culture (SILAC) has provided an effective and reproducible means of quantification between sample sets (e.g. unstimulated vs. stimulated) for proteomics studies [36]. This technique involves the metabolic incorporation of isotopically labeled amino acids, generally ^{13}C or ^{15}N labeled Lys and/or Arg, and then comparison of the peak intensities of mixed unlabeled and labeled samples. However, several disadvantages of SILAC include the expense of growing cells in labeled media and the requirement for proliferating cells in culture preventing its use in primary tissue samples such as the CLL cells.

Considerations for selecting an appropriate search database program

An additional consideration in choosing the appropriate search database is cost. Currently, there are several available open source search databases, such as InsPecT, X!Tandem, and OMSSA [37, 38]. InsPecT is particularly effective for the identification of phosphopeptides and runs in a fraction of the time compared to other search databases. However, use of a Windows browser interface is a distinct advantage to programs like X!Tandem, if the user is unfamiliar with command lines as in InsPecT, although a current version with a user-friendly Web interface is being developed at the UCSD center for computational mass spectrometry. InsPecT tutorials to aid in installation and data processing are available online. There are also commercially available search database

programs including SEQUEST, Mascot, and Spectrum Mill. Comparisons using a number of search database programs have been previously carried out [15, 39].

In many instances, a combination of strategies that include various data analysis platforms is likely to yield the most comprehensive approach to phosphoproteomics. In particular, the use of several database search engines for peptide identification is an excellent way to gather the most information from a data set, because often different database search engines will identify nonoverlapping peptides due to the inherent differences in detection and scoring strategies [15]. For example, Payne et al. demonstrated that the use of three different search algorithms—X!Tandem, SEQUEST, and InsPecT (filtered to a 1% false discovery rate)—collectively identified 1371 phosphopeptide spectra, of which 92, 116, and 203 spectra were nonoverlapping, respectively. The drawback to running a MS/MS data set against several databases is the run time. For example, in their studies, SEQUEST required 72 times longer to process the same data compared to InsPecT, a distinct advantage to using the InsPecT software package.

Additional phosphoproteomics data analysis tools

Following phosphopeptide identification, proteins can be classified through online bioinformatics tools such as Database for Annotation, Visualization, and Integrated Discovery (DAVID) (http://david.abcc.ncifcrf.gov/) and Cytoscape (http://cytoscape.org/). In addition, the phosphorylation site databases (e.g. Phosida, www.phosida.com,, and Phosphobase, http://phospho.elm.eu.org/) have been developed as a repository for phosphopeptide identifications and corollary information. Together, these tools allow data to be more easily evaluated, categorized, and visualized in different formats, thus enabling a global and/or in-depth view of particular proteins identified in various biological pathways. For example, classification of our phosphopeptide results using

DAVID revealed many candidates involved in cell death, survival, growth, proliferation, and cell cycle (Table 3.2).

Table 3.2 Functional annotation of phosphoproteomics data.

Functional Annotation (GO with DAVID)	Protein Count	% of Proteins
G protein modulator	25	10.4%
Cell death	23	9.6%
Regulation of gene expression	46	19.3%
Leukocyte activation	8	3.4%
Cell cycle	23	9.7%
Cell growth	8	3.4%
Cell proliferation	18	7.6%
Lymphocyte proliferation	4	1.7%
Cell motility	11	4.6%
Immune system development	11	4.6%
Cell development	28	11.8%
B cell activation	4	1.7%
Leukocyte differentiation	8	3.3%

Notes:
A subset of interesting categories from DAVID gene ontology functional annotation of phosphoproteins identified in the CLL cells is displayed. The number and percent of phosphoproteins implicated in regulation of particular cellular processes are indicated.

3.4 Acknowledgements

Chapter 3 was published in *Methods in Enzymology*: O'Hayre M, Salanga CL, Dorrestein PC, Handel TM. Phosphoproteomics analysis of chemokine signaling networks. *Methods Enzymol*. **2009.** The dissertation author was a co-investigator and co-first author of this methods chapter.

3.5 References

1. Thelen, M., *Dancing to the tune of chemokines.* Nat Immunol, 2001. **2**(2): p. 129-34.

2. Hubbard, M.J. and P. Cohen, *On target with a new mechanism for the regulation of protein phosphorylation.* Trends Biochem Sci, 1993. **18**(5): p. 172-7.

3. Manning, G., G.D. Plowman, T. Hunter, and S. Sudarsanam, *Evolution of protein kinase signaling from yeast to man.* Trends Biochem Sci, 2002. **27**(10): p. 514-20.

4. Kalume, D.E., H. Molina, and A. Pandey, *Tackling the phosphoproteome: tools and strategies.* Curr Opin Chem Biol, 2003. **7**(1): p. 64-9.

5. de Graauw, M., P. Hensbergen, and B. van de Water, *Phospho-proteomic analysis of cellular signaling.* Electrophoresis, 2006. **27**(13): p. 2676-86.

6. Schreiber, T.B., N. Mausbacher, S.B. Breitkopf, K. Grundner-Culemann, and H. Daub, *Quantitative phosphoproteomics--an emerging key technology in signal-transduction research.* Proteomics, 2008. **8**(21): p. 4416-32.

7. Mann, M., S.E. Ong, M. Gronborg, H. Steen, O.N. Jensen, and A. Pandey, *Analysis of protein phosphorylation using mass spectrometry: deciphering the phosphoproteome.* Trends Biotechnol, 2002. **20**(6): p. 261-8.

8. Paradela, A. and J.P. Albar, *Advances in the analysis of protein phosphorylation.* J Proteome Res, 2008. **7**(5): p. 1809-18.

9. Allen, S.J., S.E. Crown, and T.M. Handel, *Chemokine: receptor structure, interactions, and antagonism.* Annu Rev Immunol, 2007. **25**: p. 787-820.

10. O'Hayre, M., C.L. Salanga, T.M. Handel, and S.J. Allen, *Chemokines and cancer: migration, intracellular signalling and intercellular communication in the microenvironment.* Biochem J, 2008. **409**(3): p. 635-49.

11. Salanga, C.L., M. O'Hayre, and T. Handel, *Modulation of chemokine receptor activity through dimerization and crosstalk.* Cell Mol Life Sci, 2008.

12. Burger, J.A., N. Tsukada, M. Burger, N.J. Zvaifler, M. Dell'Aquila, and T.J. Kipps, *Blood-derived nurse-like cells protect chronic lymphocytic leukemia B cells from spontaneous apoptosis through stromal cell-derived factor-1.* Blood, 2000. **96**(8): p. 2655-63.

13. Mohle, R., C. Failenschmid, F. Bautz, and L. Kanz, *Overexpression of the chemokine receptor CXCR4 in B cell chronic lymphocytic leukemia is associated with increased functional response to stromal cell-derived factor-1 (SDF-1).* Leukemia, 1999. **13**(12): p. 1954-9.

14. Burger, J.A. and T.J. Kipps, *CXCR4: a key receptor in the crosstalk between tumor cells and their microenvironment.* Blood, 2006. **107**(5): p. 1761-7.

15. Payne, S.H., M. Yau, M.B. Smolka, S. Tanner, H. Zhou, and V. Bafna, *Phosphorylation-specific MS/MS scoring for rapid and accurate phosphoproteome analysis.* J Proteome Res, 2008. **7**(8): p. 3373-81.

16. Schmelzle, K. and F.M. White, *Phosphoproteomic approaches to elucidate cellular signaling networks.* Curr Opin Biotechnol, 2006. **17**(4): p. 406-14.

17. Feng, S., M. Ye, H. Zhou, X. Jiang, H. Zou, and B. Gong, *Immobilized zirconium ion affinity chromatography for specific enrichment of phosphopeptides in phosphoproteome analysis.* Mol Cell Proteomics, 2007. **6**(9): p. 1656-65.

18. Klemm, C., S. Otto, C. Wolf, R.F. Haseloff, M. Beyermann, and E. Krause, *Evaluation of the titanium dioxide approach for MS analysis of phosphopeptides.* J Mass Spectrom, 2006. **41**(12): p. 1623-32.

19. Larsen, M.R., T.E. Thingholm, O.N. Jensen, P. Roepstorff, and T.J. Jorgensen, *Highly selective enrichment of phosphorylated peptides from peptide mixtures using titanium dioxide microcolumns.* Mol Cell Proteomics, 2005. **4**(7): p. 873-86.

20. Bodenmiller, B., L.N. Mueller, M. Mueller, B. Domon, and R. Aebersold, *Reproducible isolation of distinct, overlapping segments of the phosphoproteome.* Nat Methods, 2007. **4**(3): p. 231-7.

21. Ficarro, S.B., M.L. McCleland, P.T. Stukenberg, D.J. Burke, M.M. Ross, J. Shabanowitz, D.F. Hunt, and F.M. White, *Phosphoproteome analysis by mass spectrometry and its application to Saccharomyces cerevisiae.* Nat Biotechnol, 2002. **20**(3): p. 301-5.

22. Thingholm, T.E., O.N. Jensen, P.J. Robinson, and M.R. Larsen, *SIMAC (sequential elution from IMAC), a phosphoproteomics strategy for the rapid separation of monophosphorylated from multiply phosphorylated peptides.* Mol Cell Proteomics, 2008. **7**(4): p. 661-71.

23. Motoyama, A., T. Xu, C.I. Ruse, J.A. Wohlschlegel, and J.R. Yates, 3rd, *Anion and cation mixed-bed ion exchange for enhanced multidimensional separations of peptides and phosphopeptides.* Anal Chem, 2007. **79**(10): p. 3623-34.

24. Albuquerque, C.P., M.B. Smolka, S.H. Payne, V. Bafna, J. Eng, and H. Zhou, *A multidimensional chromatography technology for in-depth phosphoproteome analysis.* Mol Cell Proteomics, 2008. **7**(7): p. 1389-96.

25. Tanner, S., H. Shu, A. Frank, L.C. Wang, E. Zandi, M. Mumby, P.A. Pevzner, and V. Bafna, *InsPecT: identification of posttranslationally modified peptides from tandem mass spectra.* Anal Chem, 2005. **77**(14): p. 4626-39.

26. Kall, L., J.D. Storey, M.J. MacCoss, and W.S. Noble, *Assigning significance to peptides identified by tandem mass spectrometry using decoy databases.* J Proteome Res, 2008. **7**(1): p. 29-34.

27. Kim, S., N. Gupta, and P.A. Pevzner, *Spectral probabilities and generating functions of tandem mass spectra: a strike against decoy databases.* J Proteome Res, 2008. **7**(8): p. 3354-63.

28. Wang, G., W.W. Wu, Z. Zhang, S. Masilamani, and R.F. Shen, *Decoy methods for assessing false positives and false discovery rates in shotgun proteomics.* Anal Chem, 2009. **81**(1): p. 146-59.

29. Moser, K. and F.M. White, *Phosphoproteomic analysis of rat liver by high capacity IMAC and LC-MS/MS.* J Proteome Res, 2006. **5**(1): p. 98-104.

30. Balgley, B.M., W. Wang, T. Song, X. Fang, L. Yang, and C.S. Lee, *Evaluation of confidence and reproducibility in quantitative proteomics performed by a capillary isoelectric focusing-based proteomic platform coupled with a spectral counting approach.* Electrophoresis, 2008. **29**(14): p. 3047-54.

31. Zhang, B., N.C. VerBerkmoes, M.A. Langston, E. Uberbacher, R.L. Hettich, and N.F. Samatova, *Detecting differential and correlated protein expression in label-free shotgun proteomics.* J Proteome Res, 2006. **5**(11): p. 2909-18.

32. Zybailov, B., A.L. Mosley, M.E. Sardiu, M.K. Coleman, L. Florens, and M.P. Washburn, *Statistical analysis of membrane proteome expression changes in Saccharomyces cerevisiae.* J Proteome Res, 2006. **5**(9): p. 2339-47.

33. Liu, H., R.G. Sadygov, and J.R. Yates, 3rd, *A model for random sampling and estimation of relative protein abundance in shotgun proteomics.* Anal Chem, 2004. **76**(14): p. 4193-201.

34. Liu, T., W.-J. Qian, E.F. Strittmatter, D.G. Camp, G.A. Anderson, B.D. Thrall, and R.D. Smith, *High-throughput comparative proteome analysis using a quantitative cysteinyl-peptide enrichment technology.* Anal. Chem., 2004. **76**(18): p. 5345-53.

35. Ong, S.E. and M. Mann, *Mass spectrometry-based proteomics turns quantitative.* Nat Chem Biol, 2005. **1**(5): p. 252-62.

36. Olsen, J.V., B. Blagoev, F. Gnad, B. Macek, C. Kumar, P. Mortensen, and M. Mann, *Global, in vivo, and site-specific phosphorylation dynamics in signaling networks.* Cell, 2006. **127**(3): p. 635-48.

37. Matthiesen, R. and O.N. Jensen, *Analysis of mass spectrometry data in proteomics.* Methods Mol Biol, 2008. **453**: p. 105-22.

38. Geer, L.Y., S.P. Markey, J.A. Kowalak, L. Wagner, M. Xu, D.M. Maynard, X. Yang, W. Shi, and S.H. Bryant, *Open mass spectrometry search algorithm.* J Proteome Res, 2004. **3**(5): p. 958-64.

39. Bakalarski, C.E., W. Haas, N.E. Dephoure, and S.P. Gygi, *The effects of mass accuracy, data acquisition speed, and search algorithm choice on peptide identification rates in phosphoproteomics.* Anal Bioanal Chem, 2007. **389**(5): p. 1409-19.

CHAPTER 4

Elucidating the CXCL12/CXCR4 Network in Chronic Lymphocytic Leukemia Through Phosphoproteomic Analysis

4.1 Summary

Chronic lymphocytic leukemia (CLL) pathogenesis has been linked to the prolonged survival and/or apoptotic resistance of leukemic B cells in vivo, and is thought to be due to enhanced survival signaling responses to environmental factors that protect CLL cells from spontaneous and chemotherapy-induced death. Although normally associated with cell migration, the chemokine, CXCL12, is one of the factors known to support the survival of CLL cells. Thus, the signaling pathways activated by CXCL12 and its receptor, CXCR4, were investigated as components of these pathways and may represent targets that if inhibited, could render resistant CLL cells more susceptible to chemotherapy. To determine the downstream signaling targets that contribute to the survival effects of CXCL12 in CLL, we took a phosphoproteomics approach to identify and compare phosphopeptides in unstimulated and CXCL12-stimulated primary CLL cells. While some of the survival pathways activated by CXCL12 in CLL are known, including Akt and ERK1/2, this approach enabled the identification of additional signaling targets and novel phosphoproteins that could have implications in CLL disease and

therapy. In addition to the phosphoproteomics results, we provide evidence from western blot validation that the tumor suppressor, programmed cell death factor 4 (PDCD4), is a previously unidentified phosphorylation target of CXCL12 signaling in all CLL cells probed. Additionally, heat shock protein 27 (HSP27), which mediates anti-apoptotic signaling and has previously been linked to chemotherapeutic resistance, was detected in a subset (~25%) of CLL patients cells examined. Since PDCD4 and HSP27 have previously been associated with cancer and regulation of cell growth and apoptosis, these proteins may have novel implications in CLL cell survival and represent potential therapeutic targets. PDCD4 also represents a previously unknown signaling target of chemokine receptors; therefore, these observations increase our understanding of alternative pathways to migration that may be activated or inhibited by chemokines in the context of cancer cell survival.

4.2 Introduction

B cell Chronic Lymphocytic Leukemia (CLL) is an adult leukemia characterized by the accumulation of B cells in the blood, bone marrow and secondary lymphoid tissues due to apparent survival advantages and/or apoptosis resistance of these cells in vivo [1]. There is significant heterogeneity in the disease progression between CLL patients. A more aggressive form of the disease, which results in lower patient survival time, correlates with markers including unmutated immunoglobulin heavy chain variable region (IgHV) status and high expression of the tyrosine kinase ZAP-70 (ZAP-70+). Although the accumulation of a monoclonal population of CD5+/CD19+ B cells is characteristic of both prognostic groups, aggressive CLL appears to have some distinct characteristics and signaling properties compared to indolent CLL [2].

Despite their enhanced survival in vivo, when CLL cells from patients are cultured in vitro, they rapidly undergo apoptosis under conditions that support the survival of normal B cells, underscor- ing the dependence of these cells on survival cues from the microenvironment [3,4]. In the microenvironment, marrow stromal cells are believed to secrete factors that promote CLL cell survival in patients; correspondingly, when monocytes isolated from peripheral blood of CLL patients are cultured, they differentiate into ‘‘Nurse-like cells’’ (NLCs) that promote CLL survival in vitro [3]. One of the factors known to be secreted by these NLCs and to support CLL survival is the chemokine, CXCL12 (SDF-1). Additionally, CXCR4, the receptor for CXCL12, is overexpressed on CLL cells compared to normal B cells, and thus has the potential for enhanced responsiveness to CXCL12 signaling [5]. Although another chemokine receptor, CXCR7, can also bind CXCL12 and was previously shown to be expressed on B cells [6], surface expression of CXCR7 was not observed on CLL B cells (Figure 4.1).

Therefore the CXCL12 signaling effects are likely mediated exclusively by CXCR4 in these cells.

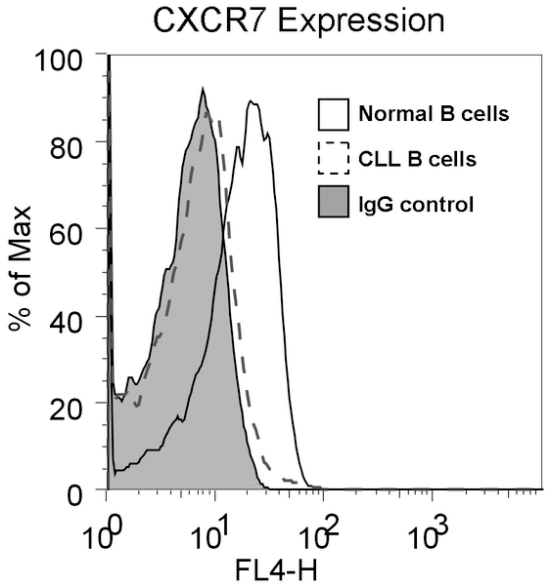

Figure 4.1 CXCR7 expression on normal B cells and CLL B cells.
Surface CXCR7 expression on Normal B cells (solid line) and CLL B cells (dashed line) was analyzed by flow cytometry and referenced to an IgG1 isotype control (filled histogram). Profiles are representative of B cells from 4 healthy donors (normal B cells) and 10 CLL patients' B cells.

While chemokines and their G-protein coupled receptors are best known for their role in directing the migration of immune cells, it is clear that these proteins are involved in many other biological functions. The CXCL12/CXCR4 axis is critical for developmental processes including lymphopoiesis, and central nervous system and cardiac development, and knockout of either the ligand or receptor in mice results in embryonic lethality [2]. Due to the involvement of CXCL12/CXCR4 in migration, angiogenesis, and development, it is not surprising that this axis is often exploited by cancer cells for metastasis as well as survival and proliferation [3]. However, the specific molecular mechanisms by which these various functions are effectuated and how these signaling pathways target different downstream signaling molecules in cancer cells compared to

non-malignant counterpart cells is largely unknown. Similarly, while it is known that Akt and ERK1/2 are activated by CXCL12 in CLL, the downstream targets of these pathways and activation of other pathways have not been elucidated [4].

Despite the upregulation of CXCR4 and strong Akt and ERK signaling demonstrated by CLL cells in response to CXCL12, the CLL cells actually migrate less efficiently to CXCL12 than B cells from healthy donors in a transwell migration assay (Figure 4.2). Thus, in CLL cells, it appears that signaling downstream of CXCL12/CXCR4 may be redirected towards survival signaling in lieu of cell migration. To better characterize the signaling responses to CXCL12 stimulation, primary CLL cells isolated from 5 patients were subjected to phosphoproteomic analysis by liquid chromatography and tandem mass spectrometry (LC-MS/MS). Rather than attempting to characterize the complete phosphoproteome of CLL cells, this approach was designed to generate new hypotheses about the CXCL12/CXCR4 signaling network in CLL survival, and to identify downstream proteins that might be good therapeutic targets. While many phosphoproteins were identified in the CLL cells, comparison of spectral counts between CXCL12 stimulated and unstimulated cells allowed identification of proteins phosphorylated as a consequence of CXCL12/CXCR4 signaling. With follow-up experiments, the tumor suppressor PDCD4 was validated as a downstream phosphorylation target of CXCL12 signaling in all CLL patient cells examined (n = 10) and HSP27 was similarly validated in a subset of CLL patients (~25%). Although these proteins have been previously linked to cancer cell survival, they have not been previously associated with CLL nor has PDCD4 been established as a downstream phosphorylation target of CXCL12 signaling. Furthermore, a number of other proteins (many of which do not have commercially available phospho-specific antibodies available) have been proposed as potential downstream phosphorylation targets of

CXCL12 stimulation based on spectral count analysis of the CLL phosphoproteomics data.

A

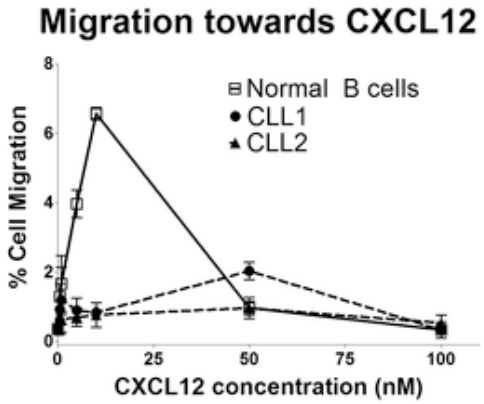

B

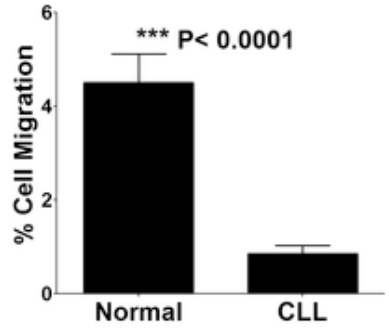

C

	B cell	CLL B cell
Max efficacy	4.5 +/- 1.2%	0.85 +/- 0.5%
Potency	10 nM	50 nM

Figure 4.2 CXCL12-mediated migration of CLL B cells and normal B cells**.** A) Representative migration assay profiles for normal B cells (solid line) compared to 2 different CLL patients' cells (dashed lines) performed in triplicate over a range of 0–100 nM CXCL12 and normalized to no chemokine. Data represents the percent of cells migrated through the transwell filter. B) Bar graph comparing the maximum percent cell migration observed in normal B cells and CLL B cells. Data represents an average of multiple transwell migration assays from separate donors, normal B cells *n* = 5, CLL B cells *n* = 7, each performed in triplicate. Differences were found to be statistically significant ($p<0.0001$) based on Student's t-test. C) Table depicting the maximum percent migration to CXCL12 (efficacy) and the concentration at which maximal migration is achieved (potency) observed in normal B cells compared to CLL B cells.

4.3 Results

4.3.1: Normal B cells migrate with higher efficacy and potency to CXCL12 than CLL B cells, despite having lower levels of CXCR4

Chemokines, including CXCL12, are best known for their role in directing cell migration, but it is well established that they can also induce cell survival and proliferation [3]. This observation can be rationalized by the fact that some of the major pathways involved in cell migration (e.g. PI3K/Akt and Raf/MEK/ERK), are also important for survival and proliferation signaling [5]. However, little is known regarding the extent to which there is overlap or divergence of the upstream and downstream effectors of these pathways in the context of migration versus survival/proliferation. Since it has been established that CLL cells have up-regulated expression of CXCR4 compared to normal B cells, and that CXCL12 stimulation of CLL cells activates Akt and ERK1/2 pathways, transwell migration assays were performed on purified CLL B cells and normal B cells to compare their ability to migrate towards CXCL12 [3, 4, 6].

Surprisingly, the normal B cells showed a significantly greater ($p<0.0001$) ability to migrate to CXCL12, with respect to both efficacy (4.5+/−1.2% migration in normal vs. 0.85+/−0.48% migration in CLL cells) and potency (~10 nM in normal vs ~50 nM in CLL cells) (Figure 4.2). Although it was expected that the CLL cells would have the stronger migratory response due to higher CXCR4 expression, these results are consistent with previously published observations that showed weak migration of CLL cells to CXCL12 compared to a much more robust response to the CCR7 ligands, CCL19 and CCL21 [7, 8]. These data suggest that the downstream effects of CXCR4 may be redirected for survival rather than migration, and led us to consider what other pathways or [7] downstream targets of Akt or ERK1/2 might be activated to bias the CXCL12 signaling

response towards survival. Taking a global approach to this question, we performed mass spectrometry-based phosphoproteomics analysis of unstimulated and CXCL12-stimulated CLL cells.

4.3.2: Characterization of phosphopeptides/phosphoproteins in CXCL12-stimulated CLL cells via mass spectrometry

Fresh PBMCs from 5 CLL patients were stimulated over an hour time course with CXCL12, and lysates were generated for IMAC enrichment and LC-MS/MS analysis. Multiple (3 separate duplicate or triplicate experiments with variable acquisition methods) phosphoproteomics data sets were acquired on lysates from the cells of a patient with ZAP-70+ aggressive CLL, referred to as “CLL A”, in order to ensure good coverage of the proteomic space. Smaller phosphoproteomics data sets (single triplicate experiments) were collected from cells of 4 additional patients (CLL B to E) for comparison.

Protein lysates from the CLL cells were trypsin digested and enriched for phosphopeptides via immobilized metal affinity chromatography (IMAC) to yield a highly enriched population of phosphorylated peptides. Phosphopeptides were analyzed by LC-MS/MS using a linear iontrap (LTQ) mass spectrometer. Data was processed using the InsPecT database search algorithm and the spectra were manually inspected for validation (see flow diagram Figure 4.3).

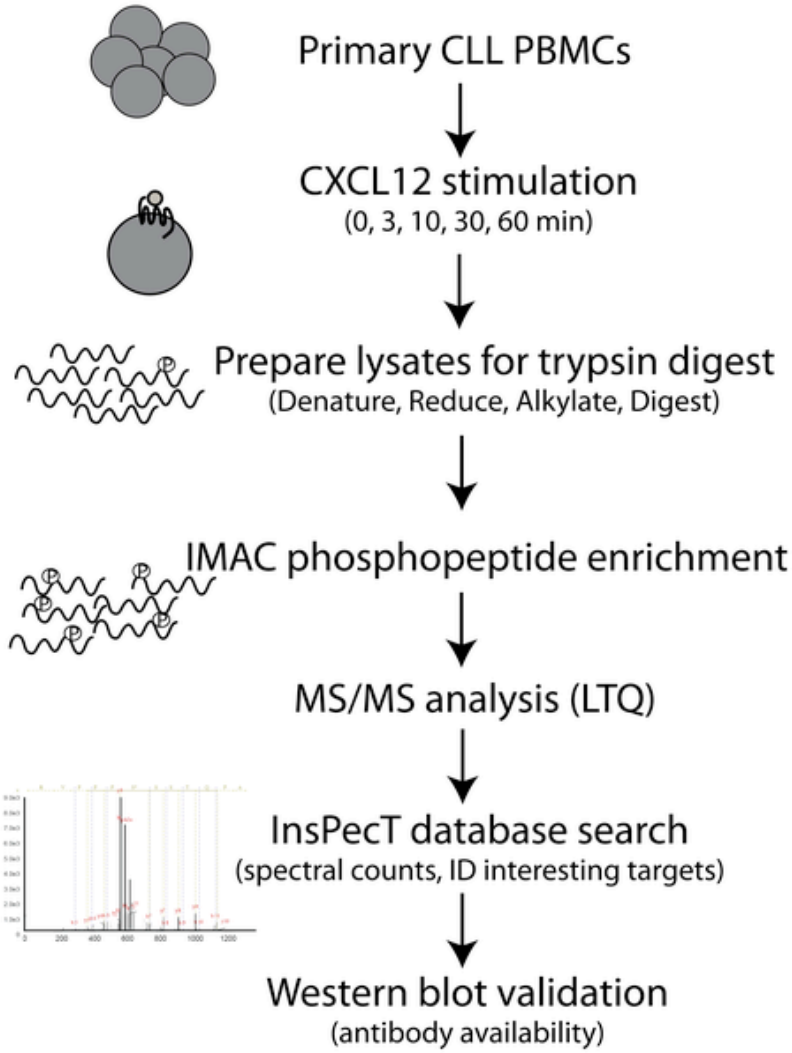

Figure 4.3 Flow chart of CLL phosphoproteomics analysis.
Lysates were prepared from primary CLL B cells that had been stimulated over an hour time course with 30 nM CXCL12. Lysates were denatured, reduced and alkylated in preparation for trypsin digest. Tryptic peptides were then enriched for phosphopeptides by IMAC and LC-MS/MS was performed. Data was analyzed using the InsPecT database search algorithm for phosphorylations on Ser, Thr, or Tyr. A decoy database and manual validation of the spectra were used as quality control. Spectral count comparisons were made as a qualitative assessment of CXCL12 stimulation response and interesting target proteins were selected for follow-up studies if antibodies were available.

Over 10,000 spectra were collected from the combined phosphoproteomics analysis of unstimulated as well as stimulated CLL cells, which was comprised of 1470 phosphopeptides (>1200 unique phosphosites) from 696 phosphoproteins. In general, a

>30% enrichment of annotated phosphopeptides was achieved from our IMAC procedure, which is on par with other phosphopeptide enrichment studies of mammalian cells [9].

To ensure that good coverage of the CLL A data set was obtained, a comparison was made of the overlapping phosphoproteins identified in the CLL A data sets and the smaller CLL B - E data sets. 538 of the 696 total phosphoproteins (>77%) identified in the CLL A data sets were also identified in data sets B - E, suggesting detection of the majority of phosphopeptides detectable by these methods. Also, many of the non-overlapping phosphoproteins identified in CLL B to E but not in CLL A were isoform variants of phosphoproteins detected in CLL A. Figure 4.4 depicts the overlap of CLL B - E with CLL A (Figure 4.4a) and the matrix shows overlap between all of the CLL samples (Figure 4.4b).

A

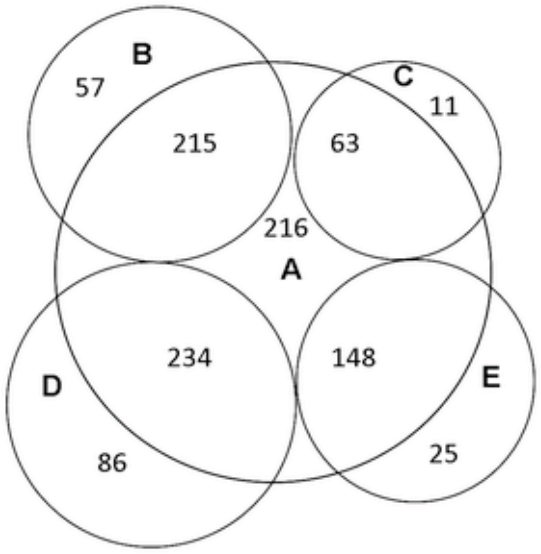

B

SAMPLE	A	B	C	D	E
A	538	215	63	234	148
B	215	271	56	178	97
C	63	56	74	58	37
D	234	178	58	320	104
E	148	97	37	104	173

Figure 4.4 Overlap in phosphoprotein identification between CLL cells from different patients. A) Venn diagram illustrating the degree of overlap between the phosphoproteins identified in CLL A compared to the phosphoproteins identified in CLL B, C and D. B) Matrix table outlining the number of overlapping phosphoproteins identified for CLL A, B, C and D.

4.3.3: Identification of phosphoproteins with prior correlations to CLL and other leukemias

Adding confidence to our phosphoproteomics results, a number of hematopoietic-specific phosphoproteins as well as phosphoproteins with prior implications in CLL and other leukemias were identified. Table 4.1 highlights 9 of the phosphoproteins detected with previous links to CLL/leukemia, including Hematopoietic cell-specific Lyn substrate (Hcls1) and SH2-containing inositol phosphatase-1 (SHIP-1). The phosphorylation status of both Hcls1 and SHIP-1 have been shown to correlate with disease aggressiveness and shorter mean survival [10-12], consistent with the aggressive characteristics of CLL A.

Table 4.1 Phosphoproteins identified by LC-MS/MS analysis with prior implications in CLL/Leukemia disease.

Protein	Gi Accession	Implications in CLL/leukemia	References
B cell novel protein 1 (BCNP1)	31542207	Overexpressed in CLL and other B cell malignancies compared to normal B cells	Boyd et al 2003
Formin-like 1 (FMNL1)	33356148	Akt interacting partner found to be overexpressed in CLL	Favaro et al 2003
Hematopoietic cell-specific Lyn substrate (Hcls1 or HS1)	4885405	Phosphorylation correlated with shorter mean patient survival time in CLL	Scielzo et al 2005
HSP-90 alpha	92859630	Stabilizes Akt and ZAP-70 signaling in CLL, highly activated in CLL, and role in CLL survival	Castro et al 2005
Lyn (Yamaguchi sarcoma viral (v-yes-1))	4505055	Overexpressed in CLL compared to normal B cells, potential anti-apoptotic function in CLL	Contri et al 2005
Minichromosome maintenance protein 2 (Mcm2)	33356547	Role in DNA replication, marker for proliferation and prognosis in B-cell lymphoma	Obermann et al 2005
promyelocytic leukemia protein (PLZF)	4505903	Correlates with apoptotic resistance, higher expression of PLZF associated with lower CLL patient survival	Parrado et al 2000
SH2 containing inositol phosphatase 1 (SHIP-1)	64085167	Phosphorylation status segregated with ZAP-70, correlated with aggressive disease in CLL	Gabelloni et al 2008
Stathmin 1 (oncoprotein 18)	44890052	Overexpressed in acute leukemia cells compared to normal lymphocytes, involved in cell growth and proliferation	Melhem et al 1991

Note:
Table listing select proteins identified by LC-MS/MS with prior implications in CLL or other related leukemias along with the GI accession number, a brief description of biological implications, and references.

Also included in Table 4.1 are phosphoproteins which have been linked to CLL but not necessarily phosphorylation status, including HSP90, B cell novel protein 1, promyelocitic leukemia protein, and formin-like 1 (FMNL1) [13-15]. These proteins have general implications in CLL, but whether differences in phosphorylation status affect the activity or function in disease is unclear. A few additional proteins including minichromosome maintenance protein 2 and stathmin 1 have been linked to disease progression of other leukemias, but not directly to CLL and thus warrant further investigation in CLL. Many of these phosphoproteins did not appear to exhibit changes in phosphorylation in response to CXCL12 or spectral numbers were too low to make an assessment of stimulation response, but HSP-90 and Mcm2 could be potential phosphorylation targets and are thus also highlighted as proteins of interest in Table 4.2.

Table 4.2 Select phosphoproteins from phosphoproteomics analysis with spectral count numbers and known functions.

Adenylyl cyclase-associated protein (CAP1)	5453595	5; 8; 14; 17; 12	Invovled in cAMP pathway, overexpressed in pancreatic cancer, correlated with poor prognosis	Yamazaki et al 2009
Heat shock protein 27 kDa (HSP27)	7706687	1; 10; 13; 7; 7	Downstream target of p38-MAPKAPK2 pathway; involvement in IkB degradation, protection from apoptosis, sequestering and inhibiting cytochrome c release, interacts with Akt	Parcellier et al 2003; Garrido et al 2006
Heterogeneous nuclear ribonuclear proteins (U, D, A1)	U (14141161), D (14110414), A1 (45044445)	U (0; 14; 11; 6; 7), D (3; 21; 25; 20; 14), A1 (13; 33;16; 40; 17)	Nucleocytoplamic shuttling proteins that shuttle mRNAs from site of transcription to start of translation; hnRNPA1 levels are increased in chronic myelogenous leukemia (CML), implications in apoptotic resistance and tumorigenesis; potentially regulated by phosphorylation by various MAPKs	Lervolino et al 2002; Eiring et al 2008; Van der Houven van Oordt et al 2000
HSP90-alpha	92859630	2; 24; 18; 21; 12	Stabilizes PI3K and Akt, pro-proliferative and tumorigenic effects, important for Jak-STAT signaling, Implicated with ZAP-70 stability and signaling in aggressive CLL, less known regarding phosphorylation	Castro et al 2005; Fujita et al 2002; Sato et al 2000; Schoof et al 2009
L-Plastin (lymphocyte cytosolic protein 1)	4504965	0; 4; 9; 1; 1	Actin binding protein expressed in hematopoietic lineage cells as well as malignant cells of non-hematopoietic origin; important for cell polarization and motility	Lin et al 1993; Morley et al 2010
Lymphocyte specific protein 1 (LSP1) (S252)	61742789	1; 9; 11; 5; 8	Downstream target of p38-MAPKAPK2 pathway, PKC, GSK3; F-actin binding protein involved in chemotaxis	Wu et al 2007
Minichromosome maintenance protein 2 (Mcm2)	33356547	2; 7; 2; 4; 2	Role in DNA replication, marker for proliferation and prognosis in B-cell lymphoma	Obermann et al 2005
Programmed cell death factor 4 (PDCD4)	21735596	5; 11; 10; 9; 14	Inhibition of AP1 transcription and eiF4A translational activity, phosphorylation by Akt and p70 S6K is inhibitory and promotes its degradation	Yang et al 2001; Yang et al 2003; Palamarchuk et al 2005; Lankat-Buttgereit et al 2009
serine/arginine repetitive matrix 1 (SRm160)	42542379	15; 57; 57; 40; 30	RNA splicing coactivator; regulates CD44 alternative splicing with potential role in tumor cell invasion	Cheng and Sharp 2006
Small acidic protein	7657234	1; 18; 10; 14; 6	Very little information available, unknown function	
Splicing factor 1 (SF)	42544125	0; 14; 13; 21; 13	Regulates premesseger RNA splicing and gene transactivation and including that of b-catenin/TCF4 complex. Phosphorylated by protein kinase KIS enhances binding to U2AF65	Shitashige et al 2007; Manceau et al 2006
UV excision repair protein RAD23 homolog A (RAD23A, hHR23)	4826964	0; 19; 10; 12; 3	Involved in nucleotide excision repair, recognition of DNA damage; implicated in p53 degradation; phosphorylation function unknown	Glockzin et al 2003

Note:
Spectral count numbers for select phosphoproteins of interest are presented for each CXCL12 (30 nM) stimulation time point (0; 3; 10; 30; 60 min). A brief description of known functions and corresponding references are also provided

4.3.4: Identification of novel downstream targets of CXCL12/CXCR4 signaling in CLL

To semi-quantitatively assess whether phosphorylation of some of the proteins is a consequence of CXCL12 stimulation, spectral counts from the mass spectrometry runs on the stimulated samples off CLL A were compared to those from unstimulated

samples. Select candidate targets of CXCL12-induced phosphorylation are reported in Table 4.2 along with their associated spectral counts. A number of known targets of survival signaling pathways including programmed cell death factor 4 (PDCD4) and heat shock protein 27 (HSP27) were identified as having more spectral counts in the stimulated versus unstimulated samples, and were selected for validation by western blot and further analysis, discussed in detail later. Validation was performed on lysates from CLL cells used in phosphoproteomics analysis (lettered CLL A to E) as well as additional patient cells not examined by phosphoproteomics (CLL1, CLL2, etc) in order to determine consistency of these responses across different patients, since CLL is a heterogeneous disease [1].

Some of the phosphoproteins identified in this study have been previously implicated in cancer malignancy such as Mcm2 and adenylyl cyclase associated protein (CAP1), while little information is available on some of the other potential targets including small acidic protein (Table 4.2). Although two of the proteins (PDCD4 and HSP27) are validated herein as targets of CXCL12-signaling in CLL, the remaining phosphoproteins, while beyond the scope of this work, pose interesting targets for future investigations.

4.3.5: CXCL12 induces the phosphorylation and degradation of PDCD4

PDCD4 is one of the phosphoproteins that appeared to be induced by CXCL12 stimulation based on spectral counts (Figure 4.5 *A* and Table 4.2). It is a known tumor suppressor, and downstream phosphorylation target of Akt, which is known to be activated by CXCL12 in CLL cells [4]. A phospho-specific antibody is also commercially available, making it attractive for follow-up studies [16, 17]. As a tumor suppressor protein, PDCD4 has been implicated in a number of cancers where it is often inhibited

and/or downregulated, disrupting its ability to inhibit eIF4A translational and AP-1 transcriptional activity, processes that are important for cell growth and survival (Figure 4.5 *G*). Phosphorylation of PDCD4 is known to occur by Akt and p70 S6Kinase (p70S6K), which inhibits its activity and leads to its ubiquitination and proteosomal degradation [16-19].

Three separate phosphopeptides from PDCD4 were detected from our analysis: R.FVSpEGDGGR.V (Ser457), R.SGLTVPTSpPK.G (Ser94) and R.DSGRGDSpVSDSGSDALR.S (Ser76) (Figure 4.6). The R.FVSpEGDGGR.V phosphopeptide corresponds to Ser457 phosphorylation, a site known to be phosphorylated by Akt [17]. Therefore, multiple CLL patient samples were examined for PDCD4 phosphorylation in response to CXCL12 by western blot. An increase in phosphorylation of PDCD4 at Ser457 was observed upon CXCL12 stimulation in CLL A cells (Figure 4.5 *B*), as well as all 9 additional CLL patient cells examined (representative western blot in Figure 4.5 *C*). Increases in PDCD4 phosphorylation levels was variable between patients and ranged from 1.7-fold to 7.4-fold and averaged to approximately 3.4-fold (n = 10), as quantified by densitometry analysis of western blots (Figure 4.5 *C*). Although variability was noted, this variation did not cluster according to disease aggressiveness.

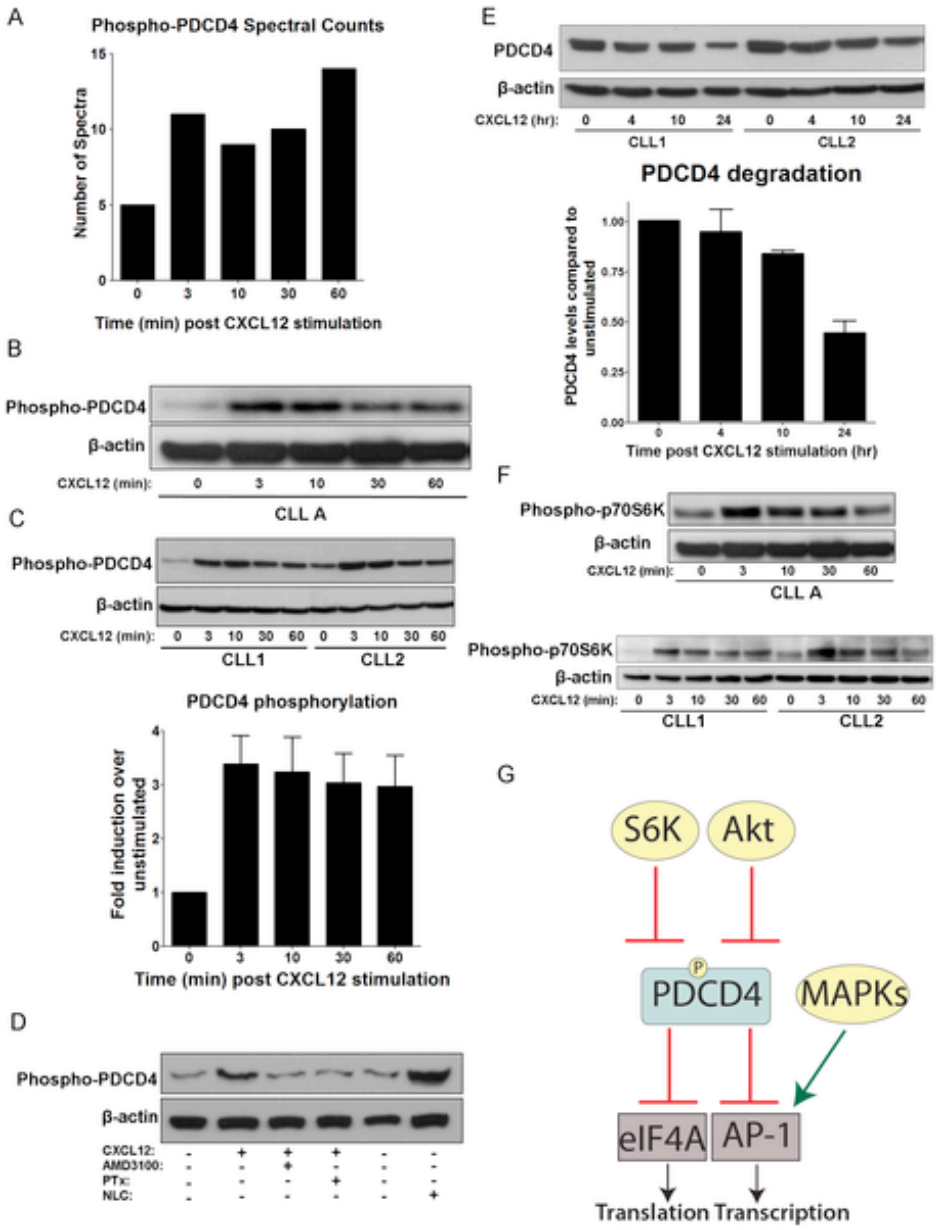

Figure 4.5 CXCL12 Induces Phosphorylation of PDCD4 at Ser457**.** (A) Spectral counts of phosphopeptides from LC-MS/MS analysis. (B) Western blot of PDCD4 phosphorylation over time upon CXCL12 stimulation. (C) (*Top*) Western blot of PDCD4 phosphorylation of additional CLL cells (*Bottom*) Densitometry analysis of PDCD4 phosphorylation levels from 10 separate CLL patient cells (±SEM). (D) Western blot of PDCD4 phosphorylation in unstimulated/untreated CLL cells or 3 min CXCL12 stimulations (30 nM) in the presence (+) or absence (−) of preincubation with AMD3100 or Pertussis toxin (PTx). NLC lysate represents CLL cells cultured in presence of NLCs . (E) (*Top*) Western blot of total PDCD4 in CLL cells (*Bottom*) Densitometry analysis of total PDCD4 western blots. (F) Western blot stripped and reprobed from Figure 4.4B for p70S6K phosphorylation (Thr389) G) Diagram of PDCD4 signaling.

A Ser457

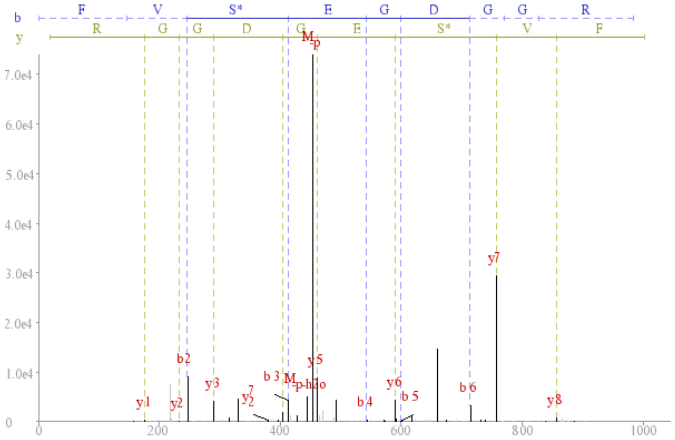

B Ser94

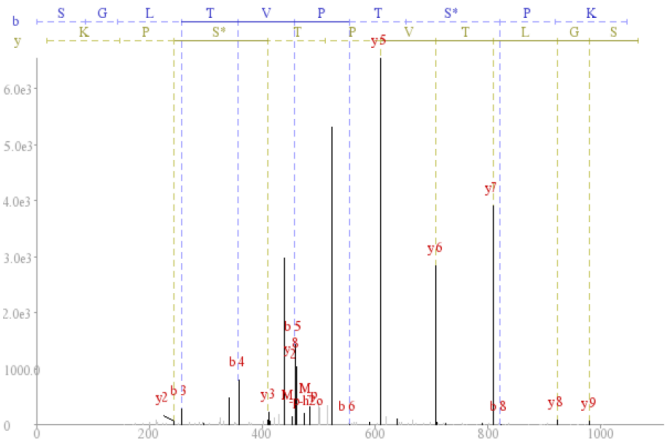

C Ser76

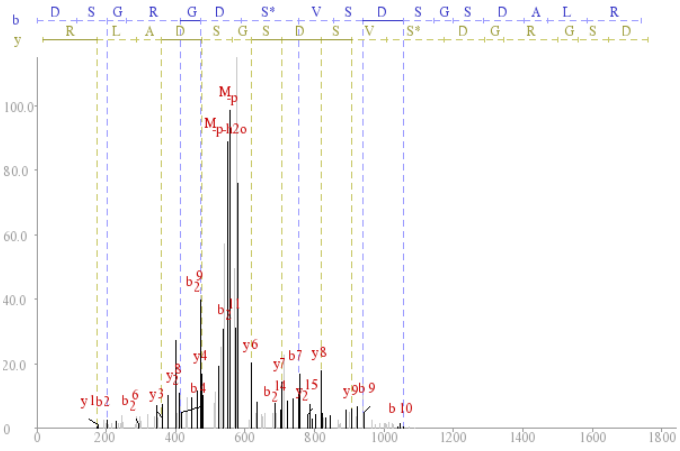

4.6 Mass spectra of PDCD4 phosphopeptides. Mass spectra from the 3 phosphopeptides from PDCD4 that were identified in the LC-MS/MS analysis. The top spectrum (A) represents the phosphopeptide with Ser457, which is the phosphosite detected by the antibody used in follow-up western blot analysis. (B) Spectrum for Ser94 phosphorylation site. (C) Spectrum for Ser76 phosphorylation site.

As a control to ensure that the phosphorylation was dependent on CXCL12/CXCR4 signaling and to determine if the effects were dependent on signaling through the G protein, Gi, CLL cells were pretreated with the small molecule CXCR4 antagonist, AMD3100, or the Gi-inhibitor, pertussis toxin (PTx) prior to a 3 min stimulation with CXCL12. As shown in Figure 4.5 *D*, both AMD3100 and PTx completely abrogated phosphorylation suggesting it is CXCR4 and G-protein signaling dependent. Furthermore, to ensure that phosphorylation of PDCD4 has relevance in a more physiological context, the levels of PDCD4 phosphorylation were examined in CLL cells that had been cultured with NLCs (+) compared to those without NLCs (−). As with CXCL12 stimulation, the coculture of CLL cells with NLCs led to an increase in the phosphorylated levels of PDCD4 (Figure 4.5 *D*).

Since the phosphorylation of PDCD4 is known to lead to its ubiquitination and degradation [17, 18], we examined levels of total PDCD4 over a 24 h time period (0, 4, 10 and 24 h) following CXCL12 stimulation. As shown in Figure 4.5 *E*, 24 h post-stimulation resulted in PDCD4 degradation to ~45% of starting levels.

Additionally, although it is well established that Akt is phosphorylated downstream of CXCL12 signaling in CLL cells [4], it has not been established whether p70S6K, another kinase known to phosphorylate PDCD4 leading to its ubiquitination and degradation, is activated in CLL cells by CXCL12. Western blot analysis revealed that phosphorylation and thus activation of p70S6K (Thr389) was induced by CXCL12-stimulation in the CLL cells (Figure 4.5 *F*).

4.3.6: HSP27 expression and phosphorylation is variable in CLL cells

The other phosphoprotein investigated further was HSP27 (phosphopeptide: R.QLSphosSGVEIR.H, Ser82) (mass spectrum shown in Figure 4.7). HSP27 was also

selected due to spectral counts indicative of phosphorylation upon CXCL12 activation of CXCR4 (Figure 4.8 *A*), its implications in cancer and protection from apoptosis, and the availability of a phospho-specific antibody at the Ser82 phosphorylation site [20-22]. Additionally, HSP27 is an interesting target since it is downstream of p38-MAPK signaling [21] which has not received much attention in association with CLL and therefore represents a pathway with potentially novel implications in CLL survival.

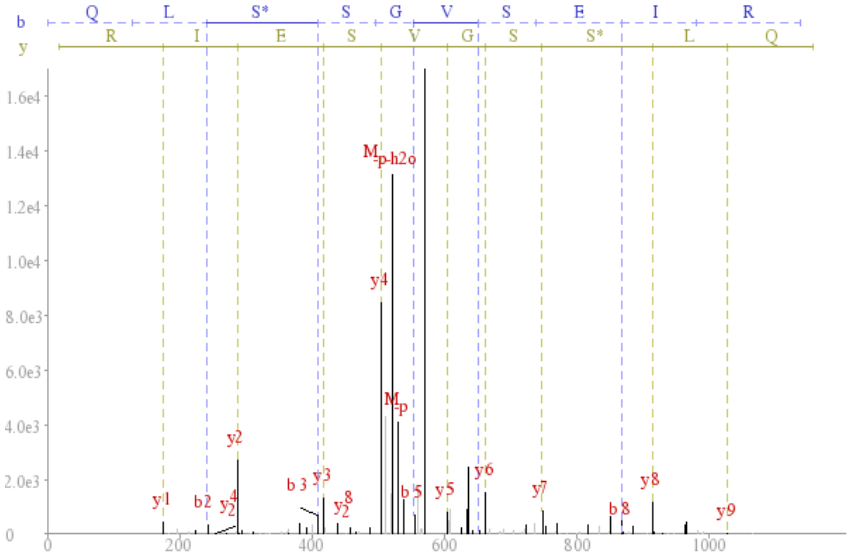

4.7 Mass Spectrum of HSP27 phosphopeptide. Mass spectrum from the HSP27 phosphopeptide (Ser 82) that was identified in the LC-MS/MS analysis.

Interestingly, while PDCD4 was found to be a common target of CXCL12 signaling in all CLL samples examined, phospho-HSP27 and total HSP27 protein were only detectable by western blot in a subset of ~25% (3 out of 12) of CLL patients examined (representative western blot Figure 4.8 *B*). Nevertheless, HSP27 was indeed present and did exhibit an increase in phosphorylation upon CXCL12 stimulation in the CLL A patient samples from which the phosphoproteomics data was collected (Figure 4.8 *B*). Since p38-MAPK is known to be upstream of HSP27 phosphorylation, we also examined p38 phosphorylation among the CLL patient samples (Figure 4.8 *C*);

correspondingly, we observed detectable p38 phosphorylation only in the samples that also exhibited the HSP27 phosphorylation (CLL A, Figure 4.8 *B*). Although no common factor could be determined among the patients examined with detectable HSP27, a larger sample size might identify common features of these cells and determine whether HSP27 is influencing the survival of this subset of CLL patients.

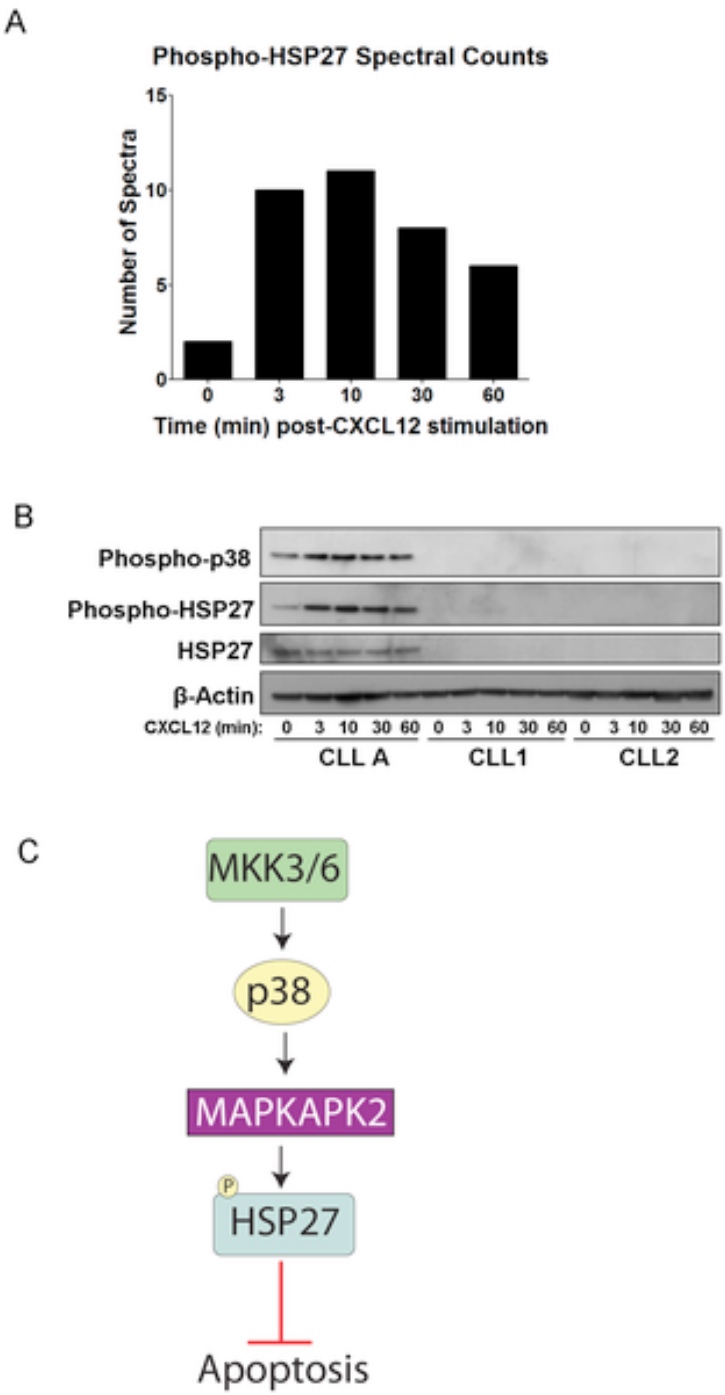

Figure 4.8 Phosphorylation of HSP27 in subset of CLL patients. (A) Bar graph depicting the spectral counts of HSP27 phosphopeptides (Ser82) observed in the LC-MS/MS analysis after CXCL12 stimulation. (B) Western blot detecting phosphorylation of HSP27 and the upstream p38-MAPK, and total HSP27 over time course of 0 to 60 min CXCL12 stimulation (30 nM) from CLL A patient cells and 2 other representative CLL patients' cells. β-actin was run as a loading control, (C) Signaling diagram of HSP27, which can protect from apoptosis, and its upstream regulation by p38-MAPK and MAPKAPK2.

4.4 Discussion

CLL is the most common leukemia in the Western world [1]. The accumulation of CLL B cells is believed to result from low rates of precursor cell proliferation and via recruitment of accessory cells that create a supportive microenvironment by producing factors that foster CLL survival [1, 23]. The chemokine, CXCL12, is one of the cytokines produced by cells in the microenvironment that enhances CLL survival *in vitro* and likely *in vivo* [4]. Although chemokines are best known for their role as chemoattractants, we show here that CLL cells are much less capable of migrating to CXCL12 compared to CLL B cells, despite an upregulation of CXCR4 on the CLL cells [6]. While the low levels of migration may still play a role *in vivo* [24], it is evident that the CXCL12/CXCR4 axis is also networked into pathways involved in survival. In contrast, CXCR7, the other receptor of CXCL12, is not expressed on the surface of CLL cells although it is expressed on normal B cells [24, 25]. Thus, while there is overlap in signaling pathways activated by CXCL12 in CLL cells and normal B cells, the differences in migration and CXCR7 expression, and the potential bias towards survival in CLL cells, suggest significant differences in the role that the CXCL12/CXCR4 axis plays in the context of the normal and pathological cells.

Phosphoproteomics analysis of CXCL12-stimulated CLL cells was performed in an effort to determine potential downstream signaling targets that could contribute to the survival and malignancy of CLL cells. As these are precious non-renewable primary patient cells, the intent of our phosphoproteomics approach was to generate hypotheses rather than an exhaustive analysis of the CLL phosphoproteome. Therefore, while it would be ideal to use a number of phospho-enrichment strategies in addition to IMAC

(e.g. TiO_2) and to employ additional liquid chromatography separation steps besides C18 (e.g. hydrophilic interaction liquid chromatography (HILIC)) to expand the number of phosphoproteins identified, we focused our efforts on well established methods [26, 27]. Along these lines, the use of quantitative phosphoproteomics strategies is limited since these cells do not replicate and cannot be cultured long term. Thus, stable isotope labeling of amino acids in cell culture (SILAC) is not possible [28]. Post-digest labeling with iTRAQ or ICAT isotopic labels [28] is also difficult due to limited sample availability, limitations in instrumentation (one-third rule with the LTQ spectrometer restricting detection of the labels in the low molecular weight range) [29], and the labile nature of phosphates and labels which causes reduced fragmentation and detection in MS/MS spectra [30]. While understanding its limitations, spectral counting was employed as a semi-quantitative assessment of the CXCL12-stimulation responses [31] and several candidates were followed up by western blot validation. In addition to the above examples with PDCD4 and HSP27, which showed that the spectral counting provides a relatively good approximation of stimulation response, spectral counts reflecting fairly even levels of phosphorylated p21-activated kinase (PAK2), another target of the PI3K pathway, was also confirmed by western blot in all six patient cells probed for phospho-PAK2 (Ser141) (Figure 4.9).

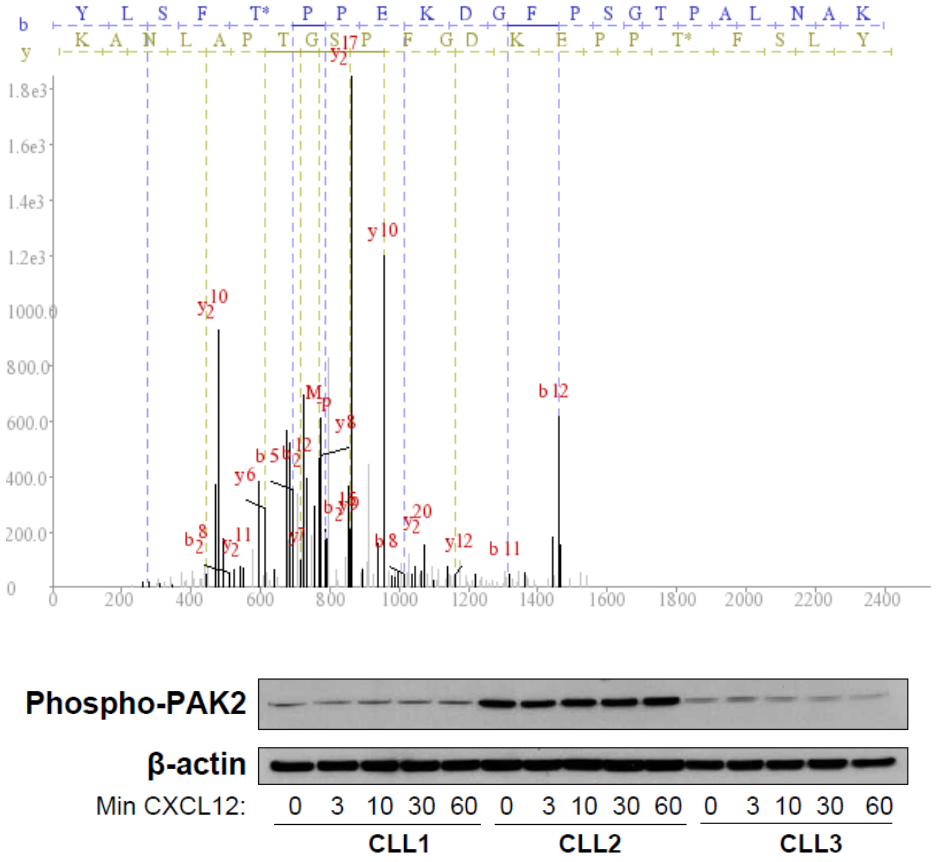

4.9 Phosphorylation of PAK2 is present but not induced by CXCL12 in CLL cells (*Top*) Mass spectrum of the phosphopeptide K.YLSpFTPPEK.D (Ser141) of PAK2, which was present in all proteomics runs but had fairly even spectral counts (1–3 spectra) in each CXCL12 stimulation time point). (*Bottom*)Representative western blot of PAK2 phosphorylation (Ser141) over 60 min time course of 30 nM CXCL12 stimulation in 3 different CLL patient's cells reflects no changes in phospho-PAK2 upon stimulation, although total phospho-PAK2 levels were variable between different patients' cells. β-actin served as a loading control.

Through this phosphoproteomics approach, we were able to confidently identify close to 700 phosphoproteins in the CLL samples, including numerous proteins previously implicated in CLL disease. Additionally, we identified many proteins that appear to exhibit changes in phosphorylation levels in response to CXCL12. This data led to the identification and validation of several previously unknown phosphorylation

targets of CXCL12 signaling. Typical approaches (e.g. western blot) for investigating signaling in response to stimuli require *a priori* knowledge of specific targets and the availability of phospho-specific antibodies, which limits the ability to globally assess cellular signaling events. Furthermore, validation studies of CLL cells are difficult since their viability in culture is limited. They are also difficult to manipulate through transfection and transduction since they do not divide in culture or infect well (e.g. they require high MOI and/or pre-activation of cells with CD40L and IL-4 [32] which could complicate interpretation of signaling analysis). Therefore, this mass-spectrometry-based approach seemed the most effective method for gaining new insight into the function of CXCL12 on CLL cell survival and possibly disease aggressiveness. Although not done in this study, comprehensive MS analysis of many patients may help to distinguish variations between patients, and with disease stratification and the identification of judicious therapeutic targets.

To our knowledge, this is the first report demonstrating that PDCD4 is a phosphorylation target downstream of CXCL12 signaling in CLL or other cell types. This finding is exciting due to the established role of PDCD4 as a tumor suppressor and as a substrate of Akt [17, 18]. Although little is known regarding the function of two of the phosphorylation sites of PDCD4 (Ser94 and Ser76) identified from the LC-MS/MS analysis, phosphorylation at Ser457 near the C-terminus of the protein is a well-established site with known functional implications. Phosphorylation at Ser457 by Akt has been shown to result in nuclear translocation of PDCD4 and a decrease in its ability to inhibit AP-1-mediated transcription and eIF4A-mediated translation [16, 19]; although Ser67 phosphorylation was not directly identified in our LC-MS/MS analysis, it is likely that this sight is also phosphorylated in response to CXCL12 stimulation since PDCD4 degradation was observed following stimulation [17, 18]. In combination, these effects

may reduce the growth regulating/tumor-suppressor capacity of PDCD4, thereby contributing to CLL cell survival and the malignancy phenotype. Validation of PDCD4 phosphorylation also led to the identification of p70S6K phosphorylation and activation downstream of CXCL12 signaling in CLL cells.

Based on the phosphoproteomics analysis, HSP27 appeared to be another promising phosphorylation target of CXCL12-signaling. HSP27 and several other HSPs have received attention in the context of cancer due to their cytoprotective/anti-apoptotic functions. Specifically, HSP27 indirectly inhibits cytochrome c release and caspase activation and it sequesters cytosolic cytochrome c. It also promotes degradation of the inhibitor of NF-kB (IkB) and p27kip, and interacts with and supports the activity of Akt under stressful conditions, all leading to protection from apoptosis [22, 33]. We identified the presence of phosphorylated and total HSP27 protein and its upstream activator p38-MAPK in a subset (~25%) of cell samples from different CLL patients. Of note, the observed variability in signaling between different CLL patient cells highlights the underlying heterogeneity of the disease. Furthermore, it serves as a reminder of how different parameters including patient differences (age and gender), variations in clinical course such as aggressiveness, stage and prognosis, and different treatments (e.g. chemotherapy, gene therapy, etc) may alter how the cells respond to different stimuli. Such variability is not unprecedented as Messmer *et al.* (submitted manuscript) have demonstrated differences in CXCL12-mediated MEK and ERK activation in different ZAP-70 subgroups of CLL, and Montresor *et al.* demonstrated differences in CXCL12-mediated lymphocyte function-associated antigen-1 (LFA-1) activation in normal B cells compared to CLL B cells and amongst the cells of different CLL patients [34]. Thus, it is reasonable to expect that different patients will exhibit different responses to stimuli,

whether it is a survival stimulus from the microenvironment or a therapeutic agent used to treat the disease.

These results showing patient variability in HSP27 expression emphasize the strength of utilizing primary cells for understanding disease pathogenesis as opposed to cell lines, which are much more homogenous, but can be less insightful and sometimes misleading. While there was considerable overlap in the phosphoproteins identified from LC-MS/MS analysis between different patients (CLL A – E), more comprehensive MS analysis of multiple patients may help to distinguish variations in signaling responses between patients. Along these lines, since HSP27 is often induced following stressful cellular events such as treatment with chemotherapeutics, its induction in certain patients could reflect a response to treatment. For example, lymphoma cells which did not express Hsp27 were sensitive to apoptosis while those expressing Hsp27 were resistant to apoptosis induced by Bortezomib (PS-341), a proteasome inhibitor [35]. Silencing of Hsp27 in the resistant lymphoma cells then rendered them susceptible to Bortezomib-induced death, demonstrating its link in resistance to this chemotherapeutic treatment [35]. Thus, a larger patient sample size may reveal if expression of HSP27 is induced by certain chemotherapeutics or in particular subsets of patients and whether there is any correlation to refractory disease, as resistance to chemotherapy is one of the major hurdles in treating CLL [23].

Herein we present follow-up data to PDCD4 and HSP27, although there are numerous other candidate phosphoprotein targets of CXCL12 signaling in CLL cells that have been proposed (Table 4.2). A summary of our findings from phosphoproteomics analysis combined with some previously established pathways of CXCL12 signaling in CLL are summarized in a signaling diagram (Figure 4.10). Overall, our data suggests that CXCL12 may preferentially activate survival signaling pathways rather than those

involved in cell migration in CLL cells, although some of the pathway components (Gi, Erk, Akt) are common nodes. We have demonstrated that the use of phosphoproteomics is a feasible and informative means of evaluating signaling responses to CXCL12 in CLL, which could be employed for investigating a variety of other stimuli in these or other primary cells. Through phosphoproteomics detection and western blot validation, PDCD4 was found to be a common phosphorylation target of CXCL12-signaling in CLL while HSP27 was present in only a subset of CLL patients. Although our focus was on CXCL12 as a survival factor, it is likely that other growth and survival stimuli may synergistically activate these pathways and downstream targets. Therefore, PDCD4 and HSP27, which have previous implications in regulation of apoptosis and carcinogenesis, may represent potential therapeutic targets for treatment of CLL. In fact, small molecule stabilizers of PDCD4, that enhance its function as a tumor suppressor by inhibiting its degradation, are currently being developed due to its potential as a therapeutic target for numerous cancers. Such agents could prove to be useful agents in combination with other therapeutic modalities for the treatment of CLL [36].

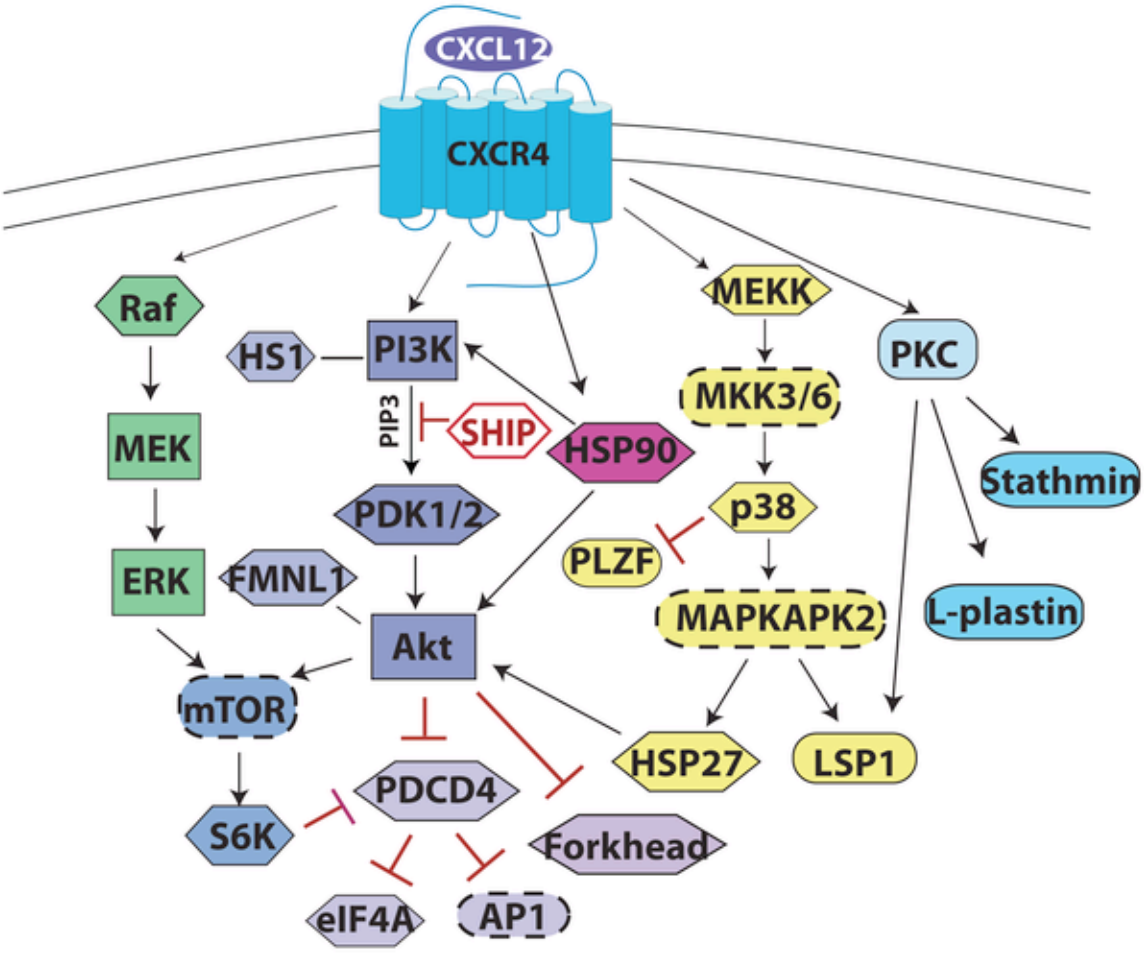

Figure 4.10 Summary of CXCL12-mediated signaling in CLL. Signaling diagram depicting pathways activated downstream of CXLC12. Through direct or indirect mechanisms, arrows indicate factors that are activated, red lines ending with a bar indicate factors that are inhibited by the upstream factor, and lines (no arrowhead) indicate interactions. Proteins in hexagons were identified and validated herein or were previously known targets also detected in the LC-MS/MS. Proteins in rectangles are known key signaling molecules of these pathways that were not detected in this LC-MS/MS data set. Proteins in ovals with dashed lines are likely intermediates/targets of the pathways based on previous studies. Proteins in oval shape were also identified by LC-MS/MS but have yet to be validated. Much of our focus has been on the PI3K/Akt and Raf/MEK/ERK pathways due to known implications in CLL cell survival and resistance to apoptosis. Furthermore, the potential involvement of the p38-MAPK pathPhway in some CLL patients with activation of HSP27 and LSP1 is outlined.

4.5 Materials and Methods

4.5.1: Cells and reagents

Peripheral blood mononuclear cells (PBMCs) were obtained from leukopheresis samples of CLL patients following written consent at the Rebecca and John Moores Cancer Center at the University of California San Diego (UCSD), in compliance with the Declaration of Helsinki. These studies were approved by the Institutional Review Board of UCSD. PBMCs were isolated by Ficoll-Paque (GE Healthcare) density gradient centrifugation as previously described [4]. The isolated PBMCs were used fresh and cultured for phosphoproteomics analysis or frozen as liquid nitrogen stocks in 90% heat inactivated fetal bovine serum (FBS)/10% DMSO for follow-up analysis by western blot. PBMCs used in the proteomics experiments were determined to be >90% CLL B cells as assessed by CD5+/CD19+ staining and flow cytometry analysis. For western blot validation, CLL B cells were purified from the PBMCs by negative selection using the magnetic associated cell sorting (MACS) (Miltenyi Biotec, Auburn, CA) by depletion of CD14+ (monocytes) and CD2+ (T cells) cells, leading to >99% CLL B cell purity. Normal B cells were purified from PBMCs from healthy donors (San Diego Blood Bank) using the MACS B cell Isolation Kit II (Miltenyi Biotec, Auburn, CA) according to the manufacturer's protocol and were determined to be >90% pure by flow analysis staining for CD19+/CD3-/CD14- cells. RPMI-1640 glutamax media and FBS were obtained from Gibco (Invitrogen, Carlsbad, CA).

4.5.2: Recombinant CXCL12 preparation

CXCL12 was expressed recombinantly in BL21 *E. coli* as previously described [26]. In brief, CXCL12 was expressed as a His-tag fusion protein and purified from

inclusion bodies. Bacterial cell pellets were sonicated and washed with deoxycholate following resuspension in 10 mM Tris pH 8.0 with 1 mM $MgCl_2$, 200 µg DNAse, and Complete Protease Inhibitor Cocktail (EDTA-free) (Roche, Indianapolis, IN). Protein was then solubilized in 6 M Guanadine-HCl, 100 mM sodium phosphate, 10 mM Tris-Cl, pH 8.0, using a dounce homogenizer. CXCL12 was purified over a Ni-NTA column and refolded with Hampton Fold-It Buffer #8 (Hampton Research, Aliso Viejo, CA), then dialyzed and concentrated using Amicon Ultra centrifugal concentrators (MWCO = 5000). The His-tag was removed by cleaving with enterokinase (NEB, Ipswich, MA) at a 1:100,000 molar ratio overnight at room temperature. CXCL12 was then purified by HPLC and the identity and purity was validated by ESI mass spectrometry. Transwell migration assays on Jurkat cells were used to validate functionality of the purified CXCL12.

4.5.3: Migration assays

Transwell migration assays (Corning, Corning, NY) were performed on purified CLL B cells and B cells from healthy donors using inserts with a 6.5 mm diameter, 5.0 µm pore size. Cells were resuspended at 2.5×10^6 cells/mL in RPMI+10%FBS and 100 µL of cell suspension was added to the inserts. CXCL12 was diluted over a concentration range of 0 nM to 500 nM in a 600 µL total volume of RPMI+10%FBS in the bottom wells. As a positive control and cell count reference, cells were added directly to the wells without inserts. Transwell migration was conducted for 2 h at 37°C/5%CO_2. Cells that had migrated into the bottom wells were then collected and counted by flow cytometry on a FACSCalibur (BD Biosciences, San Jose, CA). Data was normalized to no chemokine control and percent migration was calculated from the positive reference control.

4.5.4: Preparation of CLL lysates for proteomics

CLL cell lysates for phosphoproteomic analysis were prepared as previously described [26]. Briefly, 3×10^9 total CLL PBMCs were washed with sterile PBS and resuspended at 1×10^7 cells/mL in serum-free RPMI-1640 media. The CLL cell suspension was distributed evenly into five 15 cm plates (6×10^8 cells/plate) (Corning Inc, Corning, NY) and cultured for 2 h at 37°C/5% CO_2 prior to stimulation with CXCL12. CLL cells were then either unstimulated or stimulated for 3 min, 10 min, 30 min, or 60 min with 30 nM CXCL12. All plates were harvested at the same time with 3 mL ice cold cytoplasmic lysis buffer containing 10 mM HEPES, pH 7.9, 1.5 mM $MgCl_2$, 10 mM KCl, 0.5 mM dithiothreitol (DTT) (Sigma, St. Louis, MO), Complete Protease Inhibitor Cocktail (Roche Diagnostics, Indianapolis, IN), and Halt Phosphatase Inhibitor Cocktail (Pierce, Rockford, IL) for 30 min on ice. Lysates were clarified by centrifugation at 20,000 rcf for 20 min at 4°C. The supernatants were distributed into protein LoBind Eppendorf tubes (Eppendorf, Westbury, NY) and stored at –80°C. The total protein concentration of the CLL lysates was determined using a BCA protein assay (Pierce, Rockford, IL).

4.5.5: IMAC phosphopeptide enrichment

IMAC enrichment was performed as previously described [26]. Briefly, 2 mg of CLL lysates were denatured with 1% sodium dodecyl sulfate (SDS) (Fisher Scientific, Pittsburgh, PA), reduced with 10 mM DTT, and alkylated with iodoacetamide (Sigma, St. Louis, MO). Proteins were then precipitated with 50% ethanol/50% acetone/0.1% acetic acid (HAC). The pellets were resuspended in 6 M urea/0.1 M Tris, pH 8.0, and vortexed to solubilize the protein. The urea concentration was then diluted five-fold by addition of 50 mM Tris, pH 8.0 and protein was digested overnight at 37°C using sequencing-grade modified trypsin (Promega, Madison, WI) at a ratio of 1:50 (trypsin:protein). Trypsin was

inactivated by acidification of the digests with trifluoroacetic acid to 0.3 to 0.5% (v/v). Prior to IMAC enrichment, peptide mixtures were desalted with 50 mg Sep-pak C18 cartridges (Waters Corp, Milford, MA). IMAC beads were prepared by stripping Ni-NTA spin column resin (Qiagen, Valencia, CA) and recharging the beads with 100 mM $FeCl_3$ (Fluka reagent, Sigma, St. Louis, MO). IMAC beads were then packed into gel loading tips with glass wool and conditioned with 25% Acetonitrile (ACN)/0.1% HAC. Nonspecific peptides were removed by washing twice with 30 µL of 25% ACN/0.1% HAC/0.1 M NaCl, twice with 0.1% HAC, and twice with 30 µL of Milli-Q H_2O. Phosphopeptides were eluted with a total volume of 50 µL over three elutions with 1% phosphoric acid. All fractions were collected in protein LoBind Eppendorf tubes, speed-vac dried, and stored at –20°C until MS analysis. Analysis of IMAC washes and flow through by LC-MS/MS confirmed successful binding of phosphopeptides to the IMAC columns as less than 0.1% of these peptides were found to be phosphorylated, and the few that were detected were redundant with phosphopeptides identified in the IMAC enriched samples.

4.5.6: Mass spectrometry and data processing

IMAC-enriched CLL peptides were resuspended in Milli-Q H_2O +0.1%HAC and analyzed by reversed-phase, C18 capillary liquid chromatography and tandem mass spectrometry (LC-MS/MS) on a Thermo-Finnigan LTQ ion trap mass spectrometer. The capillary LC columns (~17 cm) were pulled and packed in-house using deactivated fused silica (100 µm) (Agilent, Santa Clara, CA) as previously described [26]. Angiotensin II (Sigma-Aldrich, St. Louis, MO) was run after every two CLL sample runs as a control for column performance. The standard method used for all samples was as follows: 95% A/5% B (buffer A = 0.1% HAC in HPLC-grade Milli-Q H_2O, buffer B = 0.1% HAC in HPLC-grade ACN) for 20 min, 60% A/40% B for 30 min, 20% A/80% B for 6 min,

followed by a final washing step of 95% A/5% B for 30 min at 250 µl/min. A flow rate of 200 to 500 nL/min through the capillary column was achieved by splitting the flow of solvent before it reached the column. Samples were run in data-dependent mode in which the spectrometer performed one full MS scan followed by six MS/MS scans of the top six most intense ions in the parent spectrum with an *m/z* ranging from 400 to 2000. The dynamic exclusion list was varied in order to get a range of coverage and spectral counts. The standard dynamic exclusion list applied had a repeat count of 1, a repeat duration of 30 s, an exclusion size of 100, an exclusion duration of 180 s, and an exclusion mass width of 1.50. Other variations included a list of the top 25 peptides with a repeat duration of 60 s, an exclusion of the top 5 most abundant peptides, and a dynamic exclusion list turned off. The spray voltage was 1.8 kV. On average, the scan rate in this experiment ranged from four to eight scans per second.

A comprehensive phosphoproteomics data set from cells of one particular patient (CLL A) with unmutated IgHV and ZAP-70+ status (indicative of more aggressive disease) was collected from two separate triplicate runs and one duplicate run in order to obtain good coverage and number of spectra for comparison. Phosphoproteomics analyses of 4 additional CLL patients' cells (CLL B – E) (each run in single triplicate experiments) were also performed to ensure reproducibility between different patient cells and stimulations. CLL B, D and E also had more aggressive (high ZAP-70) characteristics (high ZAP-70) while CLL C was of the indolent (low ZAP-70) subgroup. Following data collection, RAW data files were converted to mzXML data files using the program ReAdW (http://tools.proteomecenter.org/ReAdW.php). Data analysis of the MS/MS spectra was performed using the open-access database search tool, InsPecT [37, 38], with the UniProt human database, the UniProt shuffled human decoy database as well as common contaminants databases (e.g. keratin). Peptide sequencing searches

were defined for tryptic cleavage restraints and to allow for modification of up to two phosphorylation sites (Ser, Thr, or Tyr) on a peptide. Spectra were sorted by *p*-values according to the InsPecT scoring function and the target decoy database was used as a measure of the overall quality of MS/MS data. Peptides smaller than 7 amino acids and peptides with more than one missed cleavage were excluded from analysis. Peptides with a false discovery rate (FDR) of less than 1–2% were manually validated for positive identification.

4.5.7: Western blots and antibody reagents

For western blot analysis, patient CLL cells used for phosphoproteomics as well as additional patient's cells were used. Purified CLL B cells were cultured in serum-free RPMI at 1×10^7 cells/mL for 2 h at 37°C/5%CO_2 and then stimulated with 30 nM CXCL12 over an hour time course (unstimulated, 3, 10, 30 and 60 min) or for 4 h, 10 h, and 24 h for PDCD4 degradation analysis. For inhibitor studies, CLL cells were pre-treated with 40 μM AMD3100 (Sigma) or 200 ng/ml Pertussis toxin (List Biological Laboratories) for 1 h prior to stimulation with CXCL12. Coculture of CLL cells with NLCs was performed as previously described [39], [4] and then the CLL cells were collected and centrifuged for harvest. Cells were lysed on ice for 30 min in Ripa buffer (10 mM Tris pH 7.4, 150 mM NaCl, 1% Triton X, 0.1% Na-Deoxycholate, 0.1% SDS and 5 mM EDTA) containing Complete Protease Inhibitor Cocktail (Roche, Palo Alto, CA) and Halt Phosphatase Inhibitors (Pierce). Lysates were clarified by centrifugation at 20,000 rcf for 10 min at 4°C. A BCA protein assay (Pierce) was performed to determine total protein concentration and 20 μg of total protein was loaded into each well of a Criterion 4–12% Bis-Tris gel and run with the XT MES buffer system (Bio-Rad, Hercules, CA). Gels were transferred onto PVDF membranes (Bio-Rad), blocked with 5% milk-TBST, and

incubated overnight at 4°C with primary antibodies. Blots were washed 3 times for 10 min with Tris Buffered Saline + 0.1% Tween (TBST) and then incubated for 1 h at room temperature with secondary antibodies conjugated to HRP, washed again 3 times with TBST and then developed with Amersham ECL-plus (GE-healthcare) or SuperSignal West femto-sensitivity reagent (Pierce). Blots were stripped with Restore western blot stripping solution (Pierce) for 10 min at room temperature and then re-probed with other antibodies and/or β-actin as a loading control. Primary antibodies were diluted into 5% BSA-TBST at recommended concentrations. Phospho-PDCD4 and PDCD4 antibodies were obtained from Rockland Immunochemicals. Phospho-p38, phospho-HSP27, HSP27, phospho-S6K, and β-actin were obtained from Cell Signaling Technology. Densitometry analysis was performed using ImageJ software (NIH) and normalized to β-actin loading controls.

4.5.8: Flow cytometry

CLL B cells or normal B cells were purified for flow cytometry analysis. Cells were washed and resuspended in a 0.5% bovine serum albumin (BSA) (Sigma) in Phosphate Buffered Saline (PBS) solution and stained for CXCR7 expression using an APC-conjugated antibody (clone 11G8) (R&D systems) or an APC-conjugated IgG1 isotype control according to manufacturer's protocol (R&D systems). Flow cytometry data was collected on a FACSCalibur cytometer (BD Biosciences) and analyzed using FlowJo software.

4.6 Acknowledgements

Chapter 4 was published in *PLoS ONE*: O'Hayre M, Salanga CL, Kipps TJ, Messmer D, Dorrestein PC, Handel T. Elucidating the CXCL12/CXCR4 Signaling Network in Chronic Lymphocytic Leukemia through Phosphoproteomics Analysis. *PLoS ONE*. **2010.** The dissertation author was a co-investigator and co-author of this paper, substantially contributing to the mass spectrometry based portion of this investigation.

4.7 References

1. Chiorazzi, N., K.R. Rai, and M. Ferrarini, *Chronic lymphocytic leukemia.* N Engl J Med, 2005. **352**(8): p. 804-15.

2. Zou, Y.R., A.H. Kottmann, M. Kuroda, I. Taniuchi, and D.R. Littman, *Function of the chemokine receptor CXCR4 in haematopoiesis and in cerebellar development.* Nature, 1998. **393**(6685): p. 595-9.

3. O'Hayre, M., C.L. Salanga, T.M. Handel, and S.J. Allen, *Chemokines and cancer: migration, intracellular signalling and intercellular communication in the microenvironment.* Biochem J, 2008. **409**(3): p. 635-49.

4. Nishio, M., T. Endo, N. Tsukada, J. Ohata, S. Kitada, J.C. Reed, N.J. Zvaifler, and T.J. Kipps, *Nurselike cells express BAFF and APRIL, which can promote survival of chronic lymphocytic leukemia cells via a paracrine pathway distinct from that of SDF-1alpha.* Blood, 2005. **106**(3): p. 1012-20.

5. Lee, J.T., Jr. and J.A. McCubrey, *The Raf/MEK/ERK signal transduction cascade as a target for chemotherapeutic intervention in leukemia.* Leukemia, 2002. **16**(4): p. 486-507.

6. Mohle, R., C. Failenschmid, F. Bautz, and L. Kanz, *Overexpression of the chemokine receptor CXCR4 in B cell chronic lymphocytic leukemia is associated with increased functional response to stromal cell-derived factor-1 (SDF-1).* Leukemia, 1999. **13**(12): p. 1954-9.

7. Till, K.J., K. Lin, M. Zuzel, and J.C. Cawley, *The chemokine receptor CCR7 and alpha4 integrin are important for migration of chronic lymphocytic leukemia cells into lymph nodes.* Blood, 2002. **99**(8): p. 2977-84.

8. Richardson, S.J., C. Matthews, M.A. Catherwood, H.D. Alexander, B.S. Carey, J. Farrugia, A. Gardiner, S. Mould, D. Oscier, J.A. Copplestone, and A.G. Prentice, *ZAP-70 expression is associated with enhanced ability to respond to migratory and survival signals in B-cell chronic lymphocytic leukemia (B-CLL).* Blood, 2006. **107**(9): p. 3584-92.

9. Moser, K. and F.M. White, *Phosphoproteomic analysis of rat liver by high capacity IMAC and LC-MS/MS.* J Proteome Res, 2006. **5**(1): p. 98-104.

10. Gabelloni, M.L., M. Borge, J. Galletti, C. Canones, P.F. Calotti, R.F. Bezares, J.S. Avalos, M. Giordano, and R. Gamberale, *SHIP-1 protein level and phosphorylation status differs between CLL cells segregated by ZAP-70 expression.* Br J Haematol, 2008. **140**(1): p. 117-9.

11. Ghia, P., P. Circosta, C. Scielzo, A. Vallario, A. Camporeale, L. Granziero, and F. Caligaris-Cappio, *Differential effects on CLL cell survival exerted by different microenvironmental elements.* Curr Top Microbiol Immunol, 2005. **294**: p. 135-45.

12. Scielzo, C., P. Ghia, A. Conti, A. Bachi, G. Guida, M. Geuna, M. Alessio, and F. Caligaris-Cappio, *HS1 protein is differentially expressed in chronic lymphocytic leukemia patient subsets with good or poor prognoses.* J Clin Invest, 2005. **115**(6): p. 1644-50.

13. Sato, S., N. Fujita, and T. Tsuruo, *Modulation of Akt kinase activity by binding to Hsp90.* Proc Natl Acad Sci U S A, 2000. **97**(20): p. 10832-7.

14. Favaro, P.M., S. de Souza Medina, F. Traina, D.S. Basseres, F.F. Costa, and S.T. Saad, *Human leukocyte formin: a novel protein expressed in lymphoid malignancies and associated with Akt.* Biochem Biophys Res Commun, 2003. **311**(2): p. 365-71.

15. Castro, J.E., C.E. Prada, O. Loria, A. Kamal, L. Chen, F.J. Burrows, and T.J. Kipps, *ZAP-70 is a novel conditional heat shock protein 90 (Hsp90) client: inhibition of Hsp90 leads to ZAP-70 degradation, apoptosis, and impaired signaling in chronic lymphocytic leukemia.* Blood, 2005. **106**(7): p. 2506-12.

16. Yang, H.S., A.P. Jansen, R. Nair, K. Shibahara, A.K. Verma, J.L. Cmarik, and N.H. Colburn, *A novel transformation suppressor, Pdcd4, inhibits AP-1 transactivation but not NF-kappaB or ODC transactivation.* Oncogene, 2001. **20**(6): p. 669-76.

17. Lankat-Buttgereit, B. and R. Goke, *The tumour suppressor Pdcd4: recent advances in the elucidation of function and regulation.* Biol Cell, 2009. **101**(6): p. 309-17.

18. Dorrello, N.V., A. Peschiaroli, D. Guardavaccaro, N.H. Colburn, N.E. Sherman, and M. Pagano, *S6K1- and betaTRCP-mediated degradation of PDCD4 promotes protein translation and cell growth.* Science, 2006. **314**(5798): p. 467-71.

19. Yang, H.S., A.P. Jansen, A.A. Komar, X. Zheng, W.C. Merrick, S. Costes, S.J. Lockett, N. Sonenberg, and N.H. Colburn, *The transformation suppressor Pdcd4 is a novel eukaryotic translation initiation factor 4A binding protein that inhibits translation.* Mol Cell Biol, 2003. **23**(1): p. 26-37.

20. Parcellier, A., E. Schmitt, S. Gurbuxani, D. Seigneurin-Berny, A. Pance, A. Chantome, S. Plenchette, S. Khochbin, E. Solary, and C. Garrido, *HSP27 is a ubiquitin-binding protein involved in I-kappaBalpha proteasomal degradation.* Mol Cell Biol, 2003. **23**(16): p. 5790-802.

21. Concannon, C.G., A.M. Gorman, and A. Samali, *On the role of Hsp27 in regulating apoptosis.* Apoptosis, 2003. **8**(1): p. 61-70.

22. Garrido, C., M. Brunet, C. Didelot, Y. Zermati, E. Schmitt, and G. Kroemer, *Heat shock proteins 27 and 70: anti-apoptotic proteins with tumorigenic properties.* Cell Cycle, 2006. **5**(22): p. 2592-601.

23. Zenz, T., D. Mertens, R. Küppers, H. Döhner, and S. Stilgenbauer, *From pathogenesis to treatment of chronic lymphocytic leukaemia.* Nature Reviews Cancer, 2010. **10**(1): p. 37-50.

24. Burger, J.A. and A. Burkle, *The CXCR4 chemokine receptor in acute and chronic leukaemia: a marrow homing receptor and potential therapeutic target.* Br J Haematol, 2007. **137**(4): p. 288-96.

25. Infantino, S., B. Moepps, and M. Thelen, *Expression and regulation of the orphan receptor RDC1 and its putative ligand in human dendritic and B cells.* J Immunol, 2006. **176**(4): p. 2197-207.

26. O'Hayre, M., C.L. Salanga, P.C. Dorrestein, and T.M. Handel, *Phosphoproteomic analysis of chemokine signaling networks.* Meth Enzymol, 2009. **460**: p. 331-46.

27. Smolka, M.B., C.P. Albuquerque, S.H. Chen, and H. Zhou, *Proteome-wide identification of in vivo targets of DNA damage checkpoint kinases.* Proc Natl Acad Sci U S A, 2007. **104**(25): p. 10364-9.

28. Matthiesen, R. and A.S. Carvalho, *Methods and algorithms for relative quantitative proteomics by mass spectrometry.* Methods Mol Biol. **593**: p. 187-204.

29. Want, E.J., B.F. Cravatt, and G. Siuzdak, *The expanding role of mass spectrometry in metabolite profiling and characterization.* Chembiochem, 2005. **6**(11): p. 1941-51.

30. Macek, B., M. Mann, and J.V. Olsen, *Global and site-specific quantitative phosphoproteomics: principles and applications.* Annu Rev Pharmacol Toxicol, 2009. **49**: p. 199-221.

31. Zhu, W., J.W. Smith, and C.M. Huang, *Mass spectrometry-based label-free quantitative proteomics.* J Biomed Biotechnol. **2010**: p. 840518.

32. Huang, M.R., M. Olsson, A. Kallin, U. Pettersson, and T.H. Totterman, *Efficient adenovirus-mediated gene transduction of normal and leukemic hematopoietic cells.* Gene Ther, 1997. **4**(10): p. 1093-9.

33. Bruey, J.M., C. Ducasse, P. Bonniaud, L. Ravagnan, S.A. Susin, C. Diaz-Latoud, S. Gurbuxani, A.P. Arrigo, G. Kroemer, E. Solary, and C. Garrido, *Hsp27 negatively regulates cell death by interacting with cytochrome c.* Nat Cell Biol, 2000. **2**(9): p. 645-52.

34. Montresor, A., M. Bolomini-Vittori, S.I. Simon, A. Rigo, F. Vinante, and C. Laudanna, *Comparative analysis of normal versus CLL B-lymphocytes reveals patient-specific variability in signaling mechanisms controlling LFA-1 activation by chemokines.* Cancer Res, 2009. **69**(24): p. 9281-90.

35. Chauhan, D., G. Li, R. Shringarpure, K. Podar, Y. Ohtake, T. Hideshima, and K.C. Anderson, *Blockade of Hsp27 overcomes Bortezomib/proteasome inhibitor PS-341 resistance in lymphoma cells.* Cancer Res, 2003. **63**(19): p. 6174-7.

36. Blees, J.S., T. Schmid, C.L. Thomas, A.R. Baker, L. Benson, J.R. Evans, E.I. Goncharova, N.H. Colburn, J.B. McMahon, and C.J. Henrich, *Development of a high-throughput cell-based reporter assay to identify stabilizers of tumor suppressor Pdcd4.* J Biomol Screen. **15**(1): p. 21-9.

37. Payne, S.H., M. Yau, M.B. Smolka, S. Tanner, H. Zhou, and V. Bafna, *Phosphorylation-specific MS/MS scoring for rapid and accurate phosphoproteome analysis.* J Proteome Res, 2008. **7**(8): p. 3373-81.

38. Tanner, S., H. Shu, A. Frank, L.C. Wang, E. Zandi, M. Mumby, P.A. Pevzner, and V. Bafna, *InsPecT: identification of posttranslationally modified peptides from tandem mass spectra.* Anal Chem, 2005. **77**(14): p. 4626-39.

39. Burger, J.A., N. Tsukada, M. Burger, N.J. Zvaifler, M. Dell'Aquila, and T.J. Kipps, *Blood-derived nurse-like cells protect chronic lymphocytic leukemia B cells from spontaneous apoptosis through stromal cell-derived factor-1.* Blood, 2000. **96**(8): p. 2655-63.

CHAPTER 5

Elucidating the Roles of the Chemokine Receptors CXCR4 and CXCR7 in Breast Cancer Growth and Metastasis

5.1 Summary

Chapter 5 focuses on characterizing the role of the chemokine receptors CXCR4 and CXCR7, and their mutual ligand, CXCL12, in breast cancer growth and metastasis. Despite the lack of expression in normal breast epithelia, CXCR4 and CXCR7 are frequently found upregulated in breast cancer tissue. And while many studies have been directed towards understanding the individual roles of these two receptors in breast cancer, there is still little known about how coexpression of CXCR4 and CXCR7 on breast cancer cells may affect tumor progression. MDA-MB-231 breast cancer cells selected *in vivo* for high metastastic potential (MDA-HM), with elevated CXCR4 expression, were transfected with CXCR7 (MDA-HM + CXCR7) to understand how the coexpression of both receptors, and resulting crosstalk, affected the overall tumor growth and metastatic characteristics of the cells. Using a mouse tumor metastasis model, we found that MDA-HM + CXCR7 mice exhibited significantly reduced lung metastases compared to MDA-HM injected mice, despite normal primary tumor growth. In support of the findings that CXCR7 expression exhibits inhibitory effects on CXCR4

metastatic activity *in vivo*, we also found a decrease in CXCL12-induced calcium mobilization of MDA-HM + CXCR7 cells, as well as changes in CXCL12-mediated phosphorylation responses of downstream signaling molecules such as ERK1/2 and PDCD4, compared to MDA-HM cells. Together, these data demonstrate that crosstalk between CXCR4 and CXCR7, when coexpressed on a human breast cancer cell line, promotes down-modulation of CXCR4 functional activity *in vitro* and *in vivo.* These findings also contribute to our limited understanding of the many complexities involved in cellular signaling and regulation in cancer cells, which can have important implications in the targeting of receptors for therapeutic intervention in various disease states. Although the underlying mechanisms regulating CXCR4 and CXCR7 crosstalk in breast cancer cells is still not well understood, these effects could be related to receptor oligomerization, transinhibition, and/or ligand sequestration, all of which are currently under investigation.

5.2 Introduction

In 2001, Müller and colleagues demonstrated the integral role of chemokines in the directional metastasis of breast cancer cells [1]. Since then, it has become clear that select chemokines and their receptors are important for organ-specific metastasis by directing migration of receptor-bearing cancer cells to sites of ligand expression, as described in Chapter 1. In particular, CXCR4, and its ligand CXCL12, have been implicated in at least 23 types of cancer to date [2]. However, apart from cancer, CXCR4 and CXCL12 also play a critical role in development, whereby knockout of either CXCR4 or CXCL12 in mice is embryonically lethal due to defects in vascular development, organogenesis and haematopoiesis [3, 4]. CXCR4 and CXCL12 were considered to be an exclusive ligand:receptor pair, until 2004, when the deorphaned chemokine receptor, CXCR7, was also reported to bind CXCL12 [5, 6]. Similar to CXCR4 and CXCL12, CXCR7 was found to be important for development as CXCR7 knockout mice died at birth, mainly due to heart valve defects although haematopoiesis was unaffected [7]. In addition to binding CXCL12, CXCR7 has also been shown to bind an additional ligand, ITAC/CXCL11, although with lower affinity. Interestingly, both ligands fail to elicit normal chemokine receptor activation responses like calcium flux or cell migration in CXCR7 expressing cells [8], which is mainly attributed to CXCR7 lacking the G protein coupling “DRYLAIV” motif, and suggests a potentially distinct role for this receptor. Despite the inability to couple G protein, several groups have demonstrated that CXCR7 recruits β-arrestin2 [9-11] in a ligand dependent manner, which can lead to cell signaling apart from its classical role in mediating receptor desensitization and internalization [12, 13].

Although CXCR4 and CXCR7 are typically not expressed on normal epithelia, they are oftentimes expressed on malignant tissues [2, 8, 14, 15]. As previously discussed in Chapter 1, CXCR4:CXCL12 contributions to cancer have been well studied [2]. However, there have also been an increasing number of reports implicating CXCR7 in various aspects of cancer development, including processes such as adhesion, invasion, survival and proliferation of cancer cells [8, 14, 16, 17]. For example, using tumor cells overexpressing CXCR7, as well as RNA interference strategies directed at CXCR7, Miao et al. demonstrated that CXCR7 promoted breast and lung tumor growth *in vivo*. In addition, the described tumor promoting effects for CXCR7 were found to be independent of CXCR4 expression. Studies have also shown that addition of CXCR7 specific inhibitors in a mouse model of lung cancer was able to reduce the tumor promoting effects associated with CXCR7 expression [8], supporting a specific role of CXCR7 in tumor progression that is not necessary redundant to the role of CXCR4. Despite the well-cited involvement of CXCR4 and more recently, CXCR7, in cancer, the interrelationship between CXCR4 and CXCR7 has not really been addressed and remains unclear, providing the framework for the studies presented in this Chapter.

Thus far, it is still unclear whether CXCR7 functions through individual or redundant mechanisms as CXCR4 in cancer growth and progression. However, given the distinct differences in signaling and regulation of CXCR7, particularly the lack of G protein coupling, it is suggested that CXCR7 may serve non-redundant functions compared to CXCR4 and in fact, may modulate CXCR4 activity in some cases. In support of this, CXCR4 and CXCR7 has been shown to exhibit differential roles in the therapeutic homing of human renal progenitor where CXCR4 contributed to cell migration while CXCR7 promoted cell adhesion and survival [18]. Adding an additional level of complexity, CXCR4 and CXCR7 have also been reported to form heterodimers

[7, 11], as described in Chapter 1, although the effect of CXCR4:CXCR7 heterodimerization is not well understood. Herein, a combination of *in vivo* and *in vitro* cell based assays were used to delineate the contributions and potential crosstalk effects of CXCR4 and CXCR7 on breast cancer primary tumor growth and progression. Using an *in vivo* mouse tumor model, we found that injection of highly metastatic MDA-MB-231 cells (MDA-HM) coexpressing CXCR7 (MDA-HM + CXCR7) had an initially slowed primary tumor growth rate, although the tumor sizes ultimately resulted in slightly larger tumors at time of sacrifice. Interestingly, MDA-HM + CXCR7 injected mice led to a significant decrease in lung metastases compared to MDA-HM injected mice which only expressed high levels of CXCR4 and no CXCR7. *In vitro* cell based assays using MDA-MB-231 WT and MDA-HM cells expressing CXCR4 and/or CXCR7 further demonstrated the capacity of CXCR7 to modulate the typical activity of CXCR4 as determined by changes in CXCL12 mediated calcium flux, downstream signaling, and receptor internalization responses.

5.3 Results

5.3.1: CXCR4 and CXCR7 localization in MDA-MB-231 cells

To determine potential differences in the relative distribution of endogenous CXCR4 and CXCR7, we analyzed the cellular localization of both receptors in permeabilized MDA-MB-231 cells using mAb directed at CXCR4 and CXCR7 (Figure 5.1). The immunofluorescence microscopy images revealed distinct distribution of both receptors where CXCR7 was predominantly detected throughout the cytosol while CXCR4 mainly localized to the plasma membrane. These findings concur with other

reports showing intracellular distribution of CXCR7 [19, 20]. The distinct differences in localization for CXCR7, compared to CXCR4, may contribute, or be attributed to, the unique activity of CXCR7 compared to the classical signaling activity typically associated with chemokine receptors. These results were further corroborated by flow analysis of parental MDA-MB-231 cells showing that endogenous CXCR7 expression was predominantly expressed intracellularly, and therefore only detectable when the membrane was permeabilized allowing intracellular staining of CXCR7 (Figure 5.2). In the absence of membrane permeabilization, very little CXCR7 was detected on the cell surface indicating that endogenous expression is mostly limited to the cytosol, in comparison to MDA-MB-231 cells stably transfected with CXCR7 and expressing markedly higher surface levels of CXCR7 in addition to the intracellular expression.

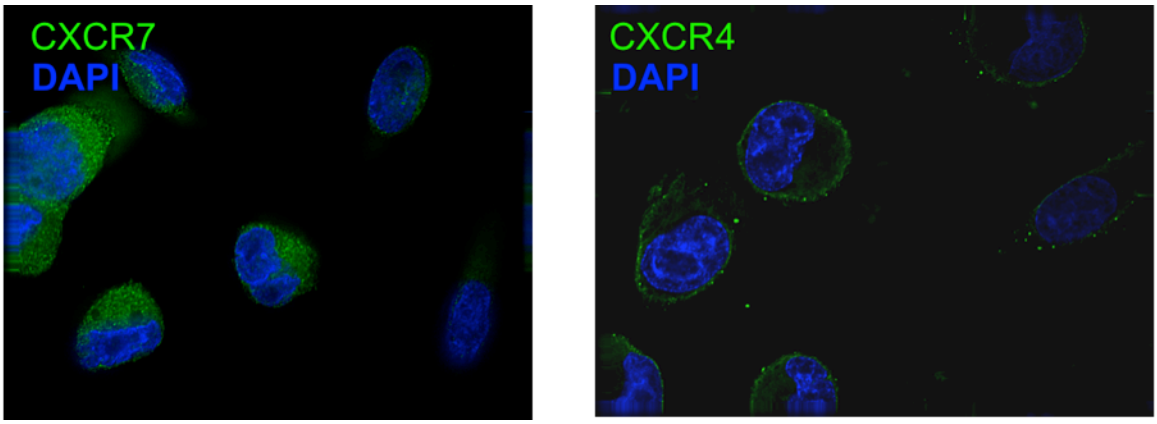

Figure 5.1 Cellular distribution of endogenous CXCR4 and CXCR7 in permeabilized MDA-MB-231 cells by immunofluorescence microscopy. Immunofluorescence staining with mAb against CXCR4 (left) and CXCR7 (right) are shown. CXCR4 and CXCR7 are colored green; DAPI nuclear stain is colored blue.

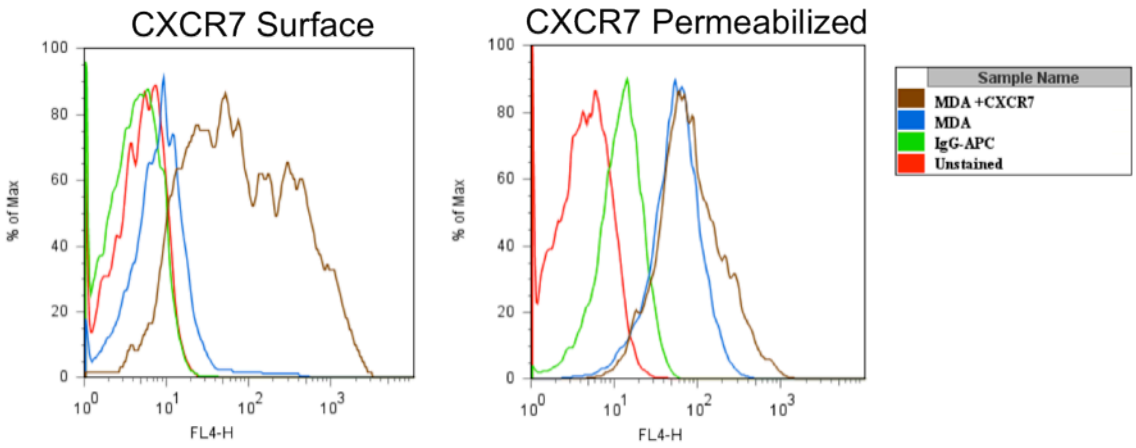

Figure 5.2 CXCR7 expression in MDA-MB-231 WT (blue) and MDA + CXCR7 (brown) cell lines. CXCR7 surface expression (*left)* as well CXCR7 staining of permeabilized cells (*right)* is shown compared to isotype control (green) as determined by flow cytometry. Transfection of CXCR7 in MDA-MB-231 WT cells resulted in an increase of CXCR7 surface levels while intracellular levels were mostly unchanged.

5.3.2: Tumor growth progression of MDA-MB-231 derived clonal lines expressing varying levels of CXCR4 and/or CXCR7

To elucidate the independent and combined effects of CXCR4 and CXCR7 in breast cancer growth and progression, we used the ATCC derived human breast cancer cell line, MDA-MB-231, stably expressing CXCR4, CXCR7 or CXCR4 and CXCR7 for the described studies. However, while culturing the ATCC derived MDA-MB-231 cells, we found that the CXCR4 levels were not stable, and in fact, the CXCR4 expression levels always increased over time while in passage (Figure 5.3). Therefore, we produced a clonal line derived from the parental MDA-MB-231 cells lines, expressing low levels of CXCR4, in order to have a reliably stable cell line with low CXCR4 expression allowing us to specifically investigate the effects of CXCR4 and/or CXCR7 receptor expression on functional activity. Using the clonal line, we then generated cell lines stably expressing CXCR4, CXCR7, or both CXCR4 and CXCR7. Surface expression of

the stable cell lines was confirmed by mAb staining and flow cytometry analysis (Figure 5.4). Interestingly, we found that coexpression of CXCR4 with CXCR7 resulted in elevated levels of CXCR7 compared to when was expressed by itself (Figure 5.4). Although the exact mechanism behind this is not known, it could potentially be due to stabilization of CXCR4 by CXCR7, by physical association (e.g. hetero-oligomerization), although this theory remains to be determined. The varying levels of CXCR4 and CXCR7 expression achieved in the clonal lines is outlined in (Figure 5.4, *bottom*) and compared to the ATCC MDA-MB-231 population as well as a highly metastatic MDA-MB-231 line (MDA-HM) that were also used in this study.

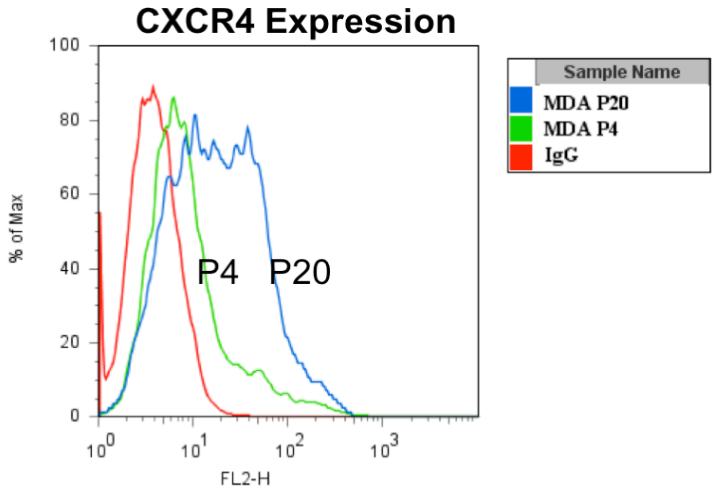

Figure 5.3 CXCR4 expression over time in MDA-MB-231 cultured cells. After 20 passages in culture (P20, blue), CXCR4 had elevated surface levels compared to the relatively low levels of CXCR4 from an early passage (P4, green), as determined by flow cytometry and compared to the isotype control (red).

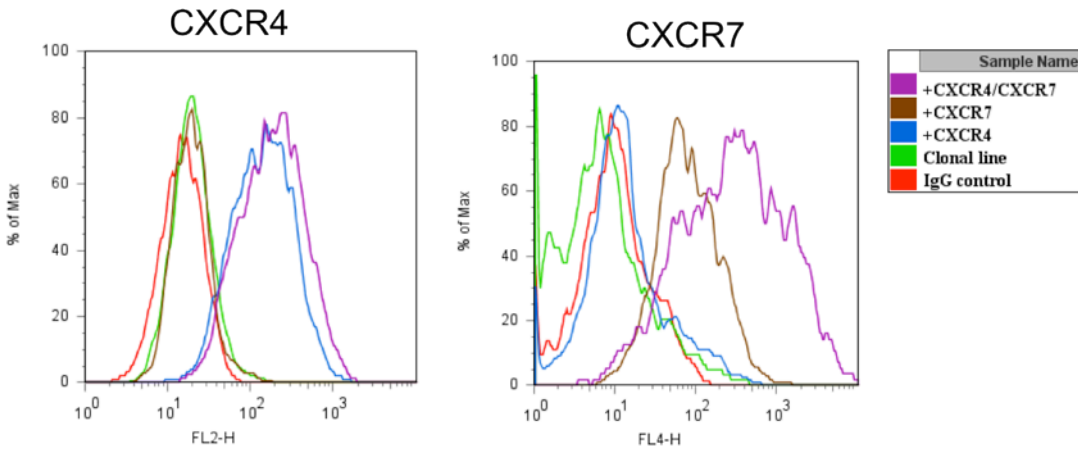

Population	% CXCR4+	% CXCR7+
ATCC MDA	21.1	4.5
MDA-HM (highly metastatic)	58.9	3.2
Clonal line	4.25	4.1
Clonal line + CXCR4	84.5	7.5
Clonal line + CXCR7	4.2	70
Clonal line + CXCR4 + CXCR7	88.9	87

Figure 5.4 Differential CXCR4 (*top, left*) and CXCR7 (*top, right*) expression of the MDA-MB-231 clonal line (green) with low CXCR4 expression. Clonal lines transfected with CXCR4 (blue), CXCR7 (brown) or CXCR4/7 (purple) compared to the isotype control (red) are shown, as determined by flow cytometry. The percentage of CXCR4 or CXCR7 expression for each population is also presented (*bottom)* and compared to the MDA-MB-231 WT (ATCC) cells and the MDA-HM line (flow data not shown).

To determine the *in vivo* tumor promoting and metastatic properties of cells expressing CXCR4 and/or CXCR7, all of the generated clonal lines (clonal, clonal + CXCR4, clonal + CXCR7, clonal + CXCR4/CXCR7) were injected into SCID mice by direct injection of the cells into the 4th inguinal mammary fat pad on both sides. Primary tumor growth was measured three times per week and the relative tumor sizes are shown in Figure 5.5. As expected, CXCR4 expressing cells robustly promoted primary tumor growth and metastasis while CXCR7 also promoted tumor growth, although to a

lesser degree than CXCR4 expressing cells, and exhibited no metastasis. These data fully support previous findings that both CXCR4 and CXCR7 individually promote primary tumor growth. However, surprisingly, the expression of CXCR7 in the presence of CXCR4 resulted in an inhibition of primary tumor growth, despite the fact that both receptors promoted primary tumor growth individually. While it is unclear why the CXCR4/CXCR7 expressing line exhibited decreased tumor growth, it could possibly be a consequence of using clonally derived cells for these studies, which could possess some defect that we are unaware of, and may also explain the unusually slow growth of the tumors in this experiment.

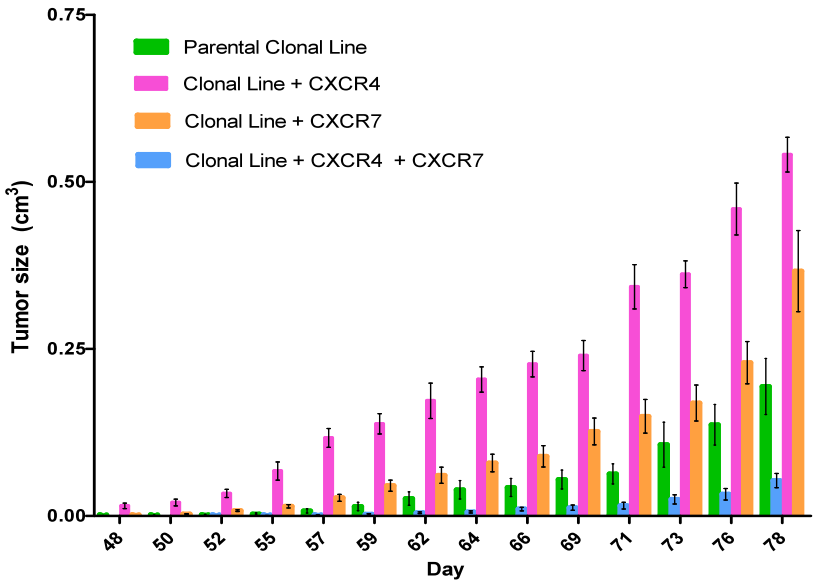

Figure 5.5 Primary tumor growth comparison of mice injected with the MDA-MB-231 parental clonal cell line (selected for low CXCR4 and CXCR7 expression) (green) or clonal line transfectants expressing CXCR4 (pink), CXCR7 (orange), or CXCR4 and CXCR7 (blue).

As described in Chapter 1, it has been well established that CXCR4, and its ligand CXCL12, are critical for the directed migration of cancer cells to distal sites of metastasis [1]. In accordance with this, we found a striking elevation in CXCR4 levels

from metastatic tissue derived from the lung and lymph node, which was markedly higher than the CXCR4 expression of the cells originating from the primary tumor. Therefore, despite slowed primary tumor growth compared to the CXCR4 and CXCR7 expressing clonal lines, and maintenance of low CXCR4 levels at the primary tumor site, cells that metastasized to distal sites exhibited increased levels of CXCR4 (Figure 5.6) and exhibited no changes in CXCR7 levels (data not shown). These data underscore the importance of CXCR4 expression for directing tumor cell migration to sites of metastasis. Despite interesting findings, a significant drawback to these experiments and use of the clonally derived cell lines extremely slow onset of tumor growth, which ranged from 48 – 60 days, correlating with tumors requiring greater than 90 days to reach the designated tumor size (1.5 cm). Therefore, we employed an alternative approach to investigating the combined effects of CXCR4 and CXCR7, which is described in the next section.

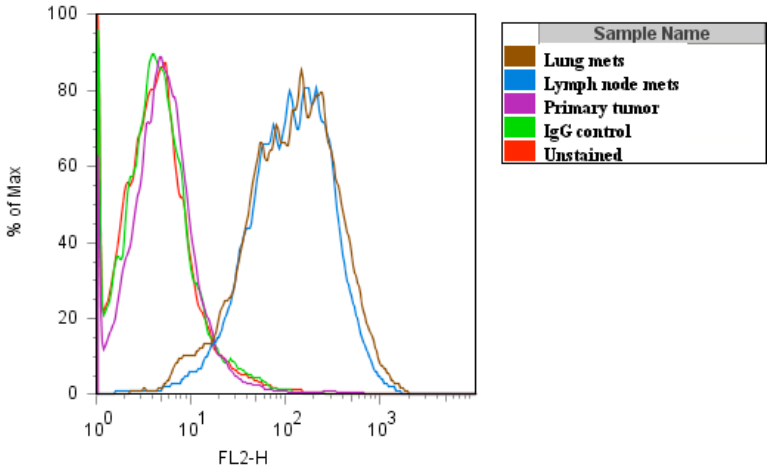

Figure 5.6 Increase in CXCR4 expression of lung (brown) and lymph node (blue) derived metastases compared to the MDA-WT parental line injected (purple) with low CXCR4 expression, all compared to the isotype control (green) and detected by flow cytometry.

5.3.3: In vivo effects of CXCR7 expression on highly metastatic MDA-MB-231 tumor growth and metastasis

Here we alternatively employed the use of a MDA-MB-231 derived cell line, which is highly metastatic and more closely corresponds to the expected tumor growth rates of cell lines expressing elevated CXCR4 levels observed in other studies. Specifically, we utilized the highly metastatic tumor cell line (MDA-HM) (see materials and methods) that was selected *in vivo* for being highly metastatic to the lung, and accordingly, expresses high levels of endogenous CXCR4. To investigate the effects of CXCR7 expression with these cells, we transfected CXCR7 constructs possessing neomycin (neo) or puromycin (puro) resistance. Figure 5.7 illustrates that while the surface levels of CXCR4 were maintained in the MDA-HM line, the CXCR7 transfectants resulted in varying levels of CXCR7 depending on the selection marker used. Neo selection resulted in medium levels of CXCR7 while puro selection resulted in high levels of CXCR7 (Figure 5.7). This “medium” and “high” expression level phenomenon has also been observed with other cell lines and receptors, making the pBabe retroviral constructs (with neo or puro resistance) useful tools for achieving varying levels of receptor expression. The observed differences in receptor levels may be related to the rate at which selection is achieved considering that puromycin selection only takes 2-3 days whereas neomycin (or G418) commonly takes up to a week to be fully selected. The longer selection times may allow the out-growth of cells possessing only low or moderate levels of receptor to survive in comparison to a rapid selection process.

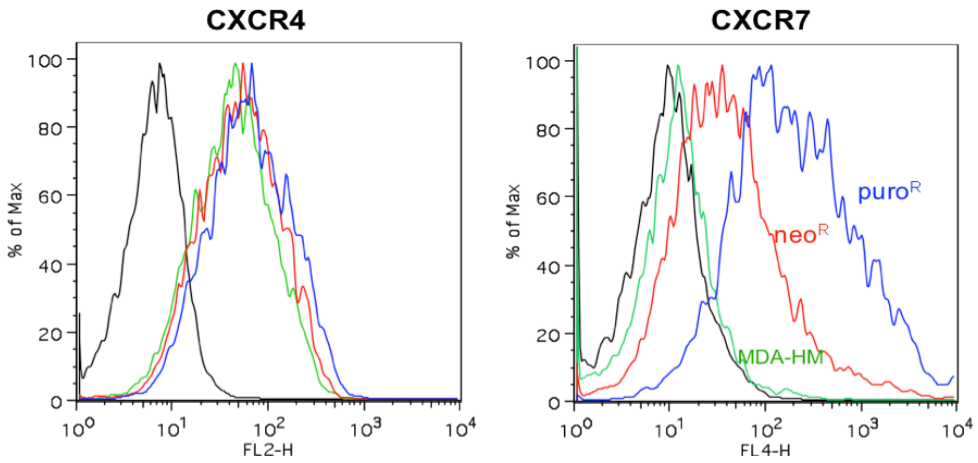

Figure 5.7 CXCR4 (*left*) and CXCR7 (*right*) expression of MDA-HM + CXCR7 transfectants with neomycin (neo) or puromycin (puro) resistance, detected by flow cytometry. While CXCR4 surface levels are maintained for the MDA-HM CXCR7 transfectant lines, puro selected cells exhibit higher CXCR7 levels compared to neo selected cells.

To understand how CXCR7 affects the well established primary tumor growth promoting properties and metastatic activity of CXCR4, mammary fat pad injections in SCID mice were performed using the MDA-HM cell line transduced with high levels of CXCR7 ($puro^R$) for all subsequent experiments, and referred to as MDA-HM + CXCR7 hereafter. The receptor expression profiles of the injected cell lines are presented in Figure 5.8 and show that while both lines have comparable CXCR4 levels, the cell lines transduced with CXCR7-puro have elevated CXCR7 levels while the MDA-HM parental lines have little to no CXCR7 expression, supporting the use of these lines to delineate receptor expression effects on activity. While MDA-HM + CXCR7 injected mice exhibited an initial delay in primary tumor growth (Figure 5.9), tumors reached levels similar to those of MDA-HM injected mice shortly thereafter (Figure 5.10). In fact, at the time of harvest, the primary tumors of MDA-HM + CXCR7 injected mice had slightly larger tumors than their MDA-HM counterpart (Figure 5.10, *B*).

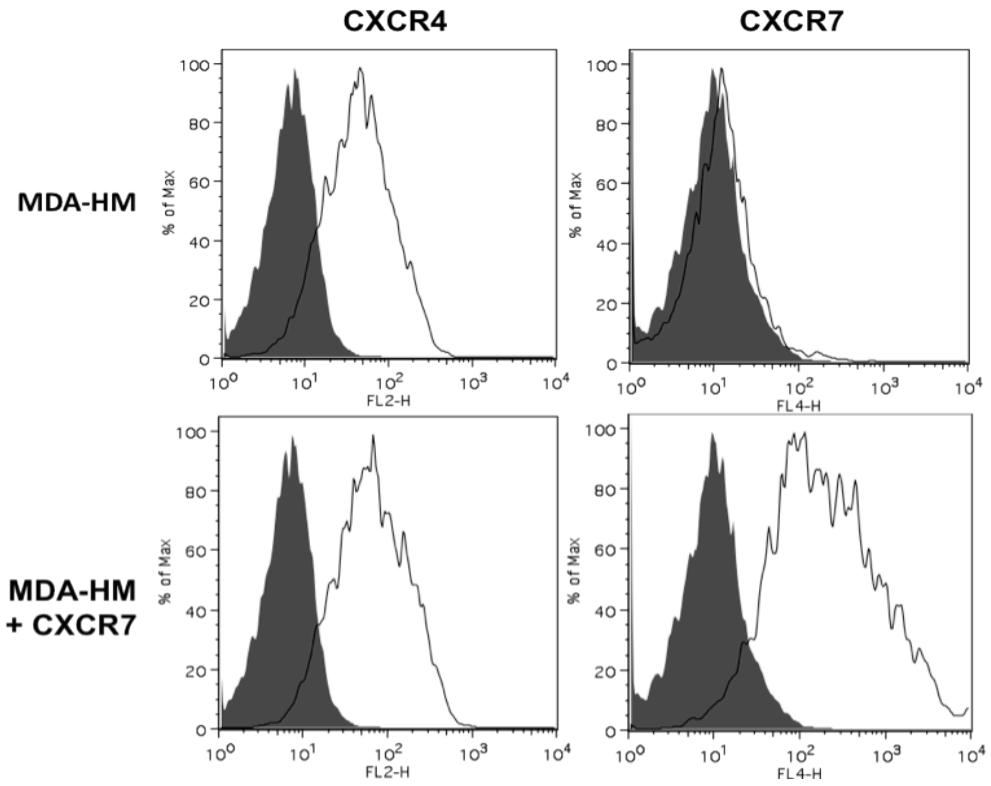

Figure 5.8 CXCR4 and CXCR7 expression of MDA-HM injected cell lines as determined by flow cytometry. CXCR4 expression is maintained for MDA-HM and MDA-HM + CXCR7 cell lines (*top left, bottom left*), while CXCR7 expression is elevated in the MDA-HM + CXCR7 cell line (*bottom right*) and not in MDA-HM cells (*top right*).

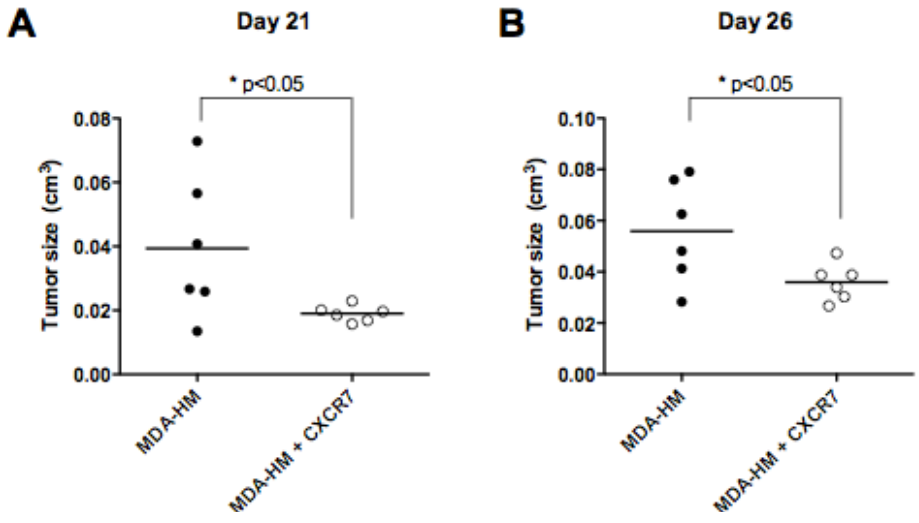

Figure 5.9 Comparison of MDA-HM and MDA-HM + CXCR7 tumor sizes 21 days (*left*) and 26 days (*right*) following injection.

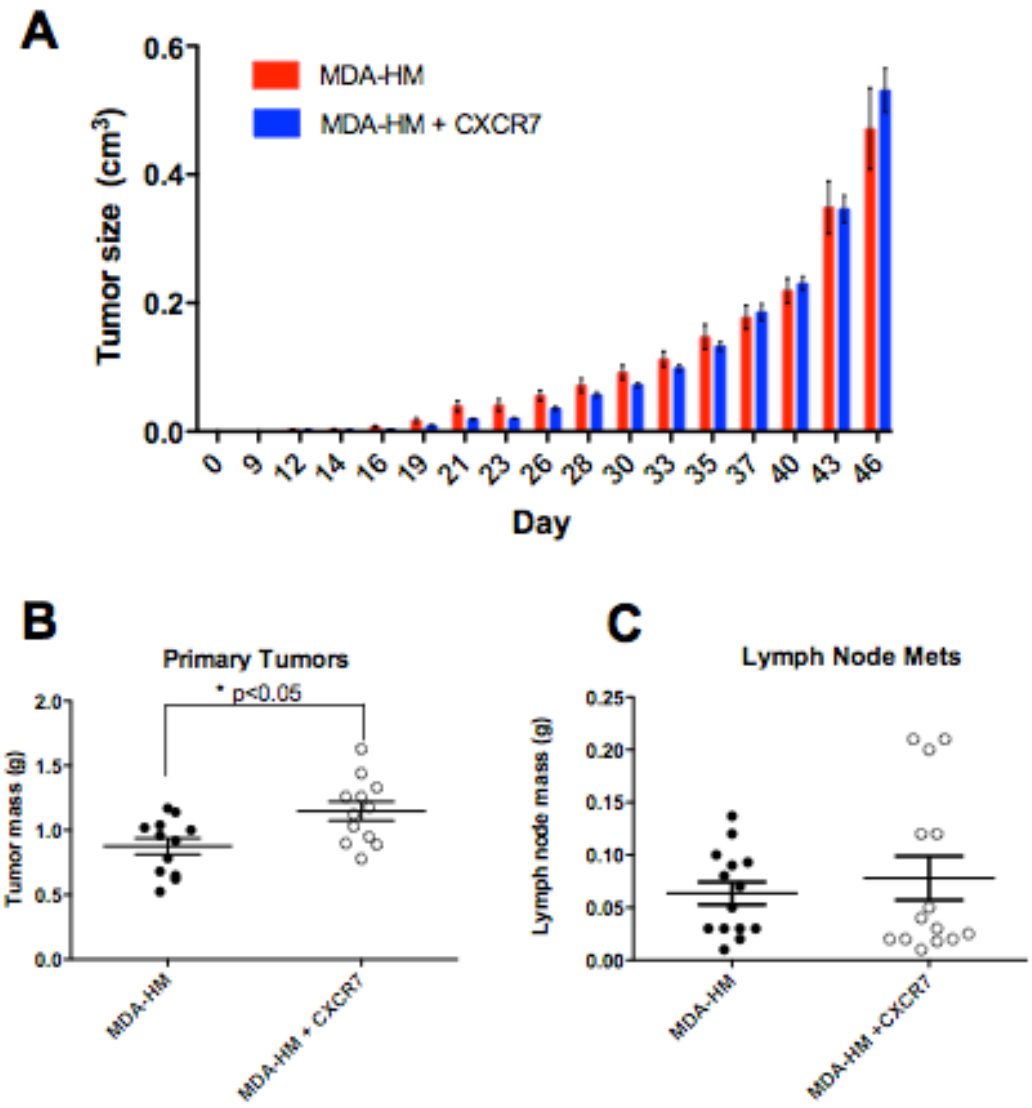

Figure 5.10 Primary tumor growth and size and tumor size comparisons of MDA-HM and MDA-HM + CXCR7 injected mice. (A) Primary tumor growth progression comparison of mice injected with the MDA-HM (*red*) or MDA-HM + CXCR7 (*blue*) show little difference in growth rates between the two cell lines. (B) Primary tumor size and (C) lymph node tumors are compared for mice injected with MDA-HM (*closed circles*) or MDA-HM + CXCR7 (*open circle*).

MDA-HM injected mice also developed lymph node tumors. However, these lymph node tumors may be attributed to excessive cell growth and escape from the primary tumor site, and drainage through the lymphatic system, ultimately leading to residence in lymph nodes. Therefore, we believe that differences in lymph node tumors do not reflect

directed migration and metastases. Accordingly, the number and size of these lymph node tumors did not differ between populations (Figure 5.10, *C*), unless mice were sacrificed slightly earlier (e.g. day 42), corresponding to smaller tumor sizes, as shown in Figure 5.11 and quantified in Figure 5.12, suggesting an age dependence on the extent of lymph node metastases observed, unrelated to the differences in lung metastases that we observed.

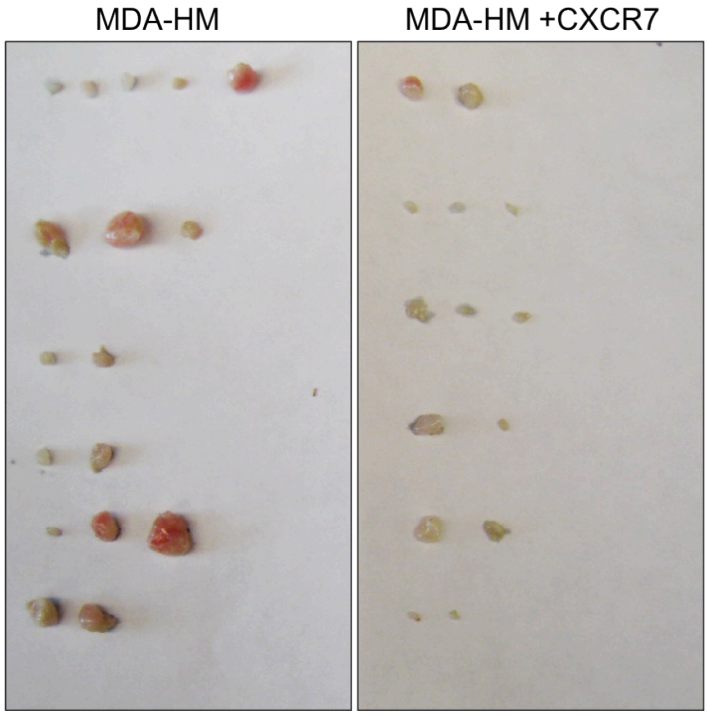

Figure 5.11 Image of lymph node metastases derived from MDA-HM (*left*) and MDA-HM + CXCR7 (*right*) mice 42 days post injection. MDA-HM + CXCR7 injected mice have smaller lymph node tumors compared to the MDA-HM injected mice.

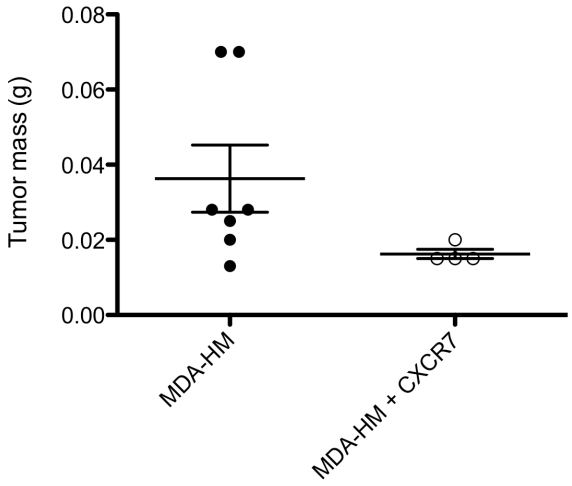

Figure 5.12 Lymph node tumor mass (g) comparisons of MDA-HM and MDA-HM + CXCR7 injected mice after 42 day of growth.

The most striking difference observed from the *in vivo* studies was the markedly decreased lung metastases of MDA-HM + CXCR7 injected mice compared to MDA-HM injected mice. Figure 5.13 shows representative fluorescence microscopy images of the lung lobes derived form MDA-HM and MDA-HM + CXCR7 injected mice, whereby the parental lines were identified by their GFP expression. Representative fluorescence images from several mice clearly indicate that the MDA-HM lines expressing CXCR7 resulted in significantly less tumor metastases than the MDA-HM injected mice, which exhibited extensive lung metastases, as expected. The extent of metastases was also quantified by comparing the fluorescent intensity of lungs derived from either control, MDA-HM or MDA-HM + CXCR7 mice, and differences were found to be statistically significant (**$p<0.005$) (Figure 5.14).

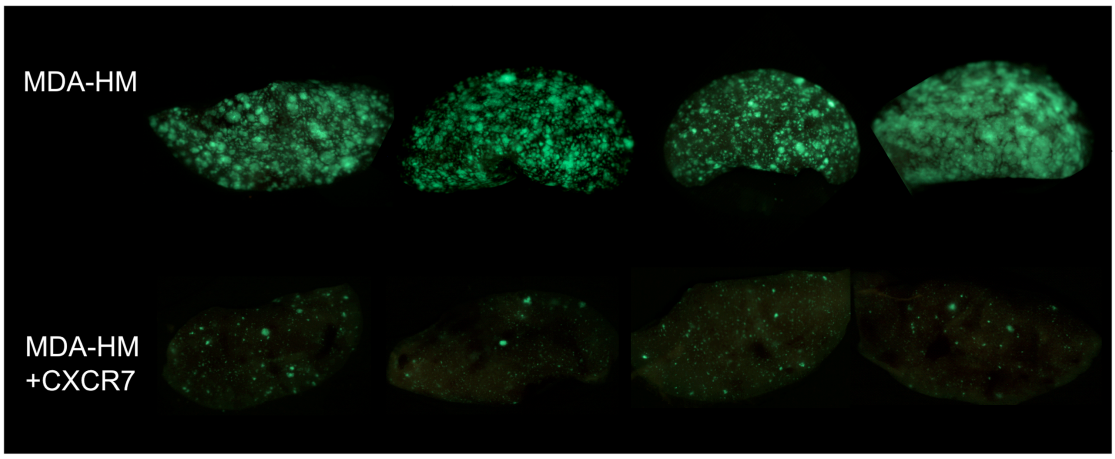

Figure 5.13 GFP fluorescence of lung lobes derived from MDA-HM (*top*) or MDA-HM + CXCR7 injected mice (*bottom*), representative images shown. MDA-HM + CXCR7 injected mice exhibited markedly decreased lung metastases compared to MDA-HM injected mice, based on fluorescence imaging microscopy.

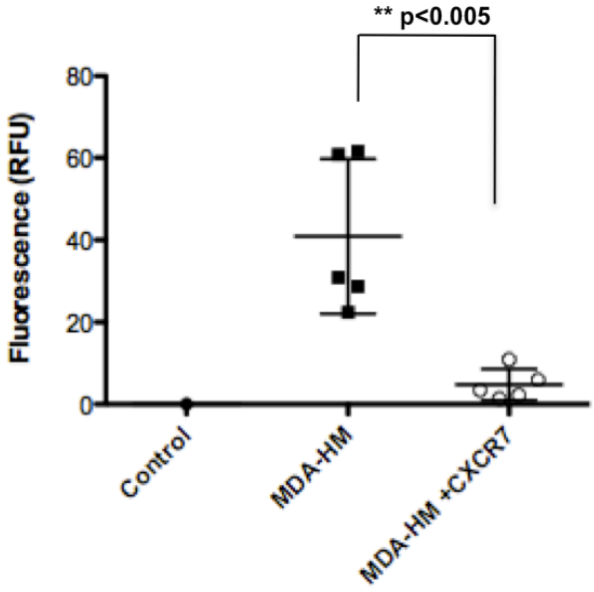

Figure 5.14 Fluorescence quantification of lung metastases harvested from MDA-HM or MDA-HM + CXCR7 injected mice compared to control lung. MDA-HM + CXCR7 exhibited significantly lower lung metastases compared to MDA-HM (**p<0.005).

These results were further confirmed by H & E staining of lungs from control, MDA-HM, and MDA-HM + CXCR7 injected mice, as shown in Figure 5.15. Collectively, these data demonstrated that expression of CXCR7 correlated with decreased lung metastases of the highly metastatic MDA-HM cell line endogenously expressing high levels of CXCR4. These observed effects may be a result of direct inhibition of CXCR4 by CXCR7, which could possibly be mediated by CXCR4/CXCR7 oligomerization and subsequent transinhibition, and is further addressed in the following sections.

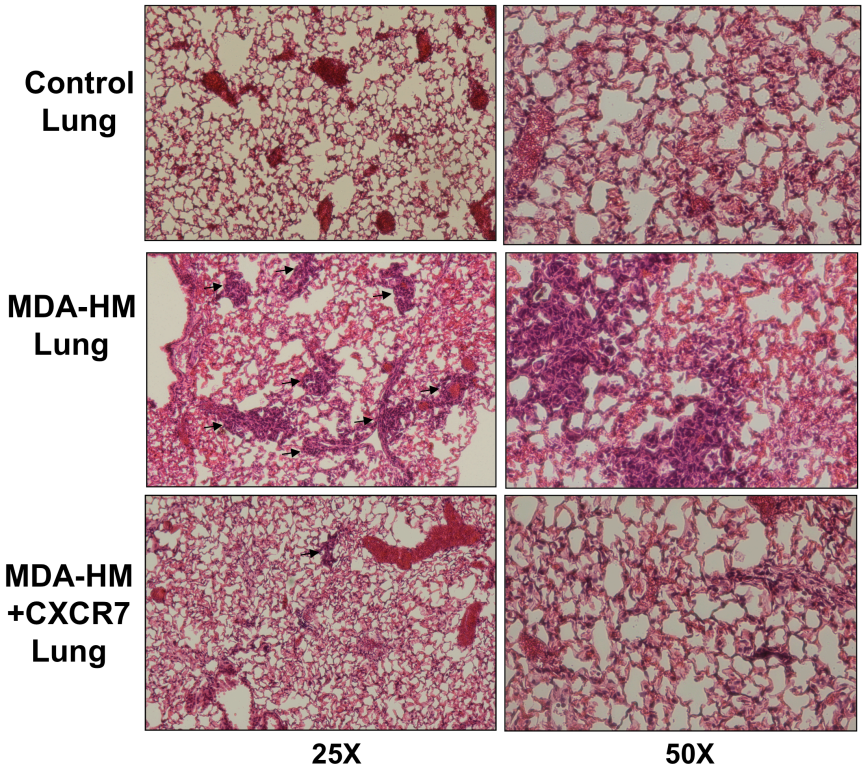

Figure 5.15 Representative H & E staining of lungs derived from a control (*top*), MDA-HM (*middle*) or MDA-HM + CXCR7 (*bottom*) injected mouse shown with 25X (*left*) or 50X (*right*) magnification. Histological analysis shows that the extent of lung metastases is higher in the MDA-HM lungs compared to the MDA-HM + CXCR7 lungs and control lungs.

5.3.4: Effect of CXCR7 expression on CXCL12-mediated signaling in MDA-MB-231 cells

As mentioned previously, unlike CXCR4, CXCR7 is unique in that it does not elicit a classical chemokine mediated calcium flux or migration response. Given the inhibitory effects of CXCR7 on CXCR4 activity observed in the *in vivo* studies, we were interested in further characterizing the CXCR4/CXCR7 crosstalk effects on the biological activity of both receptors through traditional *in vitro* methods for testing chemokine receptor activity. For consistency, we employed the MDA-HM cell lines used for the *in vivo* studies for direct comparison. To begin, we monitored calcium flux response of the MDA-HM and MDA-HM + CXCR7 cells in response to CXCL12. As expected, the MDA-HM cells exhibited a robust calcium flux signal, corresponding to their high levels of CXCR4 expression. In accordance with the inhibitory effects exhibited *in vivo*, expression of CXCR7 on the MDA-HM cells led to a reduction in CXCL12 mediated calcium flux, as shown in Figure 5.16. Possible explanations for the decreased response could be due to CXCR7 sequestration of CXCL12, as has been proposed by some groups [21], or alternatively, allosteric modulation of the receptor resulting from receptor hetero-oligomerization. To more specifically address the mechanism, we will perform additional calcium flux analyses such as pre-treating the cells with the CXCR7 specific ligand, CXCL11, or the CXCR7 specific inhibitor, CCX771, prior to CXCL12 stimulation and see if a similar response is observed. Nevertheless, since the calcium flux analysis demonstrated that the coexpression of CXCR7 affected CXCR4 calcium flux in response to CXCL12 stimulation, we went on to analyze additional CXCL12 mediated signaling responses of the MDA-HM lines including phosphorylation analysis of PDCD4 (Figure 5.17), a novel target of CXCL12 signaling [22], as well as known

targets of chemokine signaling like Akt and ERK1/2 (Figure 5.17), which are described in Chapter 1.

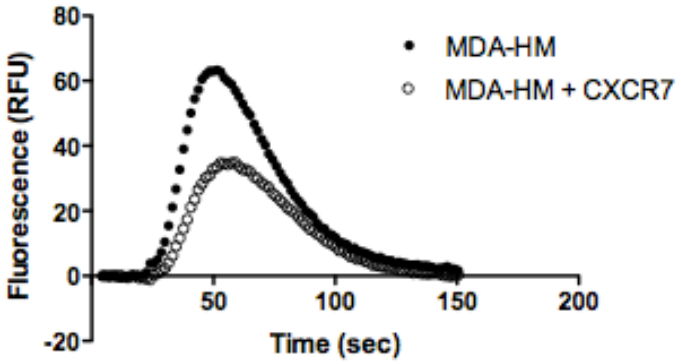

Figure 5.16 Comparison of CXCL12 mediated calcium flux of MDA-HM cells (closed circles) and MDA-HM + CXCR7 cells (open circles).

PDCD4 is a tumor suppressor protein found to be a novel downstream phosphorylation target of CXCR4:CXCL12 signaling in CLL cells based on our previous phosphoproteomics work [22] presented in Chapter 4. Here we examined the effect of CXCR7 expression on the known phosphorylation activity of CXCR4 where differences in CXCR4 and/or CXCR7 mediated phosphorylation response have potential relevance to their respective and combined contributions to breast cancer cell growth and survival. To this end, both MDA-HM and MDA-HM + CXCR7 lines were stimulated with 75 nM CXCL12 for a timecourse of 60 min (0, 3, 15, 60 min). Western blot analysis and antibody detection of phospho-PDCD4 (S457) indicated that CXCR7 expression in MDA-HM cells resulted in delayed phosphorylation of PDCD4 compared to MDA-HM cells (Figure 5.17). In addition, cells were pretreated with Pertussis toxin (PTx, a Gi inhibitor), CCX771 (a Chemocentryx CXCR7 specific inhibitor), or AMD3100 (a CXCR4 specific inhibitor) followed by stimulation with 75 nM CXCL12 for 15 min and probed for phospho-PDCD4 (Figure 5.17). While treatment of AMD3100, resulted in similar

inhibition of PDCD4 phosphorylation for both MDA-HM and MDA-HM + CXCR7 cells, the presence of CXCR7 resulted in a decreased sensitivity to PTx, compared to MDA-HM. Finally, treatment with the CXCR7 inhibitor, CCX771, also reduced the phosphorylation response in both cells lines, although to a lesser extent than AMD3100. These data suggest that phosphorylation of PDCD4 is primarily mediated through CXCR4 given that AMD3100 treatment completely abrogates the response to levels less than basal signaling. Apart from CXCR7 delaying the phosphorylation of PDCD4, compared to MDA-HM, which has a robust phosphorylation response at 3 min, the presence of CXCR7 also limits the extent of PTx inhibition of Gi signaling. Since CXCR7 does not couple to G protein, this inhibition is also mediated through CXCR4 and suggests that the presence of CXCR7 is preventing complete inhibition, potentially from CXCR4:CXCR7 heterodimerization and possible allosteric modulation of CXCR4.

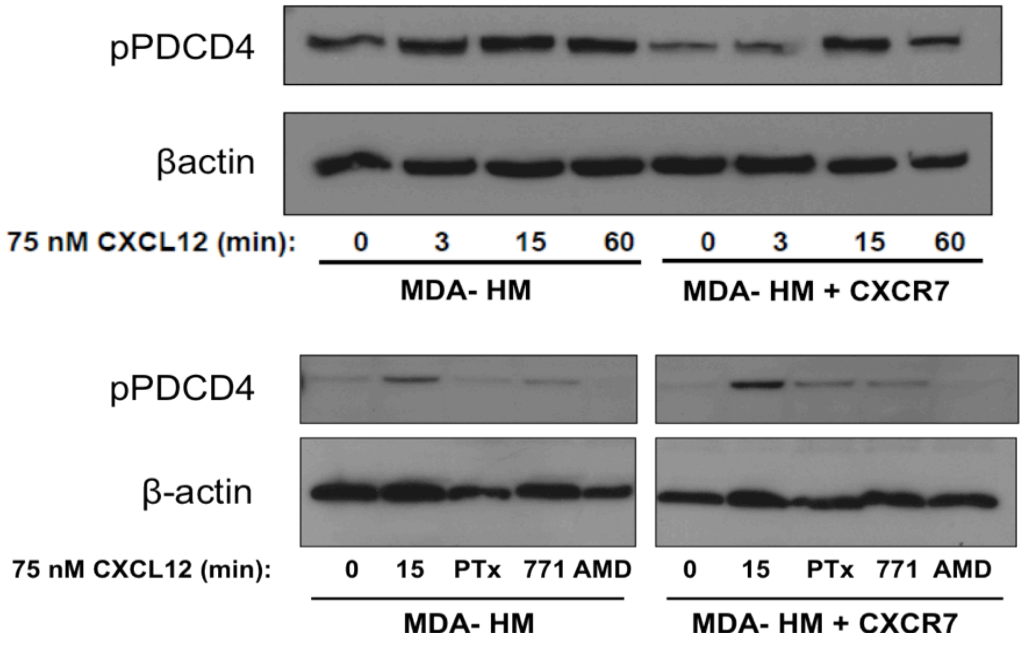

Figure 5.17 Phosphorylation analysis of PDCD4 stimulated over a timecourse of 30 min with CXCL12 (top panels) or for 15 min in the presence or absence of inhibitors in MDA-HM cells or MDA-HM + CXCR7 cells.

In addition to PDCD4, we also examined the phosphorylation profiles of Akt and ERK1/2 in MDA-MB-231 cells transfected with CXCR4, CXCR7, or CXCR4 and CXCR7 upon stimulation with 75 nM CXCL12 for a 30 min timecourse. Cells expressing CXCR4 (MDA-WT + CXCR4) resulted in Akt and ERK1/2 phosphorylation in response to CXCL12 stimulation, as well as robust phosphorylation of PDCD4 (Figure 5.18). In contrast, CXCR7 expressing cells (MDA-WT + CXCR7) resulted in ERK1/2 phosphorylation and not Akt phosphorylation. Coexpression of CXCR4 and CXCR7 (MDA-WT + CXCR4/7) showed diminished phosphorylation of Akt, ERK1/2, and PDCD4 in contrast to cells expressing CXCR4 alone. These data suggest that CXCL12 can stimulate robust phosphorylation responses of Akt, ERK1/2 and PDCD4 through CXCR4 in MDA cells; however, the presence of CXCR7 decreases the extent of these responses, as shown in Figure 5.18.

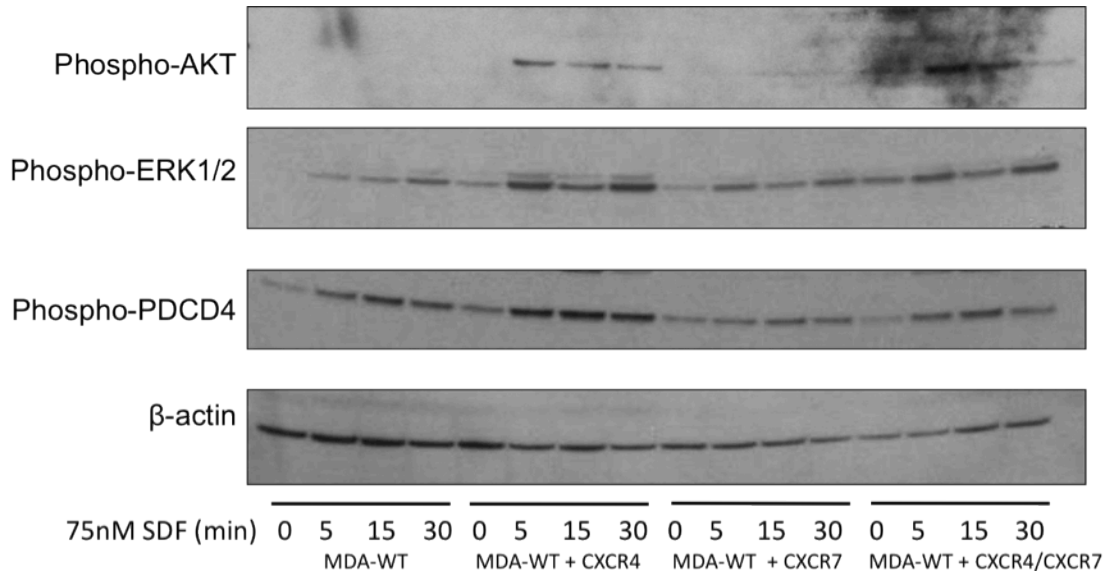

Figure 5.18 MDA-MB-231 WT (MDA-WT) cells transfected with high levels of CXCR4 (MDA-WT + CXCR4), CXCR7 (MDA-WT + CXCR7), or with moderate levels of CXCR4 and high levels of CXCR7 (MDA-WT + CXCR4/7) were stimulated over a timecourse of 30 min with 75 nM CXCL12/SDF. A western blot probing for either Akt, ERK1/2 or PDCD4 phosphorylation (S457) and β-actin as a loading control was performed.

5.3.5: Effect of the CXCR4 WHIM mutant on CXCL12 mediated internalization of CXCR4 and CXCR7

Finally, to try and determine whether there are direct interactions occurring between CXCR4 and CXCR7 in the MDA-MB-231 cells that could explain the inhibition of activity detected when CXCR4 and CXCR7 are coexpressed, we evaluated receptor internalization following CXCL12 stimulation using the C-terminal truncation mutant of CXCR4 identified in WHIM syndrome [23, 24]. As described in Chapter 1, the constitutive heterodimerization of the CXCR4 WHIM mutant with WT CXCR4 has been used to explain the retention of WT CXCR4 on the cell surface. Here, we coexpressed the CXCR4 WHIM mutant with CXCR7, to determine whether the mutant could prevent internalization of CXCR7, similar to that seen with CXCR4 WT. Cells were stimulated with 200 nM CXCL12 or PBS control for 45 min at 37 °C to allow for internalization, followed by mAb staining for CXCR4 and/or CXCR7 and flow cytometry detection. As expected, CXCL12 promoted internalization of MDA + CXCR4 cells; however, introduction of CXCR4 R334X decreased the extent of internalization by ~2-fold (Figure 5.20 and Figure 5.21). Stimulation of cells coexpressing CXCR4 and CXCR7 also led to receptor internalization of both receptors, whereas, coexpression of the CXCR4 R334X mutant in place of CXCR4 WT led to retention of CXCR7 on the cell surface as shown in Figure 5.20, and an increase in CXCR4 levels compared to WT CXCR4 dual expressing cells (Figure 5.20 and Figure 5.21). These data strongly imply that there is a direct interaction between CXCR4 and CXCR7, leading to a decreased ability for either CXCR4 or CXCR7 to be internalized normally upon ligand stimulation. Based on the mean fluorescent intensity gathered from the flow cytometry data, the percentage of

CXCR4 or CXCR7 still remaining on the surface following CXCL12 stimulation was quantified and is shown in Figure 5.21.

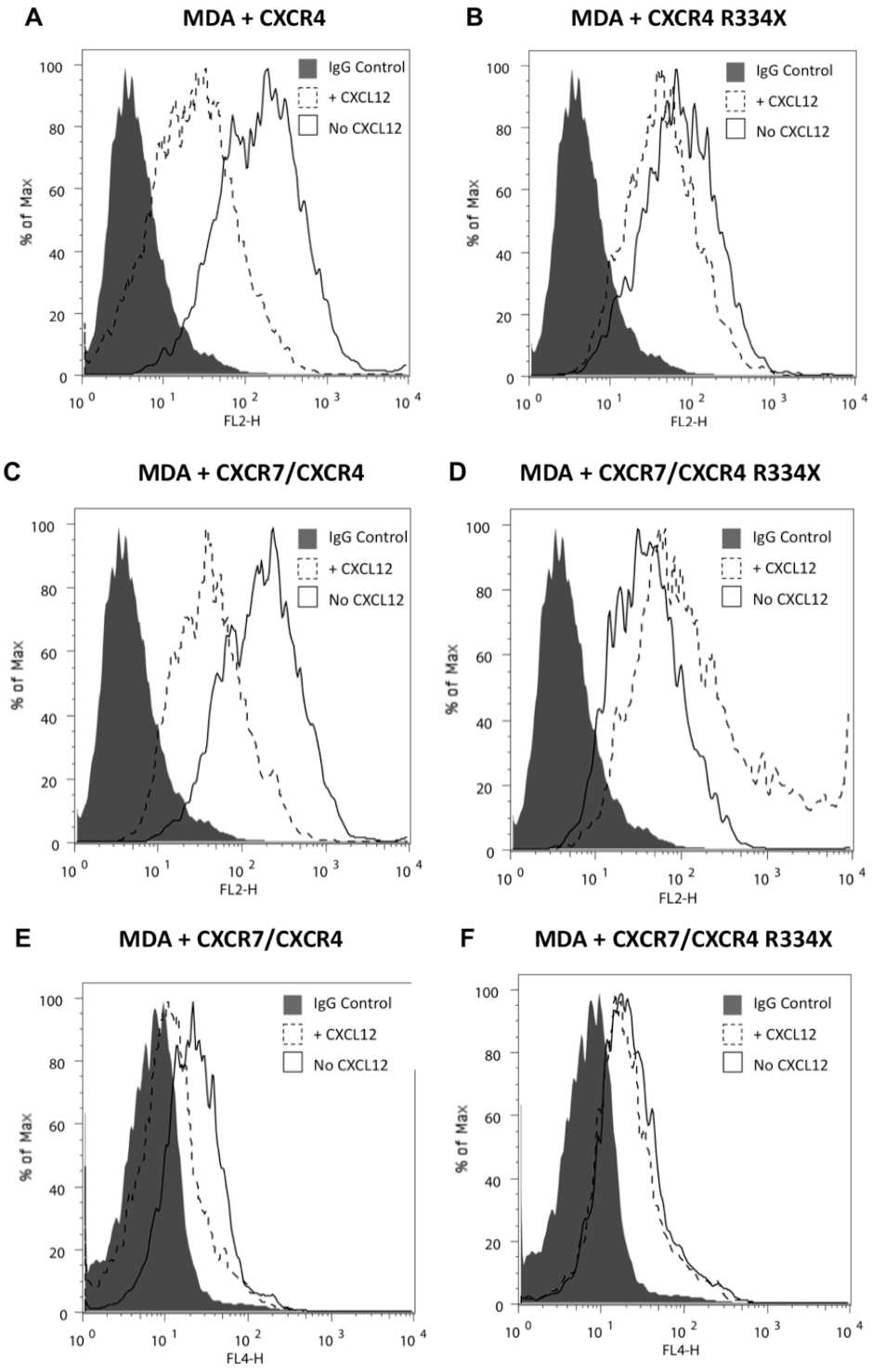

Figure 5.19 CXCR4/CXCR7 internalization of (A) MDA + CXCR4, (B) MDA + R334X, (C and E) MDA + CXCR7/CXCR4, and (D and F) MDA + CXCR7/R334X expressing cells (*right*) following treatment with CXCL12 (*dashed line*) or no chemokine (*solid line*), compared to isotype control (*filled*), as determined by flow cytometry.

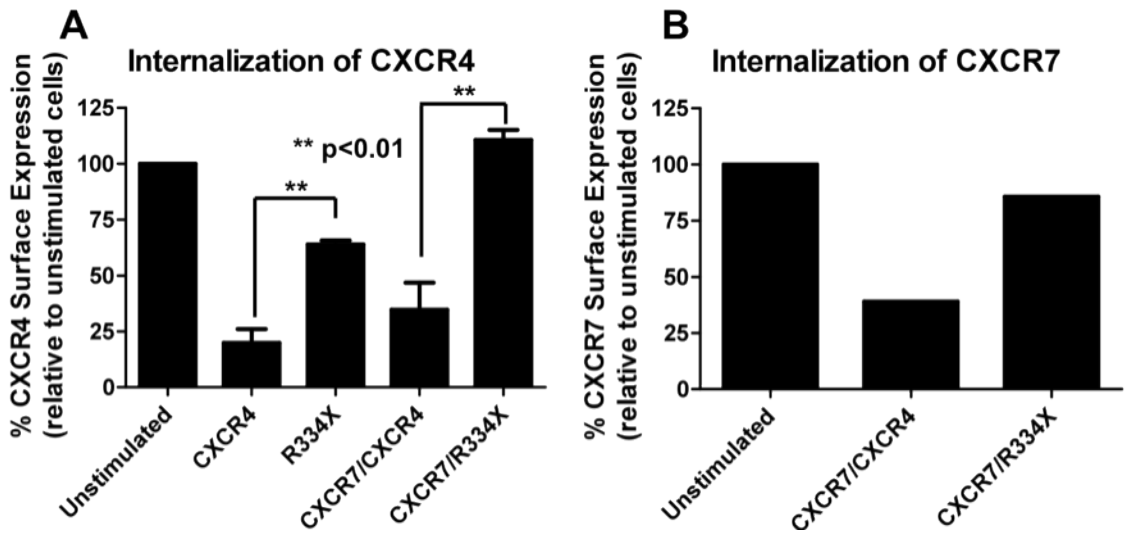

Figure 5.20 Quantification of CXCR4 and CXCR7 internalization of MDA-MB-231 cell populations. The percent of CXCR4 (A) or CXCR7 (B) levels remaining on the cell surface after treatment with 200 nM CXCL12 for 40 min are shown, as determined by flow cytometry. The relative CXCR4 or CXCR7 surface expression was calculated as 100 x (Ft – Fi)/(Fu – Fi) where Fu = Mean fluorescence intensity of untreated cells, Fi = [3]Mean fluorescence intensity of isotype control and Ft= Mean fluorescence intensity of CXCL12 treated cells.

5.4 Discussion

The functional role of CXCR4:CXCR7 crosstalk is particularly interesting as both receptors are linked to a number of cancers [8, 14, 15]. However, little is known regarding how coexpression of both receptors modulates the ligand mediated activity of each individual receptor compared to how they independently respond to chemokine. CXCR4 and CXCR7 present an especially interesting pair of chemokine receptors because they share the ligand CXCL12, in addition to CXCR7 binding to a second ligand, CXCL11, though neither ligand elicits the canonical Gαi mediated signaling of CXCR7. This lack of classic chemokine receptor activation is mainly attributed to its lack

of the G protein coupling “DRYLAIV” motif, normally present on chemokine receptors [5, 25]. Several theories have been proposed to explain the potential mechanism mediating CXCR7 activity, including mediating signaling through alternative pathways (apart from Gi), heterodimerization with chemokine receptors, or functioning as a chemokine scavenger. Although chemokine sequestration and degradation may be one component to CXCR7 activity, it seems unlikely that it is the main role considering the important contributions of CXCR7 in development, as evidenced by the early death of CXCR7 knockout mice [7]. Alternatively, studies evaluating the biochemical properties of CXCR7 have found that CXCR7 can readily form homodimers as well as heterodimers with CXCR4, providing a potential mechanism for CXCR7 activity [7, 11, 26]. Additionally, CXCR7 can readily associate with β-arrestins [9], which can also function as signal transducing molecules activating pathways such as Akt, PI3K, and MAPK [12]. Collectively, these findings have helped advance our limited understanding of CXCR7 activity but have also raised important questions regarding how the presence of CXCR7 may affect ligand mediated signaling of other receptors expressed on the same tissues.

As discussed in Chapter 1, there are several possible consequences of chemokine receptor hetero-oligomerization that can exhibit a dramatic effect on receptor activity. For example, ligand binding of one receptor could alter or interfere with the ligand binding or recruitment of intracellular proteins (e.g. G protein) of the other receptor. Additionally, binding of ligand to one receptor could potentially promote desensitization of the other receptor, and finally, hetero-oligomerization could prevent ligand mediated desensitization and internalization of a receptor, thus prolonging its responsiveness to chemokine stimulation. These mechanisms of regulation by chemokine receptor oligomerization are important considerations when studying CXCR7, given that it has been shown to heterodimerize with CXCR4, although the effect

of this association is not known, particularly with respect to cancer. To this end, we set out to investigate the individual and combined effects of CXCR4 and CXCR7 to breast cancer tumor growth and metastasis.

Using the human breast cancer cell line MDA-MB-231 stably expressing CXCR4 and/or CXCR7 in a WT or highly metastatic (MDA-HM) background, we studied the effects of receptor expression on tumor growth and progression with an *in vivo* tumor metastasis mouse model. In support of previous findings, both CXCR4 and CXCR7 independently promoted primary tumor growth, although CXCR4 resulted in more rapid growth than CXCR7 expressing cells. Interestingly, using the MDA-HM cell background, we found that coexpression of CXCR4 and CXCR7 decreased the extent of CXCR4 mediated lung metastases despite relatively normal primary tumor growth. To explore this further, MDA lines expressing varying levels of CXCR4 and/or CXCR7 were probed for activation of known signaling pathways, in response to chemokine stimulation. Coexpression of CXCR7 with CXCR4 on MDA-MB-231 cells resulted in a decreased response to CXCL12 mediated calcium flux in addition to diminished phosphorylation of Akt, ERK1/2, and PDCD4 (described in Chapters 3 and 4) in contrast to normal responses of cells expressing CXCR4 alone. Treatment with the CXCR4 specific inhibitor, AMD3100, prior to CXCL12 stimulation, resulted in similar inhibition of MDA-HM and MDA-HM + CXCR7 cells to phosphorylated PDCD4 while the CXCR7 specific inhibitor CCX771 inhibited phosphorylation to a lesser extent, suggesting that the phosphorylation effects are primarily mediated by CXCR4, and that CXCR7 does not interfere with CXCR4 inhibition by AMD3100. Interestingly, inhibition of G protein coupling by treatment with Pertussis toxin (PTx), prior to CXCL12 stimulation, inhibited the CXCR4 signaling, while CXCR7 expression was associated with a decreased sensitivity to PTx inhibition. These findings suggest that the CXCR4 and CXCR7

crosstalk may be limiting the accessibility of G protein to couple to CXCR4 based on the effects observed when CXCR7 was present. However, a more rigorous analysis would need to be performed to specifically address this notion. To look more directly at the effect of interactions between CXCR4 and CXCR7, we utilized a C-terminal truncation mutant of CXCR4 identified from WHIM syndrome. WHIM syndrome is a rare immunodeficiency disorder associated with retention of mutant CXCR4 to due to reduced desensitization and internalization. As WHIM syndrome is a mostly heterozygous disease, CXCR4 WT retention at the cell surface has been suggested to result from constitutive heterodimer formation between WT and mutant CXCR4 forms. To this end, we used the C-terminal truncation of CXCR4 (CXCR4 R334X), to determine if CXCL12 could promote CXCR7 internalization when coexpressed with mutant CXCR4, compared to WT CXCR4. Interestingly, CXCR4 R334X caused retention of CXCR7 on the cell surface upon ligand stimulation, compared to normal internalization when WT CXCR4 was expressed. These findings strongly suggest that CXCR7 is able to modulate CXCR4 activity through a direct association with CXCR4, facilitating a downregulation of CXCR4 activity when CXCR7 is present, although the biological relevance of this crosstalk effect remains to be determined. Finally, we found that in accordance with other reports, the endogenous expression of CXCR7 was predominantly localized with intracellular stores, although how this relates to the ligand mediated activation and subsequent activity of CXCR7 is unclear, considering that there are also reports of CXCR7 surface expression on other malignant cell and tissue types [14].

Overall, we are only beginning to understand the complex interaction that occurs between CXCR4 and CXCR7, and it is becoming clear that this behavior may also be completely context dependent (e.g. cell type, disease state, etc.), as has been described

for a number of other chemokine interactions presented throughout this dissertation. Nevertheless, in the context of breast cancer, we demonstrate that CXCR7 can decrease the effects mediated by CXCR4 activity, likely due, at least in part, to receptor oligomerization and crosstalk mechanisms such as receptor transinhibition. The increasingly complex biology of CXCR4 and CXCR7 involvement in cancer may have far-reaching consequences with regards to the pharmaceutical development of antagonists, considering that receptor homo- and heterodimers may elicit very different responses to stimuli.

5.5 Ongoing Work/Immediate Future Directions

To support the findings presented above, that CXCR7 inhibits the metastatic activity of CXCR4 when the receptors are expressed together in breast cancer cells, we are currently working on additional experiments to complete this work for publication. The most important remaining experiments are *in vitro* chemotaxis assays to unequivocally demonstrate the inhibitory role of CXCR7 on CXCL12 mediated CXCR4 migration. These assays are performed routinely in our lab and should be straightforward once optimized for the MDA cell line. In addition to the presented CXCL12 mediated internalization assays, we will also perform internalization assays with the CXCR7 specific ligand, CXCL11, to determine whether CXCL11 stimulation can induce internalization of CXCR4 (mutant and WT). Finally, we will perform a more rigorous signaling and functional analyses of the cells expressing CXCR4, CXCR7, and CXCR4/CXCR7 using a combination of ligands (CXCL12, CXCL11) and receptor specific inhibitors (AMD3100 for CXCR4, CCX771 for CXCR7) to further delineate the

functional effects of CXCR4:CXCR7 crosstalk on signaling in breast cancer cells. Taken together, these data will form the basis of a co-first author publication.

5.6 Materials and Methods

5.6.1: Cells and reagents

Recombinant CXCL12 was expressed and purified as described previously [27] (Appendix I , protocol K). The human breast cancer cell line, MDA-MB-231 (MDA-WT), and the HEK293T cell line were obtained from American Type Culture Collection (Manassas, VA); cells were cultured in RPMI-1640 media or DMEM media, respectively, containing Glutamax and supplemented with 10% fetal bovine serum (FBS) (Invitrogen, Carlsbad, CA). The MDA-MB-231 highly metastatic cell line (MDA-HM) was kindly provided by Dr. Anja Müller, and was originally generated *in vivo* via tail-vein injection of ATCC derived MDA-MB-231 cells into a tumor metastasis mouse model and selection of cells that were highly metastatic to the lung. MDA-HM CXCR4 and/or CXCR7 transfectants were generated by subcloning CXCR4 or CXCR7 insert into the retroviral vector, pBabe-puro or pBabe-neo with puromycin or geneticin resistance (kind gift of Dr. Jing Yang, UCSD), and then transfected into MDA-MB-231 WT or MDA-HM cells. pBabe-GFP plasmid was also generously provided by Dr. Jing Yang and stably transfected into MDA lines. The CXCR4-R334X mutation was generated by QuikChange site-directed mutagenesis (Stratagene, La Jolla, CA). mAb CXCR3 (49801), CXCR7 (11G8), and isotype control IgG_1 were obtained from R & D Systems (Minneapolis, MN) and mAb CXCR4 (1D9) and isotype control IgG_{2B} were obtained from BD Biosciences (San Jose, CA). CXCR4 inhibitor, AMD3100, was obtained from Sigma

(St. Louis, MO), CXCR7 small molecule inhibitor, CCX771, was generously provided by ChemoCentryx (Mountain View, CA), and Pertussis toxin was obtained from List Biological Laboratories (Campbell, CA).

5.6.2: Generation of stable MDA cell lines

A clonal MDA line with low CXCR4 expression was obtained by limiting dilution of ATCC derived MDA-MB-231 cell line (MDA-WT). Clones were screened for low expressing by mAb staining with PE-CXCR4 and detection by flow cytometry. To obtain cell lines with stable expression of CXCR4, CXCR7, or both receptors, retroviral transfections were performed as described previously [28]. Briefly, HEK293T cells were triple transfected with 2 μg of total DNA, including 1 μg of transfer vector, 0.9 μg of gag/pol pUCMV3 expression vector, and 0.1 μg of VSV-G expression vector using TransIT-LT1 transfection reagent (Mirius Bio, Madison, WI). Target MDA sublines (either MDA-WT, MDA clonal line (low CXCR4), or MDA-HM) were infected with 48 and 72 h viral supernatants, along with 6 μg/mL protamine sulfate (Sigma) for 4-6 h. Once MDA cells reached confluency, cells were split and selected with either 5 μg/mL Blasticidin (Invitrogen), 5 μg/mL of Puromycin (CellGro, Manassas, VA), 0.7 mg/mL of Geneticin (Invitrogen) in RPMI + 10% FBS until selection was complete. Expression of CXCR4 and/or CXCR7 was confirmed by mAb staining and analysis by flow cytometry.
In addition, the breast cancer cell lines used for the animal studies were also transfected with pWZL vector containing GFP with a Blasticidin resistance gene using the described retroviral transfection method, for visualization purposes. Following selection, GFP transfection of the target cells was verified by flow cytometry.

5.6.3: Flow cytometry

Receptor levels of ATCC derived MDA-MB-231 cells as well as MDA transfectants were assessed by flow cytometry using a PE-conjugated CXCR4 mAb (clone 1D9) or an APC-conjugated CXCR7 mAb (clone 11G8) in addition to a PE- IgG_{2B} or APC- IgG_1 isotype control (Appendix I, Protocol P). Cells were resuspended in cold buffer (0.5% bovine serum albumin (BSA) in phosphate buffered saline (PBS)), stained with antibody or isotype control for 20 min on ice in the dark, and washed 3 times with cold buffer. Data was acquired on a BD FACSCalibur Cytometer and analyzed by FlowJo Software (Tree Star, Inc., Ashland, OR). For intracellular detection of receptor, cells were first fixed with ice cold 0.1% formaldehyde solution for 30 min, permeabilized with 0.2% Tween-20 in PBS for 15 min in a 37 °C waterbath, spun down, and stained with mAb as described above.

5.6.4: Immunofluorescence microscopy

The cellular distribution of CXCR4 and CXCR7 was determined for MDA-MB-231 cells by immunofluorescence microscopy (Appendix I, Protocol U). MDA-MB-231 cells were seeded onto coverslips with 2.5 x 10^5 cells and allowed to grow for 24 h. The following day, cells were fixed for 15 min with freshly prepared 3.7% formaldehyde, washed 3 times with PBS and then permeabilized with 0.5% Triton-X 100 in PBS for 10 min. Cells were washed with PBS, blocked with SeaBlock (Pierce) for ~1 h, and then washed again with PBS. Cells were stained with CXCR4 mAb (R&D), CXCR7 mAb (R&D), or Isotype control mAb in 2% BSA in PBS, according to manufacturer guidelines for 2 h at ambient temperature, washed 3 times with PBS and then stained with Alexa Fluor 488 (Invitrogen) at a concentration of 1:500 in 0.5% BSA in PBS for 30 min. Excess antibody was washed 3 more, times with PBS, dipped briefly into double distilled H_2O to remove excess PBS, and then coverslips were mounted onto slides using

Prolong Gold (Invitrogen). Slides were allowed to dry overnight at ambient temperature and then imaged by Deconvolution Microscopy at the UCSD Cancer Center with a 40x objective. Each image underwent 10 cycles of deconvolution. Lastly, images were compared to the isotype control images and corrected for non-specific staining.

5.6.5: In vivo mouse studies

Seven to nine week old, female, CB.17-SCID mice (Charles River, Wilmington, MA) were injected into the 4^{th} inguinal mammary fat pad on both sides, with MDA-MB-231 cells (varying populations) all expressing GFP. Procedures were approved by the UCSD Institutional Animal Care and Use Committee and performed in compliance with federal regulations. Prior to injection, 2×10^6 cells were mixed with Matrigel (BD Biosciences) (50:50 v/v) and directly injected (total volume 20 µL) each fat pad. Mammary tumors were measured by caliper 3 times weekly and tumor volume was calculated using the equation $(l \times w^2)/2$. Once tumors reached approximately 1 cm in size (around day 42-48), mice were sacrificed by CO_2 asphyxiation and mammary tumors and organs (e.g. lungs, lymph nodes, spleen, liver) were excised and immediately place in either PBS for subsequent culture, GFP visualization, fluorescence quantification of lung metastases, or into freshly prepared 4% PFA for histology. To preserve the lung architecture, lung lobes were inflated by perfusing with 4% Paraformaldehyde prior to being placed into fixative overnight. The next day, samples were transferred to 70% EtOH and then processed by the UCSD Histology Core for paraffin embedding and H& E staining. Alternatively, tissues were visualized by GFP fluorescence using a microdissection microscope with varying magnification (10-40X). Select tissues were cultured by digestion with 1 mg/mL Collagenase A (Roche) in serum-free RPMI for 0.5-1 h at 37 °C with end-over-end rotation, addition of an equal

volume of RPMI + 10% FBS to stop digestion, and filtration through a 70 μm filter. Digests were spun down at 250xg for 10 min at 4 °C and supernatant was grown with RPMI-10% FBS + 1% Pen-Strep (Invitrogen). Once confluent, GFP positive MDA cells were selected with 5 μg/mL Blasticidin. Receptor expression was assayed by flow cytometry analysis as described above.

5.6.6: Calcium flux assays

CXCL12-mediated intracellular calcium flux was detected by using the FLIPR Calcium 4 assay kit (Molecular Devices, Sunnyvale, CA). Cells were lifted with 1 mM EDTA in PBS, washed twice with 0.5 % BSA in PBS to remove residual EDTA, and resuspended in assay buffer (1 x Hanks balanced salt solution, 20 mM HEPES, pH 7.4, 0.1% BSA). 100 μL of cells (at 1-2 x 10^6 cells/mL) were added to a 96 well plate along with 100 μL of calcium 4 dye (prepared in 10 mL of assay buffer) and incubated for 1 h at 37 °C. CXCL12 ligand was reconstituted in 10 mM HEPES or Tris, and prepared at varying dilutions with PBS. Using a FlexStation instrument (Molecular Devices), calcium flux response upon addition of varying concentrations of CXCL12 was monitored.

5.6.7: Western blot analysis

Cells were cultured in serum-free RPMI for 36 h, and then stimulated with 75 nM CXCL12 for a 1 h timecourse (unstimulated, 3, 15, and 60 min). For inhibitor studies, cells were pretreated with either 40 μM AMD3100, 0.2 μg/mL Pertussis toxin, or 1 μM CCX771 for 1 h at 37 °C prior to stimulation with 75 nM CXCL12 for 15 min. Cells were lysed with RIPA Buffer (10 mM Tris, pH7.4, 150 mM NaCl, 1% Triton-X, 0.1% Na-Deoxycholate, 0.1% SDS, and 5 mM EDTA) containing Complete Protease Inhibitor (Roche, Palo Alto, CA) and Halt Phosphatase Inhibitor (Pierce, Rockford, IL) on ice for

30 min. Clarified cell lysates were obtained by centrifugation at 13,200 rpm for 10 min at 4 °C and total protein concentration was determined using the BCA Protein Assay (Pierce). Protein (20 µg/well) was loaded onto a 10% SDS-PAGE gel or a CriterionXT precast 4-12% Bis-Tris gel (BioRad, Hercules, CA) and run with Tris-glycine or XT MES buffer, respectively. Gels were transferred to PVDF membrane (BioRad), blocked with 5% milk in TBS-T (Tris Buffered Saline + 0.1% Tween-20) for at least 1 h at RT, and then incubated overnight with primary antibody at 4 °C. Membranes were washed 3 times with TBS-T, incubated with secondary antibody conjugated to horseradish peroxidase (HRP) for 1 h at RT, washed again with TBS-T 3 times and developed with Amersham ECL-plus (GE Healthcare) or SuperSignal West femtosensitivity reagent (Pierce). To reprobe with additional antibodies or β-actin (Cell Signaling, Danvers, MA) as a loading control, blots were stripped for 10 min with Restore Stripping Reagent (Pierce) at RT, washed 3 times with TBS-T and incubated with additional antibodies. Phospho-ERK1/2 antibody was obtained from Upstate (Millipore, Billerica, MA), phospho-PDCD4 was obtained from Rockland Immunochemicals (Gilbertsville, PA), and phospho-Akt was obtained from Cell Signaling. All antibodies were used according to manufacturer product guidelines.

5.6.8: Internalization assays

CXCL12 mediated chemokine receptor internalization was studied with MDA-WT + CXCR4, MDA-WT + R334X, MDA-WT +CXCR7/CXCR4 and MDA-WT +CXCR7/R334X expressing cells. Briefly, cells were seeded in a 6 well plate with 700,000 cells/well. The following day, media was removed and replaced with either 3 mL of media alone or media containing 200 nM CXCL12. Cells were incubated for 45 min at 37 °C to allow for internalization and then immediately placed on ice. Wells were

washed with cold PBS, cells were lifted with 1mM EDTA in PBS for ~5 min on ice, stained for CXCR4 or CXCR7 as described above, and analyzed with a FACSCaliber flow cytometer. The percent of receptor internalized was quantified by using FlowJo software to determine the mean fluorescent intensity (MFI) of CXCL12- treated cells (M_t), untreated cells (M_u) and isotype control (M_i) and using the MFI values in the equation, $(M_t-M_i)/(M_u-M_i) \times 100$. Experiments were performed in triplicate.

5.7 Acknowledgements

The dissertation author and Morgan O'Hayre equally contributed to the material presented in **Chapter 5**. Dr. Jing Yang also substantially contributed to this study by providing expertise, guidance, and technical assistance throughout the investigation.

5.8 References

1. Müller, A., B. Homey, H. Soto, N. Ge, D. Catron, M.E. Buchanan, T. McClanahan, E. Murphy, W. Yuan, S.N. Wagner, J.L. Barrera, A. Mohar, E. Verástegui, and A. Zlotnik, *Involvement of chemokine receptors in breast cancer metastasis.* Nature, 2001. **410**(6824): p. 50-6.

2. Balkwill, F., *The significance of cancer cell expression of the chemokine receptor CXCR4.* Semin Cancer Biol, 2004. **14**(3): p. 171-9.

3. Nagasawa, T., S. Hirota, K. Tachibana, N. Takakura, S. Nishikawa, Y. Kitamura, N. Yoshida, H. Kikutani, and T. Kishimoto, *Defects of B-cell lymphopoiesis and bone-marrow myelopoiesis in mice lacking the CXC chemokine PBSF/SDF-1.* Nature, 1996. **382**(6592): p. 635-8.

4. Tachibana, K., S. Hirota, H. Iizasa, H. Yoshida, K. Kawabata, Y. Kataoka, Y. Kitamura, K. Matsushima, N. Yoshida, S. Nishikawa, T. Kishimoto, and T. Nagasawa, *The chemokine receptor CXCR4 is essential for vascularization of the gastrointestinal tract.* Nature, 1998. **393**(6685): p. 591-4.

5. Burns, J.M., B.C. Summers, Y. Wang, A. Melikian, R. Berahovich, Z. Miao, M.E. Penfold, M.J. Sunshine, D.R. Littman, C.J. Kuo, K. Wei, B.E. McMaster, K. Wright, M.C. Howard, and T.J. Schall, *A novel chemokine receptor for SDF-1 and I-TAC involved in cell survival, cell adhesion, and tumor development.* J Exp Med, 2006. **203**(9): p. 2201-13.

6. Balabanian, K., B. Lagane, S. Infantino, K.Y. Chow, J. Harriague, B. Moepps, F. Arenzana-Seisdedos, M. Thelen, and F. Bachelerie, *The chemokine SDF-1/CXCL12 binds to and signals through the orphan receptor RDC1 in T lymphocytes.* J Biol Chem, 2005. **280**(42): p. 35760-6.

7. Sierro, F., C. Biben, L. Martínez-Muñoz, M. Mellado, R.M. Ransohoff, M. Li, B. Woehl, H. Leung, J. Groom, M. Batten, R.P. Harvey, C. Martínez-A, C.R. Mackay, and F. Mackay, *Disrupted cardiac development but normal hematopoiesis in mice deficient in the second CXCL12/SDF-1 receptor, CXCR7.* Proc Natl Acad Sci USA, 2007. **104**(37): p. 14759-64.

8. Burns, J.M., B.C. Summers, Y. Wang, A. Melikian, R. Berahovich, Z. Miao, M.E.T. Penfold, M.J. Sunshine, D.R. Littman, C.J. Kuo, K. Wei, B.E. McMaster, K. Wright, M.C. Howard, and T.J. Schall, *A novel chemokine receptor for SDF-1*

and I-TAC involved in cell survival, cell adhesion, and tumor development. J Exp Med, 2006. **203**(9): p. 2201-13.

9. Rajagopal, S., J. Kim, S. Ahn, S. Craig, C.M. Lam, N.P. Gerard, C. Gerard, and R.J. Lefkowitz, *Beta-arrestin- but not G protein-mediated signaling by the "decoy" receptor CXCR7.* Proceedings of the National Academy of Sciences, 2010. **107**(2): p. 628-32.

10. Zabel, B.A., Y. Wang, S. Lewén, R.D. Berahovich, M.E.T. Penfold, P. Zhang, J. Powers, B.C. Summers, Z. Miao, B. Zhao, A. Jalili, A. Janowska-Wieczorek, J.C. Jaen, and T.J. Schall, *Elucidation of CXCR7-mediated signaling events and inhibition of CXCR4-mediated tumor cell transendothelial migration by CXCR7 ligands.* The Journal of Immunology, 2009. **183**(5): p. 3204-11.

11. Levoye, A., K. Balabanian, F. Baleux, F. Bachelerie, and B. Lagane, *CXCR7 heterodimerizes with CXCR4 and regulates CXCL12-mediated G protein signaling.* Blood, 2009. **113**(24): p. 6085-93.

12. Lefkowitz, R.J. and S.K. Shenoy, *Transduction of receptor signals by beta-arrestins.* Science, 2005. **308**(5721): p. 512-7.

13. DeWire, S.M., S. Ahn, R.J. Lefkowitz, and S.K. Shenoy, *Beta-arrestins and cell signaling.* Annu Rev Physiol, 2007. **69**: p. 483-510.

14. Miao, Z., K.E. Luker, B.C. Summers, R. Berahovich, M.S. Bhojani, A. Rehemtulla, C.G. Kleer, J.J. Essner, A. Nasevicius, G.D. Luker, M.C. Howard, and T.J. Schall, *CXCR7 (RDC1) promotes breast and lung tumor growth in vivo and is expressed on tumor-associated vasculature.* Proc Natl Acad Sci USA, 2007. **104**(40): p. 15735-40.

15. Balkwill, F., *Cancer and the chemokine network.* Nat Rev Cancer, 2004. **4**(7): p. 540-50.

16. Zheng, K., H.-Y. Li, X.-L. Su, X.-Y. Wang, T. Tian, F. Li, and G.-S. Ren, *Chemokine receptor CXCR7 regulates the invasion, angiogenesis and tumor growth of human hepatocellular carcinoma cells.* J Exp Clin Cancer Res, 2010. **29**: p. 31.

17. Wang, J., Y. Shiozawa, Y. Wang, Y. Jung, K.J. Pienta, R. Mehra, R. Loberg, and R.S. Taichman, *The role of CXCR7/RDC1 as a chemokine receptor for CXCL12/SDF-1 in prostate cancer.* J Biol Chem, 2008. **283**(7): p. 4283-94.

18. Mazzinghi, B., E. Ronconi, E. Lazzeri, C. Sagrinati, L. Ballerini, M.L. Angelotti, E. Parente, R. Mancina, G.S. Netti, F. Becherucci, M. Gacci, M. Carini, L. Gesualdo, M. Rotondi, E. Maggi, L. Lasagni, M. Serio, S. Romagnani, and P. Romagnani, *Essential but differential role for CXCR4 and CXCR7 in the therapeutic homing of human renal progenitor cells.* J Exp Med, 2008. **205**(2): p. 479-90.

19. Hartmann, T.N., V. Grabovsky, R. Pasvolsky, Z. Shulman, E.C. Buss, A. Spiegel, A. Nagler, T. Lapidot, M. Thelen, and R. Alon, *A crosstalk between intracellular CXCR7 and CXCR4 involved in rapid CXCL12-triggered integrin activation but not in chemokine-triggered motility of human T lymphocytes and CD34+ cells.* Journal of Leukocyte Biology, 2008. **84**(4): p. 1130-40.

20. Calatozzolo, C., A. Canazza, B. Pollo, E. Di Pierro, E. Ciusani, E. Maderna, E. Salce, V. Sponza, S. Frigerio, F. Di Meco, S. Schinelli, and A. Salmaggi, *Expression of the new CXCL12 receptor, CXCR7, in gliomas.* Cancer Biol Ther. **11**(2): p. 242-53.

21. Luker, K.E., J.M. Steele, L.A. Mihalko, P. Ray, and G.D. Luker, *Constitutive and chemokine-dependent internalization and recycling of CXCR7 in breast cancer cells to degrade chemokine ligands.* Oncogene, 2010. **29**(32): p. 4599-610.

22. O'Hayre, M., C.L. Salanga, T.J. Kipps, D. Messmer, P.C. Dorrestein, and T.M. Handel, *Elucidating the CXCL12/CXCR4 signaling network in chronic lymphocytic leukemia through phosphoproteomics analysis.* PLoS ONE, 2010. **5**(7): p. e11716.

23. Balabanian, K., B. Lagane, J.L. Pablos, L. Laurent, T. Planchenault, O. Verola, C. Lebbe, D. Kerob, A. Dupuy, O. Hermine, J.F. Nicolas, V. Latger-Cannard, D. Bensoussan, P. Bordigoni, F. Baleux, F. Le Deist, J.L. Virelizier, F. Arenzana-Seisdedos, and F. Bachelerie, *WHIM syndromes with different genetic anomalies are accounted for by impaired CXCR4 desensitization to CXCL12.* Blood, 2005. **105**(6): p. 2449-57.

24. Lagane, B., K.Y. Chow, K. Balabanian, A. Levoye, J. Harriague, T. Planchenault, F. Baleux, N. Gunera-Saad, F. Arenzana-Seisdedos, and F. Bachelerie, *CXCR4 dimerization and beta-arrestin-mediated signaling account for the enhanced chemotaxis to CXCL12 in WHIM syndrome.* Blood, 2008. **112**(1): p. 34-44.

25. Sierro, F., C. Biben, L. Martinez-Munoz, M. Mellado, R.M. Ransohoff, M. Li, B. Woehl, H. Leung, J. Groom, M. Batten, R.P. Harvey, A.C. Martinez, C.R. Mackay, and F. Mackay, *Disrupted cardiac development but normal hematopoiesis in mice deficient in the second CXCL12/SDF-1 receptor, CXCR7.* Proc Natl Acad Sci U S A, 2007. **104**(37): p. 14759-64.

26. Luker, K.E., M. Gupta, and G.D. Luker, *Imaging chemokine receptor dimerization with firefly luciferase complementation.* FASEB J, 2009. **23**(3): p. 823-34.

27. O'Hayre, M., C.L. Salanga, P.C. Dorrestein, and T.M. Handel, *Phosphoproteomic analysis of chemokine signaling networks.* Meth Enzymol, 2009. **460**: p. 331-46.

28. Stewart, S.A., D.M. Dykxhoorn, D. Palliser, H. Mizuno, E.Y. Yu, D.S. An, D.M. Sabatini, I.S. Chen, W.C. Hahn, P.A. Sharp, R.A. Weinberg, and C.D. Novina, *Lentivirus-delivered stable gene silencing by RNAi in primary cells.* RNA, 2003. **9**(4): p. 493-501.

CHAPTER 6

Conclusions and Future Directions

6.1 Summary

Chemokines and their receptors are involved in both the innate and adaptive immune response with chemokines being best known for their role in directing leukocyte migration [1]. Secreted chemokines form gradients along the endothelium through interactions with glycosaminoglycans (GAG), which are cell surface carbohydrates. These interactions help facilitate retention and localization of chemokines on the endothelial surface, assisting in the recruitment of receptor-bearing immune cells to sites of inflammation or to secondary lymphoid organs during routine patrol. As a result, chemokines can engage their receptors, activating a variety of signaling pathways. Together, chemokines and their receptors have multi-faceted roles in various processes such as organogenesis, hematopoiesis, and cardiac development. However, despite the prominent role of chemokines in normal physiological functions, many studies have shown that aberrant activation or expression of chemokines and their receptors is associated with numerous inflammatory disorders as well as primary tumor growth and metastasis [2, 3] (Table 1.2). Tumor cells may utilize chemokine induced signaling pathways to promote responses such as survival, growth, and proliferation. Yet, little is known regarding the molecular mechanisms that drive key interactions in the chemokine network, particularly those with chemokines (e.g. oligomerization), glycosaminoglycans

(GAGs), and chemokine receptors, and how these interactions specifically contribute to the biological activity of chemokines. In this dissertation, efforts aimed at elucidating the specific interactions of chemokines with GAGs and chemokine receptors, and the functional effects of these interactions in normal or disease states, formed the general framework for the aims presented in Chapters 2 through 5. Below is a summary of the major findings for each aim in addition to future directions.

6.2 Chapter 2

Conclusions

The first aim of this work involved the use of hydroxyl radical footprinting with mass spectrometry to identify GAG binding epitopes of the chemokine MCP-3/CCL7 in complex with the GAG, Heparin octasaccharide. As far as we know, this is the first study to date, to apply hydroxyl radical footprinting for the structural determination of GAG binding sites. Several distinct attributes of this technique distinguish it from the more traditional approaches. Mainly, hydroxyl radical footprinting is an unbiased and global approach for looking at protein complexes and is based on the general premise that certain regions of a protein will be protected from oxidative modification, due to complex formation, making it a favorable approach for studying chemokine:GAG interactions. From these analyses, two peptides, ^{13}YRFINKKIPKQRLES^{27} and ^{63}FMKHLDKKTQTPKL^{76}, were found to have lower oxidation rate constants when GAG was present, suggesting their involvement in GAG binding. The regions of these peptides were mapped to the known structure and revealed two unique binding epitopes not previously associated with MCP-3/CCL7: GAG binding, including K18K19 and the Lys rich C-terminal tail, K65K69K70K75 (termed K4x). Based on these findings, we performed directed Ala mutagenesis and functional studies to determine the contribution of these residues to MCP-3/CCL7 activity. By Heparin binding affinity chromatography, calcium flux analysis, and chemotaxis assays, we established that the mutants tested (K18AK19A and K4xA) had a lower affinity than MCP-3/CCL7 WT for Heparin binding but still maintained the ability to induce calcium flux and a migration response with receptor bearing cells, suggesting that these are GAG binding sites which do not significantly overlap with receptor binding or affect receptor activation. This last

consideration is important because the next phase of this project involves *in vivo* cellular recruitment assays with these mutants to determine their effect on chemokine induced migration of leukocytes, in order to establish a functional relevance for the identified GAG interaction sites. Details of these studies can be found under *Immediate future directions* at the end of Chapter 2.

Future directions

Extending this work to truly address the specificity of chemokine:GAG interactions on a broader scale, we are collaborating with the Complex Carbohydrate Research Center (CCRC, Univ. of Georgia), to perform GAG arrays with a large panel of chemokines. The GAG arrays are composed of a variety of synthetic GAGs (~40-50) immobilized onto a chip which are incubated with recombinant chemokine, tagged at the C-terminus with HA or myc epitopes, and binding detected by antibody against the tag(s). This approach will allow a high-throughput screen for the specificity of chemokine:GAG binding to identify preferred epitopes on the GAGs, and also for comparison of the specificity of different chemokines for different GAGs. To this end, we have cloned approximately 12 chemokines, with both HA and myc tags and are currently cloning an additional 10-15. Two have been expressed and purified for initial testing and the rest will be expressed and purified over the next two months. The specific chemokines were not randomly chosen, but rather designed to ask specific questions. For example, do the MCPs recognize similar or different GAGs, even though they all bind CCR2? Of particular relevance for the present work, how does MCP-3/CCL7, which does not oligomerize, compare to MCP-1/CCL2, which does? Many other specific comparisons will be made.

Based on the results gleaned from the GAG array, additional analyses will be carried out to further dissect the chemokine:GAG interactions. For example, we are currently developing techniques to utilize Surface Plasmon Resonance (SPR) to quantify the binding affinities of chemokines for specific GAGs, as well as their on and off rates, and their tendency to oligomerize. SPR will also enable us to more quantitatively characterize mutants in order to better understand the contribution of residues to the binding of various GAGs in a high throughput manner. Together, our efforts are aimed at elucidating the specificity of interactions within the chemokine network (mainly focused here on chemokine and GAG interactions) and identifying mechanisms that can help explain their biological activity.

Finally, to further complement this work, we will extend the focus of our hydroxyl radical footprinting studies to include another chemokine, MCP-1/CCL2 that forms dimers and higher order oligomers in the presence of GAGs. Radiolysis of MCP-1/CCL2 and MCP-1/CCL2:GAG has already been carried out and, although interpretation of this data will be more complex given the propensity of MCP-1/CCL2 to form oligomers, we have prior knowledge and will be testing the hypothesis that the GAGs truly bind along the patch shown in Figure 2.1. Collectively, this work will enable us to gain a better understanding of chemokine:GAG binding specificity between different chemokines, as well as in the context of oligomerization, which is not well understood.

6.3 Chapters 3 and 4

Conclusions

In the next set of aims, comprising Chapters 3 and 4, a mass spectrometry based approach was utilized again, this time with the goal of elucidating novel downstream targets of CXCL12/CXCR4 mediated signaling pathways involved in the survival of chronic lymphocytic leukemia (CLL) cells. As described previously, CLL is the most prevalent form of adult leukemia in the western world and is characterized by the excessive accumulation and/or apoptotic resistance of CLL B cells [4]. CLL cells are known to overexpress the chemokine receptor, CXCR4, and its ligand, CXCL12, is thought to be an important microenvironmental factor contributing to CLL survival. And while the signaling pathways associated with chemokine mediated migration are fairly well characterized, much less is known regarding pathways involved in survival and proliferation. To this end, we took a phosphoproteomics approach by employing immobilized metal affinity chromatography (IMAC) phosphopeptide enrichment followed by reverse-phase liquid chromatography and tandem mass spectrometry (LC-MS/MS). Phosphoproteomics was employed here because it possesses several distinct advantages over other techniques, mainly that it is an unbiased and global approach and allows multiple events to be detected simultaneously without *a priori* knowledge, thereby generating truly new hypotheses that can be later validated by more traditional methods (e.g. western blot, siRNA, etc.). This work identified several interesting phosphoproteins potentially involved in CXCL12-mediated survival in CLL cells, which were described in Chapter 4 and will be briefly discussed below.

Phosphoproteomics analysis was a novel strategy not previously carried out in the Handel Lab. As a result, extensive optimization and technology development was required in order to perform these experiments. In close collaboration with a fellow Handel lab graduate student, Morgan O'Hayre, we optimized a protocol for the successful enrichment of phosphopeptides originating from unstimulated and CXCL12

stimulated primary CLL cells. The details of this strategy are outlined in Chapter 3 and resulted in a co-authored methods chapter published in *Methods in Enzymology* in 2009. After testing a number of phosphoprotein/phosphopeptide enrichment strategies, we found that IMAC enrichment was an effective means for routinely obtaining greater than 30% enrichment (and upwards of 50%), which is similar to previous phosphoproteomics studies involving mammalian cells [5].

Using the phosphoproteomics methods described in Chapter 3, work elucidating the CXCL12/CXCR4 signaling network in CLL is presented in Chapter 4. This work was published in *PLoS ONE* in 2010. Due to significant efforts towards the mass spectrometry based portion of the study, the dissertation author was second author on this publication. The phosphoproteomics based analyses resulted in the identification of > 700 phosphoproteins and > 1200 unique phosphosites. Many of the phosphoproteins identified had prior implications in CLL disease and other leukemias, adding confidence to the phosphoproteomics results. In addition, there were a number of phosphoproteins identified, with no previous implication in CXCL12 mediated signaling in CLL cells. Spectral counting, a semi-quantitative analysis approach, was employed for unstimulated and CXCL12 stimulated phosphoproteomic datasets, to identify phosphorylation events potentially mediated by CXCL12. Based on the spectral count analyses, several potential downstream phosphorylation targets of CXCL12 were identified and chosen for additional follow-up studies, which are described in more detail within Chapter 4. Briefly, programmed cell death factor 4 (PDCD4) and heat shock protein 27 (HSP27), were identified as two novel targets of CXCL12 signaling in CLL cells, both with prior implications in the regulation of cancer and apoptosis. Western blot analyses confirmed that PDCD4 was a novel downstream phosphorylation target of CXCL12 mediated signaling in CLL cells, with no prior implications in CLL survival.

PDCD4 has been previously reported to act as a tumor suppressor protein, where its normal function of eIF4A translation and AP-1 mediated transcription inhibition is downregulated by phosphorylation, which can occur by Akt and p70S6k activity. In addition, HSP27 was also found to be a novel phosphorylation target of CXCL12 signaling. HSP27 has been previously associated with anti-apoptotic effects and is known to be downstream of the p38-MAPK signaling cascade, which has no previous associations with CLL survival signaling. While western blot analysis confirmed CXCL12 mediated phosphorylation of HSP27 in CLL samples exhibiting a phosphorylation response based on spectral counting assessment, only ~25% of CLL patients contained detectable total HSP27 by western blot analysis. Because HSP27 expression can be induced upon stressful cellular events like exposure to chemotherapeutics, it is possible that the presence of HSP27 in the subset of patients could potentially relate to a response from chemotherapy treatment, and refractory disease, which is a significant issue in the treatment of CLL. However, characterization of additional patient samples would be necessary to address the potential correlation between HSP27 expression and chemotherapy in CLL patients.

Future directions

In addition to the follow-up work of PDCD4 presented in Chapter 4, we have also shown that PDCD4 is a phosphorylation target of other chemokines in cells other than CLL, such as human breast cancer MDA-MB-231 cells, as described in Chapter 5. In addition, it has been shown in our lab that the chemokines CCL19 and CCL21 also robustly stimulate PDCD4 phosphorylation through their shared receptor CCR7 (data not shown). Finally, we have shown that chemokines can mediate PDCD4 phosphorylation in non-cancer cells such as HEK293T cells. As a result, we are interested in

determining which chemokines and chemokine receptor pairs are able to induce phosphorylation of PDCD4. To begin, we will transiently transfect chemokine receptors into HEK293T cells and stimulate with ligands specific to each receptor, and probe for phospho-PDCD4 by western blot. Based on these results, we will perform follow-up experiments probing the response of specific chemokine receptors endogenously expressed in more biologically relevant cell types. Collectively, we expect to determine whether PDCD4 phosphorylation is a ubiquitous signaling pathway that is utilized by many chemokines/receptors in the chemokine network, or if the phosphorylation of PDCD4 is primarily restricted to specific chemokine/receptor pairs and/or cell types.

One additional direction of significant interest is to characterize the “Nurse-like cell” (NLC)-CLL “secretome”. In the CLL microenvironment, marrow stromal cells (MSCs) are thought to secrete factors contributing to CLL survival. *In vitro*, CLL survival is supported by coculturing CLL cells with MSCs or with blood-derived monocytes that differentiate into NLCs [6] (Figure 6.1). CXCL12 is one the known factors secreted by NLCs, which can support CLL survival [6]. However, while the addition of exogenous CXCL12, and other factors, enhances CLL survival *in vitro*, it does not fully recapitulate the survival response of co-culturing CLL cells with NLCs [7], suggesting that there are additional factors being secreted by NLCs that contribute to CLL survival. Therefore, we are extremely interested in identifying the factors that drive the symbiotic relationship between CLL cells and NLCs. In particular, we want to identify factors secreted by NLCs, which support CLL survival *in vitro,* in addition to identifying factors secreted by the CLL cells, which contribute to the differentiation of blood-derived monocytes into NLCs.

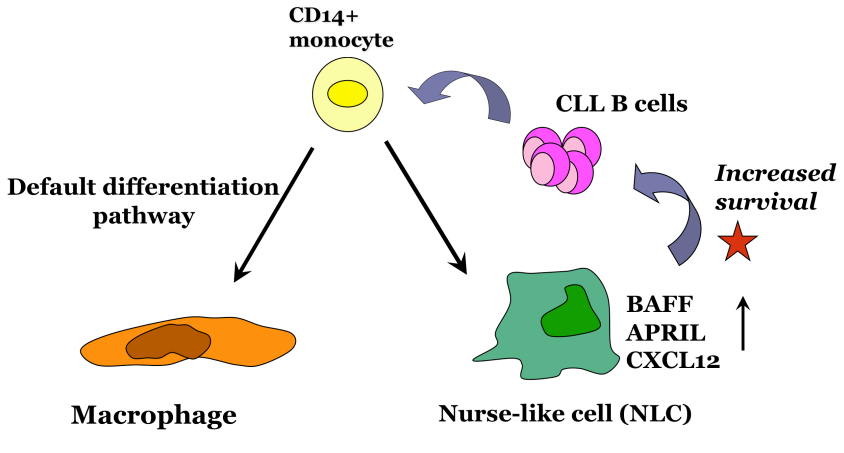

Figure 6.1 Illustration of the crosstalk between CLL cells and NLCs, referred to as the NLC-CLL "secretome"

In order to characterize factors involved in the CLL-NLC crosstalk in an unbiased and global manner, we originally planned to use a mass spectrometry based approach to identify proteins in the "secretome" using media derived from CLL cells alone and CLL-NLC cocultures. However, one significant hurdle we have had to address is the depletion of contaminating proteins originating from the human serum (e.g. albumin, immunoglobulin), which is necessary for culturing of these cells, but if left, presents a serious dynamic range issue with respect to mass spectrometry analysis, considering the proteins we are interested in typically comprise less than 1% of the plasma proteome. To address this issue, we have tried several approaches in order to deplete the contaminating serum components and enrich for the proteins of interest (e.g. small proteins ~10-40 kD in size), including spin concentration with MW cutoff filters in the presence of a denaturant (e.g. ACN), strong cation exchange chromatography, size exclusion chromatography, and elution of chemokines/cytokines factors by addition of Heparin to the cells, all with little success. One possible solution to this problem is to fractionate our samples using the Gelfree8100 fractionation system, an instrument that performs molecular weight based fractionation of complex biological samples, an

instrument which our collaborators at J&J recently acquired. Prior to the acquisition, Protein Discovery (Knoxville, TN) performed a complimentary sample workup of serum and cocultured media with the fractionation system. This system was extremely effective in separating contaminating proteins, especially the large albumin band (~66kD) present in F6 to F12 (Figure 6.2). The lower abundant and smaller MW proteins are seen mainly in F1 to F4 with no albumin overlap. In addition, depletion of the contaminating serum components was also achieved by passing samples through an Albumin/IgG affinity spin columns prior to fractionation, resulting in further separation and enrichment of the coculture samples (Figure 6.3). Together, the use of the Gelfree fractionation system in conjunction with serum depletion spin columns offer a viable method for enrichment of the CLL-NLC secretome, which can be subsequently analyzed by mass spectrometry. Elucidating the potential signaling pathways activated by CLL cells and NLCs will be fundamental towards our understanding of how the CLL microenvironment influences the survival of CLL B cells, and may potentially reveal novel therapeutic targets.

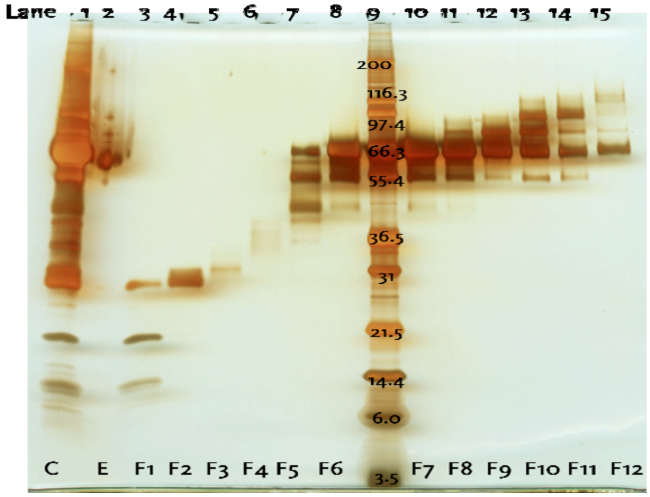

Figure 6.2 1D silver stained gel of Gelfree 8100 fractions collected from the coculture (Raw) sample showing that Fractions 1-4 contain the targeted protein range, 20-40 kDa, for the Coculture (Raw) samples.

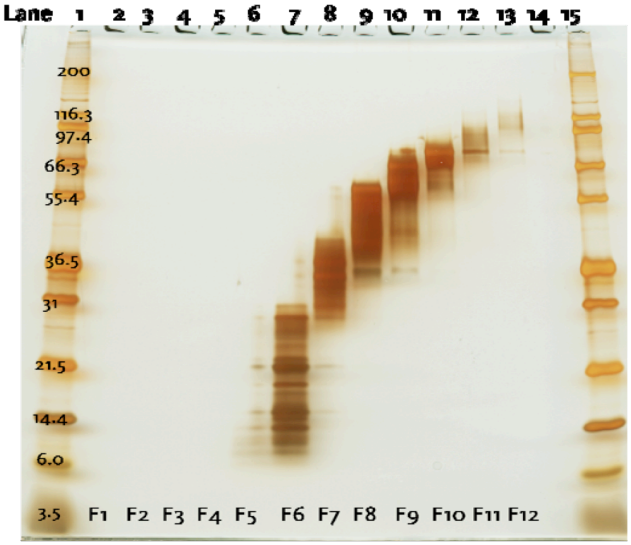

Figure 6.3 1D silver stained gel of Gelfree 8100 fractions collected from the depleted CLL-NLC coculture sample.

6.4 Chapter 5

Conclusions

In the final aim of this dissertation, the main goal of this work was to understand the individual and combined effects of the chemokine receptors, CXCR4 and CXCR7, towards breast cancer progression and metastasis. Although CXCR4, and its ligand, CXCL12 have been shown to contribute to at least 23 types of cancer [8], much less is known about CXCL12's other receptor, CXCR7, which was discovered more recently. Since the identification of CXCR7 as an additional ligand to CXCL12, there has been a relative explosion of studies in the past several years, directed at understanding the role of CXCR7 in various cancer subtypes [9-15]. Like CXCR4, CXCR7 is also not generally expressed on normal epithelia, but has been found on several types of malignant tissues as well as various cancer cell lines [9, 10, 16-20], warranting these investigations. Many

studies have investigated the functional activity of CXCR7 and/or its contributions to cancer development in isolation; however, reports have established that in some cases CXCR4 and CXCR7 are both expressed, for example through the analysis of malignant tissues derived from various sources such as breast, lung, and brain [9, 10, 15, 19]. To this end, we wanted to examine more the combined effect of CXCR4 and CXCR7 to address whether both receptors were merely redundant in function, whether there were synergistic effects towards tumor promoting properties, or perhaps the occurrence of receptor regulation by receptor mediated crosstalk. Thus far, our data indicates that CXCR7 can exhibit an inhibitory effect on CXCR4 mediated activity. Using MDA-MB-231 human breast cancer cells expressing varying levels of CXCR4 and/or CXCR7 we showed with two different mouse experimental setups that both CXCR4 and CXCR7 are tumor growth promoting; however, one major distinction between the two receptors is that CXCR4 promotes metastasis while CXCR7 does not. This is not entirely unexpected considering that has been well established by others that CXCR7 does not elicit canonical chemokine mediated responses like migration or calcium mobilization [9, 10]. Correspondingly, when both receptors were coexpressed in a highly metastatic breast cancer cell line (MDA-HM) derived *in vivo* for metastatic potential to the lung, we found that the presence of CXCR7 did not inhibit primary tumor growth but did exhibit decreased metastases compared MDA-HM injected mice. These results were quite compelling and led us to further characterize these interactions *in vitro*, to better understand on the molecular level, how CXCR7 was modulating the biological activity of CXCR4. Through signaling and calcium mobilization activity assays, we found that CXCR7 decreased the response of CXCR4 to CXCL12 mediated calcium flux as well as decreased and/or delayed CXCL12 mediated phosphorylation of signaling targets like ERK1/2 and PDCD4. Furthermore, using a C-terminal truncation CXCR4 mutant,

originally identified in WHIM syndrome, we were able to show a direct interaction occurring between CXCR4 and CXCR7, similar to what has been described to occur for CXCR4 WT and the CXCR4 WHIM mutant (CXCR4 R334X). Flow cytometry analysis of the CXCR4 and CXCR7 levels present on the surface before and after ligand stimulation showed that CXCR4-R334X did not internalize as readily as CXCR4 WT, as expected. Interestingly, CXCR4/CXCR7 expressing cells were able to normally internalize both receptors upon ligand stimulation, but when mutant was present, this actually led to an increase in the amount of CXCR4 R334X on the surface, while CXCR7 levels did not internalize nearly as well as compared to WT. These data demonstrate that CXCR4 and CXCR7 are able to physically associate, and although we do not know the exact details of this interaction (e.g. stoichiometry of homodimer versus heterodimer, propensity of occurrence), it nonetheless illustrates potential consequences of CXCR4 and CXCR7 coexpression, and the subsequent effect on modulation of receptor activity following ligand stimulation. It is important to note that evaluating CXCR4 is a significantly easier endeavor because there are several well known methods for studying chemokine receptor activation such as calcium flux, migration assays, and signaling profiling of known downstream targets (e.g. ERK1/2, Akt) that are not amenable to probing CXCR7 activity because CXCR7 does not elicit classical, and easily detectable, chemokine receptor responses.

Overall, we have described studies towards elucidating the role of CXCR4 and CXCR7 in promoting tumor growth and metastasis (findings summarized in Figure 6.4), and found that coexpression of CXCR7 on MDA-HM cells significantly limited the amount of lung metastases normally induced by MDA-HM cells. Based on the current understanding of CXCR7 activity, we hypothesize that the observed effect is due, at least in part, to a direct interaction and possible transinhibition between CXCR4 and

CXCR7 that promotes the downmodulation of CXCR7 activity, that is also corroborated through several *in vitro* cell based assays.

Future directions

An additional, more long-term future direction involves evaluating the protein-protein interactions that facilitate CXCR4 and CXCR7 mediated signaling by performing pulldown analyses with mass spectrometry of both receptors. While we have certain expectations and previous knowledge regarding what types of interactions CXCR4 is associated with (e.g. G protein coupling), much less is known regarding the intracellular interactions of CXCR7, apart from evidence that it associates with β-arrestin [21]. Therefore, applying an unbiased mass spectrometry based approach will allow us to evaluate CXCR4 and CXCR7 independently, to see what intracellular proteins they interact with that may be associated with their activity. Currently, we have generated HA-tagged CXCR4 and CXCR7 using the retroviral expression system used for the breast cancer work. We plan to transfect HEKs and breast cancer cells with both receptors, affinity purify with HA resin, and probe the resulting proteins that pulldown with either receptor by traditional proteomics approaches (e.g. trypsin digest followed by LC-MS/MS). Fortunately, we have already successfully optimized the affinity purification and elution steps for HA-tagged receptor, so this portion will be straightforward. Next, we will transfect our receptors to produce stable lines, stimulate with CXCL12, and establish that we are getting an appropriate chemokine mediated signaling response (e.g. phospho-ERK1/2) prior to carrying out pulldown analyses. If successful, we will be able to compare the protein-protein interactions of CXCR4 and CXCR7 in a high throughput manner. Targets of interest, identified by mass spectrometry would then be validated through traditional biochemical methods such as immunoprecipitation and

western blot analysis to confirm direct interactions, as well as functional assays directed at specific protein-protein interactions to establish relevance to the biological activity of the receptor.

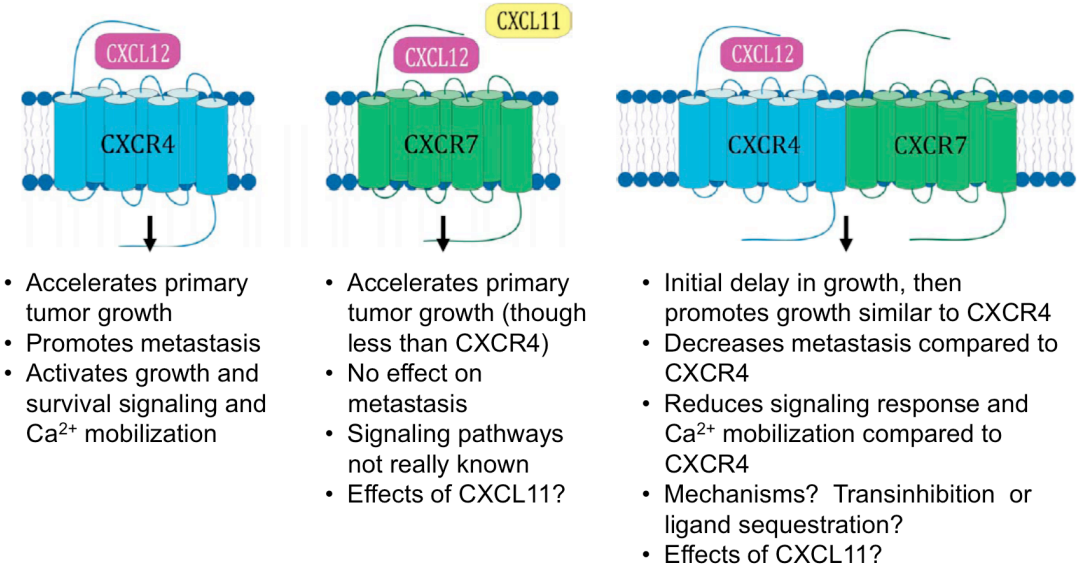

Figure 6.4 Overview of Chapter 5 studies regarding the effects of CXCR4 (*left*), CXCR7(*middle*) and CXCR4/CXCR7 (*right*) expression on breast cancer primary tumor growth, metastasis, and signaling.

6.5 References

1. Baggiolini, M., *Chemokines in pathology and medicine.* J Intern Med, 2001. **250**(2): p. 91-104.

2. Gerard, C. and B.J. Rollins, *Chemokines and disease.* Nat Immunol, 2001. **2**(2): p. 108-15.

3. Balkwill, F., *Cancer and the chemokine network.* Nat Rev Cancer, 2004. **4**(7): p. 540-50.

4. Chiorazzi, N., K.R. Rai, and M. Ferrarini, *Chronic lymphocytic leukemia.* N Engl J Med, 2005. **352**(8): p. 804-15.

5. Moser, K. and F.M. White, *Phosphoproteomic analysis of rat liver by high capacity IMAC and LC-MS/MS.* J Proteome Res, 2006. **5**(1): p. 98-104.

6. Burger, J.A., N. Tsukada, M. Burger, N.J. Zvaifler, M. Dell'Aquila, and T.J. Kipps, *Blood-derived nurse-like cells protect chronic lymphocytic leukemia B cells from spontaneous apoptosis through stromal cell-derived factor-1.* Blood, 2000. **96**(8): p. 2655-63.

7. Nishio, M., T. Endo, N. Tsukada, J. Ohata, S. Kitada, J.C. Reed, N.J. Zvaifler, and T.J. Kipps, *Nurselike cells express BAFF and APRIL, which can promote survival of chronic lymphocytic leukemia cells via a paracrine pathway distinct from that of SDF-1alpha.* Blood, 2005. **106**(3): p. 1012-20.

8. Balkwill, F., *The significance of cancer cell expression of the chemokine receptor CXCR4.* Semin Cancer Biol, 2004. **14**(3): p. 171-9.

9. Burns, J.M., B.C. Summers, Y. Wang, A. Melikian, R. Berahovich, Z. Miao, M.E.T. Penfold, M.J. Sunshine, D.R. Littman, C.J. Kuo, K. Wei, B.E. McMaster, K. Wright, M.C. Howard, and T.J. Schall, *A novel chemokine receptor for SDF-1 and I-TAC involved in cell survival, cell adhesion, and tumor development.* J Exp Med, 2006. **203**(9): p. 2201-13.

10. Miao, Z., K.E. Luker, B.C. Summers, R. Berahovich, M.S. Bhojani, A. Rehemtulla, C.G. Kleer, J.J. Essner, A. Nasevicius, G.D. Luker, M.C. Howard, and T.J. Schall, *CXCR7 (RDC1) promotes breast and lung tumor growth in vivo and is expressed on tumor-associated vasculature.* Proc Natl Acad Sci USA, 2007. **104**(40): p. 15735-40.

11. Zabel, B.A., Y. Wang, S. Lewén, R.D. Berahovich, M.E.T. Penfold, P. Zhang, J. Powers, B.C. Summers, Z. Miao, B. Zhao, A. Jalili, A. Janowska-Wieczorek, J.C. Jaen, and T.J. Schall, *Elucidation of CXCR7-mediated signaling events and inhibition of CXCR4-mediated tumor cell transendothelial migration by CXCR7 ligands.* The Journal of Immunology, 2009. **183**(5): p. 3204-11.

12. Hattermann, K., J. Held-Feindt, R. Lucius, S.S. Müerköster, M.E.T. Penfold, T.J. Schall, and R. Mentlein, *The chemokine receptor CXCR7 is highly expressed in human glioma cells and mediates antiapoptotic effects.* Cancer Research, 2010. **70**(8): p. 3299-308.

13. Grymula, K., M. Tarnowski, M. Wysoczynski, J. Drukala, F.G. Barr, J. Ratajczak, M. Kucia, and M.Z. Ratajczak, *Overlapping and distinct role of CXCR7-SDF-*

1/ITAC and CXCR4-SDF-1 axes in regulating metastatic behavior of human rhabdomyosarcomas. Int J Cancer, 2010. **127**(11): p. 2554-68.

14. Li, T., H. Li, Y. Wang, C. Harvard, J.-L. Tan, A. Au, Z. Xu, D.M. Jablons, and L. You, *The expression of CXCR4, CXCL12 and CXCR7 in malignant pleural mesothelioma.* The Journal of pathology, 2010.

15. Zheng, K., H.-Y. Li, X.-L. Su, X.-Y. Wang, T. Tian, F. Li, and G.-S. Ren, *Chemokine receptor CXCR7 regulates the invasion, angiogenesis and tumor growth of human hepatocellular carcinoma cells.* J Exp Clin Cancer Res, 2010. **29**: p. 31.

16. Salmaggi, A., E. Maderna, C. Calatozzolo, P. Gaviani, A. Canazza, I. Milanesi, A. Silvani, F. DiMeco, A. Carbone, and B. Pollo, *CXCL12, CXCR4 and CXCR7 expression in brain metastases.* Cancer Biol Ther, 2009. **8**(17): p. 1608-14.

17. Iwakiri, S., N. Mino, T. Takahashi, M. Sonobe, S. Nagai, K. Okubo, H. Wada, H. Date, and R. Miyahara, *Higher expression of chemokine receptor CXCR7 is linked to early and metastatic recurrence in pathological stage I nonsmall cell lung cancer.* Cancer, 2009. **115**(11): p. 2580-93.

18. Calatozzolo, C., A. Canazza, B. Pollo, E. Di Pierro, E. Ciusani, E. Maderna, E. Salce, V. Sponza, S. Frigerio, F. Di Meco, S. Schinelli, and A. Salmaggi, *Expression of the new CXCL12 receptor, CXCR7, in gliomas.* Cancer Biol Ther. **11**(2): p. 242-53.

19. Wurth, R., F. Barbieri, A. Bajetto, A. Pattarozzi, M. Gatti, C. Porcile, G. Zona, J.L. Ravetti, R. Spaziante, and T. Florio, *Expression of CXCR7 chemokine receptor in human meningioma cells and in intratumoral microvasculature.* J Neuroimmunol. **234**(1-2): p. 115-23.

20. Singh, R.K. and B.L. Lokeshwar, *The IL-8-Regulated Chemokine Receptor CXCR7 Stimulates EGFR Signaling to Promote Prostate Cancer Growth.* Cancer Res. **71**(9): p. 3268-77.

21. Rajagopal, S., J. Kim, S. Ahn, S. Craig, C.M. Lam, N.P. Gerard, C. Gerard, and R.J. Lefkowitz, *Beta-arrestin- but not G protein-mediated signaling by the "decoy" receptor CXCR7.* Proceedings of the National Academy of Sciences, 2010. **107**(2): p. 628-32.

APPENDIX I

PROTOCOLS

A: MCP-3/CCL7 Purification

pHUE MCP-3
MGSSHHHHHHHHHQLFVKTLTGKTITLELEPSDTVENVKAKIQDKEGIPPDQQRLIFAGK
QLEDGRTLSDYNIQKESTLHLVLRLRGGQPVGINTSTTCCYRFINKKIPKQRLESYRRTT
SSHCPREAVIFKTKLDKEICADPTQKWVQDFMKHLDKKTQTPKL

pHUE-MCP-3 (WT Ub)
MW: 19,666.5
Ex. Coeff: 10220

MCP-3
MW: 8956.4
Ex. Coeff: 8730

BUFFERS:

Resuspension Buffer:
(Store at 4°C once PI tablet and DNase is added)

10 mM Tris, pH 8
300 mM NaCl
40 mM Imidazole
Dash DNase
1 Complete EDTA-Free tablet (Roche)

Ni-Seph, Buffer A:

10 mM Tris, pH 8
300 mM NaCl
40 mM Imidazole

Ni-Seph, Buffer B:

10 mM Tris, pH 8
300 mM NaCl
250 mM Imidazole

DAY 1: TRANSFORMATION AND PREP

1. Transform BL21(DE3)pLysS Cells with 1µLof plasmid DNA. Plate 200 µL on LB/Carb plate
2. Prepare 6 x 1L LB in fernbach flasks for main growth as well as 6 x 5 mL LB in culture tubes and 3 x 100 mL LB in 250 mL shaker flasks for the starter growths

DAY 2: GROWTH

3. Inoculate each of the 5mL cultures with a swipe of colonies from the plate, shake at 30 °C
4. About 1-1.5 h later (once a bit cloudy), pool the 5mL cultures and evenly distribute into the 3 x 100 mL flasks of LB, shake at 30 °C
5. About 1.5-2 h later (once cloudy), evenly distribute the 3 x 100 mL into the 6 x 1L of LB
6. Induce with 0.5 mM IPTG (0.5 mL of 1M stock) when OD reaches 0.4-0.6 (Take 1mL aliquots before induction and every hour after induction to run on gel)
7. Harvest cultures after 3-4h of growth
8. Spin down pellets at 5.5k rpm, 15 min, 4°C
9. Resuspend in ~50mL of Resuspension buffer (make sure to add DNAse, $MgCl_2$, and EDTA-free protease inhibitor fresh)
10. Divide into 2 x 50 mL conicals, snap freeze in LN_2, and store at -80°C until ready to purify

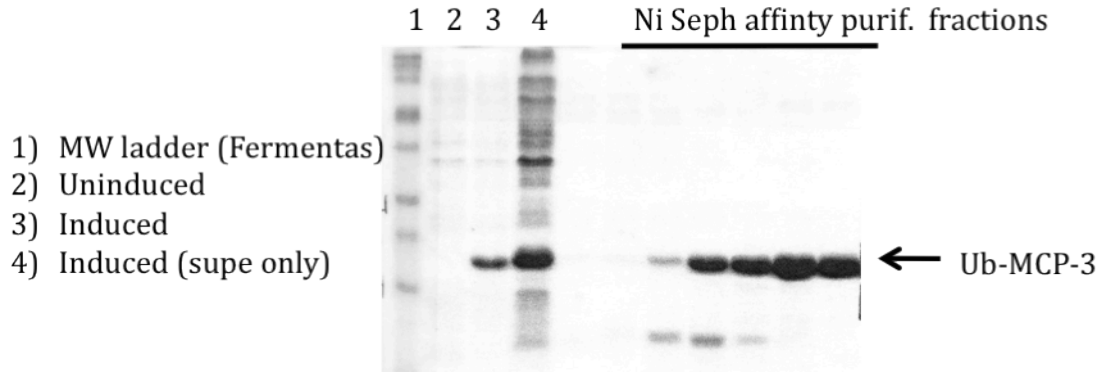

DAY 3: NI PURIFICATION ON AKTA

11. Thaw conicals containing protein in beaker of H_2O on ice for ~30 min

12. Bring volume up to approximately 100 mL with leftover resuspension buffer form the day before
13. Sonicate 4 x on ice (3 s on, 2 s off, 1 min rest in between runs)
14. Spin lysate for 30 min, 18 k rpm with JA25.50 rotor, 4 °C
15. Filter supe with durapore filter
16. Pour supe into 150 mL superloop for use with AKTA
17. Prior to running on Ni-Seph column on AKTA, be sure to equilibrate in Buffer A before hand (if stored in EtOH previously, wash with several CV's of water before equilibrating with Buffer A)
18. Run MCP-3 using "Ni Seph MCP3 gradient", just be sure to fill in column location and empty loop amount (since is different everythime). This methods does ~6 CV to wash signal to baseline (a lot of junk comes off in wash) then elutes up to 250 mM Imidazole with Buffer B. MCP-3 comes off during the middle to end of the gradient
19. Once run is complete, pool fractions containing protein (can take sample to run on gel to confirm)
20. At this point, prefer to run Ub-MCP-3 fusion over HPLC so that I don't have to purify all at once, and avoid dialysis (imidazole inhibits Usp2cc activity, so need to remove prior to cleavage step)
21. Concentrate with 3K MWCO spin filter at 4 °C until volume is appropriate to load on to HPLC
22. Acidify HPLC load with 1 M HCl to pH 2-4; filter, and load in ~4-4.5 mL aliquots (up to 20 mg total protein)
23. Run over HPLC, using a slow linear gradient from about 25-50% B then bump everything else off by going up to 100% B faster, hold there for a 10min or so to remove any contaminants, then re-equilibrate back down to 25% B (should elute around ~30-35% B). Method ~90min long
24. Freeze HPLC fractions and lyophilize
25. Store lyophilized protein in -80 °C until ready for cleavage (usually takes ~2-3 days to dry fully, depending on volume size)

USP2CC CLEAVAGE AND HPLC

1. Resuspend lyophilized protein in Uspcc cleavage buffer (20 mM Tris or HEPES, 200 mM NaCl)—be careful at this stage, some chemokines do not like to be resuspended in the presence of salt until they are more dilute
2. Cleave with 1:100 Usp2cc for ~3-4 h at RT, no need to rock/stir (take gel samples to monitor cleavage efficiency)
3. Cleanup cleavage reaction by running over Ni-NTA benchtop gravity column (use column devoted to Usp2cc cleanup for this application)
    a. Equilibrate column with 20 mM Tris, 300 mM NaCl, 40 mM Imidazole.
    b. Filter cleavage reaction and load onto Ni column
    c. Collect flow through (should contain ITAC)
    d. Wash with 1CV of 20mM Tris, 300mM NaCl, 40mM Imidazole, collect
    e. Elute Ub with 20mM Tris 300mM NaCl, 250mM Imidazole
    f. Strip and regenerate Ni column, store in 20% EtOH

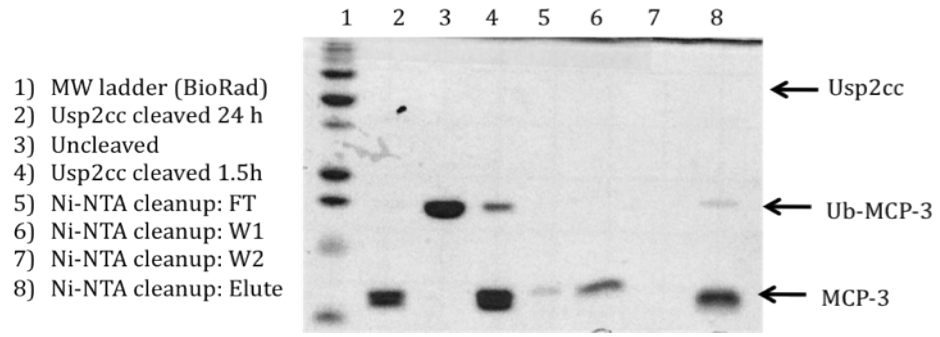

4. Concentrate the FT with a 3K MWCO spin filter at 4 °C until volume is appropriate to load on to HPLC
5. Acidify HPLC load with 1 M HCl to pH 2-4; filter, and load in ~4 mL aliquots (up to 20 mg total protein)
6. Run over HPLC, using a slow linear gradient from about 25-50% B then bump everything else off by going up to 100% B faster, hold there for a 10min or so to remove any contaminants, then re-equilibrate back down to 25% B (should elute around ~30-35% B). Method ~90min long
7. Freeze HPLC fractions and lyophilize
8. Store lyophilized protein in -80 °C until ready for use
9. Validate purity by gel and ESI-MS (ESI-MS only necessary the first time you do this)

HPLC chromatograms at 220 and 280 nM monitoring elution of Usp2cc treated MCP-3 from semi-prep C18 column. Sometimes see contamination of Ub in HPLC run, but, so long as column is not overloaded, it can be separated. Note Ub has high 220nm signal but very low 280nm signal:

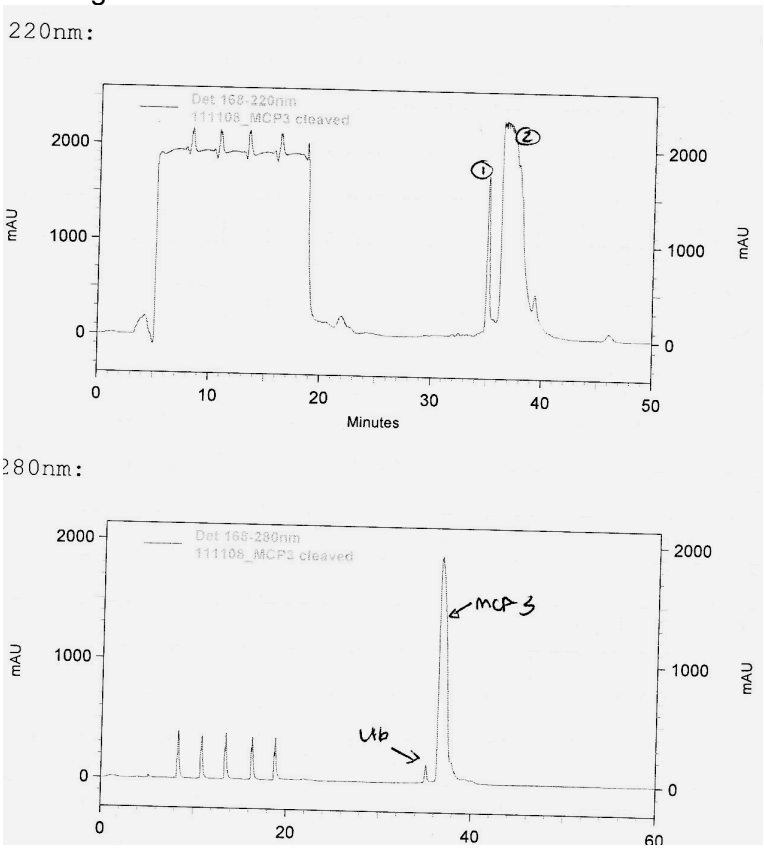

B: MCP-1/CCL2 Purification

NOTE: Protocol same as ITAC purification (see Protocol L)

pCEV37 MCP-1 (3D3-Ub)
MGSSHHHHHHHHHQLFVKTLTGKTITLELEPSDTVENVKAKIQDKEGIPPDQQRLIFAGK
QLEDGRTLSDYNIQKESTLHLVLRLRGGQPDAINAPVTCCYNFTNRKISVQRLASYRRIT
SSKCPKEAVIFKTIVAKEICADPKQKWVQDSIDHLDKQTQTPKT

Ub (3D3) MCP-1
MW: 18538.4
Ex. Coeff: 10220

MCP-1
MW: 8685
Ex. Coeff: 8730

GROWTH:

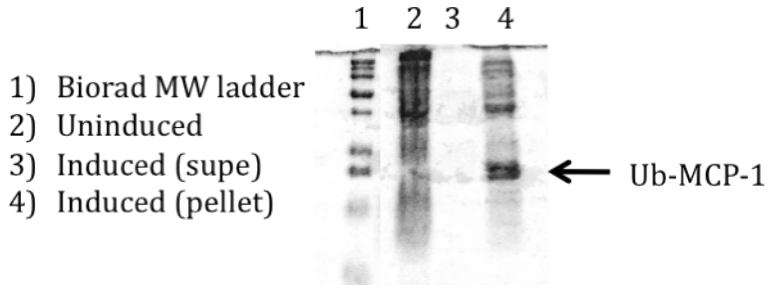

USP2CC CLEAVAGE AND NI CLEANUP:

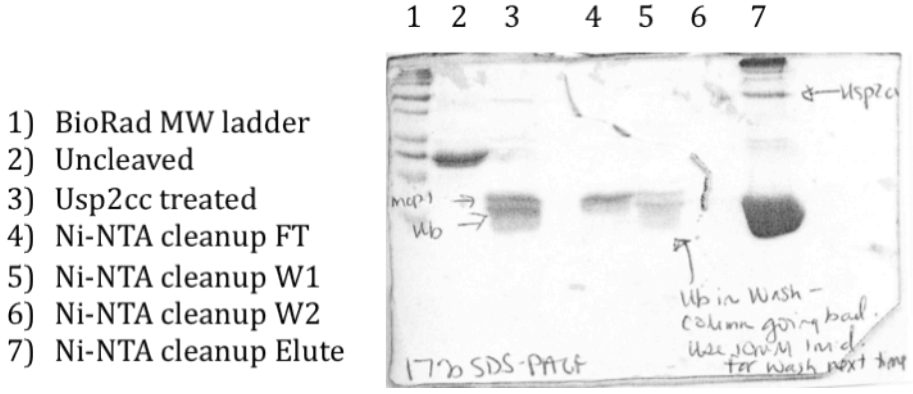

HPLC PURIFICATION

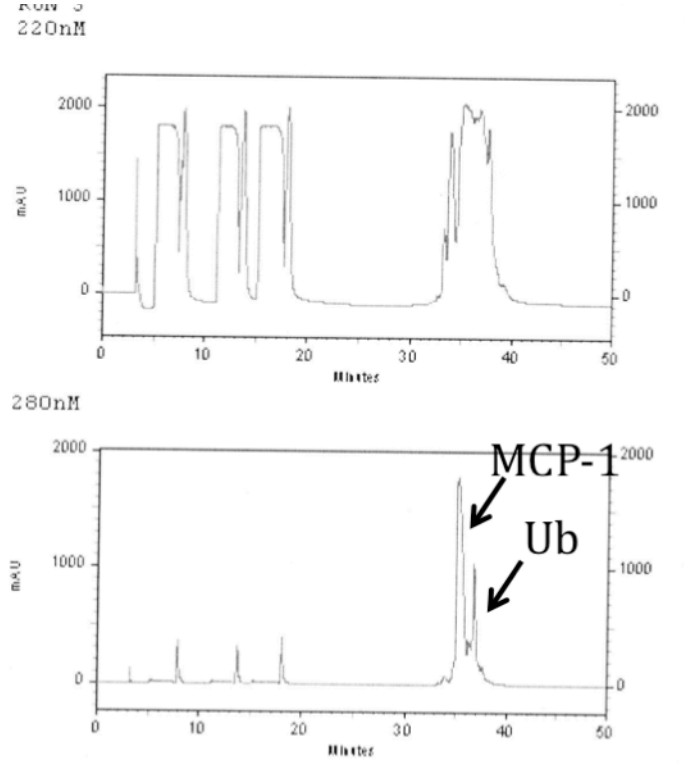

C: Maintenance and Electroporation of L1.2 Cells

(Original protocol from Etienne Danis, Yang Lab, UCSD)

L1.2 media:

RPMI 1640 + Glutamax
+ 10% FBS
+ 1% non-essential amino acids
+ 1% Na-pyruvate
+ 0.1% BME
+ 0.7 mg/mL G418 (for transfected cells)

Propagation:

Maintain at 0.5 – 4 x 10^6 cells/mL in T-25 flask (8-10 mL total volume); spin down cells at 250xg, resuspend in fresh media and place in new flask

Freezing down:

Freezing media: 90% FBS/ 10% DMSO

Prepare stocks of 1 x 10^7 cells per vial (1 mL of freezing media)

Electroporation:

1. Prewarm recovery media (RPMI + 10%FBS, 1% Na-pyruvate, 1% non-essential amino acids, 0.1% BME). Need 25 mL/electroporation.
2. Pellet 10 x 10^6 cells, 250xg, RT
3. Wash cells with PBS and repellet, 250xg, RT
4. Resuspend to 500µLwith PBS and add to individually wrapped, sterile 4 mm electroporation cuvette (yellow top, BTX, #45-0126)
5. Add 10 µg of DNA in water (or TE) to the L1.2 cells
6. Incubate at RT for 10 min swirling gently every few minutes
7. Place electroporation cuvette into electroporator device
8. Settings:
    a. 1150 µF
    b. Low resistance (25 Ω)
    c. 280 V
9. Quickly place cells in 25 mL of recovery media in T25 flask using pipettor that comes with cuvette (NOTE: some stringy cells, this is normal)

10. Incubate for 2-3 days, check viability (viability should still be ~98% +
11. After 2-3 days, spin down and bring cells up in selection media, make sure to monitor viability for ~1 week to ensure selection
12. Allow to grow ~1-2 weeks, freeze down stock of bulk electroporated L1.2s
13. Select/ screen for high expressers by limiting dilution or FACS sorting; test expression by flow cytometry

D: In Vitro Heparin Binding Assays

Protein Preparation:

1. Resuspend lyophilized protein (or thaw resuspended protein on ice) with 50 mM Tris, pH 8 (usually ~100-500 µL of buffer depending on amount of starting material)
2. Take A280, dilute close to 1 mg/mL
3. pH to 7.2 with 1M HCl
4. Take A280
5. Dilute to 1 mg/mL
6. Divide into aliquots (need 50µL/run so add enough to do in triplicates, ~180 µL is good)
7. Store aliquots at -80°C

Heparin Binding Assay:

Columns
HiTrap heparin HP (GE healthcare, cat # 17-0406-01), 1 mL column
Max pressure= 0.3 mPa
Flow Rate= 0.5-1 mL/min

SP Sepharose Column (GE healthcare, cat# 17-1151-01), 1 mL column
Max pressure= 0.3 mPa
Flow Rate= 0.5-1 mL/min

Buffers
A: 10 mM NaPhos, pH 7
B: 10 mM NaPhos, 2 M NaCl, pH 7

*For 0.1 M NaPhos Buffer, pH 7—combine 57.7 mL of 1 M Na_2HPO_4 with 42.3 mL of 1 M NaH_2PO_4 and bring up to 1 L, pH to 7

1. Columns stored in EtOH, so clean with water at 0.5mL/min for several column volumes into reach baseline absorbance
2. Equilibrate with Buffer A ~5 CV, until get good baseline
3. Attach 0.5 mL loop, clean with water and buffer
4. Prepare Protein sample
    a. Combine 50 ug (=50µL) of protein with 350 µL of 10 mM NaPhos Buffer, pH 7
5. Run Sample

    a. Method= “heparin 1 mL 30 mL wash”
6. Do in triplicate (should be +/- 0.1-0.2%) (Note—clean loop and needle between different mutants assayed)
7. Repeat with SP column

E: Calcium Flux Analysis

(Original protocol from Etienne Danis, Yang Lab, UCSD)

Volumes used: 100 µL cells (200,000 cells) + 100 µL calcium 4 dye + 50 µL ligand.

Reagents:

Calcium 4 assay kit (Molecular Devices, #R8142)
Assay buffer: 1x Hanks Balanced salt solution, 20mM HEPES, pH 7.4, 0.1% BSA
Assay plates: Biocoat 96-well plate (BD, #356640)
Compound/ligand plates: 0.3 mL v-bottom 96-well (Costar, #3357)
FACS Buffer (0.5 % BSA in PBS)

Ligand plate

1. Reconstitute ligand at a high concentration in PBS, Tris/HEPES buffer or MQ H_20 and measure concentration.
2. Dilute down to highest starting concentration in PBS and add to 300µL v-bottom assay plate (decreasing concentrations going down the plate). To begin, try 1:4 dilutions, adding 187.5 µL PBS + 62.5 µL of ligand (from above well) to each well. Using these volumes, you will need 1 column of ligand for each set of triplicate experiments.
    a. EXAMPLE: For top lane (A) to get final volume of ligand at 2 uM → A1 gets 50 µL of 10 uM ligand + 200 µL water to get final concentration of 2uM. Remaining wells are diluted as follows: 62.5 µL of ligand + 187.5 µL PBS.

NOTE: ligand plate is delivered column by column; so set up ligand and receptor plate accordingly

Receptor plate

1. Lift cells with 5 mL PBS with 1mM EDTA, incubate at 37 °C for ~20 min
2. Harvest cells and wash plates with an additional 5 mL of PBS
3. Count cells on ViCell
4. Spin at 250xg, 10min, 4 °C
5. Wash cells twice with FACS buffer
6. Resuspended cells to 2 x 10^6 cells/mL using assay buffer. (About 12 mL of cells is required per 96-well plate or 3 mL of cells for 3 lanes,)

7. Add 100 µL of cells to each well in a 96-well biocoat plate (being careful not to expel completely and create bubbles).
8. Prepare calcium 4 dye (Explorer format) in 10 mL assay buffer. Make sure it all goes into solution by pipetting up and down several times, don't shake! One vial of dye is sufficient for ~ 1 plate.
9. Carefully add 100 µL of dye to cells, trying not to disturb the cells (being careful not to expel completely and create bubbles).
10. Spin plate down for 6 min at 250xg (remember to turn down rates of acceleration/deceleration).
11. Check homogeneity of cells by microscopy and place in 37 °C incubator for 1.5 hr before measuring.
12. Read plate on Flexstation using Ca flux protocol
    a. Excitation at 485 nm, emission at 525 nm
    b. 150s read
    c. 50 µL of compound is added to 200 µL of assay plate (NOTE: if having issues with cells blowing off bottom of plate, see sharp negative dip in trace, then decrease the pipette volume height to less, e.g. 180 µL)
13. Save file once run is complete
14. Export and analyze using Excel

F: Bare-filter Chemotaxis Assays

(Original protocol from Etienne Danis, Yang Lab, UCSD)

Reagents:

24-well transwell plates, 5 μm pore size (Costar, #3421)
Chemokine (at least 100 μM concentration)
Receptor expressing cells (Induced with 1 mM Na-Butryate 12 h prior to expt)
Pre-warmed migration buffer (RPMI-10% FBS)

MCP-3 Migration Assay Protocol

1. Resuspend MCP-3 in PBS and adjust concentration to 100 uM

2. Aliquot some RPMI into a 50 mL conical for use in ligand plate dilutions

3. Prepare ligand plate using the 24 well plates. The total volume of media in the bottom of the wells needs to be 600uL. Prepare wells in duplicates or triplicates

Dilution in the well	**Volume of MCP-3 (Mi)**	**Volume of media**
No chemokine	0	600 uL
10 pM	6 uL (0.001uM stock)	594 uL
100 pM	6 uL (0.01 uM stock)	594 uL
500 pM	30 uL (0.01 uM stock)	570 uL
1 nM	6 uL (0.1 uM stock)	594 uL
5 nM	30 uL (0.1 uM stock)	570 uL
10 nM	6 uL (1uM stock)	594 uL
20 nM	12 uL (1 uM stock)	588 uL
50 nM	30 uL (1uM stock)	570 uL
100 nM	6 uL (10 uM stock)	594 uL
200 nM	12 uL (10uM stock)	588 uL
500 nM	6 uL (50 uM stock)	594 uL
1 uM	12 uL (50 uM stock)	588 uL

**Dilution of chemokines example (will vary depending on concentrations and number of replicates used)*
- For all chemokines (need 6 wells worth for each conc):

stock conc	Initial Conc	Volume to add	Final Conc	Final Volume	Volume to add of PBS
50 uM	100 uM	40 uL	50 uM	80 uL	40 uL
10 uM	50 uM	32 uL	10 uM	160 uL	128 uL
1 uM	10uM	36uL	1 uM	362 uL	326 uL

4. Prepare L1.2 CCR2 cells at 2.5 x 10^6 cells/mL in RPMI

5. Move filters to the wells containing media + chemokine
6. Add 100 µL of cells at 5 x 10^6 cells/mL in RPMI (negative control = no chemokine; positive control = cells directly into well w/ no chemokine present)
7. Incubate at 37 °C for 2 hours
8. Transfer the media in the bottom of each well to a small flow cytometry tube.
9. Count the number of events in 30 s (start with positive control to adjust settings, then process actual control

Example of Plate Setup:

0	0	0	no filter	no filter	no filter
10 6uL(1uM) **594uL**	20 12uL(1uM) **588uL**	50 30uL (1uM) **570uL**	100 6 uL (10uM) **594uL**	200 12uL (10uM) **588uL**	500 6uL (50uM) **594uL**
10 6uL(1uM) **594uL**	20 12uL(1uM) **588uL**	50 30uL (1uM) **570uL**	100 6 uL (10uM) **594uL**	200 12uL (10uM) **588uL**	500 6uL (50uM) **594uL**
10 6uL(1uM) **594uL**	20 12uL(1uM) **588uL**	50 30uL (1uM) **570uL**	100 6 uL (10uM) **594uL**	200 12uL (10uM) **588uL**	500 6uL (50uM) **594uL**

G: Preparing Cap-LC Columns

MATERIALS:

Deactivated fused silica .100mm X10m, Agilent P/N 160-2635-10, go to http://www.chem.agilent.com/scripts/Pcol.asp?lPage=2672, select Column Accessories, then Fused Silica (there is no direct link)

Column Packing Material Magic 5u 300A C18 (.50gm), Michrom Bioresources P/N PM5/66300/00**, http://www.michrom.com/catalog/index.php?cPath=22_124**

Ceramic scribe column cutter, Agilent # 5181-8836

PROTOCOL:

1. On bench, measure and mark cut length desired
    a. Suggested length- 17 cm per column
    b. For 17 cm column, cut 34 cm to make 2 columns
2. Pull out some of fused silica (be careful to only unravel a bit at a time) and measure to desired length, cut with ceramic scribe (pyromicro tecnolologies)
    a. To cut with scribe, press material into finger while passing scribe in other hand at 45deg angle over material. Adjust pressure/speed as necessary to scratch the top coating and gently tap off with finger. Don't try to cut with scribe. Should yield smooth straight edge with no jagged edges (look under microscope if necessary). Cut back further, if necessary, to obtain smooth edge.
    b. Fused silica comes in a 10 m pack – should yield approx. 60 columns (30 pieces to cut)
3. Once all pieces are cut to length, mark the middle point with black marker
4. Remove top coating of fused silica at middle point, to length of ~1 in. by *briefly* passing over medium, above blue flame
    a. Will see very brief spark of yellow/red
    b. Avoid keeping on flame for too long—don't want silica to bend or break
5. Wipe clean burned off coating with kimwipe and MeOH
    a. May need to work back/forth with kimwipe to remove all the black bits
6. ----------
7. Pull column (Tsien lab- Larry Gross) in Urey Hall, 2nd floor.
8. Use Sutter Instrument Co. Model P-2000 laser puller.
9. Turn on LHS
10. Enter in program 53 for pulling the CapLC columns:

a. Heat 330 vel 45 125pUL
b. Heat 325 vel 45 125pUL

11. Place clear region of column into the center section. Starting with left side, place the column into the grooves and hold into place with fingers, then tighten the knob to secure. Slide toward the center, then, while holding the two knobs to secure, adjust the right side of the column into the grooves. Press firmly and tighten the right knob.
12. Lower the shield and press “Pull”.
    a. Should see the light flash 2-3 times and then pull the column apart
    b. If the light stays on or flashes more than 3x, then it is not properly aligned, so press stop and try readjusting
    c. Unscrew the pulled columns and carefully store so the tips don’t break.
    d. Turn off the machine and cover.

---

13. Prepare packing material: place small spatula tip full of resin into 1.5 mL eppi; fill with ~0.5 mL MeOH to get resin suspension
14. Let resin equilibrate in MeOH for ~1 h or so prior to packing the columns
15. Use packing vessel to pack C18 resin into pulled column
    a. Use goggles to protect eyes when packing (columns can shoot out of vessel)
    b. Place open eppi with resin into center hole of vessel (may need to place something underneath to elevate to appropriate height)
    c. Screw top of vessel into place
    d. Tighten bolts
    e. Place column into vessel, pulled side up, and tighten screw around column so doesn’t fly away when pressure is applied
    f. Push column down until column bottom touches bottom of eppi
    g. Make sure both right hand (RH) and left hand (LH) valve are closed, then open main tank valve to pressure of ~600 psi
    h. Now open LH valve but keep RH valve closed
    i. Ensure that slow drip of liquid is coming out from top of column
        i. If not, hold scribe at 45deg angle and make upward sweeping motion against very top of tip...if cut, should begin to see flow

j. Begin moving column up and down in packing vessel to help mix resin (settles over time). To do this, hold column firmly with one hand while loosening screw around column with other. Lift up/down.
k. Should only take a few minutes to pack 17 cm column, check progress of the resin moving up the column
l. Let column pack further in vapor phase for ~15-20 min (this prevents loss of material out the end of the column)
m. To remove column: close LH valve and open RH valve (should vent).
n. Hold column up to light against an unpacked column, move around until you can detect a difference between the two
    i. Packed column= glowing
    ii. Not-packed= dark

16. Store columns flat until ready for use

H: Using InsPeCT

1. Connect to LTQ-MS in PSB basement by opening “My network places” on office computer (Blackdog)
   Network to access data from the MS computer downstairs:
   ftp://137.110.133.238
   Login as Guest
   Password: 9a37F_Sm

   NOTE: In order to look at the raw data with the qual browser and in order to generate the mzxml data, must have XCalibur installed on computer
   Once XCalibur software is copied into the Inspect folder, then register the following files:
   Using the command prompt, go into the Inspect folder and XCalibur subfolder→ System→programs
   Then to register type: regsvr32 XRawfile.ocx
   regsvr32 XRawfile2.dll
2. Copy .RAW files to Inspect folder on lab computer
3. Convert files to python script that is Inspect compatible (.mzXML) (note: can begin typing and select tab, will bring up correct file name...)
   a. Go to “Run” → cmd → Enter
   b. Type “cd My documents”→ enter →..... enter →“cd Inspect” (use “cd” command to change directory to until you reach the subfolder Inspect is in)
   c. Type ReadW.exe <raw file path> <c/p> → Enter
      i. Select “c” = centroid profile
   d. Generates 3 files in Inspect folder. One is mzXML, and then two other formats of it. Use the mzXML file created.
4. Prepare normal and shuffled databases (e.g. human uniprot database designated “protein.trie”, contaminants database).
   a. Preparing a shuffle database: >python ShuffleDB.py –r Database\(database to shuffle.trie – so protein.trie in this case) –w Database\(name – humanshuffleDB.RS.trie)

i. Need to then copy this generated Shuffle database into the main Inspect directory as well so it can be located

b. Creating a new database:
   i. Download database from website (e.g. Uniprot download page)
   ii. Select the .FASTA folder to download
   iii. Copy .FASTA file into main inspect folder
   iv. In command prompt type: >python PrepDB.py FASTA "uniprot_sprot".fasta (this will create the .trie and .index files of the database that are necessary to have for inspect runs

5. Open input text file and fill out information according to each sample, save by "input_name_txt". Can adjust specifications for Inspect here, to have it run based on what you want to look for (e.g. PTM)
   a. Select databases: (for example, we used protein.trie, commoncontaminants.trie, shufflehumproteinDB.RS.trie)
   b. Account for phosphorylation modification (80) (e.g. mod,80,STY,opt,phosphorylation)
   c. Allow 1 modification per peptide
   d. Make sure to copy this input file into the main inspect folder.
6. In script line, type "inspect.exe -i input file name.txt –o output file name.txt"
   a. Press enter, will eventually read, initialization successful
7. Data Processing:
   a. Can open up the output file in excel to get an idea of how many peptides you have and their quality (should cleave before and after R or K) and # of phosphorylation events (look for +80 in peptide). xxx designates a "fake" sequence. For phospho-peptides, can go back and look at spectra to see if looks reasonable- look for strong phospho peak and neutral loss of 49 Da (for 2+ charge state- H_3PO_4)
8. Generate a summary file (NOTE: be sure Python v2.5 is installed):
   >python Summary.py –r outputfile.txt –d Database\protein.trie –w resultsname.html (may want to add folder for this in which case use –w Summary(folder name)\resultsname.html –v 1 –i .\ -p 0.99
   v indicates except anything for which there is 1 peptide, could make more stringent by using 2, so need to see 2 peptides for it to be considered a

result. –p is for the p-value and can also be changed. p 0.99 is not that significant of a p value, but it doesn't really mean that much with Inspect.

I: Maintenance of MDA-MB-231 Cells

Media: RPMI-1640 with Glutamax + 10% FBS

Selection Media for Neo^R, Puromycin^R, or Blasticidin^R transfected cells:
+ 5 ug/mL Puromycin
+ 5 ug/mL Blasticidin
+ 1mg/mL Geneticin (G418)

Propagation (for cells >70-75% confluent):

1. Aspirate media
2. Rinse with 5 mL of PBS, aspirate
3. Add 1 mL of Trypsin-EDTA to plate, rock to distribute evenly
4. Incubate plate at 37°C for 2-3 min or until cells have lifted
5. Add 4 mL of media to plate and resuspend cells evenly
6. Add 8 mL of media to new 10cm plate
7. Seed the new plate with an aliquot of the resuspension (e.g. 1:12 is usually good, so cells only need to be split once/week) *

* Change media on cells 3 x per week (M, W, F is good) until confluent again. Monitor number of passages.

Freezing Down:

Materials needed:

Freezing media: 90% FBS/ 10% DMSO
Labeled cryovials (include cell line, date, initials) with labeled cap insert
2 x 15 mL conical styrofoam racks

1. Expand confluent cells from a 10cm plate to a 15 cm plate (can also seed a new 10cm plate for propagation at this time)
2. Bring media up to ~40 mL on the 15 cm plate and grow to >70% confluency (1 x 15 cm plate = 5 LN2 stocks)
3. Rinse plate with PBS
4. Add 2 mL Trypsin-EDTA
5. Incubate at 37 °C until cells have lifted
6. Add 10 mL media to plate and resuspend cells evenly
7. Transfer cells to 15 mL conical and spin on low for several min to pellet

8. Meanwhile, prepare freezing media (or can do beforehand). For 1 x 15 cm plate, we prepare 6 mL of freezing media so there is a bit extra (can freeze extra at -20°C for later use, but avoid multiple freeze/thaws).
9. EtOH tube before bringing back into hood, aspirate media
10. Resuspend pellet in 5 mL of freezing media
11. Once evenly resuspended, distribute 1 mL of cell suspension into each cryovial
12. Place cryovials into 1 styrofoam rack; cover with an additional rack
13. Place at -80°C O/N (can be at -80°C for longer if necessary)
14. Transfer cells to LN_2 storage rack

J: Retroviral Transfection and Infection Procedure

(Original protocol from Dr. Jing Yang)

1. On the day before transfection, plate 1 x 10^6 HEK293T cells onto 6cm dishes in 4-5 ml DMEM/10%FBS. The cells are ready for transfection after 18-20 hours. For 10 cm dishes, double the quantities given here.
2. Pipette 6 μl TransIT-LT1 reagent into 150 μl serum-free medium, mix by gentle pipetting, incubate at room temperature for 10-20min. DO NOT TOUCH THE TUBE WITH UNDILUTED LT1.
3. Add 2 μg total DNA (in TE). For making VSV-G retroviruses by triple transfection use 0.9 μg gag/pol expression vector (use pUMCV3 for retrovirus and use pCMVΔ8.2R for lentivirus), 0.1 μg VSV-G expression vector, and 1 μg transfer vector. It is ok to add the plasmids separately.
4. Mix by gently pipetting
5. Incubate the LT1/Medium/DNA solution at Room Temperature for 30 min
6. Drip the mixture onto the HEK293T cells that were seeded the day before
7. Incubate the cells overnight at 37 °C

The day after transfection—

8. Change the transfected HEK293T media to 4-5 mL of fresh media
9. Seed targeting cells at 2-5 X 10^5 per 6cm plate. The next day, cells should be about 20% confluency and ready to be infected with the harvested viral supes.

48h post transfection—

10. Filter the viral supes from the HEK293T plates through 0.45um filter to get rid of floating HEK293T cells and put onto target cells. Add protamine sulfate at 6ug/ml (Sigma, #P3369, make protamine sulfate stock at 6mg/ml in PBS). After 4-6 hr infection, change to fresh media.

72h post transfection—

11. Repeat the infection as in step (10) using the 72h viral supe
12. Once the infected cells are confluent, cells can be expanded to a 10cm dish and proper drug will be added to select the resulting infected cells. Be sure to also seed a control plate of target cells not infected with viral supe and treat with selection media.

13. Once cells are selected, verify protein expression by flow cytometry or other means.

NOTES ON TransIT-LT1 REAGENT (Mirius, # MIR2305):

- Always make the reaction mix by first adding serum-free-media. It's ok to add the plasmids separately to the mix.
- The transfection efficiency with LT1 is comparable to that of Calcium Phosphate, but LT1 is not toxic to HEK293T cells.
- TransIT-LT1 is the same as Fugene6 from Roche, but cheaper.

K: CXCL12 Purification

pET21a (pMS2) His-CXCL12

MKKKHHHHHHHHHDDDDKPVS LSYRCPCRFF ESHVARANVK HLKILNTPNC ALQIVARLKNNNRQVCIDPK LKWIQEYLEK ALNK

His-tag CXCL12 (pre-enterokinase cleavage)
MW: 10036.6
Ex. Coeff: 8480

CXCL12 (enterokinase cleaved)
MW: 7963.4 (reduced), 7959.4 (oxidized)
Ex. Coeff: 8480 (reduced), 8730 (oxidized)

BUFFERS:

Inclusion Body Resuspension Buffer:
(store at 4°C)

10 mM Tris 8.0
1 mM $MgCl_2$ (add fresh)
200 µg of DNAse (add fresh)
Complete protease inhibitor tablet (Roche, 1 tablet/50mL)

Tetsuya's:
10 mM Tris 8.0
200 µg of DNAse (add fresh)

"Spin Purifying Buffer":
(Store at 4°C)

10 mM Tris pH 8
0.25% deoxycholate

(Before use add: Protease Inhibitor Tablets 1 per 50 ml, stable for 1-2 weeks at 4°C)

Ni-NTA Buffers:

Buffer A (equilibration and wash 1):
10 mM Tris
100 mM NaPhos
6 M GuHCl
pH 8

Buffer B (elution):
10 mM Tris
100 mM NaPhos
6 M GuHCl

pH 4
Tetsuya's :
Buffer A (equilibration and wash 1):
10 mM Tris
6 M GuHCl
4mM DTT
pH 8

Buffer B (elution):
10 mM Tris
6 M GuHCl
4mM DTT
pH 4

Fold It Buffer #8:
Sterile filter and store at 4°C

55 mM MES pH 6.5
264 mM NaCl, 11 mM KCl
0.055% PEG 3350
1.1 mM EDTA
550 mM L-arginine-HCl

Add fresh:
1 mM GSH
0.1 mM GSSG
0.3 mM lauryl maltoside

Note: Tetsuya found that the above refolding conditions take ~3 days to get complete refolding based on analytical column, so he used modified conditions and refold at room temp- only takes 30 min-1 h (or O/N at 4°C)

Revised Fold-It buffer:
50 mM Tris
1 mM EDTA
Arginine-HCl
pH 7.5-8
No NaCl, no KCl, no PEG…

Add fresh:
1 mM GSSG

Dialysis Buffer:

20 mM Tris pH 8.0
50 mM NaCl
2 mM $CaCl_2$

HPLC Buffers:
A: 0.1% TFA
B: 90% acetonitrile, 0.1% TFA

DAY 1: TRANSFORMATION

1. Transform BL21(DE3)pLysS Cells with 1 µL of plasmid. Plate 200 µL on LB/Carb plates

2. Prepare 6 x 5 mL cultures, 3 x 100 mL and 6 x 1 L cultures for the next day with LB+100 µg/ml Carb (1:1000 dilution).

DAY 2: GROWTH

10. Inoculate each of the 5 mL cultures with a swipe of colonies from the plate, shake at 37 °C
11. ~1h-1.5 later, pool 5 mL cultures and evenly divide to inoculate into 3 x 100 mL cultures
12. ~1-1.5h later, pool the cultures and inoculate 1L cultures (prewarmed)
13. Take timepoints (doubles every 20min), monitor growth by A600
14. Induce with 0.5 mM IPTG (0.5 mL of 1 M stock) when OD reaches ~0.6-0.7
15. Harvest after ~3-4 h of growth
16. Spin down pellets at 5.5k rpm, 15 min, 4°C
17. Resuspend in ~50 mL of Resuspension buffer (for 6 L culture)
18. Divide into 2 x 50 mL conicals, store at -80°C

DAY 3: INITIAL PURIFICATION

19. Thaw the cells by placing conicals in H_2O on ice
20. Pour thawed cells into small metal sonication cup, bring volume up to ~100 mL with resuspension buffer
21. Lyse cells by sonication on ice: 4 x 30s (with 3s on, 2s off, speed 8) resting in between cycles for ~1 min
22. Add Triton-X to a final concentration of 0.1% and incubate for 15 minutes on gel shaker at room temperature or add stir bar to the metal cup and stir for 15 min. To

mix the triton-X completely in, you may have to add drop by drop or sonicate to mix 1X by 30 sec pulse.

23. Distribute into centrifuge tubes and spin lysate for 15 min in the Beckman JA25.5 rotor at 15,000 rpm, 4 °C
24. Resuspend the pellet in ~100 mL of “Spin-purifying Buffer”. Sonicate and spin as above repeatedly until supernatant is clear (~3-4 times).
25. Solubilize Pellet in ~20 mL of “Buffer A” (see above) using a Dounce homogenizer. Spin as in step 14 to remove insoluble particles. Filter supe through a 0.22 uM PVDF filter (Millipore durapore membrane).
26. Purify over benchtop Ni-NTA gravity column
    g. Use a 10-20 mL Ni-NTA Column re-equilibrated with 2 CV of Buffer A (above).
    h. Load protein onto the column with gravity flow (turns brown).
    i. Wash with 2 CV Buffer A
    j. Elute with Buffer B. Collect 2 mL fractions in glass tubes until brown color goes away (can spec A280 to ID fractions containing protein)—pool these together. Add to 1 mM DTT final concentration.
    At this point, the protein can be stored at 4°C (stable for several days in GuHCl)

DAY 4: PROTEIN REFOLDING

27. Treat with either 1mM DTT or 5 mM TCEP. Store at 4 °C O/N in reducing conditions before refolding.
28. Refold in 20 volumes of cold FoldIt Buffer #8 (e.g. for 50 mL of protein fractions, need ~1 L of buffer). Generally,for 1-3 L preps, refold into 500 mL, for 4-6 L preps, refold into 1 L. Remember to add Arginine-HCl, lauryl maltoside, GSH and GSSG fresh to the refolding buffer right before use. Note--Because of the ArgHCl, the buffer needs to be pH'd (6.5).
29. Dropwise add chemokine in GuHCl into the Hampton FoldIt #8 refolding buffer with stirring, and let sit overnight at 4°C with stirring.

DAY 5: DIALYSIS

30. Dialyze the protein into 20 mM Tris pH 8.0, 50 mM NaCl and 2 mM $CaCl_2$ using dialysis membranes (MWCO=3500). Can add ~100 mL of protein into each dialysis membrane, leave some air at top so it floats.
31. Dialyze twice against 100 X volume of protein (for 50 ml, dialyze 2 times in 5000 ml—one in the day and one overnight).
32. Filter the content of the dialysis bag with a millipore durapore membrane.
33. Concentrate the protein (using amicon Ultra-15 centrifugal filter devices, MWCO=5000). Concentrate to ~1 mg/ml for the following step (get volume down to about 15 mL from the ~280 mL after dialysis).
    k. Note:The filter devices take 15 ml at a time, spin for 40 min at 4°C at 5000rcf. Save retentate and discard the flow through.
34. Alternatively: concentrate protein after refolding in an Amicon concentrator (10kD YM10 membrane, 350 mL concentrator, 50psi; resistant to GuHCl) in delicase (4 °C) and dialyze against Dialyze against 3 L of 20 mM Tris pH 8.0, 50 mM NaCl, 2 mM $CaCl_2$ for 1 h at 4°C with stirring.

DAY 6: ENTEROKINASE CLEAVAGE

35. Concentrate chemokine to ~1 mg/mL concentration (A280 ~0.845). Determine concentration via absorbance readings.
36. Add enterokinase (NEB cat#P8070 or made in-house) to a ratio of 1:100,000 (molar ratio). Digest overnight at room temperature.
    l. For 1mg/mL protein concentration, add 0.25 µl of EK for every 100 µl of protein solution.

DAY 7: HPLC

37. Purify by RP-HPLC: acidify protein with 1 M HCL to a pH of 2.5-3.0. Filter with a syringe filter.
38. Load ~4 mL volumes of acidified, filtered protein onto C18 column by repeatedly filling (up to 20 mg total protein) under constant 2.5 ml/min flow rate in 25% buffer B/75% buffer A.
39. Run over HPLC, using a slow linear gradient over ~30 min from about 25-65% B then bump everything else off by going up to 100% B faster, hold there for a 10min

or so to remove any contaminants, then re-equilibrate back down to 25% B. Method altogether ~120min long

40. Freeze HPLC fractions and lyophilize

41. Store lyophilized protein in -80 °C until ready for use

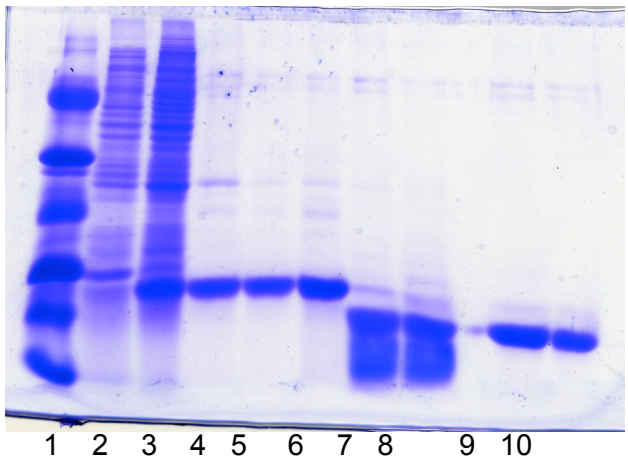

K.1 Coomassie stained gel of sample aliquots throughout the CXCL12 purification process. Lanes: 1) protein ladder 2) pre-induction 3) IPTG Induced 4) Ni-NTA purified 5) dialyzed 6) concentrated protein prior to EK cleavage 7&8) EK cleaved CXCL12 9&10) HPLC purified EK cleaved CXCL12. Sample aliquots were resuspended in Tris buffer: for OD of 0.5, use 50µL.

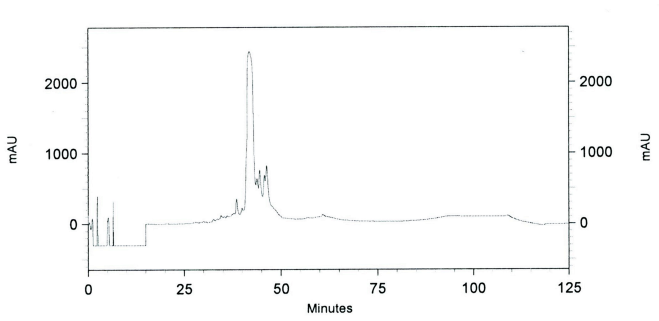

Run 3, 220 nm

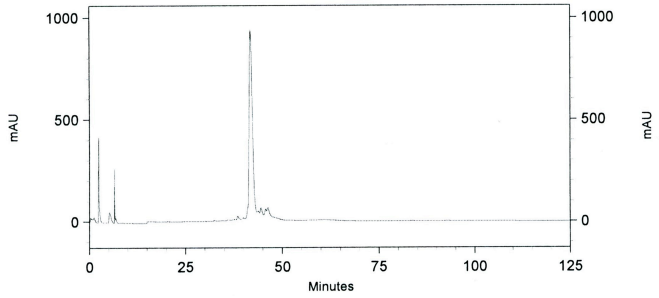

Run 3, 280 nm

K.2 HPLC trace of final CXCL12 purification. The A220 (top) and A280 (bottom) traces from the HPLC purification of CXCL12 are shown.

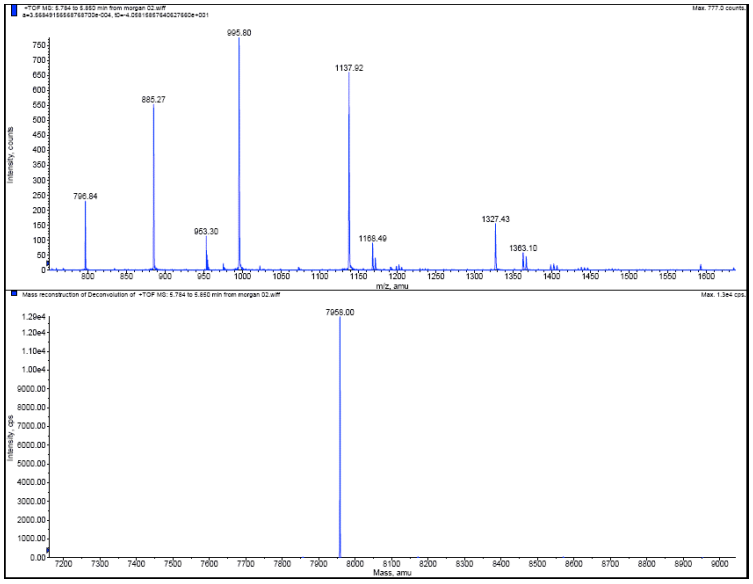

K.3 Mass spectrum of purified CXCL12.

L: ITAC Purification

pCEV33 ITAC (3D3-Ub)
MGSSHHHHHHHHQLFVKTLTGKTITLELEPSDTVENVKAKIQDKEGIPPDQQRLIFAGK
QLEDGRTLSDYNIQKESTLHLVLRLRGGFPMFKRGRCLCIGPGVKAVKVADIEKASIMY
PSNNCDKIEVIITLKENKGQRCLNPKSKQARLIIKKVERKNF

pCEV33 ITAC 4-73 (3D3-Ub)
MGSSHHHHHHHHQLFVKTLTGKTITLELEPSDTVENVKAKIQDKEGIPPDQQRLIFAGK
QLEDGRTLSDYNIQKESTLHLVLRLRGGFKRGRCLCIGPGVKAVKVADIEKASIMYPSN
NCDKIEVIITLKENKGQRCLNPKSKQARLIIKKVERKNF

Ub-ITAC
MW: 18182.1
Ex. Coeff: 3230

ITAC
MW: 8307
Ex. Coeff: 1740

Ub-ITAC 4-73
MW: 17806
Ex. Coeff: 3230

ITAC
MW: 7931
Ex. Coeff: 1740

BUFFERS:

Inclusion Body Resuspension Buffer:
(store at 4°C)

500 mL Stock *without* DNAse, $MgCl_2$:
50 mM Hepes pH 7.2
200 mM NaCl

(Before use add: a pinch of DNAse, 1µL 0.5M $MgCl_2$(10 uM final))

"Spin Purifying Buffer":
(Store at 4°C)

10 mM Tris pH 8
0.25% deoxycholate

(Before use add: Protease Inhibitor Tablets 1 per 50 ml, stable for 1-2 weeks at 4°C)

Ni-NTA Buffers:
Buffer A (equilibration and wash 1):
10 mM Tris
100 mM NaPhos
6 M GuHCl
pH 8

Buffer B (elution):
10 mM Tris
100 mM NaPhos
6 M GuHCl
pH 4

1L Hampton Foldit Buffer 13
(without Arg, reduced and oxidized Glutathione) (or make a 10X stock)
1X Stock:
55 mM Tris pH 8
264 mM NaCl
11 mM KCl
1.1 mM EDTA
Last minute add the following and re-pH because arginine drops the pH:
1 mM GSH
0.1 mM GSSG
550 mM Arginine HCl

DAY 1: TRANSFORMATION

1. Transform BL21(DE3)pLysS Cells with 1 µL of plasmid. Plate 200 µL on LB/Kan plates

2. Prepare 6 x 5 mL cultures, 3 x 100 mL and 6 x 1 L cultures for the next day with 30ug/ml Kan (1:1000 dilution).

DAY 2: GROWTH

42. Inoculate each of the 5 mL cultures with a swipe of colonies from the plate, shake at 37 °C
43. ~1h-1.5 later, pool 5 mL cultures and evenly divide to inoculate into 3 x 100 mL cultures
44. ~1-1.5h later, pool the cultures and inoculate 1L cultures (prewarmed)
45. Take timepoints (doubles every 20min), monitor growth by A600

46. Induce with 0.5 mM IPTG (0.5 mL of 1 M stock) when OD reaches ~0.7
47. Harvest after ~3-4 h of growth

48. Spin down pellets at 5.5k rpm, 15 min, 4°C
49. Resuspend in ~50 mL of Resuspension buffer (for 6 L culture)
50. Divide into 2 x 50 mL conicals, store at -80°C

DAY 3: INITIAL PURIFICATION

51. Thaw the cells by placing conicals in H_2O on ice
52. Pour thawed cells into small metal sonication cup, bring volume up to ~100-125 mL with resuspension buffer
53. Lyse cells by sonication on ice: 6 x 30s (with 3s on, 2s off) resting in between cycles for ~1 min
54. Distribute into centrifuge tubes and spin lysate for 30 min in the Beckman JA25.5 rotor at 18,000 rpm, 4 °C
55. Resuspend the pellet in ~100-150 mL of “Spin-purifying Buffer”. Sonicate and spin as above
56. Solubilize Pellet in ~20 mL of “Buffer A” (see above) using a Dounce homogenizer. Spin to remove insoluble particles. Filter supe through a 0.22 uM PVDF filter
57. Purify over benchtop Ni-NTA gravity column
    m. Use a 10-20 mL Ni-NTA Column re-equilibrated with 2 CV of Buffer A (above).
    n. Load protein onto the column with gravity flow (turns brownish).
    o. Wash with 2 CV Buffer A
    p. Elute with Buffer B. Collect 2 mL fractions in glass tubes until brown color goes away (can spec to ID fractions containing protein)—pool these together.

At this point, the protein can be stored at 4°C (stable for several days in GuHCl)

DAY 4: PROTEIN REFOLDING

58. Treat with either 1mM DTT or 5 mM TCEP. Store at 4 °C O/N in reducing conditions before refolding.
59. For 1-3 L preps, refold into 500 mL. For 4-6 L preps, refold into 1 L. Remember to add Arginine-HCl, GSH and GSSG fresh to the refolding buffer right before use. Note--Because of the ArgHCl, the buffer needs to be pH'd.
60. Dropwise add chemokine in GuHCl into the Hampton FoldIt #13 refolding buffer with stirring, and let sit overnight at 4°C with stirring.

DAY 5: CONCENTRATION/BUFFER EXCHANGE OF REFOLDED PROTEIN

61. Concentrate protein after refolding in an Amicon concentrator (10kD YM10 membrane, 350 mL concentrator, 50psi; resistant to GuHCl) in delicase (4 °C)

DAY 6: USP2CC CLEAVAGE AND HPLC

62. Dialyze against 3 L of 20 mM Tris, 200 mM NaCl (cleavage conditions) for 1 h at 4°C with stirring
63. Cleave with 1:100 Usp2cc for ~4 h at RT (Do see some ppt here form over time...could try to decrease cleavage time to reduce loss), no stirring
64. Cleanup cleavage reaction by running over Ni-NTA benchtop gravity column (use column devoted to Usp2-cc cleanup for this application)
    q. Equilibrate column with 20 mM Tris, 300 mM NaCl, 40 mM Imidazole.
    r. Filter cleavage reaction and load onto Ni column
    s. Collect flow through (should contain ITAC)
    t. Wash with 1CV of 20mM Tris, 300mM NaCl, 40mM Imidazole, collect
    u. Elute Ub with 20mM Tris 300mM NaCl, 250mM Imidazole
    v. Strip and regenerate Ni column, store in 20% EtOH

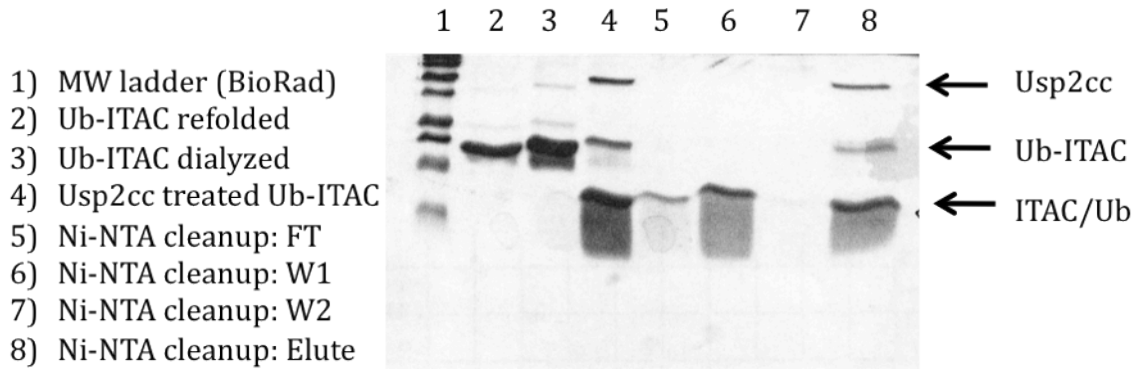

65. Concentrate the ITAC FT with a 3K MWCO spin filter at 4 °C until volume is appropriate to load on to HPLC

66. Acidify HPLC load with 1 M HCl to pH 2-4; filter, and load in ~4 mL aliquots (up to 20 mg total protein)

67. Run over HPLC, using a slow linear gradient from about 25-50% B then bump everything else off by going up to 100% B faster, hold there for a 10min or so to remove any contaminants, then re-equilibrate back down to 25% B (should elute around ~30-35% B). Method ~90min long

68. Freeze HPLC fractions and lyophilize

69. Store lyophilized protein in -80 °C until ready for use

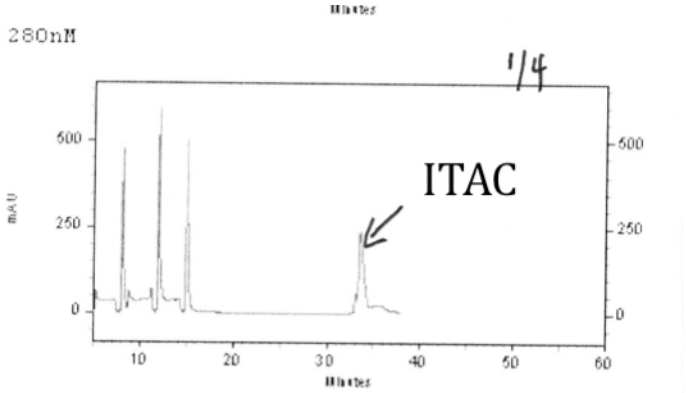

M: RNA Isolation and cDNA Synthesis

(Original protocol from Etienne Danis, Yang Lab, UCSD)

MATERIALS:

QIAshredder – Qiagen Cat. No. 79654 (for 50 units) or Cat. No. 79656 (for 250 units)
RNeasy Mini kit – Qiagen Cat. No. 74104 (for 50 units) or Cat. No. 74106 (for 250 units)
AllPrep DNA/RNA Mini kit – Qiagen Cat. No. 80204
β-mercaptoethanol/2-mercaptoethanol (RNA work only) – Sigma Cat. No. 60-24-2
Cell lifters – Sterile cell lifter from Corning/Costar Cat. No. 3008
Molecular Biology Grade (MG) Water – Cellgro 46-000-CM/CL
Ethanol (RNA work only, prepare 70% EtOH with MG Water) – Sigma E7023
RNase-free DNase set – Qiagen Cat. No. 79254
DNA/RNA LoBbind eppendorf tubes – Eppendorf 0.5 ml: 0030 108.035; 1.5 ml: 0030 108.051
High capacity cDNA reverse transcription kit – Applied Biosystems (1000 reactions) Part. No.: 4368813
*Use filter tips for pipetman in all steps of procedure

Cell lysis for RNA purification

PROTOCOL (based on using the Qiagen RNeasy mini kit):

1. Check availability for QIashredder columns, RLT lysis buffer, β -mercaptoethanol, cell lifters
2. Prepare the RLT lysis buffer + β-mercaptoethanol
    a. For $5x10^6$-$1x10^7$ cells, a 6-cm or a 10-cm plate: add 600 µL of RLT buffer
    b. For $<5x10^6$ cells or 6-well plates: use 350 µL of RLT buffer
    c. For each mL of RLT lysis buffer: add 10 µL of β -mercaptoethanol.
    d. Note: if using the AllPrep kit for DNA and RNA isolation, use the modified RLT Plus lysis buffer and add 10 µL of β –mercaptoethanol per 1 mL as above
3. Label QIashredder columns, one for each sample
4. Take plates containing cells at 80-90% of confluence from incubator and remove medium by aspiration or spin down appropriate number of suspension cells at 250 x g for 10 min and aspirate
5. Add directly RLT lysis buffer (600 µL or 350 µL) containing β -mercaptoethanol on the cells
6. Tilt the plate to make the RLT lysis buffer cover all the cells
7. Scrape the cells with a sterile disposable cell lifter, one new for each sample

8. Collect lysed cells with a Pipetman and a 1000-mL filter tip
9. Transfer the lysate in the QIashredder column to homogenize the lysate
10. Centrifuge at maximum speed (~14,000 g) and RT in a benchtop centrifuge machine for 2 min
11. Remove the column from the 2mL tube (discard column) and put a cap on the tube
12. Proceed to RNA purification step or put the tubes at -80^{o}C until later the next step, the RNA purification

RNA Purification Protocol

13. Put tubes containing cell lysates in Buffer RLT from -80°C to **37°C** for **~5-10 min**
14. Add **350 or 600 µL 70% Ethanol** (equal volume to QIAshredded lysate) , mix gently by pipetting
15. Put up to **750 µL** of this mix into the column
16. Centrifuge for **15 s at >10,000 g**, discard FT
17. If necessary, put the remaining mix on the corresponding column and centrifuge again for **15 s at >10,000 g**, discard FT
18. Add **350 µL Buffer RW1** into column
19. Centrifuge for 15 s at 10,000 g, discard FT
20. Add **80 µL DNaseI - Buffer RDD mix**
    a. Stock Solution of RNase-free DNase I: Add 550 µL RNase-free water to the lyophilized DNaseI (RNAse free), mix by inversion. Aliquot 50 µL into small epper tubes and store at -20^{o}C
    b. For each sample, add 10 µL DNase I stock solution to 70 µL Buffer RDD
    c. Mix gently and keep on ice
21. Incubate at **RT for 30 min**
22. Add directly **350 µL Buffer RW1** into the column
23. Centrifuge for 15 s at 10,000 g, discard FT
24. Tranfer column into a new 2 mL collection tube (supplied)
25. Add **500 µL Buffer RPE** into column
26. Centrifuge for 15 s at 10,000 g, discard FT
27. Add another **500 µL Buffer RPE**
28. Centrifuge for **2 min** at 10,000 g, discard FT
29. Transfer column into a new 1.5 mL collection tube (not supplied) (cap removed)

30. Centrifuge for **1 min at maximum speed**, discard FT
31. Transfer column to a new 1.5 mL collection tube (not supplied) (cap removed)
32. Add **directly 30 µL RNase free water on membrane**
33. **Incubate 5 min at RT**
34. Centrifuge for **1 min at 13,000 g to elute**
35. Quantification with nanophotometer using filter tips. A260/280 should be ~2
36. Store in -80°C or proceed to reverse transcription reaction

Reverse transcription protocol

37. cDNA synthesis with the ABI RT kit (without RNasin)

cDNA synthesis with the ABI RT kit (without RNasin)- 2x Master Mix		
10X RT buffer	2	µL
25X dNTP (100 mM)	0.8	µL
10X Random Primers	2	µL
MultiScribe Reverse Transcriptase (50 U/µL**)**	1	µL
RNase free H_2O	4.2	µL
2X RT Mix	**10**	**µL**
1 or 2 µg RNA plus RNase free H_2O to 10 µL	**10**	**µL**
Total reaction volume	20	µL

38. Mix well by pipetting up and down (no vortex!) and keep on ice
39. Set up thermal cycle run:

Thermal cycle run in the PCR machine
25°C for 10 min
37°C for 120 min
85°C for 5 min
4°C hold

40. Determine by standard curve the appropriate dilutions of cDNA to be in linear range. In general, for the 2 µg adding ~180 µL H_2O to reach 200 µL of final cDNA and use 4 µL of cDNA per real-time PCR reaction is in the linear range.
41. "-RT" cDNA synthesis without reverse transcriptase should be performed as a control for genomic DNA contamination the first time the RNA is used.

N: Quantitative Real-time PCR

(Original protocol from Etienne Danis, Yang Lab, UCSD)

MATERIALS:

Power Sybr Green 2 X Master Mix – Applied Biosystems Cat. No 4367659
Molecular Biology Grade (MG) Water – Cellgro 46-000-CM/CL
RT PCR plates – Applied Biosystems 4346906
Plate Cover strip – Applied Biosystems 4311971
Filter tips

REAL TIME PCR PROTOCOL NOTES:
Protocol for Applied Biosystems 7500 Fast

- Use specific plates from Applied biosystems
- Set up samples in either duplicate or triplicate
- Always have a GAPDH control for each sample
- Have a non-template water control for each set of primers (tells you if there is any contamination in the water)
- Use filter tips on pipetman for all procedures, ethanol down bench before use, and prepare on RNA bench with pipetman, etc. for RNA work only
- Can prepare plate with template and mix ahead of time, sequence not important
- Contents of wells should be stable O/N at 4°C
- The necessity for samples to be prepared on ice is primer dependent, in most cases, ok to be prepared at RT but to be safe **prepare on ice**
- ABI recommends 50 µL volume, but 10 µL volume using a master mix is also reproducible
- Melting curve is found under “dissociation curve” results—want a single peak, if you see multiple, could be a result of primer-dimers, non-specific binding to dsDNA

COCKTAIL:

2 X Sybr Green Master Mix	5 µL
Primer Forward (5 µM)	0.4 µL
Primer Reverse (5 µM)	0.4 µL
RNAse free H_2O	0.2 µL
Mix per well to add	6 µL/well
Template	4 µL
TOTAL	10 µL

PROTOCOL:

Sample Preparation

1. Prepare primers, template, etc. at correct concentrations using molecular grade water for any dilutions. Note: if using primers for the first time, should set up a standard dilution curve to determine the linear range of cDNA amount to use
2. Add 6 µL of mix (including master mix, primers, and H_2O to each well)
3. Add DNA template to each well. For reproducible data, use new filter tip for every well even if using the same sample in triplicate
4. Start Real Time PCR machine for "pre-heating"
5. Cover plate with the adhesive covers being sure to align properly (cover all edges of circles surrounding wells—this will ensure that there are no leaks)
    a. Use plate film applicator to press film firmly over wells and around edges
6. Spin plate in benchtop centrifuge: 4000 rpm for 1-5 min (spin longer if there are persistent bubbles, best to eliminate them but should pop when the plate heats up anyway
7. Place plate in machine

Running Samples

8. Open Applied Biosystems 7500 Fast icon on desktop
9. Select "new document"
10. Select template: Use 2 Step RT protocol (from Yang Lab), in "Handel Lab" → "Rina_Morgan" → "Templates"
    a. PROGRAM:
        i. Activation of DNA polymerase — 10 min at 95°C
        ii. DNA Amplification (x 40) — 15 sec at 95°C; 1 min at 60°C
        iii. Melting Curve — 15 sec at 95°C; 1 min at 60°C; Increase gradually over 15 min to 95°C

11. Fill in well setup information; right click and select "well inspector":
    a. Name contents in each well

   b. Select what it is (e.g. U=unknown, S=standard, or NTC=non-template control)
   c. For wells being assayed: select by check marking with GAPDH-sybr (should see green square in specific wells on template)
   d. For wells that have nothing in them: uncheck (should not see green square in those wells—makes run faster)
12. Save as (be sure saved as an .sds file)
13. Start run (will want to save again, press “save and continue”)
14. Takes about 3 h to run
15. Turn off instrument after run (don’t keep on overnight)
16. Can keep plate O/N at 4°C
17. Can test amplification:
   a. Load on gel
   b. No need to stain (sybr green fluoresces under UV lamp)
   c. Should see single band

O: Compensation on Flow Cytometer

1. Open template (e.g. “GFP and CXCR4 and 7”) or generate new one in BD Cellquest Pro

   Example:

   a. Click icon to make Dot plot, click and drag onto template layout
      i. Should read SSC on y-axis and FSC on x-axis (Normal scale)
   b. Click icon to make Histogram plot, click and drag onto template layout
      i. Select Acquisition
      ii. Select FL-X for x-axis (log scale) and automatically should read counts on y-axis
      iii. Also make plot for Acquisition dot plot with FL-X on x-axis (log scale) and SSC on y-axis
2. Acquire → Connect to cytometer
3. Acquire → Acquisition and storage (To see # of events: Acquire → Counters)
   a. Make new folder for data, and select to collect data to this folder
4. Cytometer → Detectors and Amp (if needed: Cytometer → Compensation)
5. Cytometer → Instrument settings → Open old data point similar to what you’re analyzing now → Set → Done... make adjustments as you see fit using detectors and amps tool bar you already opened
6. Adjust compensation settings according to what you want, e.g. compensation between GFP (FL1) and PE fluorophore (FL2), using various population of cells that are either stained/unstained.

   EXAMPLE of populations and associated scatter profiles to adjust to:

   a. MDA non-GFP unstained (low FL1 and FL2)
   b. MDA-GFP (high FL2, low FL1)
   c. MDA-GFP, CXCR4 stained (high FL1 and FL2)
   d. MDA non GFP, CXCR4 stained (high FL1, low FL2)

P: Detecting Chemokine Receptor Expression by Flow Cytometry

Reagents:

0.5% BSA in PBS (FACS buffer)
2% formaldehyde in PBS
0.2% Tween in PBS

anti- hCXCR3-PE mAb, clone 49801 (R&D, #FAB160P)
anti- hCXCR4-PE mAb, clone 1D9 (BD, #551510)
anti- hCXCR7-APC mAb, clone 11G8 (R&D, #FAB4227A)

anti- $IgG2_A$ isotype control-PE (BD, #553930)
anti- IgG_1 isotype control- APC (R&D, IC002A)

Prepare Cells for flow of surface expression:

1. Rinse each plate of cells with 5 mL PBS once (tilt plates and remove any excess PBS)
2. Add 1.5 mL of 1 mM EDTA-PBS to each plate to lift cells, incubate at 37 °C for several minutes (~10-20 min depending on confluency; avoid leaving low density cells incubating with EDTA for too long)
3. Add lifted cells to 2 mL V-bottom centrifuge tube, place on ice
    - Add 8 mL media back to plate→ Discard if flow is ok, continue to passage if not (or expand if necessary)
4. Count cells on ViCell using 1:5 dilution (110 µL into 440 µL PBS)-
5. Resuspend cells in appropriate volume of FACS buffer to get 5 x 10^6 cells/mL
6. Add 100 µL or 50 µL aliquots of each population for the following samples to V-bottom 96 well plate:

For detection of intracellular receptor expression:

Cell Fixation

1. Aliquot 1 x 10^6 cells (200 µL of 5 x 10^6/mL stock) in FACs buffer to a new tube
2. Bring volume up to 875 µL with cold PBS
3. Add 125 µL of cold 2 % formaldehyde solution, vortex briefly immediately after adding

4. Incubate for 30 min at 4 °C
5. Centrifuge for 5 min at 250xg, remove supe

Cell Permeabilization

6. Resuspend pellet in 1 mL of 0.2% Tween in PBS
7. Incubate for 15 min in a 37 °C waterbath
8. Add 0.9 mL of PBS and spin for 5 min at 250xg
9. Remove supe and continue with staining. Resuspend in 125 µL.
10. Aliquot 50 µL of cells to each well for CXCR7 staining of permeabilized cells and 75µL for IgG controls

For both surface and permeabilized cells, stain as follows:
(Note: for each unique cell type, include an unstained and IgG isotype control)

Unstained

- Keep on ice until other samples are ready
- Transfer to small flow cytometry tubes in 400µL total volume FACS buffer

CXCR7 only (NOTE: CXCR3 staining same procedure)

- Add 10 µL CXCR7-APC 1° Ab
- Incubate on ice, covered for 20 min
- Wash 3 x with 250 µL FACS buffer: spin with MTP rotor 5 min, 250xg, 4 °C
- Resuspend in 400 µL of FACS buffer
- Transfer to small flow cytometry tubes

APC (CXCR7) Isotype control

- Add 10 µL of IgG-APC control
- Incubate on ice, covered for 20 min
- Wash 3 x with 250 µL FACS buffer: spin with MTP rotor, 5 min, 250xg, 4 °C
- Resuspend in 400 µL of FACS buffer
- Transfer to small flow cytometry tubes

CXCR4 only

- Add 1.5 µL CXCR4-PE 1° Ab
- Incubate on ice, covered for 20 min
- Wash 3 x with 250 µL FACS buffer: spin with MTP rotor 5 min, 250xg, 4 °C
- Resuspend in 400 µL of FACS buffer
- Transfer to small flow cytometry tubes

PE (CXCR4) Isotype control

- Add 1.5 µL of IgG-PE control
- Incubate on ice, covered for 20 min
- Wash 3 x with 250 µL FACS buffer: spin with MTP rotor, 5 min, 250xg, 4 °C
- Resuspend in 400 µL of FACS buffer
- Transfer to small flow cytometry tubes

Q: Mammary Fat Pad Injections

Reagents/Supplies:

Hamilton syringe (Hamilton, # 80530)
Kimwipes
Gloves
Styrofoam blocks wrapped in aluminum foil
Lab tape
Aliquoted matrigel (BD, #354234) (on ice)
Aliquoted cells (on ice)
Sterile PBS aliquoted for saline controls
Sterile PBS in 50mL conical (for cleaning hamilton syringe)
70% Ethanol 50mL conical (for cleaning hamilton syringe)
Waste receptacle
Pipettes to mix matrigel and cells (p20, p200) and filter tips
Ear punch
Ear punch code sheet
Shaver
Surgery tools (several pairs of scissors and forceps)
Autoclaved Q-tips (Puritan, #803-WC)
Autoclip kit (BD, #427638), includes autoclip applier, wound clips, and remover
Cauterizer (WPI, #500390) and replacement tips (WPI, #500396)
Spray 70% ethanol
Microwaveable heat pad (provided by vivarium)
Notebook, pen

Surgery Injection Protocol

Cell preparation:

1. Wash cells in 15 cm plates with 5-10 mL PBS
2. Lift with 3 mL of 1 mM EDTA. Add to ~11 mL of PBS in conical and mix.
3. Remove 550 µL for cell count.
4. Spin cells at 250xg for 5-10 minutes to pellet. Aspirate supe and resuspend appropriately as described in step 6.
5. Need to prepare 2 x 10^6 cells/injection for each population and prepare centrifuge tubes with enough for 2 mice + 1 extra injection (2 injections x 2x10^^{6} cells/fatpad x 2 mice + 2x10^^{6} extra cells)= 1x10^^{7} cells needed per tube. Make 3 tubes so have enough for the 5 mice (+1 extra). Resuspend all cells at 1x10^^{7} cells/mL and aliquot 1 mL to each of 2 centrifuge tubes for each population.

   Examples:

a. Mueller-GFP: 98.8% viability
    i. Volume: 10 mL
    ii. Count: 4.7 x 10^6 cells/mL
    iii. Total cells= 4.7x10^7 cells
    iv. Resuspended at 1.6x10^^{7} cells/mL= 2.93 mL and aliquot 1 mL into 2 tubes
    v. Spun down (250xg at 4°C for 10min).
    vi. Aspirate off the supe and resuspend each aliquot in 100µL total volume with PBS (so only added 50 µL PBS since cells take up so much volume)
    vii. Mix with 100 µL Matrigel right before injecting into mice

6. Bring above listed supplies to vivarium

Surgery procedures:

7. Gather a spare cage to put mice in for recovery from surgery.

    In the biosafety cabinet located in vivarium surgery room:

    a. Set up the box for isofluorane aneasthesia
    b. Turn on isoflurane vaporizer— set O_2 levels to 1, isoflurane amount ~3-5.
    c. Place mouse in box for several minutes until no longer moving, then transfer mouse to foil-covered styrofoam rack for surgery; place mask extension immediately on mouse to keep anesthesized.
    d. Once mouse is no longer sensitive to toe pinch, then mouse is ready for surgery

8. Mount mouse, back down, on aluminum foil-covered styrofoam block in the hood and tape the limbs to immobilize (maintain isoflurane flow through mask extension to ensure constant anesthesia is being delivered)
9. Wipe down belly of mouse with EtOH and kimwipe (don't spray ethanol directly on the mouse because it may become too cold)
10. Shave belly to remove fur, wipe away the fur.
11. Make small snip incision in the belly region of mouse, ~ 1.5cm above the anal cavity.
12. Make one ~0.5-0.75cm incision up towards thoracic region. Before making the cut, be sure to keep the scissor tip pointed up and gently prod up to separate the skin from the peritoneal wall. Once tips of scissors inserted to the appropriate distance

for the cut, make the incision. Be sure to only make one cut (don't want to do a few small cuts)

13. Make two side incisions, angled toward the hind leg of the mouse between the 4th and 5th fat pads. (About the same size ~0.5-0.75 cm incision is good). Ok to be fairly conservative with incisions (so long as you can locate the fat pad) as it's easier to suture later. The 4th inguinal fat pad will be above the incision line and is used because it is the biggest of the 5 fat pads.
14. Lift skin with forceps and start peeling back skin with the Q-tip (dampen with sterile PBS to make easier). If the mouse starts bleeding- use the cauterizer to stop the bleeding- quick, gentle touch once preheated is all that is needed, then wipe away blood with a Q-tip
15. Peel back skin until you see the cross where 3 veins come together (LN's located here). If you follow the vein leading down into the dorsal side of the mouse, this is where the fat pad is located. While the skin is more of a yellow color, the fat pad is a peach color. (The fat pad placement is deeper then you might think, so keep peeling open until you can see it—it wraps around the side of the mouse)
    a. Prepare Hamilton syringe with 20 µL of 50:50 mi of cells and matrigel (10µL of each, NOTE: This is about the capacity of the fat pad, do not inject more volume than this)- make sure this is really well resuspended; be sure to pipette the suspension up and down to mix each time before injection
    b. Hold the forceps at the top of the fat pad
    c. Inject the cells with the syringe from top down (insert needle in the top of the fat pad and move down to the middle to release the cells). Should see the pouch fill out as the volume goes in. Hold fat pad up for several seconds to wait for the matrigel to start solidifying and then can bring the skin flap back down.
    d. Rinse Hamilton Syringe with PBS between injections in order to remove any residual matrigel that may solidify and make drawing up/injecting cells difficult. Ethanol and PBS the syringe between cell populations
    e. Once both fat pads have been injected, suture the incisions with woundclips
        i. Pinch skin together with forceps so the inside of the skin flaps come together. Pinch skin along the entire incision before applying wound clip.

ii. Be sure to lift up because don't want to catch the clamp on the peritoneal wall, just want to get the skin, so lift up and use forceps to clamp region of incision
iii. Hold and clamp the wound clip around the incision. Repeat for the other two incisions (total of 3 wounds clips is good for each mouse)
iv. Subcutaneous injection of diluted Buprenorphine 0.5-1mg/kg, 100 µL per mouse (as per animal protocol). EXAMPLE: For 0.07 mg/kg and ~17g mouse, need ~4µL of the stock Buprenorphine per mouse. Prepare 100µL injections, so dilute 4µL Buprenorphine + 96µL PBS per mouse (prepare 2 x 1mL aliquots).
    1. Stored in locked drawer: Code is 2464

16. Return mouse to cage in which half is placed on a pre warmed heat pad (use microwave to warm pad). Need to keep mice warm, especially in the beginning since they're cold right after surgery. Add some wood chips to cover them to keep them warm. Most mice will awake and move around in a few minutes.
17. Place "post-op" orange sticker on cages of mice that have undergone surgery, write today's date
18. Monitor mice for 5 days post-op and record appearance/health on post-op surgery form
19. Following surgery, check on mice 3 x a week (Measure weight 1/week). Once tumors become apparent, take external caliper measurements and record.

R: Mouse Tumor Harvests for GFP Imaging, Culturing, and Histology

Tissue harvest

1. Euthanize mouse with CO_2, mount mouse to styrofoam block
2. Wipe fur with 70% EtOH and kimwipe before making incision
3. Make small incision and cut an inverted Y
4. Separate skin from internal organs to expose mammary fat pads and other organs:
5. Collect various tissues to image GFP fluorescence with microdissection microscope followed by either culture and/or histology. Record Length, Width and mass (g) of tumors and any additional observations.
    a. *For fluorescent imaging/ culturing:* Place tissue (e.g. primary tumors, LN tumors, lung, spleen, liver) in sterile 6 well plate filled with sterile PBS, tissues are stable for several hours once in PBS
    b. *For histology*: Place tissue in ~10 mL of fresh 4% PFA in glass scintillation vial (see "4% paraformaldehyde preparation" below) (NOTE: lungs require special fixation protocol if preparing for histology; see "Lung fixation protocol" below)

4% Paraformaldehyde (PFA) Preparation

NOTES: Use as fixative for tissue samples that you plan to embed in paraffin to carry out histology on. Fix for 24-48 h depending on tissue size. After this time, transfer to 70% EtOH and submit for paraffin embedding/histology.

1. Weigh out 4 g of PFA (Sigma, Cat #158127) (stored at 4 °C)
2. Add to bottle with stirbar
3. Add 100 mL of PBS
4. Loosely screw on lid and place on hot/stirplate in fumehood
5. Place bottle containing 4% PFA in a beaker containing warm water (helps with even heating)
6. Bring temperature up to ~60 °C, while stirring moderately

7. Once solution has turned from cloudy to clear, take off heat and allow to cool (takes awhile)
8. Place at 4 °C (can be used for up to ~1month)

Lung Fixation Protocol

NOTES: This protocol describes infusing the lungs with PFA and inflating them for analysis by histology. This protocol also describes how to tie off one of the lobes to preserve for culturing.

Special materials needed:

Suture material (3 Gauge)

1. Cut into ribcage from diaphragm
    a. Cut with blunt scissors along both sides of ribcage extending through the thoracic cavity (not through middle), using blunt scissors will help to avoid dulling sharp scissors or accidentally injuring organs within (e.g. lungs, etc.) or major veins/arteries, blood can make difficult to navigate
    b. Once ribcage has been cleared enough to probe cavity, identify mouse's left lung lobe (should be single while right side should have 3 lobes)
2. Form a lasso loop with suture (3G) and wedge around top of individual lobe using blunt forcep to position within loop. Tie loop at top where membrane connects lobe and heart and trachea.
3. Cut lobe for culture below suture knot (to prevent formalin flow once applied later on)
4. Place lobe in sterile PBS for GFP imaging and culture
5. Find trachea and infuse fixative:
    a. Can remove salivary gland (large gland on top of trachea)
    b. Blunt dissect membrane around and under trachea to make accessible for suturing
    c. Once trachea has been cleared, place blunt forcep clamp underneath trachea, and pull suture thread through
    d. Tie a loose knot
    e. Make a perpendicular incision with small scissors to make a hole in the trachea (be sure not to cut all the way through)

   f. Using a 20G blunted needle (this is important-- don't want sharp point that can perforate trachea), insert past where knot is loosely tied and lay flat
   g. Once in position, tie knot
   h. Infuse PFA into lungs (should see lungs visibly inflate to several times their original size).
   i. Once inflation levels seem to not change anymore remove needle while firmly tying suture knot to ensure that fixative does not leak out
6. Find thymus (small whitish tissue on top of heart) and remove for culturing
7. Harvest lung lobes for histology:
   a. Clear away all the membrane and tissue (includes fat, muscle, skeletal) around trachea
   b. Cut trachea above suture knot
   c. While holding knot in an upwards fashion, start clearing and separating trachea from body, moving down towards the lung area
   d. Make sure ribcage is cleared away or this will hinder your ability to remove trachea and lobes easily
   e. Moving from trachea down, continue to cut lungs from membranous tissue until it all comes out in one package
8. Keeping suture knots firmly tied around left lung lobe and on trachea, place everything in fixative (this will prevent deflation)
9. Allow to fix for 24 h at 4 °C
10. After 24 h in fixative, place lung lobes into 70% EtOH O/N at 4 °C
11. Prepare/submit lungs for histology at UCSD histology core:
   a. Want to preserve direction of airways. Therefore, cut longitudinally from hyliss (from where it attaches to the airways) to apex (bottom corner)
   b. Be consistent when preparing lung histology samples to ensure knowledge of orientation on slide

GFP visualization using microdissection scope

1. To determine if any organs had mets, used Yang Lab (NSB) microdisssection scope
2. Turn on → Switch filter to GFP2 (need to turn mat under scope to black to see)

3. Using tweezers, remove tissue sample from PBS and place on sterile 10cm Petri dish under objective
4. Once satisfied with image, "snap"
5. Stored in RinaMorgan folder with date as subfolder: "Save as" – name "magnification, mouse #, organ"
    a. save as .tiff file
    b. resolution= 1392 x 1044 FF

Culturing primary tumors and metastases

Special Materials needed:

Collagenase A (Roche, # 11088785103)
Cell strainer, 70uM nylon (BD Falcon, # 352350)

1. Prepare fresh 1 mg/mL Collagenase A in RPMI-serum free
2. Place tissue in sterile 10 cm dish containing variable amounts of Collagenase A (depending on tissue size)
3. Mince tissue with sterile razor blade (use clamp forceps to hold blade)
4. Place minced tissue into sterile 125mL Erlenmeyer flask with stirbar at 37 °C room. Alternatively, add to 15 or 50 mL conical and rotate end-over-end in 37 °C incubator.
5. Stir or rotate for 1-2 h at 37 °C to allow Collagenase A to digest the ECM
6. Stop Collagenase A digestion by doubling volume with RPMI-10%FBS
7. Pass cells through 70um filter into new conical
8. Spin 250xg for 10 min at 4 °C, all should have visible pellets (LN pellet will be very small)
9. Seed cells depending on amount of cells expected to recover; resuspend pellet with RPMI-10% FBS + Pen-Strep (10 units/mL pen, 10 ug/mL strep) and place into appropriately sized dish or multiwall plate
    c. Primary tumors: If digested one whole primary tumor, only need to seed a fraction of the digestion to a 10 cm dish, recovery is usually very good.
    d. LN tumors: Seed in smaller dish (e.g. 6 well or 6 cm) depending on size
    e. Liver, Lung, Spleen: Depends on extent of metastases evident based on GFP detection and how much contaminating cells are likely present; will

require extensive PBS rinsing for several days after plating, recovery typically slower than that of primary and LN tumors b/c mets are less abundant

10. Incubate cells at 37 °C
11. Once cells are confluent, select or split and select into new dish with Blasticidin (RPMI+ 10% FBS + 5ug/mL Blasticidin). Only GFP+ MDA-MB-231 cells should survive selection.

S: Quantification of Lung Fluorescence for GFP-expressing Tumor Cells

(Modified from Borsig et al. Synergistic effects of L- and P-selectin in facilitating tumor metastasis can involve non-mucin ligands and implicate leukocytes as enhancers of metastasis. PNAS, 2002.)

Materials Needed:

Lysis Buffer- 20 mM Tris, pH8
70% EtOH (for cleaning homogenizer)
20% Triton X-100
96 well plate
10 mL falcon tubes (ones used for bacterial cultures work well)
2 mL eppendorf tubes

Sample Preparation

1. Harvest mice as usual (see protocol Q), keep all lung lobes in PBS (in 6 well plate is good) until ready to homogenize
2. (Optional, though good idea) Visualize lungs for detection of GFP expressing lung metastases
3. Clean up lungs being sure to get rid to any membranes (e.g. trachea, etc.) that may be left from harvesting of lungs (these tend to clog up the homogenizer and have some autofluorescence)
4. Place each set of lungs into a 10 mL falcon tube containing 2 mL of lysis buffer (this is the minimum volume to use with the homogenizer)
5. Homogenize each set of lungs for 20s, power level 3 with the IKA T18 basic Ultra Turrax homongenizer, then place lungs on ice until all samples are completed. Clean the probe between each run with 70% EtOH and Milli-Q water and use tweezers to remove any membranous tissue stuck in the homogenizer
6. Add 50 µL of 20% Triton X-100 to each tube and allow to incubate on ice for 30 min
7. Transfer homogenate to labeled 2 mL eppendorf tubes
8. Centrifuge homogenate a max speed for 10 min at 4 °C.
9. Begin warming plate reader

10. Collect about 400 µL of middle clear aqueous layer (more oily layer above) and transfer to a new tube, place on ice.
11. Pipette samples into plate reader in a total of 200 µL with lysis buffer. Can try dilutions of 1:4 to 1:20 to see what gives you the best response. Read triplicates for each.
12. Read the fluorescence at gains of 40, 50, and 60 at 485 nm excitation
13. Normalize fluorescence readings to PBS (can also compare to GFP positive primary tumor to get strong signal for comparison, though not necessary)

T: Western Blot Protocol

MATERIALS:

Ripa buffer
- 10 mM Tris pH 7.4
- 150 mM NaCl
- 1% TritonX-100
- 0.1% Na-deoxycholate
- 0.1% SDS
- 5 mM EDTA

5x sample buffer (10 mL)
- 1 M Tris/HCl pH 6.8 – 0.6 mL
- Glycerol – 5mL
- SDS – 1 g
- 2-Mercaptoethanol – 0.5 mL
- Bromophenol blue – 10 mg
- To 10 mL with mqH_2O

10x Transfer buffer (1 L)
- Tris – 30.3 g
- Glycine – 144.1 g
- To 1000 mL with mqH_2O
- Note: to prepare 1X solution for use, dilute 100 mL into 700 mL mqH_2O + 200 mL methanol

10x running buffer (1 L)
- Tris – 30.3 g
- Glycine – 144.1 g
- SDS – 10 g
- To 1000 mL with mqH_2O

10x TBS (1 L) pH 7.6
- Tris- 24.2 g
- NaCl- 87.7 g

Note: to prepare 1X solution for use, dilute 100 mL into 900 mL mqH_2O + 1 mL Tween (0.1%) (Final is 20 mM Tris pH7.5, 150 m NaCl, 0.1% Tween 20)

Complete protease inhibitor cocktail – Roche 11697498001 (or Sigma P8849)
Halt phosphatase inhibitor – Pierce/Thermo Scientific 78420
Precision Plus Dual Color protein standard- Bio-rad 161-0374
Non-fat dry milk – Apex 20-241
Bovine serum albumin (BSA) – Sigma A7906
Restore Western Blot Stripping Solution – Pierce/Thermo Scientific 21059
IgG Elution buffer – Thermo Scientific 21004
Amersham ECL Plus - GE-Healthcare RPN2132

Super signal west femto sensitivity reagent- Pierce/Thermo Scientific 34096
X-ray films (5”x7”)– Phenix F-BX57
Cell scrapers- Costar 3010 (small, for 6 well/6cm plates) 3011 (large for 10cm plates)
Eppendorf Protein LoBind tubes- Eppendorf 22431091 (1.5 mL), 22431064 (0.5 mL), 22431102 (2mL)
96-well plate (clear bottom)

PROTOCOL:

1. Prepare cell lysates for western blot analysis:
    a. Add fresh to Ripa lysis buffer: Protease inhibitor cocktail and Halt phosphatase inhibitor cocktail (can freeze extra complete Ripa buffer in -20°C)
    b. Rinse cells with PBS (can skip this for CLL cells if they are loosely adherent to plate)
    c. Add Ripa lysis buffer to cells in dish (adherent) or spun down in tube (suspension). Depending on number of cells/size of dish, vary the volume of lysis buffer appropriately:
        i. For CLL cells in 24-well or 6-well plate (~1E7-3E7 cells): generally use ~50-75 µL
        ii. For MDAs/HEKs in 6cm dish (~70-80% confluent): use ~100 µL
        iii. For 10 cm dish: can use ~200-250 µL
    d. Let cells lyse on ice in Ripa buffer for ~30 min
    e. Scrape cells with cell scrapers and transfer to 1.5 mL tubes
    f. Clarify by centrifuging at 13,000 rpm for 10 min at 4°C
    g. Transfer supernatant to new, labeled (Lo-Bind) tubes and store lysates in -80°C freezer for storage
2. Perform BCA protein assay on cell lysates to determine total protein concentration (allows equal loading of wells for western blot):
    a. Prepare a working stock of BSA standard at 0.2 mg/mL
    b. Prepare assay in duplicate or triplicate in 96-well plate
    c. Set up BSA standard wells first:
        i. 0 µg – 0 µL
        ii. 1 µg – 5 µL (of the 0.2 mg/mL solution)
        iii. 2 µg – 10 µL
        iv. 3 µg – 15 µL

v. 4 µg – 20 µL
vi. 5 µg – 25 µL

d. For all unknown samples, add 1 µL of sample to each well (if worried about low protein concentration, can use larger volume but remember to take into account at end when calculating the protein concentration
e. Prepare BCA solution mix: 1:50 ratio of clear:blue solution (so if need 10 mL, add ~9.8 mL of clear solution + 200 µL of blue solution). Mix and solution should turn green
f. Use multichannel pippetter to distribute 200 µL to each well
g. Incubate at 37°C for 30 min
h. Read absorbance using the plate reader at 562 nm
i. Determine unknown protein concentrations of samples using the BSA standard curve and linear regression.
j. Calculate volume required for 20 µg of protein lysate and volume for 5 x loading dye

3. Prepare samples for western blot: 20 µg of total protein in 5X sample loading dye. Boil samples for 5-10 min. *Note: if probing for chemokine receptors, do NOT boil because this causes their aggregation and they do not resolve (stay in upper part of gel). Can store at -80°C or -20°C for running later.
4. Prepare SDS-PAGE gels
   a. Clean the glass plates and set-up apparatus with plates
   b. Prepare resolving gel solution and pour:

      For 1 x 1.5 mm gel, 7.5 mL is sufficient, for 1 x 1 mm gel, 6 mL is sufficient for resolving gel.

      Solution for 2x1 mm 10% SDS PAGE gels:

Water	4.75 mL
30% acrylamide	4 mL
1.5 M Tris pH 8.8	3 mL
10% SDS	120 µL
10% APS	120 µL
TEMED	5 µL

      *Add TEMED and APS last. Wait until solidifies (~20-30 min).

c. Prepare stacking gel solution and pour:

Allow 2- 2.5 mL of solution for stacking per gel. Solution for 2x1 mm gels:

Water	2.75 mL
30% acrylamide	0.67 mL
1 M Tris pH 6.8	0.5 mL
10% SDS	40 µL
10% APS	40 µL
TEMED	4 µL

Wait until solidifies

5. Load samples onto SDS-PAGE gels with one lane for ~8 µL of Precision Plus protein standard.
6. Run gels at ~100V through stacking gel (~10 min) then can increase to 150- 200V through resolving gel (~40 min)

*Time varies between gel thickness, can always run at a slower voltage too and increase the run time

Run gel until the loading dye has reached the bottom of the gel

Remove the upper stacking gel before transfer

7. While gel is running, prepare 1X Transfer buffer from 10X stock and cool on ice or in fridge:
    a. 100 ml 10X buffer, 200 ml Methanol, 700 ml mq water
    b. Mix well and cool
8. Take out ~5 gel trays for soaking gels, membrane, fiber pads, and filter papers
    a. If using PVDF membranes, soak the membranes in 100% methanol (they won't wet in transfer buffer)
    b. If using nitrocellulose, soak the membranes in transfer buffer (they dissolve in 100% methanol)
    c. Soak the filter papers and fiber pads in transfer buffer
    d. Once gels are done running, let them equilibrate for ~5-10 minutes in the transfer buffer
9. Prepare Transfer Sandwich:
    a. Mark the membrane on upper right side for orientation and protein side

b. Set up transfer sandwich as follows (add transfer buffer between the different pieces of sandwich so thoroughly wet):
-Black side of plastic sandwich
-1 fiber pad
-2 filter papers
-gel
-membrane
-2 filter papers
-1 fiber pad
-clear plastic side

c. Remove air bubbles from sandwich by squeezing/rolling out

d. Insert sandwich into transfer set-up so black plastic sandwich is towards the black side, clear is towards red. Insert so the notch is at the bottom (flat side is on top).

e. Add the ice pack and a stir bar to the transfer unit

f. Fill completely with transfer buffer

10. Transfer while stirring on ice for ~1.5-2 h (need 3 h for large Criterion transfer unit) at 100 V
    a. Arrange apparatus in ice tray to stay cold, place onto stir bar and keep stirring to dissipate heat while transferring
11. Block for >1 h in 5% milk-TBST at room temperature
12. Generally want to incubate in primary antibody O/N at 4°C (check on antibody specs for recommendations for incubation time, solution, and dilution). Most Cell Signaling antibodies: dilute 1:1000 in 5% BSA-TBST and incubate O/N at 4°C. Keep in covered/sealed container so they do not dry out. For minigels, can use ~5-6 mL/gel, for large Criterion gels need 10-12 mL/gel.
    a. Note: can generally reuse antibodies, store in -20°C for later use.
13. Wash blots 3x 10 min with TBST
14. Incubate in secondary antibody >1 h at room temperature (usually dilute the secondary antibody in 5% milk-TBST)
    a. Note: for Thermo goat anti-rabbit secondary dilute 1:10,000- 1:20,000 in 5% milk-TBST when using Amersham ECL Plus to develop (stronger antibodies)

and dilute ~1:100,000 in 5% milk-TBST when using the Pierce West dura femto sensitivity reagent. (Pierce also has pre-diluted antibody which can be used at 1:1000 instead, but no longer comes in the kit)

15. Wash blots 3x 10 min with TBST
16. Develop with appropriate reagent (Amersham ECL Plus or Pierce West Dura femto) 5 min at room temperature (best to do with lights off)
17. Expose to X-ray films
18. Can strip blots for reprobing or store in fridge or freezer in TBST for later use
    a. If re-probing for different protein altogether, use the Pierce Restore stripping solution 10 min at room temperature
    b. If re-probing for same protein (e.g p-Akt and then total Akt), better to use the IgG elution buffer to strip off the antibody since it is a more mild solution (had issues with Restore stripping off the protein with the antibody sometimes)
    c. If 1st strip, usually don't need to re-block, but otherwise should re-block and then probe with new primary antibody

U: Receptor Internalization Assay

MATERIALS:

CXCL12

PBS – Ice cold

FACS buffer: PBS + 0.5% BSA

Anti-CXCR4-PE (CD184)– BD Pharmingen 551510

IgG2A-PE control– BD Pharmingen 553930

*Note: Antibody clone for CXCR4-PE is 1D9, which should NOT interfere with CXCL12 binding (binds at alternative site), so acid wash is NOT necessary. Our data initially testing with acid wash supports these results, but do NOT need to repeat acid wash steps in future.

If unsure whether antibody binding is the same as ligand binding interface, then need to do an acid wash to remove ligand before staining with antibody:

Acid wash buffer 1: 50 mM glycine +100 mM NaCl pH 3 (w/acetic acid)

Acid wash buffer 2: 150 mM NaCl +150 mM acetic acid, pH 2.7

PROTOCOL:

Analysis of CXCL12-induced CXCR4 internalization by Examining Decrease in Cell Surface Expression of CXCR4

Day 1:

1. Seed 700,000-750,000 cells into 9 wells of 6-well plates for each cell type. For CXCR4 internalization, do not need to set up acid wash wells, but shown for purposes of unknown antibody binding site
2. 9 wells are for:
    a. Unstained control
    b. IgG control
    c. Unstimulated, no acid wash, CXCR4 stain
    d. Unstimulated, Acid wash 1, CXCR4 stain
    e. Unstimulated, Acid wash 2, CXCR4 stain
    f. +200nM CXCL12, no acid wash, CXCR4 stain
    g. +200nM CXCL12, Acid wash 1, CXCR4 stain
    h. +200nM CXCL12, Acid wash 2, CXCR4 stain
    i. Seed extra well of cells to get cell count estimate

Day 2:

3. Stimulate wells with 200 nM CXCL12:
    a. Easiest to prepare stock media solution (RPMI +10% FBS) with 200 nM CXCL12 added.
    b. Aspirate wells
    c. Add fresh media to "- CXCL12 wells" or media +200 nM CXCL12 to stimulated wells
4. Incubate for 45 min at 37°C to allow for internalization.
5. Place on ice and wash with ice-cold PBS 2X.
6. Lift cells with 1M EDTA-PBS on ice- 500 µl/well.
    a. Note- next time can use normal 1mM EDTA
    b. Can also try wash with PBS, acid wash in well and then lift.
    c. Could also just have 2x10cm plates (stim and unstim) and then post-EDTA lifting do acid wash or no acid wash after distributing cells to tubes
7. Collect all the cells for staining since <1x10^6 cells per well. Take cell count for estimate with extra well.
8. After lifting cells, spin down at 250 x g for 10 min at 4°C
9. To cells for acid wash (leave non-acid wash tubes sitting on ice):
    a. Add 1 mL Acid Wash buffer (1 or 2) to tubes
    b. Invert several times
    c. Spin at 250 x g for 5 min at 4°C
10. Repeat acid wash step
11. Aspirate and wash with 1 mL FACS buffer to make sure to get out any residual acid buffer (this could interfere with antibody binding)
12. Aspirate all pelleted cell samples and resuspend in 100 µL of FACS buffer for antibody staining and aliquot into 96-well plates
13. Add 1.5 µL of IgG control or anti-CXCR4-PE antibody (BD Pharmingen) to samples. Incubate covered with foil on ice for 20 min to stain.
14. Wash 3 x 5 min with FACS buffer
15. Resuspend in total of 400 µl FACS buffer and analyze by flow cytometry
16. (Optional: can fix with 0.5 mL PBS +1% PFA) to save for analysis at later time

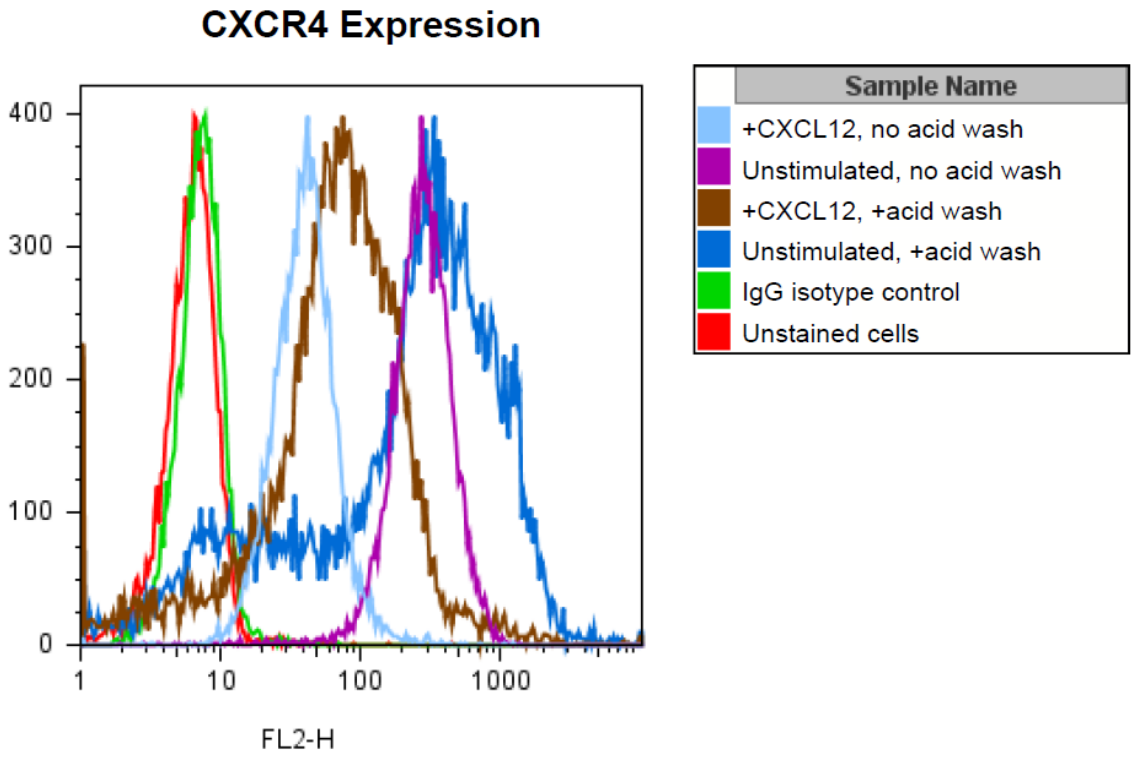

A.X CXCL12-mediated decrease in CXCR4 surface expression. Ramos cells were left unstimulated or stimulated with CXCL12 (30 nM, for MDAs use 200 nM) for 1 h at 37°C/5% CO_2, treated with (+) or without (no) acid wash, stained for CXCR4 expression and analyzed by flow cytometry.

V: Immunofluorescence Microscopy

MATERIALS:

Primary Ab	Catalog #	Stock	Recommended use	To try
Monoclonal Anti-CXCR4 (mouse ∝ hu) IgG2B	R& D MAB172	500 ug/mL	5-15 ug/mL	10 ug/mL
Monoclonal Anti-CXCR7 (mouse ∝ hu) IgG2A	R&D MAB4227	500 ug/mL (10 µL alliqouts)	8-25 ug/mL	10 ug/mL
Monoclonal mouse Anti-IgG2A isotype control	R&D MAB0031	500ug/mL	None	10 ug/mL

Secondary Ab	Catalog #	Stock	Recommended use	To try
Alexa Fluor 488 (goat ∝ mouse IgG)	Invitrogen A11001	2000 ug/mL	None	1:500 or 1:1000

Cover slips-

Prolong Gold with DAPI– Invitrogen P36935

SeaBlock – Pierce/Thermo Scientific #37527

PROTOCOL:

DAY1:

1. Seed cells onto cover slips in a 6-well plate at 250,000 cells per well
   a. 500,000 seeded previously yielded ~70-80% confluency—a bit much

DAY2:

2. Everything can be done at RT, put coverslips on parafilm for washes and staining in order to conserve reagents
3. Wash 3 x with PBS for 5 min each
4. Fix slides with freshly prepared 3.7% formaldehyde in PBS/4% paraformaldehyde for 15 mins.
5. Wash 3 x with PBS for 5 min each (at this point, can be stored O/N at 4 °C)

6. Permeabilize with ~250 µL/slide of 0.5 % Triton-X 100 in PBS for 10 min (alternatively can use ice cold methanol to permeabilize)
7. Wash 3 x with PBS for 1 min each
8. Block with ~750µL of SeaBlock or 1%BSA/10% goat serum (or whatever species 2° Ab is) for 45m- 1h
9. Wash with 3 x with PBS for 5 min each
10. Incubate with ~250 µL primary antibody for 2 h (or O/N at 4 °C)
11. Prepare antibodies in 20 mg/mL (2%) BSA in PBS
    i. Anti-CXCR4 at 10 ug/mL= 5 µL stock + 245 µL buffer
    ii. Anti-CXCR7 at 10 ug/mL= 5 µL stock + 245 µL buffer
    iii. Anti-IgG2A at 10 ug/mL = 5 µL stock + 245 µL buffer
12. Wash with 3 x with PBS for 5 min each
13. Incubate with ~250 µL of secondary antibody for 30-45 min, covered with foil (Note: spin down secondary before use)

	Volume in 1000µL total (250 µL each)
Alexa Fluor 488 (1:500)	2.0µL
0.5% BSA/PBS	998.0µL

14. Wash 1 x with PBS for 5 min
15. If not using Prolong Gold with DAPI in it, can incubate with 1:1000 DAPI-Hoescht nuclear stain for 20 min
16. Wash 3 x with PBS for 5 min
17. Dip in ddH2O to rinse off PBS
18. Remove excess moisture and allow slide to dry slightly on benchtop before applying mounting solution Prolong Gold
19. Add 1 drop of mounting solution and add coverslip
20. Allow slide to dry O/N at RT
21. Next day, image using the deconvolution microscope
    a. Samples can be viewed after 1hr, however for long-term storage dry overnight at room temperature and then store at -20^{o}C.

Using the Deconvolution Microscope at the Cancer Center Core:

Contact: Kersi Pestonjamasp kpestonjamasp@*ucsd*.edu

If first user- Turn on UV lamp (Mercury 100W) and blackbox

If last user- Turn off UV lamp (if no one is signed up after you) and blackbox, once UV lamp is off, needs to remain off for 30 min

General system:

2 computers (hardware and software)

- Toggle between the two computers by pressing the switchbox to the left of the monitor

Software for acquisition is SoftWorx- bottom left icon to view programs→ select softworx

Desktop Control:

1. Open DV instrument controller box (usually open, if not, will guide you through opening
2. File → Acquire (Acquire series for timelapse experiments)→ Yes (to initialize hardware)
3. Specify/select the following parameters in the toolbar prior to imaging:
4. Size (camera pixels)
    i. Full chip= 1300 x 1024 (larger area)
5. Exposure time (long enough to get adequate signal
    i. Generally ~0.2s-5s; 1s a good starting place
    ii. Find exposure option-will take 3 successive pictures and find the maximum pixels
6. Setup is a 12 bit camera (max range ~1000-1500)
    a. Bin- leave as 1 (only when signal is weak do you try to combine pixels, drawback is that resolution decreases)
    b. Objectives: 10X (dry), 20X (dry), 40X (oil), 60 X 1.4 aperture (oil), 100X 1.4 aperture (oil), 100X-Tirf, 1.49 aperture (oil)
        i. Signal brighter under oil
        ii. Add drop of oil onto slide and invert onto microscope
        iii. We generally use the 60X

iv. Normal numerical aperture is 1.4—tells you how close objective will be to light—higher aperture gives brighter image and better resolution. 100X-Tirf objective lets in more light with slightly higher aperture of 1.49
v. Can't discriminate below ~200nm of points apart

c. Z-spacing
i. For 60X, 1.4 aperture (smaller depth of field), ideal step size is 0.15
ii. Spacing dependent on refractive index (RI depends on type of mounting solution, cell dispersion, dry slide); if using coverslip, don't have to worry to much about the depth
iii. Remove excess mounting medium (could otherwise cause distortions)

d. Camera
i. CoolsnapHQ is default (standalone is more sensitive, but slower, use only for backup)
ii. 2 speeds (doesn't matter, so go with higher speed)
iii. Gain = 2 for all colors
iv. Blue window in toolbar- changes brightness
v. Camera settings min and max- max of 1000-1500
vi. Excitation filter (don't go below 0.5 s; if exp is too long even at ~0.2 s, can add a neutral density filter). Check that excitation and emission filters checked correspond
vii. When viewing under the microscope and taking pictures, be sure that filter on the microscope matches settings on the computer (FITC and FITC), otherwise can burn eyes with unfiltered fluorescence

e. Automated stage moves in x, y, z
f. Mark and visit (allows you to mark a point, saves the x,y,z coordinates so you can revisit)
g. Lever on right- push back for eye piece, push forward for camera
h. Emission filter (select color on computer)

<u>Microscope</u>:

7. Move to objective you designated
8. Add small drop of oil to coverslip (for 100X, need ~1/2 the amount of oil) (ideally, cells are grown on the coverslip)

9. Be sure slide is as dry as possible—press face down on kimwipe while applying pressure
10. Clean coverslip with Chloroform and Q-tip if necessary
11. Add slide oil side down (in contact with objective)
12. Lower the top piece- flip lever up to let light pass
13. Left side of microscope is the button to turn the light on/off
14. To see through eyepiece-- push stick in back position; to connect image to computer—push to forward position
15. Press bottom left hand button on joystick panel to turn on fluorescence, press again to turn off
16. In DAPI (select filter on computer and microscope when looking through eyepiece!), focus on cells with large knob, smaller adjustments with small knob
    a. Towards you—stage up
    b. Away- stage down
17. Turn bright field on for DIC- PHL- DIC analyzer, prism- use blank filter to look through
    a. Open shutter (next to fluorescence)
    b. Trans Ex shutter- exposure low
    c. post processing view blended colors- can collect fluorescent and DIC together
18. Collect series of z-stacks: ~20 sections from each slides
    a. Can start at focus and then move up and down
    b. or start at bottom and go up until through the focused image
19. Click Experiment→design→sectioning setup
    a. optical section 0.2
    b. # of optical: 10-11 (10 -11 above and below)
20. Click first box- color as DAPI, add FITC
21. File→save and exit
22. Deconvolution of Images:
    a. Transfer data- DVUser:
        i. Host: 132.239.79.91
        ii. Octane 3 132.239.74.81
        iii. user: worx passwd: ap1dv1 port: 21
        iv. Sign up for time for deconvolution computer

b. Transfer data 1 files from DV computer “scope” to Octane Softworx data folder
c. open softworx and open data
d. Process→deconvolve, OTF=60x
    i. will already add OTF file
    ii. Method- aggressive (little grainy) or conservative based on # of cycles
    iii. 10 cycles of deconvolution is default, if image is dime, use fewer cycles; detailed- use more cycles
e. Try 2 cycles and 10 cycles of deconvolution, for cytosolic proteins, less deconvolution may work better (the 2 cycles)- conservative ratio
f. Drag xxx.r3d file to inbut bar → automatically generates output file
g. Queue multiple files using run options → add to queue
h. Drag other xxx.rd3 files to input bar- should see added to queue
    i. drag/add to input
    ii. click “do it”
    iii. worx- ap1dv1 – run to que
    iv. can take a while, so leave and come back later
i. Viewing/adjusting images:
    i. open xxx.r3d_D3D_Rv file
    ii. Adjust brightness for DAPI and FITC separately:
        1. select sun icon on left hand side toolbar
        2. Drag points on like to adjust brightness/background
    iii. Save as .tiff file
        1. Rename to be more descriptive
        2. output size- 24 bit RGB
        3. Details: can select z’s to save
        4. Press “do it”, then you’re done
    iv. on left panel (half filled sun-looking icon)- scale image, copy and paste scale
    v. For each image, compare isotype control staining (non-specific staining)
        1. Once brightness for DAPI and FITC are adjusted on the sample image, select “copy scale”
        2. open IgG image→open brightness icon → select “paste scale”
        3. save image as a reference to original image

j. Downloading images
    i. Open file transfer program to get remote access to computer
    ii. IP address is 132.239.74.81 user: worx pass: ap1dv1
    iii. Find folder and transfer to lab computer

W: MTT Assay

MATERIALS:

RPMI 1640 (NO phenol red) – Sigma R7509
MTT reagent (Thiazolyl Blue Tetrazolium Bromide)– Sigma M5655 – 100 mg
96-well plates – Costar
Resolubilization buffer- 0.04M HCl in isopropanol solution:
85 µl concentrated HCl (12.1N) to 25mL isopropanol

PROTOCOL:

DAY 1:

1. Prepare cell suspensions at $1x10^6$ cells per mL for the different cell populations in serum-free RPMI or RPMI+10%FBS (NO PHENOL RED)
2. Try 2 cell densities, $0.5x10^5$ cells/well and $1x10^5$ cells/well
   a. Prepare samples in triplicate and in media + or – 10% FBS media
3. To a 96-well plate:
   a. Add 100 µl of the $1x10^6$ cell/mL suspensions in triplicate to wells for $1x10^5$ cell wells.
   b. Add 50 µl of suspension + 50 µl of media to the $0.5x10^5$cell wells.
4. Incubate overnight at 37°C/5%CO2.

DAY 2:

5. Prepare 5 mg/mL MTT reagent in RPMI w/out phenol red (enough for 10µL per well + little extra):
6. Add 10 µl reagent to each well
7. Let incubate with reagent at 37°C/5%CO_2 for ~2.5 – 3 hours
8. Aspirate the MTT reagent from the wells
9. Add 100 µl of resolubilization buffer (0.04M HCl in isopropanol solution) to each well and pipette up and down to thoroughly mix using a multichannel pipette.
10. Read absorbances at 570nm and 650nm using the plate reader, mix first for 5 seconds.

X: Pulldown of HA-tagged Receptor

(Original protocol from John Jones, Handel Lab, UCSD)

MATERIALS:

HA-affinity resin- Sigma# E6779
HA-peptide- Sigma# I2149
SilverQuest kit- Invitrogen
All lysis buffers are built upon the same base:
- 50mM Tris pH 7.4
- 300mM NaCl
- Protease inhibitor cocktail (Sigma #P2714)
- Phosphotase inhibitor cocktail I and II (Sigma #P5726 and Sigma #P2850)

Then, can vary based on detergent:

1) RIPA (**R**adio **I**mmuno**P**recipitation **A**ssay buffer)

1% IPEGAL (NP-40 substitute) (weak nonionic – lyses only cytoplasmic membranes)

0.25% Deoxycholate (mild detergent for the isolation of membrane associated proteins)

0.1% SDS (strong anionic)

10mM BME

Bare in mind…many people use the term RIPA, but it can have 1, 2, or all 3 detergents in it.

2) Ann Richmond's Buffer

0.05% Triton-X 100 (nonionic – for all membranes)

3) CHAPS buffers are typically run at 5-10mM (zwitterionic)

For most signaling/cell bio labs…RIPA is frequently used. Just remember the composition may be different. The one listed above is what my old used exclusively for Co-IPs and lysis of mammalian cells, and it is also the one used by Pascale and Bouvier for the B-arrestin pull downs.

PROTOCOL:

1. Grow cells to ~70-80% confluency in 10 cm dish

2. Wash cells with PBS
3. Serum starve with serum-free RPMI O/N (time may vary depending on the cells)
4. Stimulate w/ 30 nM CXCL12 in serum-free RPMI for 5 min at 37°C

Harvesting non-crosslinked protein lysates

5. Remove stim by aspiration and lyse with 500 µL cold lysis buffer
   a. hand rock and scrape cells off dish
   b. pipette mix and transfer to eppe tube
6. Let cells incubate on rocker at 4°C for 10 min
7. Spin at 10,000 x g for 10 min to clarify
8. Remove clarified supe to a fresh tube

Harvesting crosslinked protein lysates

9. Stop the stim with the addition of 1 ml of 20 mM DSP (2mM final)
   a. Rock with light aggition at RT for 30 min
10. If cells are still adherent, rinse with PBS, and “quench” the DSP with 4 ml of 50 mM Tris, pH 7.4 in PBS for 10min with gentle rocking, then dislodge. If cells are lifting during the crosslinking, remove supe and wash the plate with 4ml of “quench”.
11. Pellet cells (2500 rpm for 5 min) and resuspend in 10 ml of “quench”
12. Pellet once more and aspirate
13. Lyse cells with 500 µL cold lysis buffer
    a. pipette mix and transfer to eppe tube
14. Let cells incubate on rocker at 4°C for 10 min
15. Spin at 10,000 x g for 10 min to clarify
16. Remove clarified supe to a fresh screw-cap tube

Pull-downs

17. 30 µl of HA-affinity resin (Sigma# E6779) is added to 200 µg of the clarified lysates and incubated on a rocker overnight at 4°C
18. Resin is washed 2x with cold lysis buffer
19. Protein is eluted by one of the following methods:
    a. Adding 100 µl 2x SDS-PAGE sample buffer
        i. For western blot analysis (not for MS)

b. Adding 100 µl 0.2M Glycine pH 2.0 at RT for 20 min
    i. Quench with 20 µl 1M Tris pH 7.4
    ii. Note- this elution did not work very well in our hands
c. HA peptide
    i. Resuspend HA peptide at 5 mg/mL with mqH_2O
    ii. Use 100 µg/mL peptide at RT or 37°C for 20 min (work equally well at both temperatures)
    iii. This method worked great

20. Take 5 µl samples for Silver stain analysis

Gels

21. Warm sample to 60°C for 5 min (do not boil or receptors with aggregate at the top of the gel)
22. Proteins were resolved by 10% SDS-PAGE and Western blot
    a. Silver stains were performed using SilverQuest kit from Invitrogen
    b. Western blots were performed by:
        i. α-HA-HRP @ 1:750 for 1.5 h at RT